EFFECTS OF CONCRETE QUALITY AND COVER DEPTH ON CARBONATION-INDUCED REINFORCEMENT CORROSION AND INITIATION OF CONCRETE COVER CRACKING IN REINFORCED CONCRETE STRUCTURES

Jacob Olumuyiwa Ikotun

A thesis submitted to the Faculty of Engineering and the Built Environment, University of the Witwatersrand, Johannesburg, in fulfilment of the requirements for the degree of Doctor of Philosophy.

Johannesburg, 2017

DECLARATION

I declare that this thesis is my own unaided work. It is being submitted to the Degree of Doctor of Philosophy to the University of the Witwatersrand, Johannesburg. It has not been submitted before for any degree or examination to any other university.

14th day of July, 2017

ABSTRACT

Many reinforced concrete (RC) structures in inland environment deteriorate early due to carbonation-induced corrosion of their reinforcement. In some cases, the deterioration is visible within a few years of construction in the form of cover concrete cracking. This is widely accepted as one of the limit state indicators in defining the end of functional service life for existing RC structures undergoing corrosion. Many of the currently available service life prediction models are incapable of providing realistic service life estimates of RC structures beyond the corrosion initiation stage. Therefore, the need to incorporate the corrosion initiation and propagation stages in a comprehensive durability prediction approach has been receiving much research attention.

In this research, empirical models were developed for predicting carbonation rate and the amount of steel radius loss required to initiate a first visible crack in concretes exposed to Johannesburg environment. The experimental data for the models were obtained from investigations of carbonation-induced reinforcement corrosion, which were explored in three phases; (i) concrete early-age durability and strength characteristics (ii) carbonation rate of different concrete mixes exposed to the natural inland environment (iii) amount of steel radius loss required to initiate the first visible crack on the pre-carbonated cover concretes exposed to an unsheltered environment. The experimental variables for the early-age durability and strength tests were; water/binder ratio (w/b) and binder type; w/b, binder type, initial moist curing duration and exposure conditions are the experimental variables for the carbonation rate test. Cover depth, reinforcement diameter, binder type and w/b variables were considered for the corrosion cracking test.

The results showed that an improvement in concrete quality (binder type, w/b ratio and extending the initial moist curing duration) and increment in cover thickness improved the durability of the RC structures exposed to the natural inland environment. Based on the trends in the observed experimental results, models to predict carbonation rate and the amount of steel radius loss required to initiate cover cracking in concrete were developed. The proposed models' predictions are more closer to the measured values and compared well with the predictions of some previous models which indicate their respective predictive applications. They provide a general basis for durability analysis of RC structures in inland environment and can serve as basis for condition assessment of existing structures in the inland environment. Engineers can appreciate the consequences of design options on the service life of RC structures, while owners of RC structures can have information about how long their RC structures may last before any repair is envisaged.

SUMMARY

The research was aimed at developing performance-based carbonation-induced steel corrosion initiation and propagation prediction models for RC structures in the inland environment. The purpose of the models was (i) to predict carbonation rate and time to steel corrosion initiation in concrete exposed to the natural inland environment and (ii) to predict the carbonation-induced corrosion steel radius loss required to initiate a first visible crack in concrete exposed to the unsheltered inland environment.

To achieve the aims and the objectives of this research, the experimental programme was designed and carried out in three phases. Phase one was the early-age characterisation tests on the concrete specimens, using the durability indicators (oxygen permeability and water sorptivity indices). Phase two included the carbonation tests carried out on the concrete specimens exposed to the natural inland environment, which were done to determine the carbonation resistance of the test concrete mixtures. Phase three was the natural corrosion propagation tests carried out on the pre-carbonated concrete specimens using linear polarisation resistance and gravimetric mass loss methods to determine the amount of reinforcement radius loss required to initiate a first visible crack on the test concretes.

A total of 1155 cubes of size 100 x 100 x 100 mm were cast using fifteen different concretes for the durability indicator (DI), carbonation and compressive strength tests. The concretes were made using five binder types (100 PC, 70/30 PC-FA, 50/50 PC-BS, 90/10 PC-SF and 60/30/10 PC-BS-SF) and three w/b ratios (0.95, 0.60 and 0.40). The DI and compressive strength concrete specimens were cured in water (at a temperature of 22 ± 2^{o}C) for 28 days, while concrete specimens for the carbonation tests were cured in water for 7 and 28 days. The concrete specimens were immediately exposed to the natural inland environment (indoor, outdoor sheltered and outdoor unsheltered) for 2 years. The carbonation test was conducted on the concrete cube specimens at an interval of 6 months for 2 years. The test was carried out by spraying a phenolphthalein solution on the freshly cut surface of the concrete cubes and the extent of the carbonation front was observed and measured

using a Vernier caliper. The relative humidity (RH), temperature and CO_2 concentrations of the concrete exposure sites were also monitored for a period of one year.

For the corrosion propagation tests, a total of 108 RC prisms (100 x 100 x 200 mm long) and 24 unreinforced concrete prisms (12 prisms for splitting tensile strength test and 12 prisms for accelerated carbonation monitoring) were cast using six different concretes. The concretes were made using three binder types (100 PC, 70/30 PC-FA and 50/50 PC-BS) and two w/b ratios (0.95 and 0.60). Other corrosion propagation experimental variables included cover depth (12, 20 and 30 mm) and reinforcing steel diameter (8, 12 and 20 mm). The concrete samples for the corrosion test were cured for seven days in water (at 22 ± 2^{o}C) and dried under laboratory environmental conditions (temperature: 23 ± 2^{o}C, relative humidity: 50 ± 5%) for 30 days before exposure to the accelerated carbonation in a chamber with 10% CO_2 concentration at RH of 55 ± 5%. The ambient RH of the chamber was maintained using a saturated salt solution of potassium nitrate (KNO_3) and the carbonation test was carried out weekly using a phenolphthalein solution. The RC prism specimens were removed from the chamber when the observed carbonation front passed beyond the level of reinforcement and were exposed to the natural unsheltered environment. The concrete specimens were monitored daily (± 1400hrs) for the appearance of a first visible crack (visible to the naked eyes) on the concrete cover. The observation was discontinued once a longitudinal crack (parallel to the line of embedded reinforcing steel bar) appeared on the concrete cover surface. Linear polarisation resistance method was used to estimate the corrosion current density of the reinforcements while gravimetric mass loss method was used to estimate the amount of steel corrosion mass loss. The measurements were taken immediately after a first visible crack appeared on the cover concrete.

The results of the carbonation tests clearly indicated that carbonation depth and rate depend on both environmental factors (RH, temperature and CO_2 concentration) and factors related to the near-surface concrete characteristics (cover concrete penetrability and its alkalinity). The results of the early-age concrete characteristics (28-day oxygen permeability index, water sorptivity index, compressive and tensile strength) clearly reflected the influence of w/b ratio and binder type. The

investigated concrete properties were improved at a lower w/b ratio than a higher w/b ratio for a given binder type. For the same w/b ratio, all the supplementary cementitious materials (SCM) blended concretes were less penetrable with higher compressive and tensile strengths compared to the PC concretes, apart from the BS blended concretes at 0.40 w/b ratio. Even though, the concrete characteristics improved relatively with the partial replacement of PC with the SCM, the influence of concrete alkalinity was still evident in their carbonation results. The depth and rate of carbonation were greater in the blended cement concretes than the PC concretes for an equal w/b ratio, initial moist curing duration, and exposure environment. However, the silica fume blended concretes behaved differently as the depth and rate of carbonation were reduced compared to the other SCM blended concretes for an equal w/b ratio, initial moist curing duration, and exposure environment.

The effect of varying the duration of the initial moist curing conditions was also evident from the carbonation rate results. Extending the initial moist curing duration of the concretes reduced their carbonation rates in all the exposure conditions. Even though, extending the initial moist curing age of the concrete reduced the carbonation rate in the concretes, reducing the w/b ratio was assessed to be more effective and sustainable in reducing the carbonation rate in the concretes than extending the duration of the initial moist curing or using a different binder.

The results of relative humidity (RH) of the exposure sites show that the range of relative humidity measured at the indoor exposure site was relatively lower than the range of RH measured at the outdoor exposure sites for both the winter and summer periods. For a given exposure the range of relative humidity measured during the summer was higher than the range of humidity measured during the winter. For a given period, RH range of the outdoor exposures were higher than RH range of the indoor exposure. The result of the temperature measurements of the inland environment showed that the maximum and minimum temperatures measured during the summer period are higher compared to the maximum and minimum temperatures measured during the winter period. It was evident from the results that the maximum and minimum CO_2 concentrations for the indoor exposure (630–1200 ppm) was about three times higher than the maximum and minimum CO_2

concentrations of the outdoor exposures. The CO_2 concentrations for the two outdoor exposures (sheltered and unsheltered) seemed to be similar (250 – 550 ppm) considering the two periods (winter and summer) respectively. The variations in the exposure conditions of the concrete sites influenced the carbonation performance of the concrete samples. For a given concrete, carbonation depth and rate were greater in the indoor exposure than the outdoor exposures conditions. With a similar concrete, carbonation depth and rate were greater in the sheltered outdoor conditions compared to the outdoor unsheltered conditions.

The corrosion propagation test results indicate that the range of corrosion current was greater in the SCM blended concretes (0.93 - 3.96 $\mu A/cm^2$) compared to the PC concretes (0.69-2.88 $\mu A/cm^2$) for the w/b ratios (0.95, 0.60 and 0.40) and cover depths (12, 20, and 30 mm) considered. The corrosion propagation test results also showed that for a given concrete, improving its quality by reducing its w/b ratio from 0.95 to 0.60 reduced the corrosion current density and radius loss required to initiate cover cracking which consequently delayed the concrete cracking time. For a constant w/b ratio and binder type, the corrosion current density and steel radius loss required for cracking reduced with increasing cover depth; these attributes delayed the cracking time of the cover concretes. The variation in the reinforcing steel diameter seemed not to have any significant trend with the corrosion current density and the amount of radius loss required to initiate cracking and cracking time.

Based on the experimental results and their trends, corrosion initiation and propagation models were proposed. The proposed corrosion initiation model incorporates the combined influence of concrete quality (concrete penetrability, binder type, and duration of initial moist curing duration) and exposure conditions on carbonation rate. While the corrosion propagation model incorporates the combined influence of concrete quality (permeability and binder type) and cover depth on the steel radius loss required to initiate concrete cover cracking. With a known cover depth, binder type, initial moist curing duration, and exposure condition, the proposed carbonation rate model can be used to assess the corrosion initiation phase. This is with the assumption that corrosion is initiated immediately the carbonation front reaches the reinforcement regardless of whether oxygen and

moisture are sufficient to initiate corrosion or not. The two models predictions are in good agreement with the experimentally observed values and predictions from other models. However, these models are based on medium term carbonation and corrosion data; it can be updated and calibrated using long-term corrosion data in further research work.

Using a relevant carbonation-induced reinforcement corrosion rate model, with a known concrete permeability, binder type, and cover depth, the proposed corrosion radius loss model can be used to assess the corrosion propagation phase of RC structures exposed to the unsheltered inland environment. The two predicted periods (corrosion initiation and propagation) can be used to predict the service life of RC structure exposed to the unsheltered inland environment. The outcome of these models can help the design engineer in the choice of quality and cover depth of concrete to achieve a given service life. The models' application is not restricted to planning or designing stage of new concrete; it can also be applied to an existing corroding RC structure for estimation of remaining service life. Concrete construction stakeholders can have information on how long RC structures can last before maintenance. The information will help engineers in scheduling maintenance plans for RC structures, and stakeholders can have information on how long their concrete can last before maintenance.

ACKNOWLEDGEMENTS

My sincere gratitude goes to Dr. Mike Otieno and Prof. Yunus Ballim for their active supervision, guidance, and encouragement given during the study and preparation of this thesis. Their lengthy discussions helped me to understand what research is all about. I feel honoured to have worked with a team full of knowledge and passion for advancing concrete research.

Also, my appreciation goes to all academic and technical staff of School of Civil and Environmental Engineering of the University of the Witwatersrand for their technical contributions toward the success of this work.

I also thank The Concrete Institute (TCI) formerly known as Cement and Concrete Institute (C&CI), South Africa, Bradlow Foundation and Postgraduate Merit Award of the University of the Witwatersrand for their financial supports during the study.

Finally, I appreciate my wife, Abiodun Motunrayo and my son, Toluwanimi Epaphras Ikotun for their prayers, endurance, and encouragement during this study. The Lord bless you all.

Ikotun Jacob Olumuyiwa

July, 2017

TABLE OF CONTENTS

CONTENTS Page

ABSTRACT 3

SUMMARY 4

ACKNOWLEDGEMENTS 9

TABLE OF CONTENTS 10

LIST OF FIGURES 16

LIST OF TABLES 20

LISTS OF SYMBOLS 22

CHAPTER 1 23

1 INTRODUCTION 23

1.1 Background 23

1.1.1 Corrosion-induced service life models 25

1.1.2 Classification of South African inland environment 27

1.1.3 Durability Design of RC Structures 28

1.2 Research Motivation and Significance 30

1.3 Research Aims and Objectives 32

1.4 Research Conceptual Framework 33

1.5 Thesis Outline 33

CHAPTER 2 35

2 LITERATURE REVIEW 35

2.1 Introduction 35

2.2 Concrete Composition and Durability 35

2.2.1 Influence of concrete composition on its durability 36

2.2.2 Fluid transport properties of concrete 37

2.2.3 Concrete durability indicators (DI) 39

2.3 Mechanism of Steel Corrosion in Concrete....40
2.4 Thermodynamics of Corrosion....42
2.5 Reinforcement corrosion initiation in concrete....45
2.5.1 Concrete carbonation rate....46
2.5.2 Effect of concrete cover depth on corrosion initiation time....57
2.6 Concrete Carbonation Tests....57
2.6.1 Accelerated carbonation....58
2.6.2 Carbonation experiment under natural exposure conditions....60
2.6.3 Measurement of carbonation depth....61
2.7 Predicting the Time to Carbonation Induced Corrosion Initiation....62
2.7.1 Review of some existing corrosion initiation models....65
2.8 Corrosion Propagation of Steel in Concrete....74
2.8.1 Exposure environment....74
2.8.2 Concrete quality....77
2.9 Corrosion Propagation Assessment Techniques....78
2.9.1 Electrochemical techniques....79
2.9.2 Gravimetric mass-loss technique....82
2.9.3 Concrete resistivity....82
2.10 Effects of Corrosion on Concrete....85
2.11 Corrosion Steel Mass loss and Corrosion rate....87
2.12 Factors affecting corrosion-induced cover cracking....88
2.13 Review of Some Existing Cover Cracking Models....91
2.13.1 Empirical corrosion-induced cover cracking models....92
2.13.2 Analytical corrosion-induced cover cracking models....96
2.14 Corrosion Cracking Control Parameters....101
2.14.1 Corrosion rate....101

2.14.2 Critical amount of corrosion products....102
2.14.3 Cover concrete geometrical parameters....103
2.14.4 Material properties of concrete....104
2.15 Summary of the Previous Corrosion-induced Cracking Models....105
2.16 Summary....108
CHAPTER 3....110
3 EXPERIMENTAL WORK....110
3.1 Introduction....110
3.2 Experimental Variables....111
3.3 Concrete Mix Proportions....115
3.4 Number of Concrete Specimens....117
3.5 Specimen Casting....120
3.5.1 Concrete batching and mixing....122
3.5.2 Casting and curing of the concrete specimens....122
3.6 Tests Procedures....122
3.6.1 Natural carbonation....122
3.6.2 Accelerated carbonation....123
3.6.3 Corrosion propagation....125
3.7 Test Measurements....126
3.7.1 Concrete characterisation tests (Durability index)....126
3.7.2 Carbonation depth....130
3.7.3 Reinforcement Corrosion current density....130
3.7.4 Gravimetric mass loss....137
3.7.5 Other tests....140
3.8 Summary....141
CHAPTER 4....143

4 EXPERIMENTAL RESULTS, ANALYSES AND DISCUSSION.....143
4.1 Introduction 143
4.2 Exposure Conditions at the Concrete Sites 143
4.3 Quantification of Concrete Quality 145
4.3.1 28-day oxygen permeability index.....146
4.3.2 28-day water sorptivity index.....148
4.4 Compressive Strength and Split tensile strength 150
4.5 Carbonation Depth 152
4.6 Carbonation Rate 153
4.6.1 The effect of natural exposure conditions on carbonation rate 157
4.6.2 The effect of w/b ratio and binder type on carbonation rate 159
4.6.3 Effect of initial moist curing duration on carbonation rate 160
4.7 Relationship between Carbonation Rate and Permeability 163
4.8 Corrosion Propagation Test Results, Analyses and Discussion 166
4.8.1 Reinforcement corrosion current density 166
4.8.2 Steel corrosion radius loss required for cover cracking 170
4.8.3 Reinforcement corrosion rate 173
4.8.4 Corrosion Cover Cracking Time 177
4.9 Conclusion 180
4.10 Specific Conclusion 183
CHAPTER 5 186
5 DEVELOPMENT OF SERVICE LIFE MODELS 186
5.1 Introduction 186
5.2 Statistical Modelling.....186
5.3 Carbonation-Induced Corrosion Initiation Model 187
5.3.1 Carbonation rate prediction model.....188

5.3.2 Carbonation depth prediction model 193
5.3.3 Time to corrosion initiation prediction model 193
5.4 Comparison with some Existing Models 197
5.4.1 Summary 201
5.5 Modelling the Propagation Phase of Carbonation-Induced Corrosion 202
5.5.1 Predicting corrosion steel radius loss required for cracking 203
5.6 Graphical Representation of the Proposed Steel Radius loss Model 205
5.7 Evaluation of the Proposed Cover Cracking model 207
5.8 Summary 210
CHAPTER 6 212
6 CONCLUSION AND RECOMMENDATIONS 212
6.1 Introduction 212
6.2 Effect of concrete quality on the concrete early-age characteristics and carbonation-induced steel corrosion 213
6.3 Effect of concrete cover depth on carbonation-induced corrosion 215
6.4 Empirical Carbonation-induced Corrosion Initiation Model 217
6.5 Empirical Carbonation-induced Corrosion cracking Model 219
6.6 Practical Implications and Limitations of the Models 220
6.7 Contributions to Knowledge 221
6.8 Recommendations for Further Research 222
7 REFERENCES 224
APPENDICES 241
Appendix A: Experimental data and preliminary results 241
Appendix B: Experimental results: Durability index (OPI and WSI) 243
Appendix C: Experimental results - Carbonation test results 244
Appendix D: Experimental results - Concretes corrosion propagation data 254

Appendix E: Regression analysis output – Carbonation rates 260

Appendix F: Regression analysis output – corrosion propagation.....262

Appendix G: Derivation of a multiplying factor (11.6) for converting corrosion current density ($\mu A/cm^2$) to corrosion rate (μm/year).....263

Appendix H: Regression analysis outputs in a CD 264

LIST OF FIGURES

FIGURES Page

Figure 1:1 Corrosion service life of RC structure....25

Figure 1:2 Corrosion service life showing different stages of propagation (Busba, 2013)....26

Figure 1:3 Map of South Africa showing the current study area (Google Map) 28

Figure 2:1 Corrosion process in concrete 41

Figure 2:2 Simplified Poubaix diagram for iron in water (Sohail, 2013)....44

Figure 2:3 Annual mean CO_2 at Mauna Loa, Hawaii (Fitzpatrick, 2014)....48

Figure 2:4 Average monthly CO_2 variations for the exposure sites (Alhassan, 2014)....48

Figure 2:5 Effect of carbon dioxide concentration on the carbonation depth of the concrete (Papadakis and Vayenas, 1991) 49

Figure 2:6 Effect of percentage replacement of PC with SCM on carbonation depth of concretes (Papadakis, Fardis and Vayenas, 1992) 53

Figure 2:7 Effect of w/c ratio on carbonation depth of concrete 54

Figure 2:8 Effect of a/c ratio on carbonation depth of concretes....55

Figure 2:9 Effect of relative humidity on corrosion rate (Tuutti, 1982)....75

Figure 2:10 Effect of temperature on corrosion rate (Tuutti 1982) 75

Figure 2:11 Corrosion current as a function of outdoor Temperature and RH (Soroka, 2003) 76

Figure 2:12 Photograph of four-probe Wenner's method for resistivity measurement (Photograph adapted from Proceq Resipod users manual)....84

Figure 2:13 Corrosion-induced cover cracking in concrete (a) cracking mechanism (b) cracking modes 86

Figure 2:14 Corrosion-induced cracking - a thick-walled cylinder approach (Jamali *et al*., 2013)....97

Figure 3:1 Indoor exposure site 114

Figure 3:2 Sheltered exposure site....114

Figure 3:3 Outdoor unsheltered exposure site 114

Figure 3:4 Aggregates particle size distribution 117

Figure 3:5 Cross-section of a reinforced concrete prism 118

Figure 3:6 Photograph of the wooden moulds....121

Figure 3:7 Schematic diagram of a pre-conditioned typical reinforcing steel bar....121

Figure 3:8 Accelerated carbonation chamber 124

Figure 3:9 Pre-carbonated RC specimens exposed to natural unsheltered inland environment.....126

Figure 3:10 Oxygen permeability test set up rig (SANS 3001-CO3-2, 2015). ..128

Figure 3:11 Schematic diagram of water sorptivity test adapted from Otieno (2008) 129

Figure 3:12 Photograph of Coulostat corrosion rate measurement set-up.....133

Figure 3:13 Photograph of Coulostat corrosion rate meter showing the underneath electrodes 133

Figure 3:14 Schematic measurement diagram of Coulostat corrosion rate meter.....133

Figure 3:15 A typical Coulostat V3 input and data analysis page.....135

Figure 3:16 A typical result summary page for corrosion rate measurement.....136

Figure 3:17 A typical result plots of corrosion current density 137

Figure 3:18 Photograph of split reinforced concrete prisms showing the corroding reinforcements 138

Figure 3:19 A schematic representation of a corroded reinforcing steel cross-section (homogeneous corrosion).....139

Figure 4:1 28-day OPI results (error bars represents $\mu \pm (\sigma / n^{0.5})$)146

Figure 4:2 28-day water sorptivity (WSI) results (error bars represents $\mu \pm (\sigma / n^{0.5})$) 149

Figure 4:3 28-day compressive strength results (error bars - $\mu \pm (\sigma / n^{0.5})$ 151

Figure 4:4 Carbonation depth versus exposure time – Indoor exposure 152

Figure 4:5 Carbonation rate versus water/binder ratio, binder type and exposure conditions for the concretes initially moist cured for seven days ...155

Figure 4:6 Carbonation rate versus water/binder ratio, binder type and exposure conditions for the concretes initially moist cured for 28 days 156

Figure 4:7 (a) Indoor carbonation rate (K_{i7}) versus outdoor sheltered carbonation rate (K_{s7}) (b) Indoor carbonation rate (K_{i7}) vs outdoor unsheltered carbonation rate (K_{u7}) (c) Outdoor sheltered (K_{s7}) vs outdoor unsheltered (K_{u7}) 157

Figure 4:8 (a) Indoor carbonation rate (K_{i28}) versus outdoor sheltered carbonation rate (K_{s28}) (b) Indoor carbonation rate (K_{i28}) vs outdoor unsheltered carbonation rate (K_{u28}) (c) Outdoor sheltered (K_{s28}) vs outdoor unsheltered (K_{u28}).....158

Figure 4:9 (a) Indoor carbonation rate (K_{i7}) vs indoor carbonation rate (K_{i28}) (b) sheltered carbonation rate (K_{s7}) vs sheltered carbonation rate (K_{s28}) (c) Outdoor unsheltered (K_{u7}) vs outdoor unsheltered (K_{u28}).....161

Figure 4:10 Relationship between K_i (indoor exposure carbonation rate) and OPI 164

Figure 4:11 Relationship between K_s (sheltered exposure carbonation rate) and OPI 164

Figure 4:12 Relationship between K_u (unsheltered exposure carbonation rate) and OPI 165

Figure 4:13 Corrosion current density results (PC concretes) 167

Figure 4:14 Corrosion current density results (PC-FA concretes) 167

Figure 4:15 Corrosion current density results (PC-BS concretes).....168

Figure 4:16 Average corrosion current density results 168

Figure 4:17 Average steel radius loss required to initiate cover concrete cracking 170

Figure 4:18 Average steel radius loss versus cover depths (a) 0.95 w/b ratio (b) 0.60 w/b ratio.....173

Figure 4:19 Measured Average corrosion rate results 174

Figure 4:20 Average corrosion rate versus cover depth (a) 0.95 w/b ratio (b) 0.60 w/b ratio.....175

Figure 4:21 Comparison between the I_{RP} and I_{ML} 176

Figure 4:22 Pre-carbonated concretes with visible cracks along the line of reinforcement after exposure to unsheltered inland environment ...177

Figure 4:23 Observed average cracking time 178

Figure 4:24 Average cover cracking time versus cover depth (a) 0.95 w/b (b) 0.60 w/b 179

Figure 5:1 Measured values versus estimated values of K_c (mm/year$^{0.5}$).....192

Figure 5:2 Predicted time to corrosion initiation (t_i) vs concrete cover depth..195

Figure 5:3 Predicted time to corrosion initiation vs concrete quality (OPI).....196

Figure 5:4 Effect of binder type on the predicted time to corrosion initiation .197

Figure 5:5 Effect of initial curing duration on the predicted time to corrosion initiation 197

Figure 5:6 Comparison of the RILEM's, Alhassan's and the proposed time to carbonation induced corrosion initiation (t_i) model 199

Figure 5:7 Comparison of the RILEM's, Alhassan's and the proposed time to carbonation induced corrosion initiation (t_i) models.....199

Figure 5:8 Comparison between the Alhassan's and proposed carbonation induced corrosion initiation time (t_i) model 201

Figure 5:9 Comparison between the predicted and measured corrosion amount required for cover cracking 205

Figure 5:10 Plot of the predicted steel radius loss versus Cover depths.....206

Figure 5:11 Plot of the predicted steel radius loss versus OPI 206
Figure 5:12 Comparison between the predicted radius loss and measured steel radius loss of slab specimens of Liu (1996).....210

LIST OF TABLES

TABLES Page

Table 1:1 South African inland environmental classes for carbonation-induced corrosion 27

Table 2:1 Binder coefficients (RILEM 14 1996) 71

Table 2:2 Environment coefficients (RILEM 14 1996) 71

Table 2:3 Air content coefficients (RILEM 14 1996) 71

Table 2:4 Probability for corrosion (ASTM C876: 1991) 80

Table 2:5 Relationship between resistivity and corrosion risk 85

Table 3:1 Percentage composition by mass of the binders as used in this study 112

Table 3:2 Concrete mix proportions of the concretes used for the characterisation and carbonation tests 115

Table 3:3 Concrete mix proportions of the concretes used in the corrosion test 116

Table 3:4 Reinforced concrete prism matrix for the corrosion propagation test 119

Table 3:5 Summary of the concrete specimens pre-conditioned for various tests 120

Table 4:1 Exposure conditions at concrete specimen exposure sites (±1400 hours) 144

Table 4:2 Percentage reduction in carbonation rate K_c (mm/year$^{0.5}$) due to extension of the initial curing period from 7 days to 28 days 162

Table 4:3 Percentage reduction in carbonation rate, K_c (mm/year$^{0.5}$) due to decrease in w/b ratio from 0.95 to 0.60 163

Table 4:4 Percentage reduction in carbonation rate, K_c (mm/year$^{0.5}$) due to decrease in w/b ratio from 0.60 to 0.40 163

Table 5:1 Characterisation of the input and output variables 190

Table 5:2 Dummy variable coding for the exposure conditions 190

Table 5:3 Dummy variable coding for the curing 190

Table 5:4 Regression coefficients and adjusted R^2 for Equation 5.4 191

Table 5:5 Selected corrosion initiation models and their input parameters 198

Table 5:6 Characterisation of the input and output variables 204

Table 5:7 Dummy variable coding for Binder type 204

Table 5:8 Input parameters for graphical representation of Equation 5.7 206

Table 5:9 Selected previous and proposed empirical steel radius loss models 209

Table 5:10 Experimental data for the slab specimens (Liu 1996).....210

LISTS OF SYMBOLS

c	cover depth
d	Reinforcement diameter
x	Depth of carbonation front
f_c	28-day compressive strength
f_t	28-day tensile strength
i_{cor}	Corrosion current density
k	Coefficient of permeability
K_c	Carbonation rate
K_7	Carbonation rate of concrete initially cured in water for 7 days
K_{28}	Carbonation rate of concrete initially cured in water for 28 days
K_i	Carbonation rate of indoor concrete
K_s	Carbonation rate of sheltered concretes
K_u	Carbonation rate of unsheltered
I_{ML}	Corrosion rate by linear polarisation resistance
I_{RP}	Corrosion rate by gravimetric steel mass loss
t_c	Corrosion cracking time
t_i	Corrosion initiation time
t_p	Corrosion propagation time
t_{sr}	Corrosion service life

CHAPTER 1

1 INTRODUCTION

1.1 Background

Concrete is a heterogeneous composite material consisting of binder, water, aggregates, and admixtures. In a hardened state, concrete produces different characteristics such as strength and durability which determines its service life. Service life is the period after construction during which concrete is able to fulfill specified requirements with an acceptable level of safety and serviceability (Heiyantuduwa and Alexander, 2009). It depends largely on the depth and the quality of the concrete cover zone (Beushausen *et al.*, 2016).

The desire of many concrete infrastructure owners is for their concrete to complete its specified service life without major repairs. However, most concrete structures fail to achieve the specified service life due to the influence of environmental conditions and material factors. Many concrete structures reach their specified service lives at a high cost of maintenance and repairs. Jones et al. (2000) attributed the short service life of most of the reinforced concrete (RC) structures to the inability of the owners/engineers to determine the durability potential of concrete in the environment. In the UK alone, about £20 billion of yearly expenditure has been spent on repairs and maintenance of RC structures (Jones *et al.*, 2000). In South Africa and many other parts of the world, a lot of money is spent annually on repairs and rehabilitation of existing concrete structures.

In recent times, it was discovered that the service environment of many RC structures is harsher than the exposure conditions for which they were designed. This has resulted in early deterioration of these structures (Ahmad, 2003; Song & Saraswathy, 2007). The cause and the process of premature deterioration in concrete have been reported in the literature to be complex and depending directly on physical, chemical and environmental factors (Visser, 2012); Jones et al., 2000). The present day concrete construction which is characterized by the use of many different binders, innovative designs and construction for sustainable development presents engineering challenges to most existing and new concrete structures. It is pertinent to note that many of the current RC structures have shown severe

serviceability failures due to lack of durability at ages considerably less than their design service life. These have initiated several investigations into factors that influence concrete early deterioration.

One of the principal causes of the concrete early deterioration is corrosion of steel reinforcement, and this is caused by the chemical effect of the external aggressive agents such as air carbon dioxide (CO_2), oxygen (O_2), chlorides (Cl^-) and sulphates (SO_4) (Zhou *et al.*, 2014). The severity of the attack by these external aggressive agents depends on the exposure conditions (temperature, relative humidity (RH), nature and concentration of the aggressive agents at the exposure location) of the RC structure, concrete quality, and cover depth.

South Africa is ranked the 12th largest generator of CO_2 in the world (South Africa Department of National Treasury, 2010). The vast majority of South Africa's CO_2 emissions are produced by the electricity sector, steel, and transport industries. Given the developing nature of the South African economy, it is expected that the emissions will increase as development goals are pursued. This is expected to have a considerable effect in reducing the service life of RC structures.

Coastal RC structures (structures located less than 15 kilometres from the Sea) are primarily prone to the chloride attack. Inland RC structures (structures located more than 50 kilometres away from the Sea coast) are mainly prone to the CO_2 attack (carbonation) while buried structures can be at risk of sulphate or chloride attack (Haque, Al-Khaiat and John, 2007). However, the primary focus in this study is CO_2 initiated deterioration in concrete located in the South African inland environment, and one of the final results of early deterioration is cracking of the cover concrete caused by the expansive force of the corroding reinforcing steel. Concrete deterioration impairs not only the physical appearance of the structure but also its durability, strength and hence safety (Apostolopoulos and Papadakis, 2008).

There have been some attempts to study carbonation-induced reinforcement corrosion damage in RC structures. These studies have developed into various models that can be used to predict the onset and propagation of deterioration. However, many of these models are not explicit enough to explain the complex interaction between the various factors that cause carbonation-induced concrete

failures. Therefore, such models may not be useful to predict the onset of concrete deterioration. To develop a model that will be useful in predicting the service life of RC structures in the natural inland environment, an in-depth understanding of the factors that affect the deterioration process at the initiation and propagation stages is important. A service life model will afford RC design engineers a useful tool in optimising the economy of a building project in the long term. Also, in respect of the total cost, the durability factors offer a better understanding of service life and real economic benefits.

1.1.1 Corrosion-induced service life models

The different mathematical or empirical models for predicting reinforcement corrosion proposed by various authors are based on the conceptual model initially introduced by Tuutti (1982), where corrosion service life is idealized as a two-stage process (Figure 1.1).

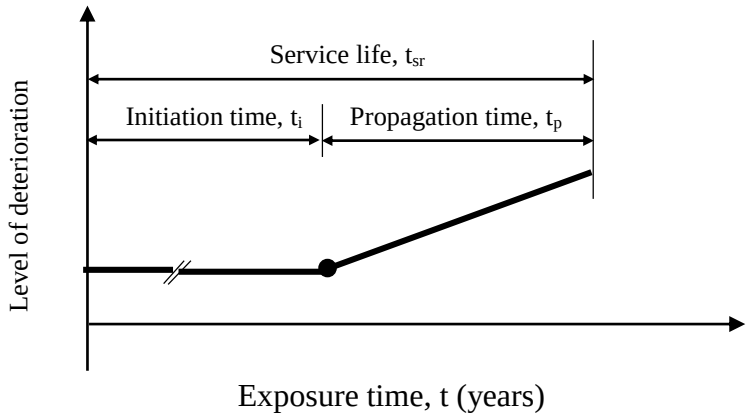

Figure 1:1 Corrosion service life of RC structure

The first stage is the initiation period, t_i (years) during which CO_2 progresses in a time-dependent manner into the depth at which it encounters the reinforcement in concrete. This stage is followed by the propagation period, t_p (years) in which corrosion progresses to the time at which unacceptable damage is visible on the concrete. The addition of the two periods represents concrete service life, t_{sr} (years) which is usually expressed as:

$$t_{sr} = t_i + t_p \quad 1.1$$

As shown in Figure 1.1 and Equation 1.1, Tuutti's service life model gives fundamental insights into corrosion process in reinforced concrete and is favoured by most researchers due to its practicality and simplicity in its approach (Ahmad, 2003; El Maaddawy and Soudki, 2007). However, it presents a generalized corrosion propagation period which does not show the different stages of corrosion-induced damage in the propagation phase. To account for corrosion's different stages in concrete, Busba (2013) sub-divided the corrosion propagation phase into sub-phases as shown in Figure 1.2.

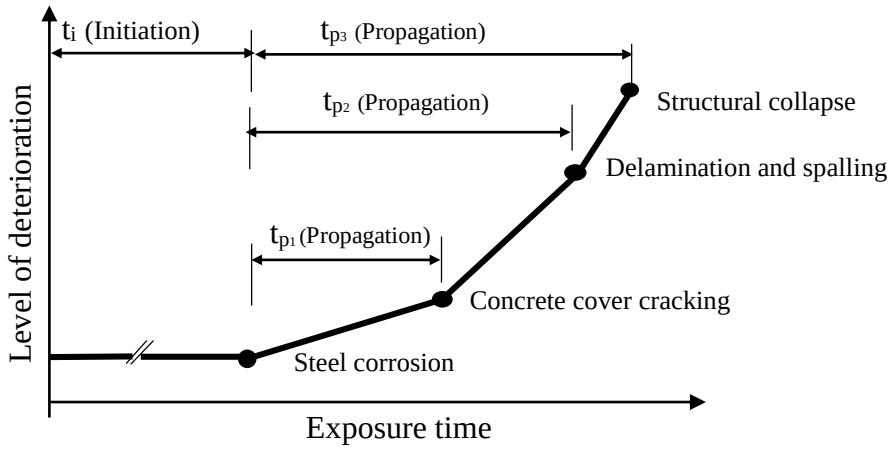

Figure 1:2 Corrosion service life showing different stages of propagation (Busba, 2013)

The diagram in Figure 1.2 shows the boundaries between these sub-phases and can be defined by different limit states such as:

- Appearance of surface corrosion-induced cracks (El Maaddawy and Soudki, 2007)
- Loss of concrete-steel interface bond - spalling and delamination (Busba, 2013)
- Reduction of member's ultimate load capacity – structural collapse (Apostolopoulos & Papadakis, 2008).

The approach to service life design presented in Figure 1.2 is preferable to Tuutti's model because it offers a selection of different limit states for a service life design. This approach makes it possible to compare and evaluate alternative solutions objectively plan for maintenance and repair of RC structures (Otieno, 2014). In this study, the appearance of a first visible crack on the surface of the concrete cover is considered as the limit state of the concrete deterioration. The appearance of a first visible crack on the surface of the concrete cover is considered in this study as the end of RC service life based on the fact that the appearance of visible crack impairs the aesthetic of the structure. It also allows other aggressive agents into the concrete resulting in a further deterioration (Alonso, Andradel and Diez, 1998). Also, repairing RC structure at this stage will reduce the total maintenance cost.

1.1.2 Classification of South African inland environment

As mentioned earlier, carbonation-induced corrosion is one of the main causes of early deterioration in RC structures located in the inland environment. With respect to carbonation-induced reinforcement corrosion in concrete, the inland environment is usually classified into 4 classes depending on the severity of carbonation-induced damage on concrete over a given time. The classification adopted in this study is that of BS EN 206-1: 2006 replicated in Table 1.1. The environmental classifications have been considered suitable for natural South African inland conditions (Ballim, Alexander and Beushausen, 2009).

Table 1:1 South African inland environmental classes for carbonation-induced corrosion

EN 206-1 classifications	Description of concrete environment
XC1	Permanently dry or permanently wet
XC2	Wet, rarely dry
XC3	Moderately humidity (60-80%) - (exterior concrete sheltered from rain)
XC4	Cyclic wet and dry

This study focuses on three exposure classes for the corrosion initiation part - XC1 representing indoor exposure, XC3 representing the outdoor sheltered exposure and XC4 representing outdoor unsheltered exposure (Table 1.1). The corrosion propagation part of the study focuses on XC4 representing the unsheltered exposure. This is mainly because the unsheltered environment is considered the most common aggressive inland environment regarding carbonation-induced reinforcement corrosion in concrete (Ballim and Lampacher, 1996; Alexander, Mackechnie and Yam, 2007). The South African inland environment referred to in this study is represented by Johannesburg area as indicated in Figure 1.2.

Figure 1:3 Map of South Africa showing the current study area (Google Map)

1.1.3 Durability Design of RC Structures

Concrete durability is the capability of maintaining the serviceability of a concrete structure over a specified time (Pommersheim and Clifton, 2010). In an environment, a more durable concrete is generally agreed to have a longer service life while a less durable concrete is expected to have a shorter service life (Rostam, 2000). The present national building and design standards, for example, SANS

10100-2000 do not usually require the estimation of service life. The durability of the concrete structure is ensured through requirements on strength grade, fluid transport properties, exposure conditions, and cover concrete geometry (cover depth and reinforcing steel diameter). Satisfying these requirements is assumed to guarantee adequate service life, even though their exact effects and quantification of their effects on service life are not yet well known and explored (Vesikari, 1988).

In the durability design of RC structure, the time factor is taken into account only when mathematical service life models are available, with the help of which the influence of various factors on the service life of the concrete structure can be estimated. Thus, factors such as local concrete material properties, cover concrete geometry, and exposure environment become part of real durability design parameters and solutions deviating from the minimum requirements specified in national building codes and standards can be arrived at.

One of the main parameters that quantify durability of concrete is its quality. It can be defined as the ability of concrete to satisfy the durability requirements which may be resistance to the fluid movement within the cover of hardened concrete. The quality of concrete controls most of the concrete properties and service life. Higher quality means a more durable concrete while a lower concrete quality means a lesser durable concrete (Tuutti, 1982). Therefore, in developing a model to predict service life, a measurable parameter must be used to quantify the concrete quality. The parameters quantifying the quality of concrete should preferably be such that they can be determined afterward from the hardened concrete since most of the early deteriorations occur in the hardened state of concrete. The test methods to assess the concrete quality must be reliable, fast and not too expensive (Beushausen and Alexander, 2008; Vessikari, 1988).

In the context of this study, the 28-day oxygen permeability index (OPI) and water sorptivity index (WSI) tests are used to assess the quality of various concretes for a service life modelling. The oxygen permeability of concrete is defined as a property characterising the ease by which oxygen gas subjected to a known pressure passes through the concrete (Bjegovic *et al.*, 2016). The water sorptivity of concrete is a property characterising the ease by which water under the action of capillary forces

moves through the concrete. Both properties depend on the concrete properties (e.g. water/binder ratio, porosity, narrowness and tortuosity of the pores, etc.). The OPI and WSI are widely accepted as durability related properties of concrete (Torrent *et al.*, 2016).

1.2 Research Motivation and Significance

Several models have been developed from laboratory as well as field investigations to predict the initiation and propagation phases of carbonation-induced corrosion of RC structures. It is important to note that many of these models purport to forecast a total service life, but their critical assessment suggests that only initiation or propagation part of the service life is predicted. Ignoring either the initiation or propagation phase of corrosion may incorporate conservatisms and reducing the safety margin of the model.

Corrosion initiation results in the literature (Alhassan, 2014; Ballim, 2009; Dhir, Hewlettt and Chanz, 1989; Salvoldi, Beushausen and Alexander, 2015) show the presence of a strong correlation between carbonation (chemical reaction between CO_2 and concrete alkaline content) and fluid transport properties of concrete. But hardly any model has managed to develop a universal relationship between carbonation and fluid transport properties of concrete for a service life prediction. Some of the existing models developed from a particular set of data in a specific environment usually overestimate or underestimate the service life of RC structures located in a different environment (Ikotun and Ekolu, 2012). This indicates an underlying complexity in attempting to determine an empirical function capable of adequately capturing the key parameters affecting corrosion activity in RC structures in an environment.

Corrosion of reinforcing steel produces expansive material with a bigger volume compared to the original steel. Due to the volumetric expansion of this material, the capillary pores are filled with corrosion products which exert pressure on the surrounding concrete causing cracking and spalling of the cover concrete (Ahmad, 2003; Zhou *et al.*, 2014). This suggests that the knowledge of corrosion amount

needed to initiate the first crack at the cover concrete when exposed to corrosive environment and rate of corrosion production are essential in service life modelling.

It is a common belief that corrosion in the inland environment of South Africa is insignificant compared to its coastal environment due to the inland's moisture condition. However, the presence of cracks along the line of reinforcement on some of the RC structures located in the inland environment shows the evidence of reinforcing steel corrosion (Ananmalay, 1996; Ballim and Lampacher, 1996). Therefore, it is important to investigate carbonation-induced steel corrosion in the inland environment, with the influencing factors. Such influencing factors should include concrete durability property, exposure conditions, cover depth, reinforcing steel diameter and the rate at which carbonated concrete corrodes when exposed to the environment.

Corrosion mechanism has been extensively studied in the past. This has allowed research into model development for many applications. It is noted that most of these attempts have taken place in the North America and Europe, suiting their exposure conditions and binder systems. Little or no published information is available for inland exposure conditions of South Africa. This implies the necessity of research into the performance of concrete structures vis-à-vis corrosion in the inland environment of South Africa. Such research would facilitate the prediction of RC service life under inland exposure conditions.

There have been significant improvements in the application of concrete as a construction material. This arises from improved design procedures, better quality of cement and greater understanding of engineering performance of the material. Also, new techniques that reduce construction time are now emerging. The use of industrial waste materials such as metakaolin (MK), blast furnace slag (BS), fly ash (FA) and silica fume (SF) are now common in concrete applications (Ballim & Alexander, 2005). These developments make concrete more resistant to early deterioration caused by the aggressive agents. However, the use of these materials in arresting carbonation-induced reinforcement corrosion has not been successful due to a reduction in alkalinity of the carbonated concrete. Hence, the need for a

performance based carbonation-induced corrosion service life model for inland RC structures.

In developing a model that can predict corrosion service life, it is essential to first examine the accuracy and suitability of a corrosion service life model that will account for the governing parameters that are relevant to the local environment and concrete material properties. Concrete material properties should be those that are related to near-surface concrete where corrosion deterioration occurs. This rules out the inclusion of strength related properties of concrete as part of the main parameter in a corrosion service life model. However, strength can be used to grade concrete into different classes as used in many concrete codes.

A useful model is expected to be practically simple to execute, easily understood and should utilize readily available or easily obtainable data (Ikotun and Ekolu, 2012). It thus becomes necessary to consider the exposure conditions (relative humidity-RH, temperature, and CO_2), reinforcing steel diameter, thickness and quality of cover concrete as part of the governing parameters for a useful model that can adequately predict carbonation-induced corrosion service life.

1.3 Research Aims and Objectives

The research aims at developing performance-based carbonation-induced steel corrosion initiation and propagation prediction models for RC structures in the natural inland environment. The purpose of the models will be (i) to predict time to carbonation-induced corrosion initiation of reinforcement in concrete exposed to the natural inland environment and (ii) to predict the steel radius loss required to initiate a first visible crack in RC structure exposed to the unsheltered inland environment. The aim will be achieved through these specific objectives:

(i) to explore and quantify the transport mechanisms of fluid substances (CO_2, oxygen, and moisture) in concretes;

(ii) to understand the carbonation-induced corrosion initiation and propagation processes in RC structures exposed to the natural inland environment;

(iii) to quantify from durability point of view the time to corrosion initiation in concretes exposed to inland natural environment, and the amount of steel radius loss required to initiate a first visible crack in RC structures when exposed to the unsheltered inland natural environment

1.4 Research Conceptual Framework

The research work was undertaken at the School of Civil and Environmental Engineering, University of the Witwatersrand, Johannesburg, South Africa. The research project was initiated with an extensive literature review on topics related to carbonation-induced concrete deterioration, the model for predicting periods of corrosion deterioration and RC service life.

The experimental work was carried out in 3 phases as follow:

Phase 1- concrete early-age characterisation

Phase 2- corrosion initiation in the concretes

Phase 3- corrosion propagation and cracking of the pre-carbonated concretes.

The three phases produced the results which were used to generate data to develop an empirical carbonation-induced corrosion model for RC structure in the South African natural inland environment.

1.5 Thesis Outline

This thesis is divided into six chapters. The 1st Chapter, the introduction gives a brief framing of the whole thesis. It includes a background of corrosion deterioration in concrete, the motivation and significance of the research, the objectives and conceptual framework of the research.

The 2nd Chapter contains a literature review that focusses on concrete compositions and effect of it on durability. The carbonation-induced corrosion as one of the primary sources of concrete early deterioration in the natural inland environment was discussed in two parts – corrosion initiation and propagation. Corrosion mechanisms and several factors influencing corrosion initiation and propagation in

concrete are highlighted and discussed. Some of the existing models used to predict carbonation-induced corrosion process in concrete are critically reviewed.

The 3rd Chapter describes the experimental investigation. It shows the test procedures of obtaining data used in modelling the two periods of corrosion that define the concrete service life in the natural inland environment.

The 4th Chapter presents the results, analyses, and discussion of the experimental investigations carried out in Chapter 3. The various factors influencing both stages of carbonation induced corrosion in the inland environment of South Africa are discussed. Functional relationships among the variables are established and defined.

The 5th Chapter presents the application of the established functional relationships derived in Chapter 4 to model the corrosion initiation period in concrete as well as the amount of radius loss required to initiate a first visible crack in the concrete. The chapter also includes the models' practical application, accuracy, and evaluation.

The 6th Chapter gives the general conclusion of the chapters and the overall summary of the thesis. It also presents practical implications and limitations of the proposed corrosion models. It recommends further studies

The Appendix contains both Tables and Figures that are not included in the chapters and are not necessary for the adequate appreciation of the Chapter contents. However, they are necessary expansions of the chapter contents.

CHAPTER 2

2 LITERATURE REVIEW

2.1 Introduction

The literature review is presented in this chapter, and it is organised as follows:

- Concrete composition and its effect on concrete durability
- Mechanism of reinforcement corrosion
- Carbonation process and assessment techniques
- Carbonation-induced corrosion initiation
- Carbonation-induced corrosion propagation and assessment techniques
- Damage effects of carbonation-induced corrosion on RC structure
- Existing models for the prediction carbonation-induced corrosion initiation and propagation periods in RC structures.
- Summary of the findings.

2.2 Concrete Composition and Durability

Concrete is a composite material made up of aggregates, a cement, admixture and mixing water. It becomes a multi-phase material when the cement hydrates. The hydrated cement consists of a binder phase, filler phase and interfacial transition zone (ITZ). The binder phase is known as hardened cement paste (hcp), which is made up of a solid phase (calcium silicate hydrates – CSH, calcium hydroxide – CH, calcium sulphoaluminate – CASH and unhydrated clinker grains); voids (interlayer space in C-S-H, capillary and air voids) and water phase - capillary water, adsorbed water, interlayer and chemically combined water (Mehta, 1993). The filler phase consists of the coarse and fine aggregates, while the ITZ is the space between the bulk cement paste and aggregates. The ITZ is composed of the same elements as the hcp but its microstructure and properties are different. It is the weakest and more permeable zone between the binder phase and filler phase (Garboczi and Bentz, 1996).

The deterioration of concrete and its long-term durability performance is dependent on the structure and composition of the hcp and ITZ (Ballim, Alexander and

Beushausen, 2009). Moreover, the ability of concrete to protect embedded reinforcing steel and withstand various forms of degradation mechanisms depends on the structure and compositions of the hcp and ITZ. The hcp and ITZ are also responsible for the concrete fluid transport and chemical properties (Ballim, Alexander and Beushausen, 2009). The influence of hcp and ITZ on durability performance of concrete is discussed in the next section (section 2.2.1).

2.2.1 Influence of concrete composition on its durability

Carbonation is a primary factor in reinforcing steel corrosion in the inland environment (Ahmad 2003). This is a chemical reaction that occurs when atmospheric CO_2 comes into contact with calcium hydroxide present in the concrete pore structure of hardened cement paste (Ballim et al. 2009). The carbonation reaction is influenced by the proportion and properties of the binder phase in concrete (hcp and ITZ). The properties of the binder phase in concrete depend on its microstructure (the type, amount, distribution of solid and voids in the hcp as well as ITZ). The size and continuity of pores in the hcp and ITZ in concrete determine its fluid transport and strength properties to a large extent. Fluid transport properties and strength are closely related to the capillary porosity and the solid-space ratio (Ballim, Alexander and Beushausen, 2009; Naik 1997).

The capillary pores and their degree of interconnectivity as well as entrapped air influence the pore structure of the concrete, while the composition of the solid phase in the hcp and ITZ determine the concrete interaction (Mehta, 1993). Fluids can flow more easily through large capillary pores and air voids compared to gel pores found in the solid phases (Naik, 1997). The capillary pores and air voids present in the concrete reduce the mechanical strength of the concrete. Naik (1997) attributed this to the stress concentration effects due to the fluid and ion movements in the large capillary pores. Thus, the presence of large capillary pores and air voids is detrimental to both permeability and strength of concrete.

In determining the resistance to carbonation-induced corrosion of reinforcement, not only the size and interconnectivity of the capillary pores should be considered but also the composition of the CSH and CH that exist in the hcp and ITZ (Alhassan

2014). The microstructure of concrete determines its resistance to aggressive compounds thereby making the fluid transport properties increasingly important (Neville, 2011). Most deterioration mechanisms involve the movement of gases, liquid, and ions through the concrete pore structure. Hence the fluid transport property of concrete is an important determinant of its ability to resist deterioration (Mehta 1993; Alhassan 2014).

The durability performance of concrete exposed to a given aggressive environment is also influenced by the chemical interaction between the constituents of the hcp and the aggressive agents (i.e., CO_2, Cl^-, O_2, and H_2O). The chemical composition of concrete which is derived from the thermodynamic stability of its hydrates determines its resistance to aggressive agents in the environment (Mehta, 1993). Similarly, the nature of aggressive agent with the paste component of concrete also contributes to its resistance. This it does by blocking the capillary pores with the chemical reaction products thereby reducing further intake of the aggressive agents. The composition of hcp influences the concrete chemistry and can be responsible for the chemical protection of steel reinforcement (Mehta, 1993).

It is understood that the size and the amount of pores available in concrete as well as its chemical composition play important roles in concrete durability. Hence, fluid transport parameters (permeability, absorption, and diffusivity) are evaluated to ascertain the movement of aggressive substances through concrete pores. These transport mechanisms are briefly discussed under fluid transport property of concrete.

2.2.2 Fluid transport properties of concrete

Transport properties of concrete are important in predicting their durability since deterioration mechanisms such as chemical attack, chloride ingress, and carbonation, all relate to the ease with which a fluid or ions can move within the concrete microstructure (Ballim, Alexander and Beushausen, 2009). The transport characteristics of concrete are predominantly affected by the structure of hcp and ITZ (Mehta, 1993). The passage of potentially aggressive fluids is primarily influenced by the concrete penetrability which is described as the degree to which

the concrete permits gases, liquids or ionic species such as chlorides and sulphates to move through its pore structure. The transport property of concrete relates to the concepts of permeation, sorption, diffusion, and migration which are quantified in terms of the transport parameters (Alexander and Mindess, 2005).

The processes involved in fluid and ion movements include the distinct mechanisms of capillary action, flow under pressure and flow under a concentration gradient (Ballim, Alexander and Beushausen, 2009). The mechanisms are characterised by the material properties of permeability, sorptivity and diffusivity respectively (Ballim and Alexander, 2005; Alhassan, 2014). The transport mechanisms are important for assessing concrete deterioration processes and are discussed below.

Permeation: This is the movement of gases, liquids, and ions through a concrete pore structure under an externally applied pressure whilst the pores are saturated with that particular fluid or ion (Ballim, Alexander and Beushausen, 2009). Permeability is therefore a measure of the capacity for concrete to transfer fluid or ion by permeation and depends on the concrete microstructure, the moisture condition of concrete and the characteristics of the permeating gas, fluid and ion such as CO_2, H_2O, and Cl^- (Ballim, Alexander and Beushausen, 2009; Wong et al. 2006). Since permeability is a function of the concrete microstructure (size, amount, and connectivity between the pores), it can be used to assess concrete quality as well as predicting its resistance to carbonation and moisture penetration which is responsible for corrosion deterioration of concrete in the inland environment.

Absorption: This is the process whereby liquids and ions are drawn into a porous, unsaturated concrete by capillary suction (Wong, Buenfeld and Head, 2006). The capillary forces are dependent on the concrete pore geometry and its degree of saturation (Neville 2011; Alexander and Mindess, 2005). Water absorption caused by wetting and drying of the concrete surface is an important transport mechanism at the concrete near-surface. However, water absorption becomes less significant with depth. The rate of movement of a wetting front through the concrete pores under the action of capillary forces is defined as sorptivity. Sorptivity is influenced by the size of capillary pores and their degree of interconnectivity. These two attributes of sorptivity are directly affected by the hydration of the outer concrete

surface. Sorptivity is also influenced by the concrete mix proportion, initial moist curing age, aggregate orientation, and distribution (Kropp and Alexander, 2007).

Diffusion: This is the process by which liquid, gases and ions move through a concrete under a concentration gradient. Diffusion occurs in partially or fully saturated concrete and is an important internal transport process for most concrete structures exposed to chloride based salts such as located near the Ocean (Otieno, 2008). Concrete structures in the South Africa inland environment are not prone to chloride and sulphate attacks except the buried structures in contaminated soil with chloride or sulphate.

The major mechanism in the carbonation of concrete is the diffusion of CO_2 which is dependent on the concrete diffusivity. Fick's laws of diffusion are widely used to describe the carbonation depth which forms the basis for most of the prediction models. However, measuring CO_2 diffusion in concrete is usually a complex process and cannot be easily applied directly on the site. Hence, a measurable parameter such as permeability can be adequately applied on site and in the laboratory. It provides useful information with regards to durability and it is particularly sensitive to changes in the pore size and pore interconnectivity which can be used to quantify concrete quality in terms of concrete durability. Therefore, permeability can be used as governing parameter to quantify the service life of concrete exposed to inland environment.

2.2.3 Concrete durability indicators (DI)

Two of the durability indicators (DI), commonly used in the South africa inland environment to measure the quality of concrete are oxygen permeability index (OPI) representing permeation and water sorptivity index (WSI) representing absorption. They provide a qualitative measure of concrete resistance to fluid and ion transport in concrete (Beushausen and Alexander, 2009). The DI tests have been shown to be sensitive to construction quality and environmental factors that affect durability and they provide reproducible engineering measures of the concrete microstructure (Ballim and Alexander, 2005). The tests characterise the quality of concrete as affected by choice of concrete mix material and proportion, placing,

compaction, duration and curing techniques as well as the concrete environment (Alhassan 2014). The DI test equipment and procedures are described in detail in a research monograph published in South Africa by Alexander, Ballim and Mackechnie, (2007); SANS 3001-CO3: Part 1-3 (2015).

In a comparative international study of various test methods for durability indicators by Beushausen & Alexander (2008), OPI was found to detect changes in w/b ratio, binder type, and curing condition on a highly significant statistical level. The same study reveals that results obtained with South African oxygen permeability index test equipment correlate with other existing permeability test methods (Cembureau and the Torrent permeability).

Regarding the use of oxygen permeability index and water sorptivity index to assess concrete quality, a higher OPI value or a lower WSI represents a less permeable concrete which means that the quality of the concrete is relatively high. A lower OPI or a higher WSI means a more permeable concrete which depicts a low quality concrete. High quality concrete depicts that the concrete microstructure is relatively closely packed which retards the rate at which corrosion causing agents penetrate the concrete compared to a more permeable concrete.

Tuutti (1982) explained that more permeable (low quality) concretes are usually characterised with large and interconnected pores which easily permit fluid to pass through the concrete microstructure. Such concrete is referred to as lower quality concrete. Even though large and connected pores can act as storage void for corrosion products and can delay corrosion cracking in RC structures this attribute should not be desired in concrete as there is no early indication of corrosion and the steel reinforcement may be severely weakened before corrosion is detected. The severely impaired reinforcement can jeopardize the structural integrity of such RC structures.

2.3 Mechanism of Steel Corrosion in Concrete

Corrosion of steel is an electrochemical reaction that involves anode, cathode, and electrolyte through which the current flows. The surface of reinforcing steel in concrete acts as combined electrodes (anode and cathode) connected through the

body of steel (Figure 2.1). Concrete pore fluid functions as an electrolyte completing the electrochemical cell (Shetty, 2011). In a favourable corrosion environment oxidation and reduction reactions take place on the steel surface with the dissolution of iron ions at the anode and evolution of hydroxyl ions at the cathode expressed as:

Anode reaction: $Fe \rightarrow Fe^{2+} + 2e^{-}$ 2.1

Cathode reaction: $2e^{-} + H_2O + \frac{1}{2}O_2 \rightarrow 2(OH)^{-}$ 2.2

The hydroxyl ions OH^- migrate to the anodic site and electrically neutralises the Fe^{2+} ions in the concrete pore water to form a solution of ferrous hydroxide at the anode (Equation 2.3).

$Fe^{2+} + 2OH^{-} \rightarrow Fe(OH)_2$ 2.3

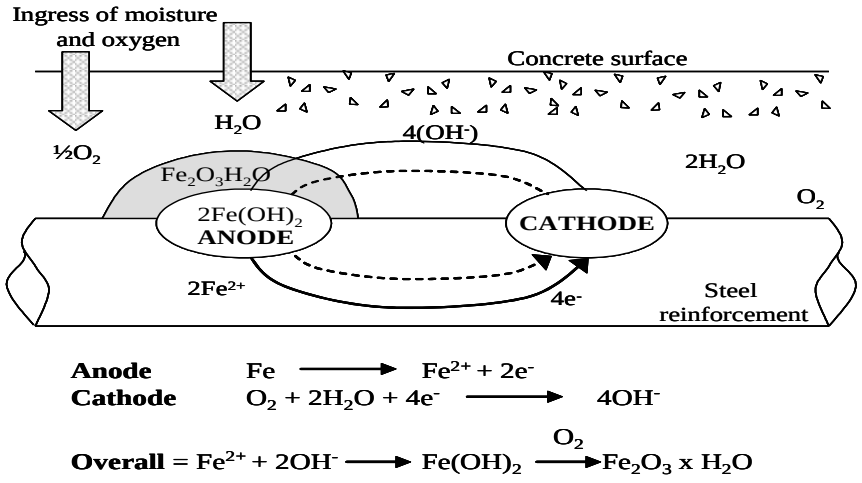

Figure 2:1 Corrosion process in concrete

Iron oxide (Fe_2O_3) further reacts with additional external hydroxide and oxygen to form the insoluble red corrosion products known as black corrosion (Fe_3O_4). Other ferric/ferrous oxides and hydroxides are also formed which are orange to red-brown in colour (Sohail, 2013). Chloride hydrates are also formed when chlorides are involved in the corrosion process (Shetty *et al.*, 2012; Parrott, 1987).

Unhydrated ferric oxide (Fe_2O_3) has a volume of about twice that of the original steel when it becomes hydrated it swells even more and becomes a porous layer at the steel-concrete interface (Jaffer and Hansson, 2009). At this stage, the volume is increased to about ten times the original steel at the steel-concrete interface (Nasser *et al.*, 2010). The increased volume of the hydrated iron generates a higher pressure that cracks and spalls the concrete cover when the tensile strength capacity of the concrete is exceeded (Sohail, 2013).

2.4 Thermodynamics of Corrosion

The progress of electrochemical reactions in concrete can be determined by chemical thermodynamics using Gibbs free energy (ΔG) of the chemical compounds involved or the electrochemical potential of the galvanic cell. The Gibbs free energy and electrochemical potential are related through the expression:

$$E = -\frac{\Delta G}{nF} \tag{2.4}$$

where E is electrochemical potential (V), ΔG is the free energy of reaction (J/mol), n is the number of electrons transferred during the electrochemical reaction and F is Faraday's constant (96487 *As/mol*). Therefore, Gibb's free energy or electrochemical potential of the galvanic cell can be used to determine the progress of corrosion in concrete. Electrochemical potential is a driving force that affects the rate of cathode and anode reactions. Anode electrode potentials (E_A) can be derived using the Nernst Equation as:

$$E_A = E^o{}_A + \frac{R_G T}{nF} In \frac{[Fe^{2+}]}{[Fe]} \tag{2.5}$$

where $E_A{}^0$ is standard electrode potential of steel at the anode, R_G is the gas constant, F is Faraday's constant (i.e., 96500 Coulomb per mole of electrons or Ampere-second), *'T'* is absolute temperature, and n is number of electrons taking part in the reaction.

Ahmad (2003) simplified the anode electrode potential (V) in terms of $[Fe^{2+}]$ as:

$$E_A = -0.44 + 0.00296 \log[Fe^{2+}] \tag{2.6}$$

where $[Fe^{2+}]$ is the concentration of Fe^{2+} in moles per liter of electrolytes, which is related to the mass concentration of $Fe(OH)_2$ per unit volume of concrete and amount of capillary pore water per unit volume of concrete. Similarly, referring to the cathodic reaction (Equation 2.2), the cathode electrode potential, E_c can be expressed by Nernst equation as:

$$E_C = E^o{}_C + \frac{R_G T}{nF} In \frac{[O_2][H_2 O]^2}{[OH^-]^4} \quad 2.7$$

where E_c^0 is standard electrode potential of steel at the cathode, *log* $[OH^-]$ = pH 14. The simplification of Equation 2.7 is obtained through substitution of standard values of the equation parameters; the full details can be found in Ahmad (2003). The simplified cathode electrode potential equation is given as:

$$E_c = 1.229 + 0.0148 \log[O_2] - 0.059\, pH \quad 2.8$$

where $[O_2]$ is the concentration of oxygen expressed in molarity and the amount of capillary pore water per volume of concrete.

The cell potential *'e'* of the corroding reinforcement involving anode and cathode reactions is expressed as:

$$e = E_c - E_A \quad 2.9$$

Substituting the Equations 2.6 and 2.8 into the Equation 2.9, gives an equation for cell potential *'e'* (*V*) (Equation 2.10) as:

$$e = 0.789 + 0.0148 \log[O_2] - 0.059\, pH - 0.0296 \log[Fe^{2+}] \quad 2.10$$

In a galvanic cell, the cell potential *'e'* drives the corrosion current through the electrolyte from the cathode to the anode. It is evident from Equation 2.10 that the corrosion current is affected mainly by the following factors (Ahmad, 2003):

- The pH of the electrolyte in concrete
- The availability of oxygen and capillary water
- The concentration of Fe^{2+} in concrete near the reinforcement

When the cell potential moves toward the positive values (i.e., $e > 0$), the anode reaction is stimulated, and the rate of cathode reaction decreases. The cathode reaction is stimulated when cell potential moves toward negative values (i.e., $e <$

0), this decreases the anode reaction. When *'e'* is zero the system is at equilibrium and the anodic and cathodic currents are equal to each other and no net current flows through the electrode (Sohail, 2013).

Nernst equation gives the instantaneous potential of an electrochemical cell which is related to the activities of the products and reactants as shown in anode and cathode potential equations. Nernst equation has been used to construct the potential-pH diagram (Figure 2.2) which indicates possible corrosion conditions. The diagram in Figure 2.2 is referred to as the Poubaix diagram and is based on equilibrium thermodynamics of corrosion (Sohail, 2013).

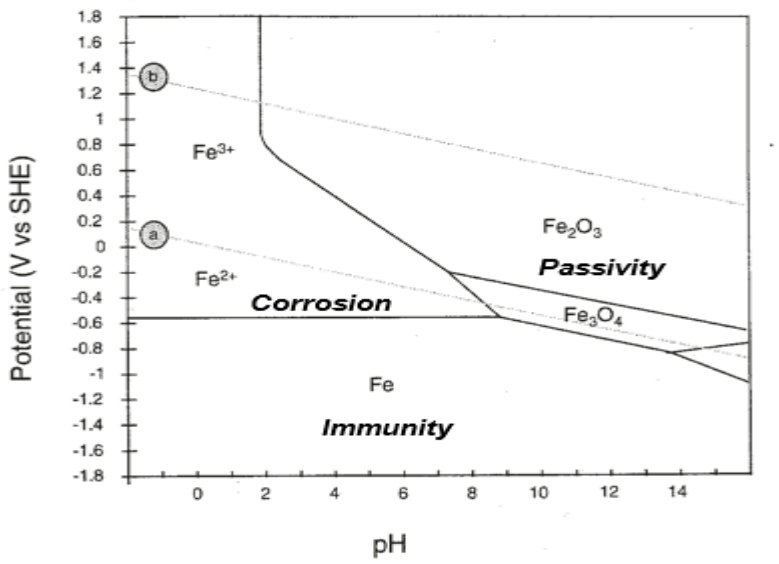

Figure 2:2 Simplified Poubaix diagram for iron in water (Sohail, 2013)

Poubaix diagram can be used to show at a glance the specific conditions of potential and pH under which the iron either reacts to form specific oxides or complex ions. Also, it determines the potential and pH domains in which a metal is stable (Sohail, 2013; Uhlig and Revie, 1985). Three regions can be identified in the Poubaix diagram as immunity, corrosion and passivity regions. In the immunity region, the steel is regarded as thermodynamically stable and is immune to corrosion. The region where the steel ions are thermodynamically stable with every possibility that corrosion will occur at a rate which cannot be predicted thermodynamically is

known as the corrosion region. In the passivity region, compounds of steel are thermodynamically stable. This region protects the steel from corrosion reactions at a higher pH in a process known as steel passivation. However, this protection by the passive film can be lost due to carbonation reaction when concrete pH falls below 9 depending on the steel potential. The process is known as "steel depassivation" and at this point of the reinforcing steel, corrosion is initiated.

Moreover, even though Poubaix diagram for reinforcing steel determines the potential and pH domains in which a metal is stable and immune to corrosion, it is a thermodynamic diagram that cannot indicate the rate at which the most stable state will be achieved.

2.5 Reinforcement corrosion initiation in concrete

Corrosion initiation in concrete is the process of continuous breakdown of the passive protective layer on the steel surface. It can be caused by several factors e.g ingress of chloride ions, carbon dioxide, stray electric currents and bacterial attack. In the inland environment, one of the main causes of reinforcing steel corrosion in concrete is carbonation. This chemical reaction takes place in concrete when gaseous carbon dioxide (CO_2) dissolves in the concrete pore solution to form carbonic acid (H_2CO_3) as shown in Equation 2.11 (Zhou *et al.*, 2014). The carbonic acid further reacts with the calcium hydroxide to precipitate mainly as calcium carbonate (Equation 2.12);

$$H_2O + CO_2 \rightarrow HCO_3 + H^+ \qquad 2.11$$

$$Ca(OH)_2 + 2H^+ + CO_3^{2-} \rightarrow CaCO_3 + 2H_2O \qquad 2.12$$

Carbonic acid can also penetrate into the pore structure of hardened cement paste (hcp) through CO_2 dissolved in rainwater. Calcium carbonate which is one of the carbonation reaction products is insoluble in pore solution with a higher volume than original reactants. It precipitates and blocks the concrete pores thereby reducing the porosity and permeability while it increases the compressive strength of the exposed concrete. This change is viewed as beneficial to strength and fluid transport properties of concrete (Chi, Huang and Yang, 2002; Song and Kwon,

2007; Czarnecki and Woyciechowski, 2015). However, this becomes a serious challenge to RC structures, especially when the advancing carbonation front (the narrow layer at which the carbonation reaction takes place) reaches the vicinity of the reinforcing steel.

One of the major effects of carbonation reaction in concrete is the depletion of the hydroxyl ions (OH^-) in the concrete pore solution. The depletion of the hydroxyl ions (OH^-) reduces the pH of the pore solution from above 12 to below 9.0 (Loo *et al.*, 1994; Zhou *et al.*, 2014). At this low pH, corrosion is initiated when the passive layer of gamma ferric oxide on the surface of the reinforcing steel breaks down (depassivates) and propagates in the presence of sufficient oxygen and moisture (Ballim and Lampacher, 1996).

The time taken for the carbonation front to reach the reinforcing steel and breakdown its passive layer, is known as time to corrosion initiation. The time to corrosion initiation depends on the rate at which the carbonation front advances in concrete and concrete cover thickness.

2.5.1 Concrete carbonation rate

Concrete carbonation rate is defined as the advancement of the carbonation front with time in concrete. It is influenced by exposure conditions (relative humidity-RH, temperature, and CO_2 concentration) and concrete composition (w/b ratio and binder type) which determines the fluid transport properties (permeation, absorption and diffusion) of the concrete. The duration of early-age curing, coating, and cracks in concrete have been reported to also have influence on concrete carbonation rate (Ballim, 1993; Hills *et al.*, 2015)

2.5.1.1 Effect of exposure environment on carbonation rate

RC exposure environment can be classified into mild, moderate and severe depending on the aggressiveness of the environment to carbonation reaction (Schiessl, 1988). However, under any of the exposure classes, a reinforced concrete structural member can be categorized into the following exposure types:

(i) Indoor exposure

(ii) Outdoor sheltered from rain

(iii) Outdoor unsheltered from rain

A considerable number of researches has been conducted on the effect of exposure conditions on the rate of carbonation and the general trend is that indoor concrete samples carbonate faster than outdoor concrete samples. The same concrete samples placed outdoor but sheltered from rain carbonate much quicker than samples exposed to rain (Hills *et al.*, 2015). Nischer (1984), investigated the carbonation rate of concretes exposed to both outdoor and indoor environments for three years and reported that the carbonation rate for the indoor concrete was higher compared to the outdoor concrete. Kokubu and Nagatakis (1989) found that carbonation of indoor exposure is about 2 times that of outdoor exposure.

The main quantifying variables that describe a given exposure environment are relative humidity (RH), carbon dioxide concentration, and temperature (T). The progress of carbonation has been observed by many researchers to be strongly affected by relative humidity in the concrete pores (influenced by ambient relative humidity), air temperature and carbon dioxide concentration in the atmosphere (Khunthongkeaw, Tangtermsirikul and Leelawat, 2006).

(a) Carbon dioxide (CO_2**) concentration**

Over the years, there has been an increase in global CO_2 concentrations in the atmosphere, which has been because of recent industrialisation especially using fossil fuel. The normal level of CO_2 in the air is approximately 0.035% (350 ppm). (Ballim and Lampacher, 1996; Khunthongkeaw, Tangtermsirikul and Leelawat, 2006). However, concentrations higher than 350 ppm (0.035%) have been recorded in some cities, a case in-point is Mauna Loa city in Hawaii where average CO_2 concentration growth is shown in Figure 2.3 (Fitzpatrick, 2014). This is not far from the average concentration of CO_2 found in the South African inland environment (Figure 2.4) as investigated by Alhassan (2014).

The increase in CO_2 concentration in urban areas over the years can be attributed to concentration of industrial activities in the urban areas; where human activities

(e.g., combustion of fossil fuel from traffic; domestic heating, power generation, etc (Stewart, Wang and Nguyen, 2011; Peng and Stewart, 2014)) cause most of the CO_2 emissions (Ballim and Lampacher, 1996). An approximately 20% of human-produced CO_2 is generated from heavy motor vehicle traffic which is a feature in most urban environments (Ballim & Lampacher, 1996). Peng & Stewart (2014) recorded CO_2 concentration of > 575 ppm near one of the street in Brno city (Czech Republic). This can have significant deteriorating effect on the RC structures especially those located in vicinities where motor vehicle traffic is high.

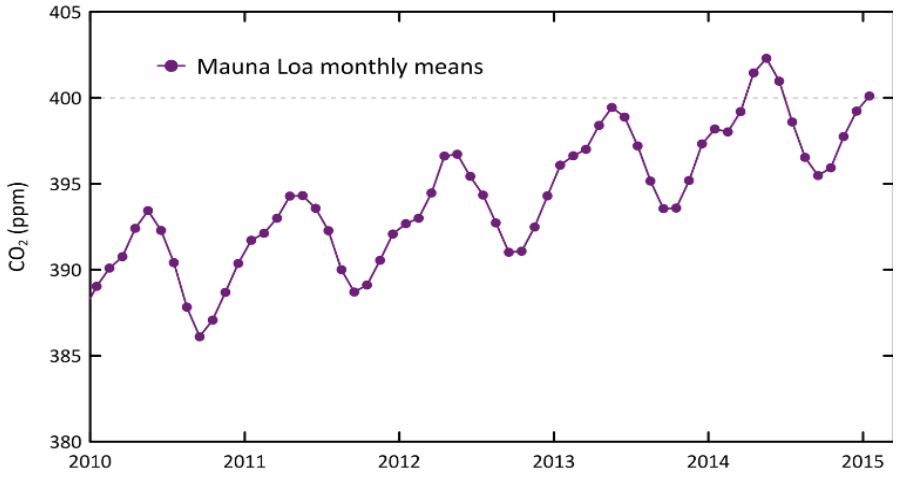

Figure 2:3 Annual mean CO_2 at Mauna Loa, Hawaii (Fitzpatrick, 2014)

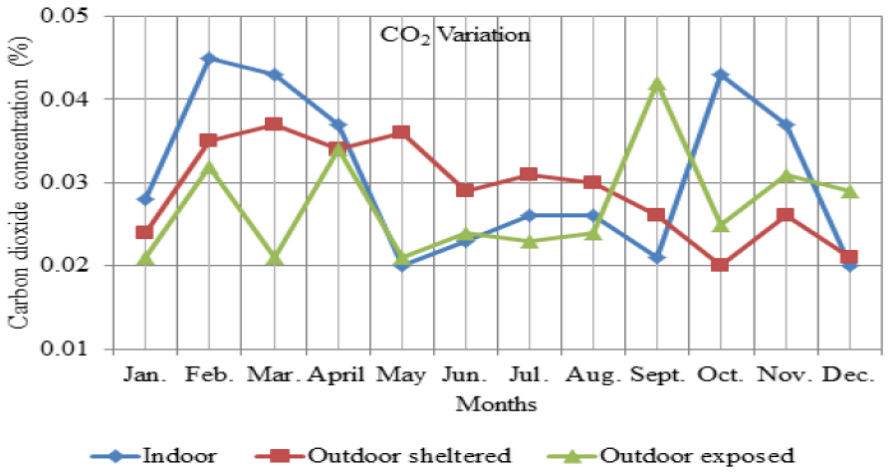

Figure 2:4 Average monthly CO_2 variations for the exposure sites (Alhassan, 2014)

Many studies (Loo *et al.*, 1994; Stewart, Wang and Nguyen, 2011; Peng and Stewart, 2014) have shown that the rate of carbonation increased with an increase in the concentration of CO_2. Papadakis, Fardis and Vayenas (1992) investigated the influence of CO_2 concentration on concrete carbonation, although this was in an accelerated experiment where CO_2 concentration was increased above normal concentration in the air. They found that at a given w/c ratio and RH, an increase in the concentration of CO_2 resulted in an increase in carbonation depth (Figure 2.5). A similar trend was also observed by other researchers (Thiery *et al.*, 2005; Borges *et al.*, 2010; Thiéry, Faure and Bouteloup, 2011).

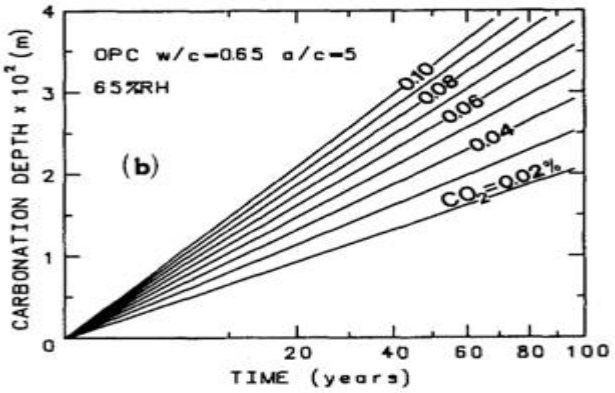

Figure 2:5 Effect of carbon dioxide concentration on the carbonation depth of the concrete (Papadakis and Vayenas, 1991)

The concentration of CO_2 is greater in the urban areas than the countryside due to increased industrial activities in the cities. Khunthongkeaw, Tangtermsirikul and Leelawat, (2006) found that CO_2 concentration in the city of Bangkok was twice that of the rural areas. This is not far from the level of urbanisation in Johannesburg city as a representative of the South Africa inland environment considering that both cities are capitals. This presents an opportunity of experimenting with RC structures exposed to the natural environment of Johannesburg city.

It is important to note that CO_2 concentration varies from one exposure to the other within the same locality. This was reported in an investigation conducted by Alhassan (2014) where Johannesburg area was categorised into two exposure sites (indoor and outdoor), it was found that the concentration of CO_2 in the indoor

environment was greater than the outdoor environment as a result of poor indoor ventilation.

(b) Ambient relative humidity (RH)

The carbonation of concrete is a diffusion process and it is sensitive to the internal humidity of concrete. In most of the carbonation experiments, concrete ambient RH is mostly used for conditioning the concrete samples, this is as a result of insensitivity of concrete internal humidity to carbonation (Alexander, Mackechnie and Yam, 2007). This assertion is contrary to a research report by Parrott (1987) who found that the concrete internal relative humidity is mostly responsible for the rate of carbonation. Hence, carbonation can occur in a concrete exposed to a lower ambient relative humidity.

It is understood that the depth of carbonation reaches a maximum at a relative humidity of between 50 and 70% (Hills *et al.*, 2015). This means that below 50% and more the 70% RH, carbonation tends to decrease and no carbonation seems to take place when the pores are completely dry or when they are completely saturated with moisture. This is because CO_2 diffusion within the concrete is low when the concrete pores are completely dry or saturated (Galan *et al.*, 2010).

Schubert (1987) showed that the periodic wetting of outdoor unsheltered concrete significantly reduced its carbonation rate and was attributed to the slower rate of carbon dioxide diffusion through partially saturated pores of the cement paste matrix. Wierig (1984) also investigated the carbonation rates of an existing outdoor concrete. It was discovered that walls protected from rain showed a greater carbonation rate in comparison to the same structure exposed to rain. However, the optimum relative humidity for carbonation and corrosion are relative values, which vary depending on concrete quality (Ballim & Lampacher, 1996).

(c) Air temperature (T)

Carbonation reaction in concrete is a chemical reaction which can be influenced by temperature change (Tuutti, 1982). An increase in temperature increases the molecular mobility which in turn increases the rate of carbonation reaction. This occurs mostly in tropics and sub-tropics where temperatures can be more than of 20^oC (Haque, Al-Khaiat and John, 2007). However, temperature may not be

significant to the carbonation reaction especially in the temperate regions where temperatures can be less than zero degrees during the winter season (Haque and Al-Khaiat, 1997; Mikhailov, Strekalov and Panchenko, 2008). In such case, other factors such as relative humidity and carbon dioxide concentration can be responsible for the carbonation reaction. Matsuzawa, Kitsutaka and Tsukagoshi, (2010) investigated the combined effect of relative humidity and temperature on the carbonation rate under accelerated test conditions where CO_2 was fixed at 5% relative humidity was varied at 30, 45, 60 and 80% and temperatures of 20^{o}C and 60^{o}C were used. The 60^{o}C temperature was considered so as to depict conditions in a nuclear power plant structure. The findings were in accordance with the general trend that carbonation rate is higher with an increase in temperature (Tuutti, 1982; Papadakis and Vayenas, 1991; Matsuzawa, Kitsutaka and Tsukagoshi, 2010).

2.5.1.2 Effect of concrete composition on carbonation rate

The main factors that determine hardened concrete properties are pore structure and chemical composition. These two factors are also responsible for carbonation reaction. The concrete microstructure is largely dependent on w/b ratio, binder type, cement content, mix composition and concrete production practices such as mixing, placing, compaction and curing (Alhassan, 2014). The chemical composition of concrete is mainly controlled by the binder type, cement content and the degree of hydration. The effect of these factors on carbonation rate will be discussed further. Some of these factors are discussed further as they affect the carbonation rate in concrete.

- ***Binder type*:** Binder type has a significant effect on the concrete carbonation rate through the concrete capillary pore solution. The pore solution is an electrolyte which is physically absorbed in the concrete pores due to the capillary suction (Guangling & Ahmad 1998). It contains various ions such as sodium (Na^{2+}), potassium (K^{+}), calcium (Ca^{2+}), magnesium (Mg^{2+}), aluminum (Al^{3+}), Iron (Fe^{2+}), silica (Si^{+}) and hydroxyl ions (Andersson *et al.*, 1989)). The elements and compounds in the pore solution can vary in the concrete depending on the binder type used and concrete age (Guangling and Ahmad, 1998). Also,

the amount of calcium hydroxide available for the carbonation reaction varies with different binders which in turn influences their engineering properties of the concrete (Igarashi and Watanabe, 2006). The enhanced strength and durability properties of SCM blended cement concretes are mostly attributed to micro-filler effect due to their fine particles that block the pore spaces and reduce permeability.

There are many literature asserting the role of SCM in enhancing the durability property of concrete. However, apart from SF concrete, the application of SCM in improving the carbonation and corrosion resistance of concrete exposed to the inland environment has not been successful. This may be attributed to the pozzolanic and carbonation reaction of the SCM which play dominant roles more than the permeability effect especially with BS and FA concretes.

Concrete with SF has been reported to have a greater resistance to carbonation compared to concretes made with PC, and other SCM (Dalage and Aitcin, 1983; Turk, Karatas and Gonen, 2012). This is due to the fineness of its particles which is about 100 times smaller than average cement particle (Ananmalay, 1996). This improves the packing structure of the capillary pores which consequently enhances the concrete impermeability. This shows that permeability is more a controlling factor than the pozzolanic reaction in carbonation performance of SF concrete. It implies that SF behaves more like micro-filler than pozzolanic materials (Ananmalay, 1996). The incorporation of SF in concrete essentially eliminates pores between 50 and 0.5 microns and reduces the size of pores in the 500 to 50 micron range (Dalage and Aitcin, 1983). This attribute suggests the reason for its better performance in resisting the ingress of CO_2 and moisture into concrete

Moreover, SF is usually used at 5% to 10% of the total binder, which is lower than BS (50%) and FA (30%) contents. Low SF content in concrete can as well account for its better performance in lowering carbonation rate in concrete (Figure 2.6). This can be because small percentage of PC is replaced with SF compared to BS and FA. Therefore more calcium hydroxide is available for the carbonation reaction.

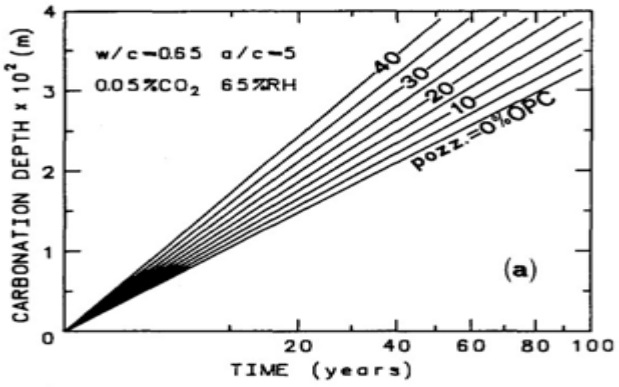

Figure 2:6 Effect of percentage replacement of PC with SCM on carbonation depth of concretes (Papadakis, Fardis and Vayenas, 1992)

Finally, the characteristics of SCM depends on the composition of the raw materials and methodology involved in the processing of such SCM (Ikotun, 2010). Extensive research has been conducted on the effect of SCM in concrete. However, the findings cannot be applied locally, due to the variability of SCM compositions (Ananmalay, 1996). This demands experimenting with local SCM for the development of a service life model that can be useful for inland RC structures.

- ***Concrete mix proportion:*** A concrete mix design is a process of determining the proportion of ingredients that make up a particular concrete of desired quality. Typical concrete ingredients include the cement (binder), water, admixtures, and aggregate (Ballim, Alexander and Beushausen, 2009). The main objective of the concrete mix proportioning is to produce a desired concrete quality at both fresh and hardened state at a reasonable cost. This means that concrete mix proportions have a considerable effect on the concrete quality with consequential effects on its durability and strength (Ahmad, 2003). To study the influence of water and binder content on the concrete quality, the ratio of water to binder content (w/b) is usually used. This is a measure of the degree of dispersion of binder particles in the "effective water", i.e the distance between neighboring binder particles that has to be bridged by hydration products (Tor*rent et al.*, 2016). The w/b ratio determines gel/space ratio, capillary porosity and hence concrete permeability (Loo *et al.*, 1994).

At a fixed water content, an increase in cement content results in a w/b ratio reduction. This reduces concrete permeability which in turn improves the concrete quality. As mentioned earlier, concrete with lower w/c ratio usually has a lower carbonation rate due to a reduction in porosity. Papadakis, Fardis and Vayenas (1992) and Tuutti (1982) found that increasing the w/c ratio of a mix increased the carbonation depth. This was due to an increase in porosity and the effective diffusivity of the concrete. The effect of w/c ratio on carbonation depth is shown in Figure 2.7 where an increase in w/c ratio causes an increase in carbonation depth.

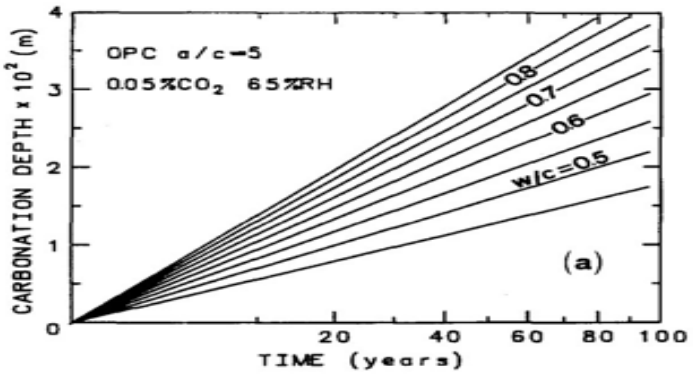

Figure 2:7 Effect of w/c ratio on carbonation depth of concrete (Papadakis, Fardis and Vayenas, 1992)

An attempt was made by Loo *et al.* (1994) in a laboratory experimental investigation, where the effects of varying cement content for a fixed water content and varying the water content for a fixed cement content on carbonation rate were examined. The results show that for a fixed water content increasing the cement content reduces the w/c ratio which has an insignificant effect on the carbonation rate. However, for a fixed cement content increasing the water content increases the w/c ratio which significantly affects the carbonation rate. This suggests that cement content may not be an important parameters that can be considered for a useful carbonation rate model.

Papadakis, Fardis and Vayenas (1992) investigated the effect of varying aggregate/cement ratio (a/c) on carbonation depth of concretes. The result is shown in Figure 2.8, where it can be observed that increasing a/c ratio slightly increases the carbonation depth and this can be because of the reduction in the molar concentration of Ca $(OH)_2$ and CSH hydrates. As shown in Figure 2.8, the effect of a/c ratio on the carbonation depth is relatively smaller compared to the effect of w/c ratio on the carbonation depth shown in Figure 2.7. Therefore, a/c ratio can be ignored as a part of the input variable for a carbonation model (Papadakis, Fardis and Vayenas, 1992).

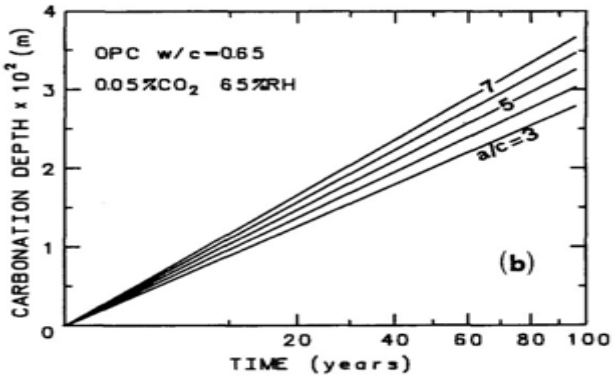

Figure 2:8 Effect of a/c ratio on carbonation depth of concretes (Papadakis, Fardis and Vayenas, 1992)

- ***Initial moist curing duration*:** Among other variables, early-age moist curing of concrete facilitates strength development, reduction in porosity and permeability for an improved durability and structural strength performances. Initial moist curing is done by keeping the concrete completely saturated or close to saturation until originally water-filled pores within cement paste have been filled to the extent desired by the products of hydration of cement and associated binders (Federation International du Béton (fib Bulletin) 2000). Powers, (1948); Patel *et al.* (1985) and showed that hydration progresses at a maximum rate when the concrete is fully saturated and can be greatly reduced when the relative humidity within the capillary pores drops below 80%.

Nagatakis, Ogha and Kim (1986) reported on the influence of curing on hydration property of blended cement concretes. They observed that hydration was very slow in a concrete not adequately cured or exposed to a dry environment at an early age. The effect of curing on the resulting pore structure of the concretes was reported to include large and connected pores. The presence of large connected pores in concretes has been reported in many publications to be responsible for an increased penetrability of moisture and CO_2 into the concrete pores leading to an advancement of carbonation front. Ballim (1993) showed that a relatively greater influence on the durability of concrete regarding its permeability and sorptivity could be beneficial by extending the period of early-age moist curing rather than decreasing the w/b ratio. A similar trend was also reported by Dhir et al. (1989), where the carbonation rate was significantly influenced by extending the initial moist curing age. Alhassan (2014) conducted an investigation into the effect of varying the duration of initial moist curing on carbonation characteristics of various concretes. The durations of 3, 7, and 28 days were used to moist cured the concretes after casting before exposing them to the environment; the order of carbonation depth (maximum to minimum) at every testing age regarding the initial moist curing was found to be 3-day → 7-day → 28-days for a particular concrete.

It is difficult to specify a curing age for a structural element; the duration of curing is best determined based on the extent of the required properties of that particular concrete. The minimum prescriptions of initial curing age made in some literature are dependent on the binder type, curing type and the average temperature on curing periods. However, for a laboratory concrete, 7 days has been noted to be sufficient for initial moist curing at an average temperature greater than 5^{o}C (M*indess et al*., 1981). This is also recommended by structural durability research monograph authored by Alexander et al. (2003). Previous studies have shown that the effect of curing beyond 14 days on carbonation rate is negligible (Dhir et al., 1989; Calavera, 2001; Nagatakis, Ogha and Kim, 1986). Also, 7 days was used by EI Maaddawy & Soudki (2003) to initially moist cure the concrete samples used for a corrosion test. The curing attempt was to control the rate of moisture loss and to prevent concrete premature

shrinkage cracking for a reliable corrosion data that can be used in modeling the time to initiate corrosion cover cracking in concrete. However, an unnecessary increase in the initial moist curing duration on site presents a challenge on time and material optimization in concrete construction.

2.5.2 Effect of concrete cover depth on corrosion initiation time

Concrete cover depth provides the initial resistance to the corrosion causing agents such as CO_2, oxygen and moisture. Therefore, the thickness, quality and exposure condition of the concrete cover have significant effects on the corrosion initiation time. Concrete cover depth mainly influences the ingress of carbon dioxide, oxygen and moisture into the concrete. Hence, an increase in concrete cover depth increases the travel path for the CO_2 and oxygen to the embedded steel in concrete which in turn increases the time which CO_2 reaches the depth of reinforcement. A significant portion of a RC structure service life may be lost if the cover thickness is reduced while an excessive thick cover may result in wider flexural cracks, which consequently impairs concrete durability. Therefore, cover depth can only be increased up to a limit of 80-90 mm (Neville, 2011; Otieno, 2008). If this requirement is not satisfactory for the required durability, then concrete quality rather than the thickness should be increased (Otieno, 2008).

2.6 Concrete Carbonation Tests

Concrete carbonation test is conducted under two conditions; controlled exposure conditions and natural exposure conditions. Carbonation under controlled exposure conditions is usually employed in accelerated carbonation experiments to shorten the test duration and to predict the long-term performance under natural conditions (Jones et al., 2000). This is because carbonation takes longer time in natural environment due to low CO_2 concentration (0.03% to 0.05%) in the environment (Khunthongkeaw, Tangtermsirikul and Leelawat, 2006). However, both tests involve a similar carbonation depth measurement method.

Apart from a few studies that used the natural environment for concrete carbonation test, most researches employ accelerated laboratory tests with high CO_2 concentrations. Chang & Chen (2006) used CO_2 concentration of 5% to 40% at 60% to 80% RH to obtain full carbonation depth of the concrete specimens. The results were obtained between 14 and 60 days, and it was concluded that it is feasible to study the carbonation process of concrete under natural conditions by using accelerated carbonation techniques. Other accelerated tests have made use of pressurised CO_2 to carbonate concrete specimens with the intention of obtaining carbonation data in a short time (Reardon, James and Abouchar, 1989). However, the process of relating the pressurised carbonation process to natural carbonation process is not known.

In a comment about accelerating carbonation in concrete using pressurised chamber at a pressure of 45 kPa, Ballim (personal communication, June 12) mentioned that pressurising concrete can induce micro-cracks and at the same time destroy the micro-structure of the concrete at the cover zone. This is in line with research findings of Reardon, James and Abouchar (1989) where a substantial number of micro-cracks were developed on the concrete when pressurised CO_2 was used to carbonate the concrete specimens. The concrete damage was attributed to the repeated cycles of pressurisation and depressurisation rather than the carbonation. Further research study is necessary to determine the actual pressure that can be used to carbonate a given concrete without resulting in any physical damage. This would promote the applicability of pressurising technique in concrete carbonation experiment and the results can be used as well to determine the porosity, and permeability changes in concrete due carbonation (Reardon, James and Abouchar, 1989).

2.6.1 Accelerated carbonation

Accelerated carbonation test is done by introducing higher concentration of carbon dioxide (above normal CO_2 concentration in the air) to the concrete samples in a tight chamber kept at a relative humidity of 65%. At a higher CO_2 concentration, more CO_2 molecules arrive at the carbonation front within a given period, dissolve

and dissociate. This increases the dissolution rate of calcium from hardened cement paste constituents. Thus, the calcium supply that goes into the reaction is depleted faster, and carbonation front progresses faster.

Sisomphon & Franke (2007) postulated using Fick's first law that for a given concrete, the rate of carbonation is accelerated by an amount equal to the ratio of the square root of accelerated concentration of CO_2 divided by the square root of natural CO_2 concentration (Visser, 2012; Sisomphon & Franke, 2007);

$$\frac{K_{acc}}{K_{env}} = \frac{\sqrt{c_{1,acc}}}{\sqrt{c_{1,env}}} \qquad 2.13$$

where K_{acc} and K_{env} (mm/year$^{0.5}$) represent the carbonation rate under the accelerated conditions and natural exposure environment. The $c_{1,\text{acc}}$ and $c_{1,\text{env}}$ represent the CO_2 concentration under accelerated and natural exposure conditions.

For example, using a CO_2 concentration of 4% to accelerate a carbonation process whereas in a conventional environment CO_2 concentration is about 0.04%. Thus, the carbonation process is increased 10 times the concentration of the natural carbonation test. This shows that carbonation process can be accelerated as much as one wishes by increasing the CO_2 concentration accordingly. Although, accelerated carbonation is based on the constant conditions of 65% RH and 20^{o}C temperature. It does not take into consideration the variations in the real environment. The fact that concrete properties have not been developed fully before exposing them to a relatively high concentration of CO_2 jeopardises the reliability of accelerated carbonation results compared to a long-term behaviour of concrete under natural test conditions (Visser, 2012). Hence, results of carbonation tests obtained from accelerated tests can cause a serious error in estimating the concrete service life. However, accelerated carbonation test results can be used to indicate the relative resistance of different concretes in different environments (Pihlajavaara, 1984).

Regarding the application of accelerated carbonation to predict concrete service life, no experimental results have been found in the literature on use of accelerated carbonation results for predicting RC service life (Sanjuan, Andrade and Cheyrezy,

2003). Although, accelerated carbonation allows for an easier control of the exposure conditions, but the diffusion rate of CO_2 may change during the conditioning of the concrete samples (Sagues *et al.*, 1997). Previous studies (Reardon, James and Abouchar, 1989;Tuutti, 1982; Hakkinen, 1993; Thiery *et al.*, 2005) established the consequential effects of accelerated carbonation test on the products of carbonation. Such effects include the small size of calcium carbonate crystals, the difference in solid phases of cement and lower pH of the aqueous phase compared to natural carbonation. Bier, Kropp and Hilsdorf (1987) investigated the effect of accelerated carbonation on cement blended with SCM. It was found that accelerated carbonation led to the formation of coarse capillary porosity which was larger than capillary pore volume found with carbonated PC. Therefore, it may be necessary to take into account the differences in behaviour of binders when interpreting the result of accelerated carbonation, especially when using such data to predict the concrete service life.

2.6.2 Carbonation experiment under natural exposure conditions

Carbonation is a slow process under natural environment. This is due to low concentration of CO_2 in a natural environment which is within a range of 0.03-0.04% by air volume. The CO_2 concentration in the air depends on the location and level of urbanisation in a particular locality (Ballim and Lampacher, 1996).

Moreover, the natural carbonation process gives true carbonation data for model development. Although, this may be difficult to conclude in the interest of time. Long-term natural carbonation experiment can be used to validate short-term accelerated carbonation tests and can serve as an indicator of concrete durability (Dhir et al., 1989). Alhassan (2014) used a natural carbonation experiment to obtain data which was used to predict the carbonation rate in concrete exposed to the South African inland environment. Although, the developed models did not account for the effect of using different binder types, the carbonation rate predictions were comparable to most of the existing models predictions. For a useful service life model, it is more important to consider natural carbonation rather than accelerated carbonation. Although, the experimental duration may have to be compromised,

such data is more reliable and can be used in further studies such as stochastic analysis of service life.

2.6.3 Measurement of carbonation depth

The usual method for monitoring the depth of carbonation involves spraying a concrete cut surface with a solution of phenolphthalein, which acts as an indicator. The solution is a mixture of 50 to 100 ml of alcohol and 50 ml of water with 1 g of phenolphthalein (Parrott, 1987). When the phenolphthalein solution is applied to the freshly cut concrete surface, the carbonated part remains colourless due to the reduction in the pore solution pH (< 9). Other parts not affected by carbonation change to a pink colour due to their alkalinity (pH >12) of the concrete. The carbonated surface zone can be easily measured by Vernier caliper or measuring tape. The phenolphthalein indicator method of monitoring the depth of carbonation is convenient to use and can give reproducible results *(Jones et al*., 2000).

Moreover, phenolphthalein indicator method indicates the zone where the pH is about 9, however, this does not necessarily correspond to either the border between un-carbonated and partially carbonated concrete or the boundary between the partially carbonated and fully carbonated concrete. Litvan and Meyer (1986) asserted that this is an incomplete representation of carbonation depth since it does not show the width of the carbonated zone, even though the width of the carbonation front can be so small compared to the depth of reinforcement in the concrete. This can be considered insignificant and may not be relevant to the determination of time at which the carbonation front reaches the depth of reinforcement.

Alternative methods of determining the carbonation depth include X-ray diffraction, infra-red absorption and thermal analysis. These methods involve measuring the increase and reduction of calcium hydroxide and various forms of carbonate. Villain, Thiery and Platret (2007) explained the effectiveness of using other methods apart from the phenolphthalein method to obtain carbonation data for a carbonation model development. However, most of these alternative methods are expensive, inconclusive and may yield misleading results. Therefore, it is necessary to supplement them with other methods to obtain more reliable

carbonation data that will be suitable for developing a service life model. The alternative methods cannot be compared to phenolphthalein indicator method in terms of convenience, fast/quick result, and reproduceable data that can be suitable for a service life prediction model.

2.7 Predicting the Time to Carbonation Induced Corrosion Initiation

The approach to determining concrete carbonation rate follows the Fick's law of diffusion. In this case, the concentration gradient of CO_2 between the concrete and the environment is a driving force for carbon dioxide penetration into concrete capillary pores (Visser, 2012; Sisomphon and Franke, 2007). According to Fick's first law of diffusion, the amount of CO_2 ingress into concrete can be expressed as:

$$J = -D\left(\frac{\partial c}{\partial x}\right) = DA\frac{(c_1 - c_2)}{x} \qquad 2.14$$

where J represents the carbon dioxide flux (g/m^2s), D is the diffusion coefficient (m^2/s) of CO_2 in concrete, c_1 is a CO_2 concentration in the environment, c_2 is the measured CO_2 concentration of the concrete sample. A (m^2) represents the concrete surface area exposed to CO_2, x represents the depth of carbonation front from the exposed surface. The negative sign suggests a linear decline in the CO_2 rate of penetration over the carbonation depth (Visser, 2012;Otieno, Alexander and Beushausen, 2010).

Assuming that the carbonation front will not progress untill all the carbonating materials have reacted with the penetrated CO_2 within a reference concrete volume (Adx), the total mass of CO_2 (dM) that will be transported to the carbonation front to react with the carbonating material can be given as;

$$dM = C_0 A dx \qquad 2.15$$

where dM represents a unit mass of CO_2 that penetrated into the concrete, C_0 represents the amount of CO_2 (kg/m^3) required to react with CH phase contained in a unit volume of a concrete sample. x (m) is the location of the carbonation front and dx (m) is a unit progress of the carbonation front. The unit mass of the gaseous

CO_2 diffusing into the concrete with respect to time can also be expressed as given by Equation 2.16 (Sisomphon and Franke, 2007).

$$dM = DA\frac{c_1 - c_2}{x}dt \qquad 2.16$$

Assuming that the CO_2 flux that goes through a unit volume of a reference concrete spent a reference time, *dt*), therefore, Equation 2.15 and 2.16 can be simplified (see Equation 2.17) and integrated to obtain the carbonation depth (Equation 2.18).

$$DA\frac{c_1 - c_2}{x} = C_o A\frac{dx}{dt} \qquad 2.17$$

$$x = \sqrt{\frac{2D}{C_0}(c_1 - c_2)}t^{0.5} \qquad 2.18$$

The concentration of CO_2 in the concrete reacting with the $Ca(OH)_2$ can be very small and thus neglect c_2, Equation 2.18 becomes:

$$x = \sqrt{\frac{2Dc_1}{C_0}}t^{0.5} \qquad 2.19$$

Therefore, the carbonation coefficient (rate) *K* can be expressed as:

$$K = \sqrt{\frac{2Dc_1}{C_0}} \qquad 2.20$$

Substituting for *K* in Equation 2.19 yields a well known square root time relationship (Equation 2.21) which seems to be reasonably applicable to all types of concrete in any exposure condition, but with some assumptions (Visser, 2012; Alexander, Mackechnie and Yam, 2007).

$$x = Kt^{0.5} \qquad 2.21$$

Equation 2.21 shows that the rate of carbonation is dependent on the concrete diffusion coefficient and the amount of bound CO_2 and concentration of CO_2 in the air (Ballim and Lampacher, 2004; Alexander, Mackechnie and Yam, 2007 and Neville, 2011). The application of Equation 2.21 in practice assumes the following:

- Uniform pore structure across the concrete depth and constant exposure environment

- The quality of the pore structure remains constant across the concrete depth
- The degree of hydration and the amount of calcium hydroxide remain constant across the depth of the concrete

However, in reality, the assumptions may not hold since the carbonation reaction itself influences the pore structure, by causing pore volume reduction (Thiery *et al.*, 2005). The calcium carbonate, which is the main carbonation product, blocks the air pores in the concrete and causes a reduction in diffusivity which in turn decreases the rate of carbonation with time. Hence, depth of carbonation can be generally expressed as:

$$x = Kt^n \qquad 2.22$$

where n is the time exponent value which varies with concrete properties (pore structure) and the exposure environment (Sisomphon & Franke, 2007 and Alexander et al. 2007).

Therefore, the application of Fick's law of diffusion, using constant parameters is limited even though many service life prediction models have been derived based on $t^{0.5}$ theory. The value of n may be less than 0.5 if the concrete is subject to wetting and drying cycles since the diffusion of carbon dioxide is slower through moisture filled pores. On the other hand, the value of n may be greater than 0.5 in the case of cracked concrete; the presence of cracks provides a direct pathways for carbon dioxide (Alexander, Mackechnie and Yam, 2007). Also, in old concrete, the depth of carbonation is often less than expected, this is contrary to the square root of time relation. In controlled climates such as the laboratory, satisfactory carbonation rate results may be obtained using $\sqrt{t}$. However, its correlation with actual carbonation rate is often weak and yields misleading results, especially for outdoor exposure with changing temperature and humidity conditions (Alhassan, 2014).

In an environment such as the Cape Peninsula, the sustained periods of rain in winter coupled with dense concrete pore structure usually reduces the rate of carbonation with time. Therefore, the theoretical value of 0.5 for the time exponent may not be adequate for concrete in such an environment. Taking various factors into consideration, the n value for concretes in coastal areas of South Africa was taken as 0.4 (Alexander, Mackechnie and Yam, 2007). For Johannesburg locality,

a more conservative *n* value of 0.5 is selected due to its relatively drier environment (within the optimum RH range for carbonation) which allows rapid carbonation throughout the year Alexander, Mackechnie and Yam, 2007).

Time to corrosion initiation is defined as the time required for the carbonation front to reach the level of reinforcement and assumes to initiate corrosion. The carbonation depth required to initiate corrosion is the concrete cover depth *'c'*, while the time (t_i) required for carbonation front to reach the reinforcement is the corrosion initiation time 't_i' this is expressed as:

$$t_i = \left[\frac{c}{K}\right]^2 \qquad 2.23$$

where *K* is the carbonation rate (mm/year$^{0.5}$). As shown in Equation 2.22, the main factors that control the corrosion initiation time in any environment are concrete cover depth and carbonation rate. Carbonation rate is influenced mainly by the concrete quality and exposure conditions as mentioned in Section 2.6.

2.7.1 Review of some existing corrosion initiation models

There are several empirical models describing the carbonation rate in literature, and each model is based on different sets of parameters and experimental designs. Some of the corrosion initiation models are reviewed in this section.

(a) Papadakis at al.'s model (1992)

Papadakis, Fardis and Vayenas (1992) worked on an experimental investigation of the physicochemical process of concrete carbonation. Carbonation depth (*d*) was empirically modelled using the ambient concentration of CO_2, the molar concentrations of the carbonating constituents (CH and CSH) as well as the effective diffusivity of CO_2 in carbonated concrete (Equation 2.24).

$$d = \left(\frac{2[CO_2]^2 D_{c,CO_2}}{[CH]+3[CSH]}t\right)^{\frac{1}{2}} \qquad 2.24$$

$$D_{c,CO_2} = \left(1.64x10^{-6}\right)\varepsilon_p^{\,1.8}\left[1-(RH/100)\right]^{2.2} \qquad 2.25$$

$$\varepsilon_p = \varepsilon \frac{1+(w/c)(\rho_c/\rho_w)(a/c)(\rho_c/\rho_a)}{1+(w/c)(\rho_c/\rho_w)} \quad 2.26$$

where $D_{c,co2}$ is the diffusion coefficient represented by Equation 2.25 and is given as a function of the porosity of hardened cement paste, ε_p is the cement paste porosity (Equation 2.25). ε is the total porosity of the concrete, *a/c* is the aggregate/cement ratio, and ρ_c/ρ_w is the ratio of concrete to water densities. The CH and CSH are in molar concentrations, while ρ_c/ρ_a expresses the ratio of concrete and aggregate densities. The diffusion coefficient, $D_{c,co2}$ is given as a function of the porosity of hardened cement paste.

The model suggests that carbonation depth with time is a function of the chemical composition of cement, mix proportion of the concrete, CO_2 concentration, concrete diffusion coefficient, and ambient relative humidity. It is considered to be valid when the concrete is in a state of CO_2 equilibrium with the environment. Quillin (2001) asserted its application to indoor and external sheltered exposure due to initial assumption of the constant environment and completed hydration reaction while the diffusion coefficient remains constant. However, the application of the model for predictive purposes requires knowledge of a concrete chemical composition as well as the pore relative humidity which may not be easily obtainable on site.

(b) Liang & Lin's model (2003)

Liang & Lin (2003) worked on mathematical modelling of concrete carbonation using Fick's first and second laws of linear diffusion to express the three-dimensional equations of conservation of mass for predicting carbonation depth at corners and general surface of concrete structures. The following analytical models were proposed:

$$d = 2\left(\frac{DC_0}{m_0}t\right)^{\frac{1}{2}} \qquad d = \left(\frac{2DC_0}{m_0}t\right)^{\frac{1}{2}} \quad 2.27$$

i. Corner surface ii. Surface

where C_0 is the CO_2 concentration at the outer edge of the concrete, m_0 is the unit volume (kg/m^3) of absorbed CO_2 and *D* is the diffusion coefficient.

The expression derived by Liang & Lin (2003) suggests a greater carbonation at concrete corners compared to the flat surfaces. This supports a numerical study by Saetta & Vitaliani (2004) who used two-dimensional finite element analysis and found that the maximum carbonation depth at concrete corners is 40% greater than the carbonation depth on flat surfaces. The two assertions by Liang & Lin (2003) and Saetta & Vitaliani (2004) can be due to two directions at which CO_2 penerates and progresses at the corner of the concrete structure.

The results show the relevance of concrete geometry on carbonation rate which many carbonation models do not consider especially during testing. Most studies tend to concentrate on measurements done on flat concretes surfaces. Carbonation is greater at the corners of a structural member as shown in Equation 2.27. The models indicate that measurements based on flat concrete surfaces may not provide the worst case scenario for estimating concrete service life. However, the Liang & Lin (2003) model provides the engineering reference on the basis of reinforcement repairs of existing RC structures.

c. Parrot's model (1998)

In an attempt to show the relationship between the transport property and performance of concrete for in-situ assessment of concrete resistance to carbonation, Parrot (1998) used the oxygen permeability of cover concrete to model the carbonation depth in concrete. The influence of moisture conditions of the cover concrete on CO_2 penetration was studied regarding of relative humidity within the concrete pores. The empirical relationship between the parameters was proposed as;

$$d = \frac{aK^{0.4}t^{n}}{c^{0.5}} \qquad 2.28$$

where K is the air permeability at 60% RH, t is the time for corrosion initiation in years, and c is the alkaline content in the cement that can be responsible for the rate of carbon dioxide penetration.

The calcium oxide content depends on the cement composition, exposure condition and proportions of cement reacted (Sagues *et al.*, 1997; Quillin, 2001). Parameter

'n' is the attenuation factor that depends on the exposure conditions and can be obtained using an empirical relation shown in Equation 2.30. The parameter r is the relative humidity

$$n = 0.01785r - 0.0001623r^2 + 0.02536 \quad 2.29$$

The experimental investigation revealed the role played by relative humidity in controlling CO_2 penetration into concrete. This is shown by the attenuation power factor (n) which depends on the rate-controlling factors such as CO_2 diffusion, pore structures, the amount of lime and relative humidity. The attenuation power factor can be very close to 0.5 for an indoor exposure, but decreases as the relative humidity rise above 70%. The time at which the internal relative humidity reaches an equilibrium with ambient relative humidity depends on the concrete cover thickness and the pore structure (Sagues *et al.*, 1997). In addition, Parrot's model was empirically developed to suit European climatic conditions which will need modification before it can be suitable for predicting carbonation depth of concrete in South Africa's inland environment.

(c) Salvoldi et al.'s model (2015)

Salvoldi, Beushausen and Alexander (2015) used South African concrete durability design method to model the carbonation depth in concrete. The model is presented as:

$$x = \frac{2D_{dry}c\beta t_e}{a} \quad 2.30$$

$$D_{dry} = \left(1.4x\left(\frac{k}{10^{-11}}\right)^{22}\right)x10^{-11} \quad 2.31$$

where D_{dry} is the dry diffusion coefficient, k is the permeability coefficient, c is the ambient CO_2 concentration in mol/m^3, β is the relative humidity, t_e is the effective time of exposure, and a is the amount of carbonating material in mol/m^3.

The model incorporates oxygen permeability, coefficient of exposure conditions in terms of ambient CO_2 concentration, ambient relative humidity, amount of carbonating materials in concrete as the input parameters to make the model robust in the application. Even though it is a good practice to account for many parameters

in a single model, however, it should be noted that the largeness of model input parameters is not a criterion for its superior performance over the simple ones. A model is only superior when the input parameters are reliably quantified (Jamali *et al.*, 2013).

The model enables prediction of time-dependent carbonation depths of concretes based on environmental exposure, mix design and oxygen permeability of the concrete. However, the model was developed using the data obtained from accelerated tests where the exposure conditions were controlled in the interest of time. Following a constant carbonation depth, a relationship between accelerated (t_{acc}) and natural carbonation times (t_{nat}) was established as:

$$t_{nat} = 51 t_{acc} \qquad 2.32$$

Even though Equation 2.32 can predict the carbontion exposure time of concrete to natural environment, the model may not be suitable for predicting natural carbonation in concrete due to (i) heterogeneous property of concrete (ii) the fact that the type of natural exposure environment is not specified with the model.

(d) Dhir et al.'s model (1989)

Dhir, Hewlettt and Chanz (1989) examined the feasibility of using intrinsic permeability to predict the potential resistance of concrete to carbonation. This is with the aim of controlling the quality of in situ cover concrete. The carbonation depth prediction model is shown in Equation 2.33 and it has a correlation coefficient (R^2) of 0.95.

$$D_t = (t/20)^{0.5} (22.8 \log k - 6.9) \qquad 2.33$$

where D_t (mm) is the carbonation depth measured after t (years) in a normal exposure, t (years) is the design life of the concrete structure, and k (m^2) is the intrinsic permeability. The model illustrates a direct relationship between the depth of carbonation and intrinsic permeability. A similar trend was also observed by the same authors (Dhir, Hewlettt and Chanz, 1989) when Figg air index test was used to show the relationship between the carbonation depth and permeability of concrete (Equation 2.34). The correlation coefficient (R^2) of the equation is equal to 0.97.

$$D_t = (t/20)^{0.5}\left(82 - 34\log F_d\right) \quad 2.34$$

where F_d is the Figg air index (s), D_t (mm) is the depth of carbonation measured after t (years) in a normal exposure, t (years) is the design life of the concrete structure.

The two models show good correlations as their R^2 values are near unity. This indicates that either of the two models can be used to predict the carbonation resistance of concrete. The Figg air index test equipment is more portable, cheap, and simple to operate compared to other permeability devices (Dhir, Hewlettt and Chanz, 1989). The main limitation in the application of the two models is that they may not be suitable for predicting carbonation depth in concretes with different binders and natural exposure conditions. The data used to developed the two models was obtained from controlled accelerated experiments which did not specify the exposure conditions. Also, the effect of binder types on carbonation depth of concrete was not accounted.

(e) Hakkinen's model (1993b)

To overcome some of the limitations in Dhir et al.'s model, (Hakkinen, 1993) proposed a model that considers different types of binders and their compressive strengths. The model considers carbonation rate as a function of concrete compressive strength as shown in Equations 2.35 and 2.36.

$$d = v\sqrt{t} \quad 2.35$$

$$v = af^{b} \quad 2.36$$

where d (mm) is the depth of carbonation, v is the carbonation rate (mm/√year), t (years) is time, f (MPa) is the compressive strength, while a, b represent the constants that depend on binder type. Although, the model is empirically based, its application to predicting the service life of RC structures in a particular environment cannot be generalized based on the variations in the mineralogical composition of different binders as well as variations in the environmental conditions.

(f) RILEM's model (1996)

RILEM 14 (1996) modified the model proposed by Hakkinen (1993) to include different exposure conditions represented by the exposure coefficient (C_{env}), concrete porosity in terms of the air content coefficient (C_{air}) and concrete characteristic compressive strength, f_{cm} (MPa). The coefficients 'a' and 'b' depend on the binder type. The various constants are shown in Tables 2.1, 2.2 and 2.3.

$$K_c = C_{env} C_{air} a (f_{cm})^b \qquad 2.37$$

Table 2:1 Binder coefficients (RILEM 14 1996)

Binder types	a	b
100%PC	1800	-1.7
72%PC + 28%FA	360	-1.2
91%PC + 9%SF	400	-1.2
30%PC + 70%BS	360	-1.2

Table 2:2 Environment coefficients (RILEM 14 1996)

Environment conditions	C_{env}
Structures sheltered from rain	1
Structures exposed to rain	0.5

Table 2:3 Air content coefficients (RILEM 14 1996)

Air entrainment	C_{air}
Non – air entrainment	1
Air entrainment	0.7

RILEM's model classifies the exposures into two categories; sheltered and unsheltered exposure from rain (see Table 2.2. It does not consider indoor exposure which has significant effect on carbonation in terms of CO_2 concentration

(Alhassan, 2014). It considers air content which may not be relevant to the inland climate of South Africa due to the absence of severe winter conditions. Although, air content can be used to illustrate cover concrete pore system. Besides, the RILEM model is based on compressive strength which is mainly governed by the concrete bulk while durability is primarily controlled by the concrete cover depth (Alexander, Santhanam and Ballim, 2010). The benefit of RILEM's model is that it can be applied to RC structures with various strength grades.

(g) de Fontenay's model (1985)

de Fontenay (1985)proposed a carbonation model that shows the influence of early-age curing on carbonation depth of concrete. The model showed that carbonation depth is greater in non-cured concrete compared to 28-day cured concrete.

28-day cured: $d = 0.43(a/c - 0.4)\left(12(t-1)\right)^{0.5} + 0.1$ 2.38

Non-cured: $d = 0.53(a/c - 0.2)(12t)^{0.5} + 0.2$ 2.39

where, d (mm) is the carbonation depth, a/c is the ratio of aggregate content to cement content and t (year) is the exposure time

A similar trend was observed by Kokubu and Nagatakis (1989). However, some previous studies showed that the effect of curing beyond 14 days on carbonation rate is negligible (Nagatakis, Ogha and Kim, 1986; Dhir, Hewlettt and Chanz, 1989; Calavera, 2001)**.**

(h) Alhassan's model (2014)

Alhassan (2014), developed a comprehensive carbonation rate model in terms of w/b ratio, early curing age, and exposure type.

$$K = 5.63 + 10.01(\text{w/ c}) - 0.02C + \alpha_1 + \beta] \quad 2.40$$

where K (mm/years$^{0.5}$) is the carbonation rate, C (kg/m^3) represents the cement content, α_1 β are the coefficients representing the early moist curing age and exposure conditions. The model is plausible as it contains many parameters that seem to be useful for a carbonation model. The w/c ratio parameter in the model represents the concrete quality. However, the model is limited to the design stage of concrete, as it may be practically difficult to obtain accurate w/c ratio data from

existing concretes. It becomes apparent that a fluid transport parameter would be a better and more convenient way of representing concrete quality in the model. Moreover, the effect of binder types on carbonation rate is not accounted for by the model, which may limit its application.

(i) Basheer et al.'s model

In regression analysis, the addition of an independent parameter usually improves the correlation coefficient of a model (Montgomery & Runger, 2011). Basheer et al. (1999), proposed a multiple linear regression carbonation model using compressive strength and durability index parameters as shown in Equation 2.40.

$$K = \gamma_0 + \gamma_1(\mathrm{f}_{cu}) + \gamma_2(API) + \gamma_3(SI) + \varepsilon_i \qquad 2.41$$

where K is the rate of carbonation, γ_1, γ_2, and γ_3 are multipliers for the independent variables. The f_{cu}, API, and SI are the compressive strength, air permeability index and sorptivity index respectively, and ε_i is the random error associated with the variables.

The addition of each variable in the regression analysis used by Basheer to develop the carbonation rate model expressed in Equation 2.40 improved the model by presenting a better correlation. It is generally understood that the dominant mode of concrete early deterioration in carbonation environment is mainly through the ingress of oxygen, moisture, and CO_2. This suggests the adequacy of OPI and WSI as the appropriate parameters that can be used to predict carbonation rate in concrete. Ballim (1993) suggests that permeability or water sorptivity can represent a durability indicator in predicting carbonation rate in concrete. Ballim's suggestion was based on the fact that permeability and water sorptivity measure the concrete pore network system and are sensitive to variations in binder type and w/b ratio. However, it will not be reasonable to include the two parameters in a single model to avoid violation of multicollinearity assumption of regression analysis which can give a biased result if not avoided.

Moreover, the findings of Basheer, Russell and Rankin (1999) are based on accelerated carbonation under controlled exposure conditions. A different result might be obtained if natural carbonation and a single index parameter that relates

to the gaseous mode of transport in concrete are used. This will avoid the normalisation error usually encountered when converting an accelerated carbonation result to natural carbonation result.

2.8 Corrosion Propagation of Steel in Concrete

Corrosion is initiated, when the passive film on the surface of reinforcing steel is destroyed as a result of decrease in the pH value of concrete pore solution from above 12 to below 9 (Sohail, 2013). It proceeds into the propagation stage when the corrosion agents (O_2 and H_2O) are sufficient at the corrosion sites (anode and cathode). Corrosion propagation is characterised by active corrosion which produces expansive material with bigger volume compared to the original reinforcing steel. Due to the volumetric expansion of this material, the capillary pores are filled thereby exerting pressure on the surrounding concrete causing cracking and spalling of the cover concrete (Ahmad, 2003; El Maadawy & Soudki, 2007 and Liu, 1996).

As mentioned in Section 2.3, reinforcement corrosion is mainly influenced by the environmental conditions, concrete quality (concrete penetrability and composition of its pore solution), and the concrete cover depth (Ahmad, 2003; Zhou, 2005). Tuutti (1982), explained that progress of corrosion in concrete is mostly dependent on environmental factors rather than material properties. However, it is expected that concrete quality will affect corrosion propagation in a similar way as environmental conditions (RH and temperature) do. The two corrosion influencing factors are reviewed further.

2.8.1 Exposure environment

The main environmental components that affect corrosion propagation are relative humidity, temperature and oxygen. Corrosion propagation increases with an increase in relative humidity. It reaches a peak at about 95% RH and then reduces to a very low level near saturation as shown in Figure 2.9 (Tuutti, 1982). The rate

at which corrosion propagate is at minimum when the relative humidity is below 85%.

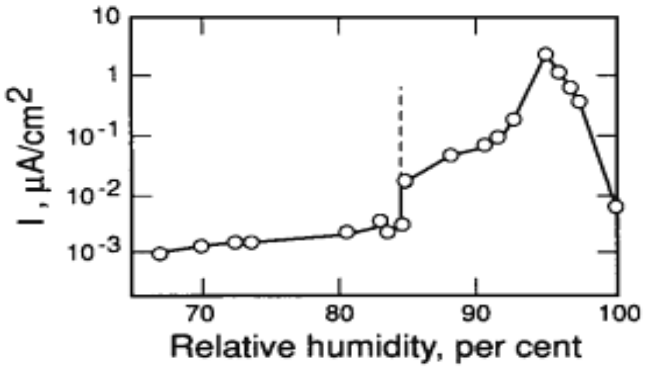

Figure 2:9 Effect of relative humidity on corrosion rate (Tuutti, 1982)

Figure 2.10 illustrates the effect of temperature on corrosion current density. At a higher temperature, the corrosion ions are more agitated and move faster between the anode and cathode which contributes to the increase in the corrosion current density. Tuutti (1982) investigated the effect of a higher temperature on corrosion current density and found that corrosion current increased ten times when the temperature rose from 0 to 20^{o}C. He attributed the increase in the corrosion current to the fact that corrosion is a chemical reaction and an increase in temperature usually increases the rate of a chemical reaction.

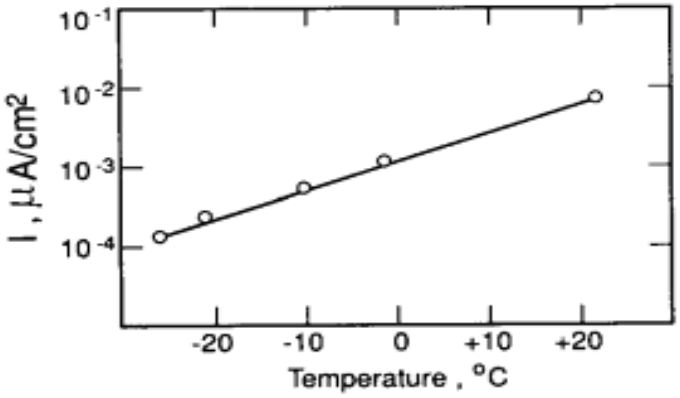

Figure 2:10 Effect of temperature on corrosion rate (Tuutti 1982)

Uhlig & Revie (1985) argued that, an increase in temperature can release the dissolved oxygen in the concrete pore for more corrosion reaction to occur. Figure 2.10 shows that at the lowest end of the temperature scale, below the freezing point of the pore solution, it is difficult for the ions to move, this limits the corrosion reaction (Soroka, 2003).

It is evident from Figure 2.11 that the effect of temperature on corrosion current density can be ignored at lower relative humidity as temperature becomes significant only when the relative humidity exceeds 85% (Soroka, 2003). Low corrosion performance of RC structure at elevated relative humidity of greater than 95% may be attributed to the low diffusion of oxygen at the cathode and anode sites of the electrochemical cell.

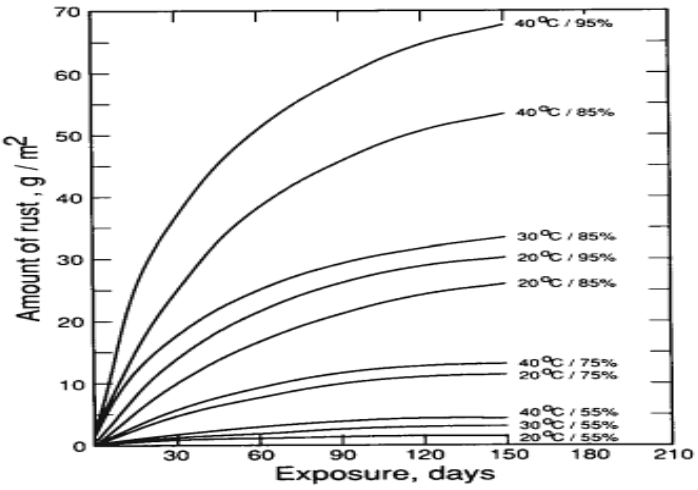

Figure 2:11 Corrosion current as a function of outdoor Temperature and RH (Soroka, 2003)

The results of Raphael and Shalon, (1964) cited by Soroka (2003) for carbonated mortar, showed an increase in corrosion current density with an increase in relative humidity up to 95% at 20 - 40ºC (Figure 2.11). The presence of moisture and oxygen are necessary for corrosion of reinforcement in concrete. Moisture fulfills the electrolytic requirement of a corrosion cell while moisture and oxygen combined, help in the formation of more OH^- thereby producing more corrosion products such as $Fe(OH)_2$ (Liu, 1996). Availability of sufficient oxygen also

influences the progress of cathodic reactions of reinforcement corrosion. In the absence of sufficient oxygen, even after depassivation, corrosion will not progress due to cathodic polarisation (Ahmad, 2003 and Sohail, 2013). The rate of oxygen supply is dependent on concrete pore system, the degree of pore moisture content and cover thickness. This means that concrete quality and cover thickness are more significant to corrosion propagation than exposure environment.

2.8.2 Concrete quality

Early deterioration in RC structure is often associated with the ingress of deleterious agents from the exterior, and the cover concrete quality largely controls its durability (Beushausen and Alexander, 2008). A more permeable concrete is usually regarded as a low quality concrete with well-connected large pores that can quickly transmit oxygen and moisture which enhance corrosion activities. For a low permeable concrete, the aggressive substances would find it difficult to access the reinforcement and thus the possibility of the reinforcement corrosion could be greatly reduced.

The permeability of concrete is mainly controlled by the porosity of the cover concrete and its pore size distribution, which depends on the w/b ratio. A lower w/b ratio decreases the concrete permeability, which in turn reduces oxygen diffusion. However, a lower w/b ratio does not, by itself assure low permeability in concrete. For example ‘no fines’ concrete can have a low w/b ratio and yet be permeable. Hence, in addition to lowering the w/b ratio, the concrete must be properly proportioned and compacted to produce a less permeable concrete.

Corrosion activity in carbonated SCM blended concretes (FA and BS) has been reported by Arachchige (2008). Despite the improvement in permeability of FA and BS blended concretes, Arachchige (2008) observed an increase in the corrosion rates of FA and BS concretes compared to PC concrete. Similar observation was also reported by Parrot (1994), Tuutti (1982), Arachchige (2008); Dhir, Jones and Mccarthy, (1992). The increase in corrosion current density of carbonated FA and BS blended concretes was attributed to the reduced pore solution alkalinity and increased ionic mobility due to PC partial replacement, pozzolanic and carbonation

reactions. The pozzolanic and carbonation reactions of these binders (FA and BS) tend to marginally reduce the ionic concentrations of the pore fluid particularly calcium ions (Dhir, Jones and Mccarthy, 1992; Arachchige, 2008; Diamond, 1981). The reduction in the ionic concentration of the pore solution reduces the average distance between the ions which in turn increases the ionic mobility. Consequently, the resistance to ionic movement is reduced and the corrosion in carbonated FA and BS blended concretes are increased (Arachchige, 2008).

Morandeau, Thiéry and Dangla (2014); Thiery *et al.* (2005); Borges *et al.* (2010) attributed the increased corrosion activities of FA and BS blended concretes to increased coarse capillary porosity due to pozzolanic and carbonation reactions compared to PC concrete. Also, poor curing adversely affects the concrete microstructure, resistivity and pore solution alkalinity of FA and BS concretes (Arachchige, 2008).

2.9 Corrosion Propagation Assessment Techniques

Corrosion of reinforcement is not visually evident until the damage appears at the external surface of the reinforced concrete with a sign of corrosion spots, cracks, delamination and spalling of the cover concrete (Liu, 1996). To estimate the service life of RC structure, assessment of the concrete needs to be carried out to ascertain the present level of its deterioration. There are many assessment techniques for laboratory and field corrosion surveys of reinforcement corrosion in concrete broadly classified into non-destructive and destructive techniques (Guangling & Ahmad, 1998). The application of a technique depends on the expected accuracy and characteristic of the concrete structure. The complex nature of the corrosion process has made the development of accurate corrosion monitoring device difficult and the use of different devices on the same structure has led to variability in corrosion measurements (Liu, 1996).

Electrochemical techniques have been successfully used for measuring the corrosion rate of reinforcing steel in concrete for both laboratory and field concretes. The techniques include half-cell potential, electrical resistivity and linear polarisation resistance methods. They are regarded as the most reliable non-

destructive techniques in field and laboratory corrosion measurements (Guangling & Ahmad, 1998). Papavinasam (2008) explained the main advantages of electrochemical techniques which include:

- Sensitivity to low corrosion rate
- Short experimental duration
- Well established theoretical understanding of the corrosion mechanisms

Guangling and Ahmad (1998); Song and Saraswathy, 2007; Ahmad (2009) reported that most of the electrochemical techniques do not give a direct measurement of the corrosion rate. The gravimetric mass loss method overcomes some of these challenges in spite of being a destructive method of assessing and measuring corrosion rate in reinforcement steel. Though, it gives accurate results, it is not sensitive to low corrosion rate measurement (Guangling & Ahmad, 1998). However, it is the most accurate method compared to other electrochemical methods that use sophisticated equipment.

2.9.1 Electrochemical techniques

(a) Half-cell potential (HCP) method

Half-cell potential (HCP) is a non-destructive electrochemical test used widely as a qualitative index for ascertaining whether or not reinforcement is likely to be corroding, and also for obtaining a contour plot to delineate anodic and cathodic portions of the RC structure under investigation (Polder, 2001; Ahmad, 2003). It involves measuring the electric potential of the embedded steel bar against a standard reference electrode. Half-cell potential is a standardized method recognized for the corrosion assessment of reinforced concrete structures. The method identifies the regions where corrosion activity is probable as described in ASTM C876: 1991 and the evaluation criteria is related to the typical reference electrodes such as calomel, copper/copper sulphate and silver/silver chloride electrodes. This criterion of probable identification of corrosion regions is most suited for localized corrosion such as pitting corrosion. Its use in uniform corrosion induced by carbonation often leads to inconclusive results.

The limitation of this method is that the actual corrosion rate cannot be quantified due to the effects of oxygen polarization, concrete porosity and resistivity of the concrete (Alonso, Andradel and Gonzalez, 1988). However, the method has received wide acceptability for determining the probability of corrosion in RC structures (Alonso, Andradel and Gonzalez, 1988).

Interpretation of half-cell potential test results is usually carried out as per the ASTM C 876 guidelines (Table 2.4). Note that the application of Table 2.4 is only useful for interpreting HCP results when $Cu/CuSO_4$ (CSE) reference electrode is used, the interpretation is different for other electrodes.

Table 2:4 Probability for corrosion (ASTM C876: 1991)

HCP related to CSE electrodes (mV)	Probability of active corrosion
< -350	90%
-350 to -200	50%
> -200	10%

(b) Linear polarization resistance (LPR) method

This is a very widely used electrochemical method for quantitative determination of instantaneous corrosion propagation in concrete. The main feature of this approach lies in the relationship between measured polarization resistance and the corrosion current density of the reinforcing steel in concrete. The Stern-Gary equation expresses the instantaneous corrosion rate as given in Equation 2.42 for a simple corroding system (Andrade and Alonso, 1996).

$$I = \frac{\beta}{R_p} \qquad 2.42$$

$$\beta = \frac{\beta_a \beta_c}{2.3(\beta_a + \beta_c)} \qquad 2.43$$

where β is a constant with a voltage unit and can be theoretically determined by the cathodic and anodic Tafel slopes (β_a and β_c are anodic and cathodic Tafel slopes in mV/dec) illustrated in Equation 2.43. I is the applied current (μA) and R_p is the polarisation resistance (Ω), which can be calculated as:

$$R_p = \frac{\Delta E}{\Delta I} \quad 2.44$$

$$i_{corr} = \frac{\Delta I}{A} \quad 2.45$$

where ΔE is the shifting in potential due to polarised voltage (E_{cor}) of the corroding system (mV), ΔI is the corresponding current change due to shift in potential applied (μA). A is the polarised steel area (cm^2) and i_{corr} is the corrosion current density ($\mu A/cm^2$). Hence, i_{corr} can be calculated using Equation 2.45.

The polarisation resistance technique is based on the assumption that when a small polarising potential is applied to a steel solution interface, the system must be allowed to settle to a steady state before the current response is recorded (Gulikers 1999). Moreover, failure to achieve a steady state can result in overestimation or underestimation of corrosion rate which depends on the initial time in the transient region at which the current is recorded. In concrete, the value of β is usually taken as 25 mV to 52 mV for a particular electrochemical cell. However, these values have been widely used in both laboratory and field corrosion studies (Guangling & Ahmad, 1998). Gowers *et al.* (1994) cited in Guangling & Ahmad (1998) developed a programmable linear polarisation meter for on-site corrosion measurement. This development has made LPR method more widely applied for estimating corrosion rate.

Additionally, linear polarisation method is relatively simple, quick and a practical technique of evaluating corrosion rate of reinforcing steel in both new and existing concrete structures without necessarily destroying the concrete (Proverbio, 1999). It can also adequately reflect the change of corrosion rate of reinforcing steel in concrete (Guangling & Ahmad, 1998). Linear polarisation resistance is mainly used for uniform corrosion, the application of it in localised/pitting corrosion has not been successful due to its significant variation with time (Andrade, 2008). Gulikers (1999) mentioned voltage drop (IR) across the electrodes, and rapid fluctuating corrosion potentials as factors that affect the successful application of polarisation resistance technique in practice. Other factors include localised corrosion, uncertainty about polarised areas and perturbation of electrodes by small direct

current polarisation necessary to obtain a measurable response. These mitigating factors when not properly attended to in practice can consequentially underestimate or overestimate the corrosion propagation period in concrete thereby making modeling of service life complex.

Several commercial devices have been developed based on the polarisation resistance technique for estimating the corrosion rate on reinforced concrete structures. Nevertheless, the performance of these instruments has not been satisfactory due to the complexity in the steel and concrete system. This has made electrochemical measurements difficult to make, and the interpretation of its output data remains ambiguous and uncertain (Proverbio, 1999).

2.9.2 Gravimetric mass-loss technique

The gravimetric mass loss method is a destructive method of obtaining corrosion rate in concrete structures. The method is commonly applied with the intent of overcoming some practical difficulties usually experienced when interpreting the measurement results obtained by electrochemical means. Tuutti (1982) regarded the method as suitable for investigating corrosion rate in the propagation phase and for determining the amount of steel radius loss that results in cover concrete damage. The data obtained can be easily used in developing a service life model. However, due to its destructive nature, the method is only suitable for laboratory investigation of corrosion propagation in concrete.

The gravimetric mass-loss method, though simple, offers solutions to most of the shortcomings usually experienced by the electrochemical techniques. Tuutti (1982) used this method to study the corrosion rate of steel in cracked and un-cracked concrete cover and the results compared very well with other methods.

2.9.3 Concrete resistivity

The resistivity of concrete describes its ability to withstand the movement of corrosion current. Concrete resistivity is one of the major factors that influences corrosion rate in concrete. It is an indirect parameter that depends mainly on the RH of the concrete pores, temperature, and binder type as well as the ionic

concentration of the pore solution (Ahmad, 2003). The chemical composition of the pore structure also affects the resistivity.

The electrical resistivity of concrete has been studied extensively as indicated in the literature, and most of the measurements obtained are incomparable with one another. This has been attributed to the different experimental procedures and electrochemical cells (Alonso, Andradel and Diez, 1998). The relationship between resistivity and corrosion rate is still scarce in the literature. Few research works that have been done on the relationship between resistivity and corrosion rate are more of chloride induced than carbonation induced corrosion. Most of resistivity studies had been conducted using accelerated corrosion method (partial immersion and impressed current) where samples are conditioned to a particular environment. The results can be different from those obtained when concrete samples are exposed naturally. The correlation between the resistivity of concrete samples exposed to natural environment and resistivity of conditioned concrete samples is still not known, and where such exist, the result cannot be generalized due to variability in the exposure conditions and heterogeneity of concrete (Andrade and Alonso, 1996). Therefore, resistivity study is an important aspect of corrosion study of inland RC structures.

Despite the importance of resistivity in corrosion studies, there is no standardised technique of measuring resistivity in concrete, apart from two probes and Wenner's method that consists of 4 probes as shown in Figure 2.12.
The Wenner's device uses alternating current with frequencies of 50 and 1000 Hz. The apparent resistivity (ρ) in Ω-cm is expressed as:

$$\rho = \frac{2\pi aV}{I} \qquad 2.46$$

where V is the voltage drop in Volts, I is the applied current in Amperes and 'a' is the electrode spacing in cm.

For low temperature and high relative humidity, especially during winter in cold regions, the alternating current frequency is usually increased to obtain a reasonable result (Polder, 2001). The result can be different when using the same equipment in a region like Johannesburg area where the winter period is usually dry with low temperature and relative humidity (Alexander, Mackechnie and Yam, 2007). This

makes calibration of the equipment an important process to ensure useful results. The calibration of the resistivity equipment can be difficult to perform considering the variability of the environment and heterogeneous property of concrete (Polder, 2001 and (Vennesland, Raupach and Andrade, 2007). Therefore, any calculated resistivity value may contain a considerable scatter (Vennesland, Raupach and Andrade, 2007). Errors up to 25% have been noted when using Wenner's resistivity method for field concretes, while less error (about 10%) has been reported for laboratory concrete specimens cast from the same mix and exposed to identical environment (Polder, 2001). This suggests that resistivity may not be a realistic parameter that can be included in a service life prediction model.

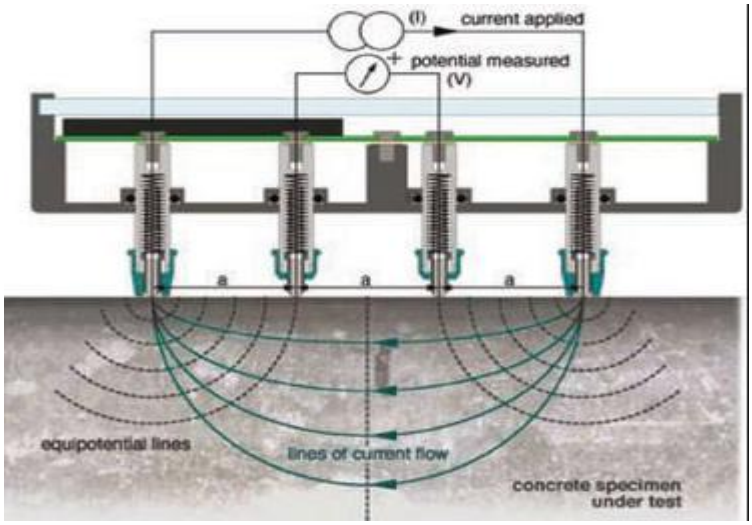

Figure 2:12 Photograph of four-probe Wenner's method for resistivity measurement (Photograph adapted from Proceq Resipod users manual)

Classification of the likelihood of corrosion occurrence in reinforcement, for non-saturated concrete in an environment can be obtained from the values given in Table 2.5 as proposed by Andrade & Alonso (1996). Electrical resistivity is an independent geometry parameter (Hornbostel, Larsen and Geiker, 2013) which is best suited when half-cell potential measurements indicate that corrosion is possible (Ahmad, 2003).

Table 2:5 Relationship between resistivity and corrosion risk
Andrade & Alonso (1996)

Resistivity (kΩ-cm)	Risk level
> 100 - 200	Very low corrosion rate in CO_2 contaminated
50 - 100	Low corrosion rate
10 - 50	Moderate to high corrosion rate
< 10	Resistivity is not the controlling variable

2.10 Effects of Corrosion on Concrete

Once reinforcement corrosion has initiated, its propagation is primarily controlled by the supply of oxygen, moisture and concrete quality (Tuutti, 1982). The length of the propagation stage is the time from onset of corrosion to a well-defined limit state. However, there are various damage indicators associated with different limit states in concrete and steel during corrosion propagation. These include (i) loss of bond strength between steel and concrete interface (ii) concrete cover cracking, spalling and delamination (iii) loss of significant reinforcement steel cross-sectional area with a consequent structural failure.

The increased steel surface roughness created by the corrosion causes an initial increase in the bond between reinforcement steel and concrete (Busba, 2013). The bond later reduces when the corrosion products migrate away from the corrosion site through the concrete pores and cracks (Lu, Jin and Liu, 2011). This creates more voids at the steel-concrete interface which consequently reduces the bond between the concrete and the reinforcing steel. The loss in the bond can also be explained by the loss of the reinforcement ribs to corrosion and lubricating effect of the flaky thick corrosion layer surrounding the original steel causing the reinforcement to slide within the space of its confirmment. (Pantazopoulou and Papoulia, 2001).

Deposition of corrosion products at the concrete pores causes corrosion-induced cover cracking. The deposition is assumed to occur in a relatively small and uniform ring-shaped volume located around the reinforcing steel (Jamali *et al.*, 2013). As a result of the limited pore size, deposition of solid corrosion products exerts an outward pressure on the surrounding concrete. As a consequence, tangential tensile

stresses are developed in the concrete surrounding the reinforcing steel. Once the tensile stresses from the corrosion products exceeds the tensile strength capacity of the concrete, it cracks at the concrete-steel interface and appear at the concrete surface as shown in Figure 2.13. The reinforcing steel radius loss that causes the concrete to crack is referred to as the critical amount of corrosion products which is also known as critical attack penetration (δ_r) in most literature.

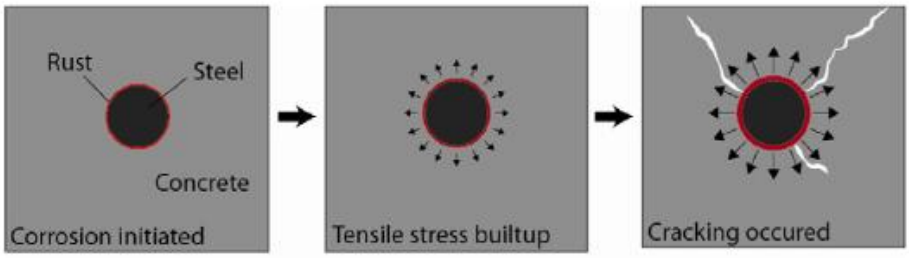

(a)

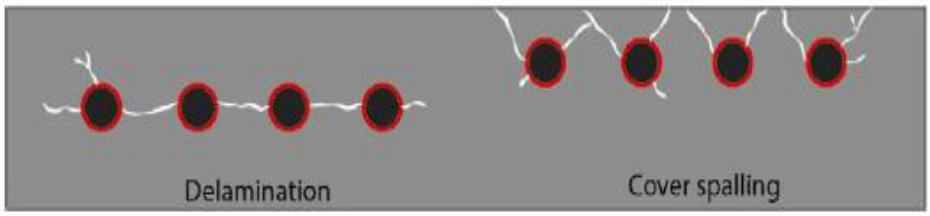

(b)

Figure 2:13 Corrosion-induced cover cracking in concrete (a) cracking mechanism (b) cracking modes

Regarding the effects of reinforcement corrosion on concrete, cracking of the cover concrete is the most important indicator that mark the end of service life of a RC structure. The time to cover cracking is a meaningful index of the intensity of the corrosive environment to which the RC member is exposed. Therefore, estimating this quantity is a necessary step in assessing the residual development capacity of a RC structure. It becomes necessary to investigate the underlying factors that influence the time to cover cracking in RC structure. These factors are (i) corrosion production rate (ii) amount of radius loss that causes cover concrete cracking and (iii) cracking time (time between corrosion initiation and cracking of the cover concrete).

2.11 Corrosion Steel Mass loss and Corrosion rate

In the propagation phase of corrosion, Faraday postulates that the mass of iron consumed over time is related to the amount of current that flows through the electrochemical corrosion cell. The equation supporting Faraday's postulation is given as:

$$\frac{dm_l}{dt} = \frac{IA}{nF} \tag{2.47}$$

$$m_l = \frac{IAt}{nF} \tag{2.48}$$

where m_l (g) is the mass of iron consumed, I (ampere) is the corrosion current, A (g/mol) is the atomic weight of the ions being dissolved, and F is the Faraday's constant taken as 96500 C/mol. n is the valency of the corrosion reaction which depends on the chemical composition of the reaction products usually taken as two assuming that the corrosion product is $Fe(OH)_2$. However, this assumption may not be valid since corrosion composition strongly depends on many factors e.g., ionic concentration of the pore solution, oxygen, and moisture supply which determine the composition of corrosion products. Therefore, the uncertainty of corrosion valency (n) may likely be the source of scatter usually observed between the corrosion rate measured by the electrochemical and gravimetric mass loss methods.

Moreover, integrating the right side of Equation 2.48 over time produces the total mass of iron consumed in the corrosion reaction. Faraday's law implies that at a constant corrosion rate, the dissolution of iron at the anode site increases with time.

In a more complicated case of variable corrosion current in an electrochemical cell, Liu and Weyers (1998) found that rate of corrosion production decreases with time (Pantazopoulou and Papoulia, 2001). This is because iron ions were found to be inversely proportional to the oxide layer thickness (Liu and Weyers, 1998). The governing equation is expressed in Equation 2.49 (Pantazopoulou and Papoulia, 2001).

$$\frac{dm_l}{dt} = \beta \int dt \tag{2.49}$$

where β is a function of corrosion current and is given as $3.328 \times 10^{-10} \pi d i_{cor}$ (note that i_{cor} (A/m^2) is the corrosion current, t (seconds) is the exposure time, and d (m) is the diameter of steel). m_l (kg/m) is the mass of corrosion products per unit length of anode. The solution of Equation 2.49 is expressed as:

$$m_l = (2\beta t)^{0.5} \qquad 2.50$$

Equation 2.50 can be used in estimating the corrosion mass loss and the corresponding corrosion time for a case of variable corrosion rate (particularly useful for estimating the time between the initiation and cracking of the cover concrete).

It is evident from the two postulations that the time to reach the critical value of mass loss using the square root model (Equation 2.50) will be longer than the linear model (Equation 2.48). Therefore, caution must be taken when interpreting the outcome of the two models, even though, the mass loss was assumed to be constant in the two models. The two models (Equations 2.48 and 2.50d) have been used in all published corrosion cracking models. The main parameters involved in the corrosion cracking process in concrete are evident from the two models; (i) steel mass loss required to initiate cracking (ii) rate of corrosion production and (iii) propagation or cracking time (time between corrosion initiation and cracking of the cover concrete).

Similar to corrosion rate, the steel mass loss parameter is complicated and depends on many factors such as the type of corrosion products formed, space available for deposition (concrete porosity), cover depth and material properties of concrete. Some of the main factors that influence the amount of radius loss required to initiate cracking are discussed further in section 2.12.

2.12 Factors affecting corrosion-induced cover cracking

There are many factors that affect the amount of corrosion products needed to crack cover concrete. The main important factors are cover concrete geometry (cover depth and steel diameter) and concrete quality. The two influencing factors are

discussed in this section, they provide a basic information desirable for modelling corrosion cracking time.

(a) Cover concrete geometry (cover depth and steel diameter)

The influence of cover concrete geometric parameters such as cover depth and reinforcement steel diameter on the amount of steel radius loss required to initiate a crack width of 0.05 mm on cover concrete was investigated by Alonso, Andradel and Diez, (1998). The limit state was defined as the appearance of a 0.05 mm crack which is barely visible to the human eye. It was found that, higher depth of cover needed a significant amount of radius loss (corrosion amount) to induce a surface crack on concrete. It was also pointed out that at a constant cover depth the higher the steel diameter, the lower the amount of corrosion products required to initiate cracking. This also applies to findings of Rodriguez *et al.* (1996); Al-Harthy, Mullard and Stewart (2011). However, this is contrary to observations made by Morinaga (1989) and Bazant (1979) where a large reinforcing steel diameter needed more corrosion products to induce cover concrete cracking. In the literature, the effect of reinforcing steel diameter corrosion amount necessary for cracking is inconclusive and can be investigated further.

The effect of cover depth on corrosion amount was also reported by Andrade, Alonso and Molina (1993). It was found that the amount of corrosion required to crack concrete increased by 48% when the cover depth was increased from 20 to 30 mm. This can be attributed to the fact that in a given concrete increasing the cover thickness increases the void spaces compared to a smaller concrete cover. This means that the amount of corrosion products required to cause crack is greater in a large cover thickness compared to a smaller cover thickness for the same concrete. Furthermore, thick cover concrete protects the reinforcement from corroding and extends the corrosion cracking time. Therefore, increasing the concrete cover depth improves structural durability (Lu, Liu and Jin, 2010).

(b) Concrete quality

Alonso, Andrade and Diez (1998) studied the effect of concrete quality on the amount of radius loss required for cover crack initiation and propagation. Reinforcing steels were embedded at both top, and bottom cast positions in concrete

made with 0.60 and 0.65 w/b ratios. It was found that for a constant reinforcing steel diameter and cover depth concrete specimens manufactured using 0.60 w/b ratio required a lesser amount of corrosion radius loss to initiate crack compared to specimens manufactured using 0.65 w/b ratio. This was attributed to the presence of large void spaces in the concrete specimens with higher w/b ratio as the void accommodate the corrosion products without inducing any tensile stress on the surrounding concrete. Alonso, Andrade and Diez (1998) also found that top cast concrete required more corrosion radius loss to induce a given crack width than bottom cast concrete. This was attributed to the extra void space created by the bleed water as it rises to the concrete surface.

Furthermore, corrosion products exert a higher pressure on the surrounding concrete due to availability of few voids to accommodate the corrosion products in concrete with low w/b ratio. It is generally understood that corrosion induced cracks are initiated when the induced stresses from the corrosion products exceed the concrete tensile resistance. This emphasises the significance of tensile strength in the corrosion cracking process of cover concrete.

Rashid *et al.* (2010) and Shanmugavadivu *et al.* (2014) investigated the effect of concrete tensile strength on corrosion cracking resistance and found that the latter increased with increase in concrete strength. This trend is similar to to the analytical study conducted by Lu (2010). It was reported that the cracking time increased when concrete tensile strength increased although, the increase in the cracking time was negligible. This was attributed to the simultaneous improvement in the elastic modulus of the concrete when the tensile strength increased. A similar trend was also observed by Liu (1996). Hence, concretes of higher strength grade may provide better resistance to reinforcement corrosion cracking initiation in concrete (Andrade et al. 2006). However, this is in conflict with the observations of Rodriguez *et al.* (1996) and Al-Harthy, Mullard and Stewart (2011), where an increase in concrete tensile strength reduced its resistance to cracking and shortened the cracking duration in a given concrete. The argument is that high strength concretes are usually characterised with fewer voids that require a lesser amount of corrosion to induce cracking. However, the weaker microstructure of a low strength concrete can allow localized crushing of the concrete around the reinforcing steel relieving

some of the induced tensile stress thereby lengthened the cracking time (Mullard and Stewart, 2009; Rashid *et al.*, 2010)

It is difficult to draw a definite conclusion from both assertions (influence of concrete tensile strength on the amount of corrosion products and cracking time), as it presents a challenge when strength is included as part of essential parameters in modelling the time to corrosion-induced cracks in concrete. However, the fact is that strength is not a near-surface property of concrete where deterioration occurs as it may be difficult to measure the strength of cover concrete since strength is a bulk property of concrete. Therefore, tensile strength may not be an appropriate property to substitute with concrete porosity in a corrosion-induced cover cracking initiation model.

2.13 Review of Some Existing Cover Cracking Models

In recent years, there have been increasing effort to quantify the damage progress in reinforced concrete due to steel reinforcement corrosion. This is of great importance in the structural assessment and residual service life estimation of existing RC structures.

Several models have been developed to predict time to corrosion induced cover cracking. Even though these cracking time prediction models usually have several input parameters, it is clear that the amount of radius loss required to initiate cover cracking is a function of other parameters which govern their outcome either in terms of time to attain a pre-defined limit state or its severity at a given time (Otieno, Beushausen and Alexander, 2011). The success in incorporating cracking time in the service life of RC structures will therefore depend on how accurately and realistically the amount of corrosion products required to crack a given concrete can be predicted. Some of the existing corrosion cracking models are reviewed in this chapter. They are categorised under empirical and analytical models.

2.13.1 Empirical corrosion-induced cover cracking models

Empirical models are based on the assumed direct relationship between two or more variables that define a system (Otieno, 2010). They are primarily based on regression analysis of experimental data and observations e.g., cracking time (t_{cr}) and steel radius loss are expressed in terms of the parameters deemed important. These parameters include material properties, cover geometric variables and corrosion rate (Jamali *et al.*, 2013). The experimental data which form the basis of deriving the empirical corrosion models are obtained under accelerated conditions (e.g. through using external impressed voltage or currents and partial immersion in chloride salt solution). Even though these methods of corrosion acceleration may not represent corrosion under natural environmental conditions, they show a basic understanding of the process that is involved in corrosion-induced cover cracking. Additionally, the results are obtained in a reasonable length of time. Some empirical corrosion-induced cracking models are presented:

(a) Rodriguez & Andrade's model (1990)

Rodriguez & Andrade (1990) studied the amount of steel radius loss needed to initiate a cover crack at the concrete surface in accelerated corrosion tests. A relationship between the corrosion current density and steel radius loss at cracking of the cover concrete was obtained as:

$$\delta_r = 0.0115 i_{cor}\left(t - t_i\right) \qquad 2.51$$

where δ_r (mm) is the reinforcing steel radius loss due to corrosion required for cracking, i_{corr} ($\mu A/cm^2$) is corrosion current density assumed to be constant and t-t_i = t_{cr} (years) is the time difference between corrosion initiation (t_i). t (years) is the total time from casting of the concrete to the time at which a first crack was observed on the cover concrete. 0.0115 is a conversion factor from $\mu A/cm^2$ (corrosion current density) to mm/year (corrosion rate). It can be observed from Equation 2.51 that the amount of radius loss required to crack the cover concrete depends upon the corrosion current density and time between the onset of corrosion and cracking of the cover concrete. Equation 2.51 is expanded to obtain the cover cracking time in years, expressed as:

$$t_{cr} = 86.96\left(\frac{\delta_r}{i_{cor}}\right) \quad 2.52$$

Equations 2.51 and 2.52 assume that i_{cor} is constant and it does not vary with time and environmental conditions such as relative humidity and temperature. The use of Rodriguez & Andrade' model in a new structure may not be feasible because obtaining i_{corr} and δ_r for the new structure may not be realistic. Moreover, other physical parameters that influence time to corrosion-induced cracking such as cover depth, reinforcing steel diameter and concrete material properties are not accounted for in this model.

(b) Alonso et al.'s model (1998)

Alonso, Andradel and Diez (1998) investigated the key parameters controlling the steel radius loss required to induce cover cracking in concrete under a uniform corrosion condition. The corrosion was accelerated by applying a constant current density of 100 μA/cm^2 through the reinforcing steel embedded in concrete manufactured using w/b ratios of 0.52, 0.60 and 0.65. The diameters of reinforcing steel bar used were 3, 8, 10, 12 and 16 mm at cover depths of 10, 15, 20, 30 and 50 mm respectively to produce different concrete cover depth/reinforcing stee diameter ratios (c/d). The data obtained from the accelerated corrosion experiment was used to develop an empirical model that can be used to estimate the steel radius loss required to produced a first visible crack width of ~ 0.05 mm. The empirical model is shown in Equation 2.53.

$$\delta_r = 7.53 + 9.32\,c/d \quad 2.53$$

where δ_r is the amount of steel radius loss (μm) needed to produce the first visible crack width of < 0.05 mm, while c (mm) and d (mm) are the cover depth and reinforcing steel diameter respectively. The model show a good linear relationship between radius loss and c/d ratio with a correlation coefficient of 0.92. However, the influence of concrete material properties is not accounted for by the model and can be a limitation to its pratical application.

(c) Rodriguez et al.'s model (1996)

Rodriguez *et al.* (1996) used experimental data obtained from accelerated corrosion experiments to develop a model that estimates the amount of steel radius loss required to initiate cover cracking in concrete. The corrosion was accelerated by applying a constant external current density of 10 μA/cm^2 and 100 μA/cm^2 through reinforcing steels of diameter 3, 8, 10, 12 and 16 mm embedded at a concrete cover depths of 10, 15, 20, 30, 50 and 70 mm respectively. The reinforcing steel and cover depths arrangement yielded various c/d ratios. The split tensile strength of the concrete ranged between 2.4 and 3.85 MPa. The corrosion data obtained from the experiment was modelled using regression analysis. The model shown in Equation 2.54 was proposed.

$$\delta_r = 83.8 + 7.4\frac{c}{d} - 22.6\, f_t \qquad 2.54$$

where f_t (MPa) is the concrete tensile strength. The experimental and model results showed that amount of steel radius loss required for cracking primarily depended on c/d ratio and quality of concrete (represented by the concrete split tensile strength). The model was developed using accelerated corrosion results. Its validation using data from natural corrosion tests is necessary. However, the Rodriguez et al model is currently used in DuraCrete though its validation using data from natural corrosion tests has not been conducted.

(d) Morinaga's model (1989)

Morinaga (1989) investigated the effect of material and geometric parameters on cracking pressure. For series 1, pressurised oil was used to induce crack on RC elements while series 2 was an accelerated corrosion test. The test concretes were hollow cylinders of 100 mm and 150 mm diameters and 100 mm high, reinforced singly with steel rods of diameters of 9, 19 and 25 mm. The test concretes were admixed with 0.5%, 1% and 5% calcium chloride (by weight of cement) and the systems were impressed with 1.5, 3, 6 and 12 V external voltage. The data obtained from the two experiments were combined to propose a model for estimating the mass of corrosion required to initiate cover cracking in concrete (Equation 2.55).

$$Q_{cr} = 0.602d\left(1 + \frac{2c}{d}\right)^{0.85} \qquad 2.55$$

The model was further developed to predict the time taken after corrosion initiation to corrosion cracking as shown in Equation 2.56.

$$t_{cr} = 0.022\, j_r^{-1}\left(\frac{2c}{d}+1\right)^{0.85} \qquad 2.56$$

where Q_{cr} (g/cm^2) is the critical mass of corrosion products required to initiate cover cracking, j_r (g/mm^2/year) is the rate of corrosion production which is assumed to be constant throughout the corrosion process. While the t_{cr} (years) is the cover cracking time.

One of the experimental objectives was to investigate both stress and strain properties of concrete at the time of the first crack. However, stress and strain properties were not directly reflected in the model. In other words, the model does not account for the mechanical properties of the concrete which would significantly affect the time to corrosion cracking of concrete. Hence, the model may not be generalised to predict the time to corrosion–induced cover cracking of concretes with different mechanical properties.

(e)Torres-Acosta and Sagues's model (2004)

Torres-Acosta and Sagues (2004)experimentally investigated the critical steel radius loss required to crack concrete in localised and uniform corrosion using a cylinder and prismatic concrete samples. For the series 1, concrete cylindrical samples were produced with a reinforcing steel of diameter 21 mm at cover depths of 27.5 mm to 65.7 mm. The series 2 were made up of prismatic concrete samples, produced with reinforcing steel diameters of 6 mm and 13 mm at the cover depth of 13-39 mm. The concrete samples were mixed at w/b ratios of 0.47, 0.49 and 0.51 and had compressive strengths that ranged between 40-53 MPa. The test concretes were admixed with 2% calcium salt by weight of cement. The corroding lengths of the reinforcing steel ranged between 8-390 mm. The prepared concrete samples were impressed with 100 µA/cm^2 external current and were put in a controlled humidity environment of about 85% and observed daily for crack appearance.

From the experimental data, an empirical model was proposed for estimating the amount of corrosion required for cracking as a function of c/d and c/L_s ratios as shown in Equation 2.53.

$$\delta_r = 0.011\left(\frac{c}{d}\right)\left(\frac{c}{L_s}+1\right)^n \qquad 2.57$$

where L_s is the length of the corroding part of the reinforcing steel, and 'n' is exponent factor that depends on the shape of the laboratory concrete specimen (cylindrical or prismatic shape).

It is evident from Torres-Acosta and Sagues's model that concrete material properties are not accounted for and this presents a limitation in predicting a reliable service life for concrete with different characteristics. Also, the model was developed using accelerated corrosion results, validation of the model is necessary using data from natural corrosion tests.

2.13.2 Analytical corrosion-induced cover cracking models

The analytical corrosion cover cracking models are primarily based on the concepts of solid mechanics *(Jamali et al*., 2013). The theory is related to the mechanics of cracking where an input variable i_{cor} describes the corrosion process. However, the chemistry and electrochemistry of these corrosion phenomena are treated in a practical manner (Jamali *et al.*, 2013). Thus analytical models are semi-empirical models. The corrosion cover cracking analytical models involve modelling corroding reinforced concrete structures as a thick-walled cylinder (Figure 2.14) acted upon by internal stresses created by the advancing corrosion products (Liu, 1996; Liu & Weyers, 1998).

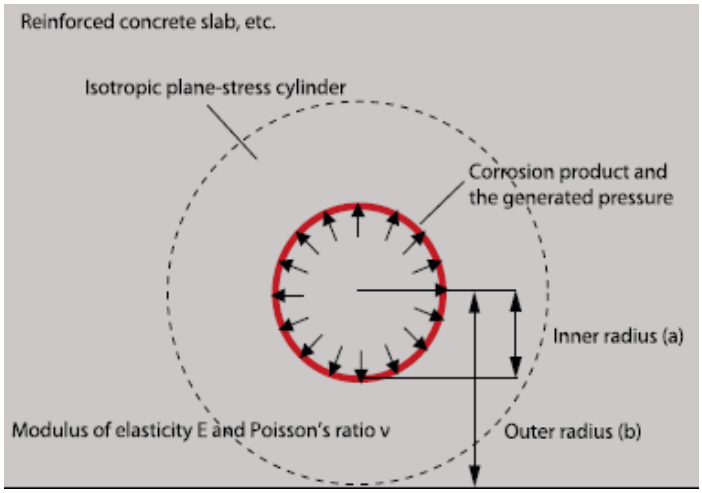

Figure 2:14 Corrosion-induced cracking - a thick-walled cylinder approach (Jamali *et al*., 2013)

The thick-walled cylinder approach is based on these assumptions:

i. Corrosion is uniform along the corroding reinforcing steel with a uniform distribution of stresses around the corroding reinforcing steel.

ii. The presence of a porous zone around the steel reinforcment (zone around the steel reinforcement which corrosion products must fill before inducing internal stresses on the surrounding concrete). Park & Pauay (1975) reported on the presence of a soft and spongy porous layer of concrete around the steel reinforcing bars caused by bleed water under coarse aggregate particles and the steel reinforcement.

iii. The volume expansion caused by corrosion products creates strain only in the surrounding concrete while strain in the reinforcing steel is neglected. This assumption seems to be reasonable because Young's modulus of steel is about one order of magnitude higher than that of concrete.

iv. The mechanical properties of concrete adjacent to the steel reinforcing bars are assumed to be the same as those of the bulk concrete.

v. Cracks are assumed to occur on the concrete ring when the tensile stresses in the circumferential direction at every part of the ring have exceeded the concrete tensile strength.

The following analytical corrosion cracking models are reviewed:

(a) Bazant's Model (1979)

Based on a comprehensive mathematical formulation of the corrosion process in reinforced concrete, Bazant (1979) developed an analytical model for estimating the time to corrosion-induced cracking of the cover concrete. The model is expressed in Equations 2.58 and 2.59. The model can be used to estimate cracking time when reinforcment spacing < 6d.

$$t_{cr} = \left(\frac{1}{\rho_r} - \frac{1}{\rho_s} \right)^{-1} \frac{f_t c k'}{s j_r} \qquad 2.58$$

$$k' = \frac{2d^3}{s^2 E_{ef}} + \frac{d}{E_{ef}} (1 + \upsilon_c) + \frac{d^3}{4c(c+d)E_{ef}} \qquad 2.59$$

where t_{cr} (s) is time to concrete cracking, jr (g/mm^2/year) is the rate of corrosion production per unit area, c (mm) is the cover depth, ρ_r (kg/m^3) is the density of corrosion product, ρ_s (kg/m^3) is the steel density, k' (mm/MPa) is the hole flexibility. d (mm) is the steel diameter, s (mm) is the spacing between reinforcements, υ_c is the poisson's ratio and E_{ef} (MPa) is the effective modulus of elasticity of concrete

Bazant (1979) proposed other model that can be used to estimate the time to corrosion spalling and delamination in concrete (Equation 2.60).

$$t_{cr} = \left(\frac{1}{\rho_r} - \frac{1}{\rho_s} \right)^{-1} \frac{f_t k' (s - d)}{s j_r} \qquad 2.60$$

The increase in steel diameter was estimated by applying a uniform pressure around the reinforcing steel assuming concrete to be homogeneous elastic material, and corrosion rate is time-invariant. However, these assumptions may not be realistic in practice due to the heterogeneity of the concrete material. Moreover, Bazant's

models are comprehensive, simple and can be applied to estimate the steady-state corrosion of laboratory RC samples.

In an attempt to improve the Bazant' models, Newhouse & Weyers (1996) investigated its prediction capability. They found that Bazant's models significantly underestimated the time to concrete cracking when compared to the experimental cracking times. The underestimation was attributed to (i) the presence of voids and microcracks surrounding the reinforcing bars which act as repositories for the corrosion products (ii) the variation in corrosion rate over time due to varying exposure conditions and build-up of layers corrosion products.

Liu (1996); El Maaddawy & Soudki (2007) and Lu et al. (2011) reworked Bazant's model using a much simpler description of corrosion rate and assuming a porous zone around the reinforcing steel. A good agreement was obtained between their predictions and the experimental values when the porous zone was accounted for.

(b) Liu's model (1996)

Liu (1996) used the concept of a thick-walled cylinder to analytically derive a relationship for estimating the critical mass of corrosion products required for cover cracking as follows:

$$W_c = \rho_{corr}\left[\pi\left(\frac{cf_t}{E_e}\left(\frac{a^2+b^2}{b^2-a^2}+\upsilon\right)d_o\right)d+\frac{m_l}{\rho_{st}}\right] \quad 2.61$$

$$a = 0.5d + d_o \quad 2.62$$

$$b = c + a \quad 2.63$$

$$E_e = \frac{E_c}{1+\varphi_c} \quad 2.64$$

where W_c (g) is the critical mass of corrosion products required to crack the cover concrete, a and b are the inner and outer radii of the corroded steel as shown in Figure 2.14. The parameters ρ_{corr} (g/mm^3), ρ_{st} (g/mm^3), c (mm), f_t (MPa) represent the density of corrosion product, the density of steel, the cover depth, tensile strength. The parameters υ, d_o (mm), m_l (g), d (mm) and E_e (MPa), the concrete Poisson's ratio, thickness of porous interfacial zone, mass of steel loss to corrosion,

diameter of steel and effective elastic modulus of the concrete respectively. The E_c (MPa) and φ_c represent the concrete elastic modulus and the creep coefficient respectively.

The critical mass of corrosion products per unit length required to crack the cover concrete is shown by the model to be mainly influenced by the cover depth, steel diameter, elastic modulus of the concrete, tensile strength and properties of the porous zone. The model was extended to estimate the time to cover cracking given as:

$$t_{cr} = \frac{W_c^2}{2k_p}$$

2.65

where W_c (g) is the critical mass of corrosion products required to crack the cover concrete, t_{cr} (years) is the time to cover cracking. k_p is the rate of corrosion product which is related to the rate of steel mass loss expressed in terms of corrosion current density, steel diameter and type of corrosion products.

$$k_p = 2.59x10^{-6}(1/\alpha)\pi d i_{cor} \qquad 2.66$$

where α is related to the types of corrosion products and i_{corr} ($\mu A/cm^2$) is the annual mean corrosion current density. The model accounts for the influences of voids, microcracks surrounding the reinforcing steel and the variable corrosion rate on cracking time of cover concrete. These considerations make its predictions reasonable and comparable to experimental data.

However, even though, Liu' predictions agree well with experimental observations, its non-linear variable rate of corrosion and non-compliance with Faraday's law of electrolysis creates a marked difference between its predictions and other accelerated tests. Chernin & Val (2011) and Pantazopoulou and Papoulia (2001) investigated the accuracy of Liu model using accelerated tests. They found that Liu's predictions were 2 - 4 times longer than the linear models by the accelerated tests. Additionally, Liu's model may not be practical as it is too complicated to be conveniently used by engineers. It requires much input information that may be difficult to obtain in practice. However, it has the advantage of incorporating the theory of corrosion production with time.

(c) El Maaddawy & Soudki's model (2007)

In an attempt to further account for the effect of concrete characteristics on cracking time of cover concrete, El Maaddawy & Soudki (2007) used thick-walled cylinder theory to proposed a modified analytical cracking model shown in Equation 2.63.

$$t_{cr} = \left[\frac{7117.5\left(d + 2\delta_o\right)\left(1+\nu+\psi\right)}{i_{cor}E_{ef}}\right]\left[\frac{2cf_t}{d} + \frac{2\delta_o E_{ef}}{\left(1+\nu+\psi\right)\left(d+2\delta_o\right)}\right] \quad 2.67$$

$$\psi = \frac{1}{\frac{c^2}{d+2\delta_o} + c} \quad 2.68$$

where c (mm) is the cover depth, f_t (MPa) is the tensile strength of the concrete, υ is the poisson ratio, E_{ef} is the concrete elastic modulus (MPa), d (microns) is the initial diameter of the reinforcing steel. δ_o (microns) is the thickness of the porous layer (zone around the steel reinforcement which corrosion products must fill before inducing internal stresses on the surrounding concrete). It is evident that the porous layer is mainly dependent on the concrete quality which can be measured using a concrete characteristic parameter that relates to near-surface concrete.

2.14 Corrosion Cracking Control Parameters

It is understood that various factors affect the corrosion-induced cracking of concrete which has led to the development of several prediction models. Some empirical and analytical models were highlighted and discussed in Section 2.12. This section discusses the model control parameters that are common to both empirical and analytical cracking models mentioned in Section 2.12.

2.14.1 Corrosion rate

The corrosion rate is an important parameter that influences corrosion cracking in concrete. It varies with environmental conditions e.g. oxygen, moisture, and temperature. The alkalinity of concrete pore solution and concrete penetrability also

contribute to variation in corrosion rate. This later parameter is affected by numerous factors which include concrete quality, cover depth, and environmental conditions. The reaction kinetics of the corrosion process may slow down over time due to the formation of corrosion product layers that render part of the steel surface inaccessible for electrochemical reactions. In some models (Liu, 1996; Balafas & Burgoyne, 2010; Lu et al., 2011), it is reflected that the production rate of corrosion products is inversely proportional to the amount of corrosion products. This hypothesis was criticised by Chernin & Val (2011) who found that rate of corrosion production is proportional to the amount of corrosion products and inversely proportional to the cracking time.

However, the natural corrosion rate in structures is typically in the order of 1 $\mu A/cm^2$ whereas corrosion-induced cracking experiments are usually performed using impressed anodic currents in the range of 10 to 100 $\mu A/cm^2$ or higher. Such severely accelerated conditions do not reflect the actual site conditions, and there may be possible damage to concrete microstructure (Jamali et al., 2013). In all the models an increase in corrosion rate reduces the cracking time for a given concrete since corrosion rate appears explicitly in the denominator of both empirical and analytical models.

2.14.2 Critical amount of corrosion products

This is usually referred to as the amount of corrosion products required to initiate concrete cover cracking. In some literature, it is referred to as the amount of steel radius loss or steel section loss (radius loss multiply by a factor of 2) that induces cover cracking while others use the term, 'attack penetration' that induces concrete cover cracking. In all the cracking models considered in this review, it is observed that the cracking time increases with increase in the critical amount of corrosion products. The critical amount of corrosion products is a relevant parameter in estimating the time to corrosion cracking and residual service life of RC structures. It is being affected by the composition of corrosion products and thickness of corrosion accommodating region (pores within the steel-concrete interface) which most of the corrosion cracking models do not considered especially the empirical

cracking models. Few analytical studies considered the thickness of the corrosion accommodating region to be in the range of 10 to 20 µm, although, more extreme range of 2 to 180 µm have been reported in literature (Jamali *et al.*, 2013).

While it is well understood that corrosion products may move through pores and voids and they exert no pressure before these pores and voids are filled with corrosion products, Jamali et al. (2013) disputed this idealisation of a cylindrical gap around the reinforcing steel. The argument was that the thickness of the corrosion accommodating zone cannot be measured as it does not physically exist and it does not have a clearly defined border with the bulk concrete. Therefore, it may be difficult to draw the line between the porous zone and bulk concrete.

Additionally, the porosity at the steel-concrete interface may significantly vary around the reinforcing steel. The top side of the reinforcing bar is usually denser than the bottom side due to the bleed water being trapped at the underside of reinforcement bar (Jamali *et al*., 2013). Therefore assuming a constant thickness for the porous zone may not be reasonable if it exists. A reasonable assumption is that corrosion products diffuse through the concrete capillary pores and air voids which can be measured using a parameter that is related to the fluid transport properties of concrete. However, it is pertinent to note that in many empirical prediction models, the phenomenon relating to kinetics and chemistry of corrosion products deposition have been ignored. Such studies are important for the development of a comprehensive service life model.

2.14.3 Cover concrete geometrical parameters

The cover concrete geometric parameters include cover depth (*c)*, reinforcing steel diameter (*d)* and spacing (*s)*. The common geometric parameters mostly mentioned in the literature are cover depth and reinforcing steel diameter especially in the empirical and analytical models. However, in corrosion-induced cracking studies based on Finite Element Method, the reinforcement spacing can be included to account for the effect of reinforcement confinement (Balafas and Burgoyne, 2010).

It is generally understood that the cover depth strongly influences the corrosion process in various ways such as (i) movement of deleterious substances within the

concrete, (ii) repositories for the corrosion products. Moreover, all the experimental and analytical investigations agreed on a common trend in terms of increasing or decreasing the cover depth. For a given concrete, the corrosion amount required to initiate a cracking and cracking time increased with increase in cover depth. This trend was observed in both empirical and analytical models. All the empirical models mentioned in this study explicitly include cover depth as a parameter.

The models also consider the influence of reinforcement diameter. Most of the experimental investigations indicated that the use of larger reinforcement diameter accelerates cracking as reflected in their proposed models. Out of the empirical models considered in this study, only the Morinaga's model predicts extended cracking time with an increase in reinforcing steel diameter. Based on this controversy, it is difficult to make a definite conclusion about the influence of reinforcing steel diameter on corrosion cracking process in concrete. Reinforcement spacing influences the mode of concrete deterioration as proposed by Bazant (1979). Bazant's model suggests that increasing spacing more than six times diameter of the steel can lead to concrete spalling instead of cracking. Apart from Bazant's model none of the empirical and analytical models explicitly include a spacing parameter in their models.

2.14.4 Material properties of concrete

Corrosion cracking occurs when the capillary pores and air voids around the reinforcement bar are filled with the corrosion products, and the advancing pressure from the corrosion products exceeds the tensile strength capacity of the concrete. Thus, crack formation depends not only on the amount of corrosion and type of corrosion products formed but also concrete characteristics such as the tensile strength and elastic modulus.

Most of the present analytical models considered the effect of tensile strength on cover cracking process. However, few empirical models illustrated the effect of tensile strength on the amount of corrosion products required for cracking. The Rodriguez' model suggests that the radius loss required to induce cracking decreases with an increase in tensile strength. This was as a result of experimental

investigation where cracking was observed to occur faster in higher tensile strength (high quality) concrete than a lower tensile strength (low quality) concrete. This was probably due to the higher amount of pores and air voids in a lower quality concrete which acts as repositories for the diffusing corrosion products and thus relaxes the internal stresses (Rodrigu*ez et al*., 1996). However, other studies such as Liu (1996) and Mullard and Stewart (2009) reported a slight increase in cracking time with an increase in tensile strength of concrete. While some other studies do not recognise any effect of concrete tensile strength or have observed inconsistent effects (Jamali *et al.*, 2013). Most analytical models suggest that the increase of tensile strength leads to an extension in cracking time when other parameters are kept constant.

Concrete strength is an age-long concrete characteristic parameter that is readily available on site. However, its use as a durability indicator for estimating concrete service life is questionable. This is because cover cracking occurs at the surface of concrete and therefore a parameter that relates to the near-surface concrete chracteristics will be reasonable to predict its resistance to cracking.

The adequacy of strength in predicting concrete deterioration that occurs at the concrete surface has been challenged severally in the literature. Concrete strength is a bulk property of concrete that measures the core resistance of concrete to stress without failure (Perrie, 2009). Therefore, concrete strength may not be a right parameter to illustrate a corrosion-induce cover cracking process. An appropriate parameter for illustrating the cracking process in concrete will be the fluid transport parameters which is a dominant mode of concrete deterioration. Fluid transport properties of concrete quantify the size and amount of pores as well as given an indication of their interconnectivity. Hence, it can be used as an input parameter to predict corrosion-induced cracking process in concrete.

2.15 Summary of the Previous Corrosion-induced Cracking Models

The empirical models investigated are based on relatively simple mathematical expressions derived from regression analysis of their corrosion experimental data; while the analytical models are based on mathematical expression derived from

mechanics of corrosion cracking. The analytical models involve more parameters than the empirical models. The involvement of many parameters in analytical models can be an advantage. However, some shortcomings are observed with the models which were similarly observed with the empirical models. The observations are listed as follows:

- The influence of binder type on the corrosion-induced cracking in concrete is not accounted for in any of the models. It is understood that different binders do not have the same concrete characteristic due to differences in their chemistry, hence, the variation in their corrosion cracking performance should be expected and accounted for in a model. For example Parrott (1994) found that concrete blended with slag required a larger amount of corrosion products and a shorter carbonation-induced corrosion cracking time compared to plain PC concrete of the same w/b ratio, cover depth and reinforcement diameter. This is similar to the observation made by Tuutti (1982).

- In most of the models uniform corrosion was assumed irrespective of their corrosion type. This is because analysing the amount of corrosion products required to cause cracking in a localised corrosion is a complex task compared to a uniform corrosion. Corrosion induced by using chloride admixtures is noted to be a localised corrosion with a larger steel loss area compared to uniform corrosion which is a feature of carbonation-induced corrosion. Therefore, a model built using localised corrosion data for carbonation-induced corrosion may underestimate the cracking process in a concrete.

  Moreover, admixing chloride to a fresh concrete to accelerate the corrosion may likely alter the chemistry of the concrete pore solution, porosity and the corrosion morphology (J*amali et al*., 2013). Impressed currents upset the time-related effects of transport, saturation, and precipitation of the corrosion products. Thus, it is suggested that a proposed model should be developed based on the specific agents that commonly cause corrosion deterioration in a particular environment. For example, in inland environment, carbonation seems to be predominant, therefore a corrosion cracking model that is based on carbonation as a means of corrosion inducement will be reasonable; while

chloride-induced corrosion cracking model will be appropriate in coastal environment.

- It is equally observed that none of the models accounts for the influence of concrete exposure environment, although this is not surprising since most of the models are built using experimental data from accelerated corrosion tests. However, this may limit their application in practice.
- Most data used to develop the corrosion empirical models are obtained from accelerated corrosion experiments with higher corrosion rates than what is obtainable in natural corrosion. Correlating such predictions with other predictions from natural corrosion may present a challenge. Even though accelerated corrosion test gives an understanding of the corrosion-induced cracking process, using their model to estimate the amount of corrosion products required for cracking in the natural environment may lead to a biased result. Therefore, data from natural corrosion test is appropriate to develop a generalised model that can be used to estimate the amount of corrosion required for cracking in a real RC structure, data from natural corrosion test is be suggested.
- There are variations in the input parameters of all the models. Amongst all the parameters, the corrosion rate is prominent in all the corrosion cracking models. This is in agreement with the fundamental concept of corrosion expressed by Faraday's law which says that the propagation period is proportional to the critical amount of the corrosion products; while propagation period is inversely proportional to the rate of corrosion (Andrade, Alonso and Molina, 1993). In the empirical models, the amount of corrosion products required for cracking variable is related to the cover depth and reinforcement diameter. This is with an assumption that the amount of corrosion required to initiate cracking is primarily determined by cover depth and reinforcement diameter. On the other hand, analytical models use more refined formulations that include concrete mechanical properties, geometric variables, and thickness of steel-concrete interface to express the amount of corrosion required for cracking. The individual effect of these influencing parameters on the overall model predictions can then be responsible for the scatter.

- The use of assumed porous zone thickness in analytical solutions is also questionable. It is a fitting parameter that has no direct evidence of existence to indicate its appropriateness neither can it be measured experimentally. It is suggested that a parameter that quantify the amount of pores and their connectivity in concrete be used instead.
- Additionally, the pore spaces available to accommodate the corrosion products before leading to expansive pressure may vary considerably in reality. This depends on the pore network system of cover concrete and the presence of microcracks particularly the bleed-water zone. Concrete pore network system is a function of concrete compositional parameters e.g., w/b ratio and binder type which determines concrete characteristics. Therefore, it is more important to include a concrete characteristic parameter that relates to the near surface properties of concrete where cracking occurs. Such parameter should be able to adequately quantify the pore network system of concrete and be sensitive to binder type and w/b ratio.

2.16 Summary

This literature review presented an overview of concrete composition and its effect on concrete durability. The electrochemical principles of corrosion and mechanisms of steel corrosion in concrete were discussed in two stages namely; corrosion initiation and propagation in concrete. The focus was on carbonation-induced corrosion in the inland environment.

Carbonation mechanisms in concrete and its damaging effects on steel reinforcement were critically discussed. Moreover, the damage effects of carbonation-induced corrosion on RC structure and some influencing factors such as concrete quality, cover depth, reinforcing steel diameter are also highlighted and discussed in this review to provide a holistic understanding of the underlying carbonation-induced corrosion process and its influencing factors.

This chapter closes with the review of some existing corrosion damage models. The review identified various factors and parameters considered by different authors in modelling the steel radius loss required to initiate cracking and time from corrosion

initiation cover concrete cracking. Based on the present evaluation, the following conclusions are drawn:

- Most of the existing models were developed using data obtained from accelerated corrosion experiment which does not represent practice-related conditions. This limits their application to the field structures.
- None of the models described the most important factors involved in steel corrosion process in concrete.
- It is very difficult to identify a superior model either by using more input parameters or the appropriate corrosion mechanism and the accuracy of their prediction. The empirical models are as good as the analytical ones.
- The use of unrealistic parameter (porous zone) in the analytical models is identified, and a more reasonable parameter was suggested.

Conclusively, it is recognised that an analytical model would provide a more robust solution but the process of corrosion-induced cover cracking is highly complicated and dependent on a large number of variables. As such, any analytical model would require a large number of assumptions which introduces scope of errors in prediction and therefore may not be well suited to Monte Carlo based reliability applications (Al-Harthy, Mullard and Stewart, 2011). The use of an empirical model is fast and accurate in predicting corrosion cracking times based on input parameters that are readily available. Therefore, empirical models are suitable for use in reliability based analyses. This forms a motivation for developing the empirical predictive models in this study.

The preceding chapter 3 will discuss the materials and methods of obtaining the data that will be used in modelling the carbonation and corrosion processes in concrete.

CHAPTER 3

3 EXPERIMENTAL WORK

3.1 Introduction

To achieve the aim and objectives stated in Chapter 1, this chapter presents the experimental methods used to obtain data to develop models for predicting carbonation-induced corrosion initiation, and propagation processes in different concretes exposed to the South African natural inland environment. The experimental programme was designed in 3 phases as follows:

Phase 1- concrete early-age characterisation

Phase 2- steel corrosion initiation in various concretes

Phase 3- steel corrosion propagation in different pre-carbonated concretes.

Phase 1 of the experimental programme was the laboratory investigation into the durability (oxygen permeability index (OPI) and water sorptivity index (WSI)) and strength (compressive and tensile strengths) characteristics of different concrete mixtures. The experimental variables used for the concrete characterisation tests were w/b ratio and binder type. Phase two of the experimental programme was the laboratory investigation into the corrosion initiation process in concrete exposed to the natural inland environment of the Johannesburg area. The experimental variables used for the corrosion initiation phase included w/b ratio, binder type, duration of initial moist curing and exposure conditions. The carbonation performance of the concretes was assessed using a phenolphthalein indicator test conducted on the test samples for two years exposure to the natural inland environment.

Phase 3 of the experimental programme involved a laboratory investigation in determining the amount of steel radius loss or corrosion required to initiate a first visible crack in pre-carbonated cover concretes exposed to a natural unsheltered inland environment. The experimental variables considered for this phase were cover depth, reinforcing steel diameter, w/b ratio, and binder type. Gravimetric steel mass loss measurements were performed in accordance with ASTM G1-3 (2011). Corrosion current density measurements were conducted to ascertain the corrosion

condition of the reinforcing steel when the concrete cover cracked. The corrosion measurements were taken immediately the concrete samples cracked. Many factors influence carbonation-induced steel corrosion damage in the natural inland environment as found in the literature. It is not within the scope of this study to considered all the factors. An attempt was made in this study to considered only those factors mentioned in the research objectives

3.2 Experimental Variables

The experimental variables for the carbonation-induced corrosion initiation process included the water/binder ratio (w/b), exposure condition, binder type, extent of initial water curing and a structural configuration (cover depth). The experimental variables considered for corrosion propagation were w/b ratio, binder type, structural configurations (reinforcing steel diameter, and concrete cover depth). The variables considered nature and properties of Portland cement concrete and provided a means of comparing the properties of each concrete from the durability perspective. The selection of the experimental variables was based on engineering judgement of other researchers, where the selected variables were found to have some significant influence on the intended experimental programmes. Besides, the variables were chosen to allow comparison of prediction models with corrosion initiation and propagation experimental data reported in another similar study. The materials used for the test concretes were selected reflecting local availability for construction works.

Binder types: Plain Portland cement (PC) of strength class 52.5 (CEM I 52.5 N) was used in this study. Also, fly ash (FA), ground granulated blastfurnace slag (BS) and silica fume (SF) were used for partial replacement of PC. These are industrial waste products, usually used to improve the engineering properties of concrete. The binder materials, as stated by the manufacturer, conform to SANS 50197 Part 1-2: 2000; and SANS 1491-Part 1-3:2005 requirements. The percentages of PC blended with the supplementary cementitious materials (SCM) are indicated in Table 3.1. The percentage replacements are based on what is commonly used in South Africa

as well as acceptable durability and strength performance reported by some previous studies (Alhassan, 2014; Ananmalay, 1996).

Table 3:1 Percentage compositions by mass of the binders

Binder types	% compositions
PC	100
PC-FA	70-30
PC-BS	50-50
PC-SF	90-10
PC-BS-SF	60-30-10

Water/binder ratio: Water/binder ratios (w/b) of 0.40, 0.60 and 0.95 were used for the carbonation, oxygen permeability, water sorptivity and compressive strength tests. Water/binder ratios of 0.60 and 0.95 used for the corrosion experiments. The 0.95, 0.60 and 0.40 w/b ratios were used representing concrete strength grades of < 25 MPa, 25-50 MPa and > 50 MPa respectively for each of the binder type. Concrete strength grade of < 25 MPa was included to represent the case of unsatisfactory site practices in concrete production (Adewole, Ajagbe and Arasi, 2015) while 25-50 MPa and > 50 MPa strength grades are common in concrete applications. Moreover, the decision to use different w/b ratios was to study concrete samples over a range of pore structure characteristics and to enable comparison of the concretes in terms of their investigated properties.

Initial moist curing age: The concrete samples used for the carbonation test were initially cured in water for 7 and 28 days. The decision to use the two initial moist curing periods was aimed at producing specimens with different pore structures. This is because initial moist curing of concrete has a greater influence on its pore structure (Alexander, Jaufeerally and Mackechnie, 2003; Ballim, Alexander and Beushausen, 2009).

Concrete cover depth: To study the corrosion of reinforcing steel in concrete due to carbonation, concrete cover depths of 12, 20 and 30 mm were used. South African concrete design code (SANS 10100:2-2000, 1992) specifies the minimum

concrete cover depths of 20 and 30 mm for a normal density concrete exposed to mild and moderate environmental conditions, such as common in the inland environment. Hence, 20 and 30 mm concrete covers were among others used in this study where applicable. The 12 mm concrete cover depth was included to represent a poor site practice.

Reinforcing steel bar: High yield deformed steel bars of 8 mm, 12 mm and 20 mm diameters were used to manufacture the RC specimens. These are common sizes of reinforcing steel bars used in practice and therefore adopted in this study. The preliminary tensile strength test conducted on the steel samples showed that the average ultimate tensile strengths are 651, 737 and 625 MPa for 8, 12 and 20 mm steel diameters respectively (see Figure A1 of Appendix A). The results showed that the average ultimate tensile strengths of the reinforcing steel are greater than 450 MPa conforming to SANS 920: 2011 requirement for a structural reinforced concrete.

Natural exposure environment: To assess the effect of exposure conditions on the carbonation depth of the concretes, three exposure environments were used. Those were indoor, outdoor sheltered and outdoor unsheltered exposure from rain. They were chosen based on classification specified by BS EN 206-1 (2006) as XC1, XC3 and XC4 representing moderate, less severe and severe carbonation-induced corrosion exposures. The exposure sites are located in the Hillman building at University of the Witwatersrand, Johannesburg. The lower rooftop of the Hillman building was used as the unsheltered outdoor exposure site. Underneath of a concrete tank placed at the upper rooftop of the Hillman building was used as a sheltered exposure site. A laboratory room inside the Hillman building was used as the indoor exposure site for the carbonation concrete samples. The exposure sites were decided upon based on the results of a trial study using five other locations around the University of the Witwatersrand, Johannesburg. It was found that the exposure conditions of relative humidity (RH), CO_2 concentration and temperature were similar in all the exposures considered. Therefore, to avoid disturbance or loss of concrete samples that might have a significant effect on the experimental results, Hillman building was used to expose the concrete specimens. The indoor, outdoor

sheltered and outdoor unsheltered exposure environments are shown in Figures 3.1, 3.2 and 3.3 with concrete cube samples in position.

Figure 3:1 Indoor exposure site

Figure 3:2 Sheltered exposure site

Figure 3:3 Outdoor unsheltered exposure site

3.3 Concrete Mix Proportions

Concrete mix design is a process of selecting the mixture ingredients required to meet some specific properties of concrete at both fresh and hardened states. The C&CI volumetric mix design method developed in South Africa was employed to determine the mixture proportions of the concretes. The method involves calculating mix constituents by mass per unit volume of a concrete type. The various proportions of mix constituents are shown in Tables 3.2 and 3.3.

Table 3:2 Concrete mix proportions of the concretes used for the characterisation and carbonation tests

Mix label	Binders (kg/m^3)				Aggregates (kg/m^3)		Water (kg/m^3)	w/b	Super-plasticiser l/m^3	Slump (mm)
	PC	FA	BS	SF	Crushed granite sand	Crushed granite stone				
PC	255	-	-	-	910	1002	242	0.95	-	-
	350	-	-	-	849	1015	210	0.60	1.00	70
	450	-	-	-	800	990	180	0.40	2.00	30
PC-FA	178	77	-	-	910	1002	242	0.95	-	-
	245	105	-	-	849	1015	210	0.60	0.67	120
	315	135	-	-	800	990	180	0.40	1.00	55
PC-BS	127	-	128	-	910	1002	242	0.95	-	-
	175	-	175	-	849	1015	210	0.60	0.67	100
	225	-	225	-	800	990	180	0.40	1.33	45
PC-SF	230	-	-	25	910	1002	242	0.95	-	-
	315	-	-	35	849	1015	210	0.60	0.50	100
	405	-	-	45	800	990	180	0.40	1.17	30
PC-BS-SF	153	-	77	25	910	1002	242	0.95	-	-
	210	-	105	35	849	1015	210	0.60	2.00	60
	270	-	135	45	800	990	180	0.40	2.67	35

The aggregates used in this study were crushed granite stone and crushed granite sand (nominal size of 4.75 mm) obtained from Midrand quarry in the Johannesburg area. The particle size distributions of both coarse and fine aggregates are shown in Figure 3.4. The maximum size of 19 mm coarse aggregate was used to produce concrete mixtures used for the carbonation, durability index, compressive and splitting tensile strength tests specimens. A maximum size of 12 mm coarse aggregate was used to produce concrete mixtures for the corrosion test specimens. The 12 mm coarse aggregate used in the corrosion concrete mixes was to comply

with SANS 10100:2-2000 (1992) which specifies that maximum coarse aggregate should not exceed the cover of reinforcement. The minimum cover of reinforcement used in this study was 12 mm, and for uniformity and comparison of the concrete properties, 12 mm coarse aggregate was used in all the corrosion concrete mixtures.

Table 3:3 Concrete mix proportions of the concretes used in the corrosion test

Mix label	Binders (kg/m^3)			Aggregates (kg/m^3)		Water (kg/m^3)	w/b	Super-plasticiser l/m^3	Slump (mm)
	PC	FA	BS	Crushed granite sand	Crushed granite stone				
PC	255	-	-	910	1002	242	0.95	-	-
	350	-	-	849	1015	210	0.60	1.00	60
	450	-	-	800	990	180	0.40	2.00	30
PC-FA	178	77	-	910	1002	242	0.95	-	-
	245	105	-	849	1015	210	0.60	0.67	105
	315	135	-	800	990	180	0.40	1.67	60
PC-BS	127	-	128	910	1002	242	0.95	-	-
	175	-	175	849	1015	210	0.60	0.67	95
	225	-	225	800	990	180	0.40	1.67	40

The fineness modulus (FM) of the sand aggregate is 2.98 (Table A2 of Appendix A). It is within the range of 2.0 to 3.0 recommended by SANS 1083 (2006) as a preferable sand used for the manufacture of high-quality concrete. From the sieve analysis, both coarse and sand aggregates as received from the quarry were good for concrete production as they meet the requirements of SANS 1083 (2006). The aggregates were air dried in the laboratory (at temperature: 23 ± 2^{o}C and relative humidity: 50 ± 5%)

A super-plasticiser of modified phosphates group stated to comply with BS EN 934-2:2009 requirements as written on the container was added to the mixtures to improve the workability of the fresh concrete mixtures where necessary. This was also to ensure a minimum slump of 30 to 60 mm, particularly for the mixes of 0.40 and 0.60 w/b ratios. All the concrete mixtures having w/b ratio of 0.95 gave collapse slumps, therefore, slump measurement was not taken for such concrete mixtures.

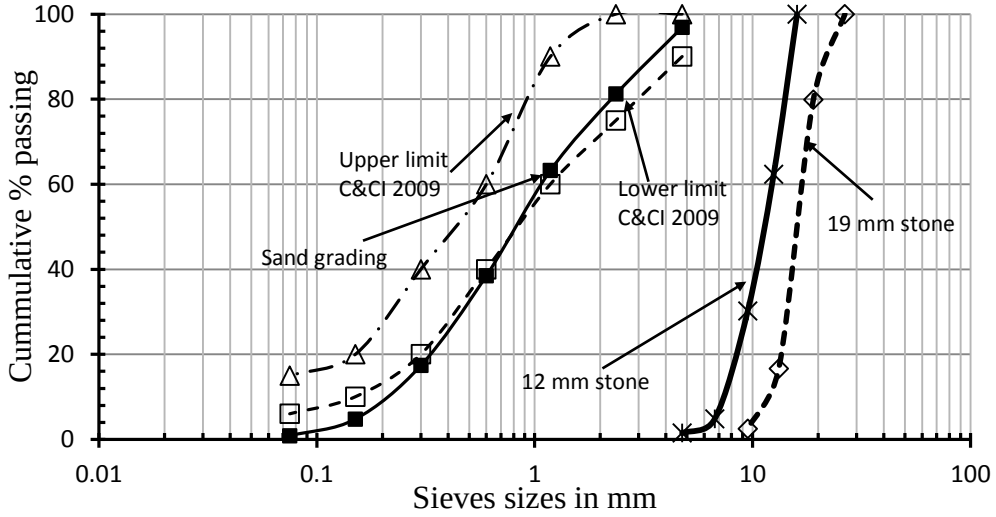

Figure 3:4 Aggregates particle size distribution

3.4 Number of Concrete Specimens

A total of 1155 cubes (100 mm^3) were cast using fifteen different concrete mixtures for the durability indicator, natural carbonation, and compressive strength tests. For the carbonation and compressive strength tests, three concrete cube specimens were used for each mix, while two concrete cube specimens per a mix were used for the durability index tests. It is well understood that similar studies in the literature used concrete prism specimens for carbonation test. This procedure involves removing the concrete prism from the exposure site to the laboratory where a smaller part of the concrete prism is cut for the carbonation test and the remaining part of the concrete prism is returned to the exposure site. This procedure could interrupt the in-take of CO_2 by the remaining prism, therefore, to avoid the CO_2 interruption, concrete cube specimens were used in this study which were discarded immediately after use.

For the corrosion propagation tests, a total number of 108 RC prism (100 x 100 x 200 mm long) were cast using six different concrete types. Prismatic configuration was adopted for the RC specimens based on the fact that it is easier to use corrosion rate meter (coulostat device) on a prismatic specimen compared to a cylindrical specimen. It is understood that corrosion test carried out on small-sized specimens may not be a representative of a real RC structure in terms of corrosion-induced

damage. However, due to cost, space constraints in the laboratory and the fact that the extent of the effect of corrosion specimen size on corrosion experimental result is seldom discussed in the literature, small-sized concrete prism specimens (100 x 100 x 200 mm long) were used in this corrosion study.

For each binder type, w/b ratio, cover depth and reinforcing steel diameter, two specimens were cast with two reinforcing steel bars embedded at an equal cover depth as shown in Figure 3.5. In many corrosion studies (Tuutti, 1982; Andrade, Alonso and Molina, 1993; Molina, Alonso and Andrade, 1993; Parrott, 1994) several reinforcing steel bars were placed parallel to each other in cover depths ranging from 7 to 76 mm (Hornbostel, Larsen and Geiker, 2013). Apart from Al-Harthy, Mullard and Stewart (2011) that reported an equal corrosion rate found in the parallel reinforcing steel bars placed at an equal cover depth, to what extent the number of reinforcement influences corrosion experimental investigation is rarely discussed in the literature. Two reinforcing steel bars placed parallel to each other at an equal cover depth (Figure 3.5) were used in this study.

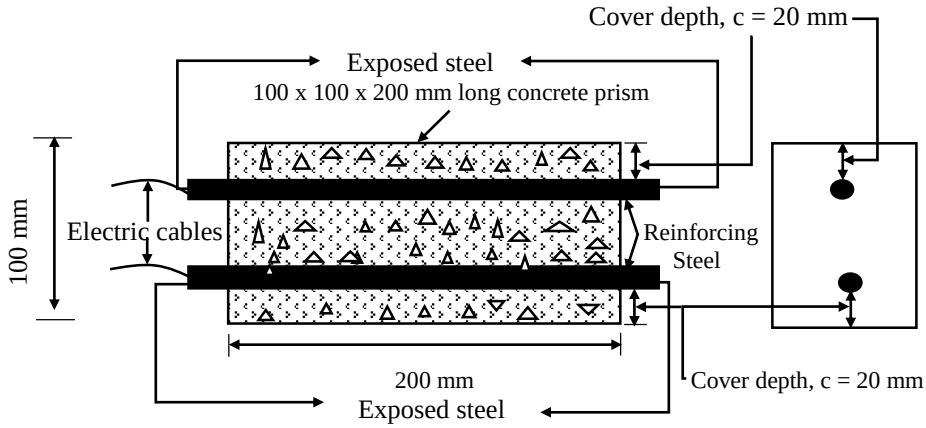

Figure 3:5 A typical cross-section of a reinforced concrete prism

Tables 3.4 shows the RC prism matrix and the number of samples for each concrete mixture. Five companion prisms (100 x 100 x 200 mm long) were cast per concrete mix without reinforcement for the splitting tensile strength test and to monitor the

progress of carbonation in the exposure chamber. The summary of various concrete samples pre-conditioned for different tests is shown in Table 3.5.

Table 3:4 Reinforced concrete prism matrix for the corrosion propagation test

Binder types	w/c	Steel diameters mm	Cover depths mm	Number of specimens
PC, PC-FA and PC-BS	0.95	8	12	2
		8	20	2
		8	30	2
		12	12	2
		12	20	2
		12	30	2
		20	12	2
		20	20	2
		20	30	2
PC, PC-FA and PC-BS	0.60	8	12	2
		8	20	2
		8	30	2
		12	12	2
		12	20	2
		12	30	2
		20	12	2
		20	20	2
		20	30	2

Table 3:5 Summary of the concrete specimens for various tests

Tests	Initial water curing ages (days)	Size and number of specimens per a mix	Pre-conditioning	Testing age
Compressive strength	28	3 cubes (100 mm x 100 mm x 100 mm) per a mix	Concrete tested at water saturated condition	28 days
Splitting tensile strength	28	3 prisms (100 mm x 100 mm x 200 mm) per a mix	Concrete tested at water saturated condition	28 days
Durability index tests (Oxygen permeability and water sorptivity)	28	4 concrete discs (70 $\pm$ 2 mm diameter and 30 $\pm$ 2 mm thickness	Oven dried for 7 days ± 4hrs at a temperature of 50 ± 2^{o}C	Between 30 to 40 days
Natural carbonation test	7 and 28	3 concrete cubes (100 mm x 100 mm x 100 mm) per a mix	No pre-conditioning after initial curing	6, 12, 18 and 24 months
Accelerated carbonation	7	2 concrete prisms (100 mm x 100 mm x 200 mm) per a mix	Laboratory air drying for 30 days after initial curing	Weekly
Corrosion current density and gravimetric steel mass loss	7	2 RC prisms (100 mm x 100 mm x 200 mm)	Pre-carbonated beyond the depth of cover	Immediately after the appearance of the first visible crack

3.5 Specimen Casting

- **Wooden moulds for the reinforced concrete prisms**

Wooden moulds of size 100 x 100 x 200 mm were prepared in the laboratory using 22 mm thick plywood. They were used to cast the concrete specimens used for corrosion and splitting tensile strength tests. Each of the moulds was made with two holes at both ends to position two reinforcing steel at a specified cover depth as shown in Figure 3.6. The mould compartment was designed to accommodate three concrete prisms of a similar reinforcing steel diameter at different cover depths (12, 20 and 30 mm). The arrangement was chosen to optimise the wooden materials usage. A releasing agent (motor engine oil) was applied to the inner sides of the wooden panels to prevent concrete from sticking to the wooden boards.

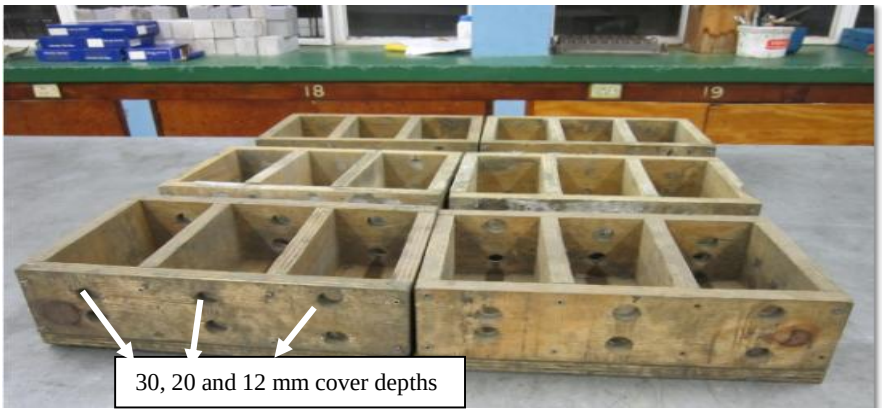

Figure 3:6 Photograph of the wooden moulds

- **Preparation of reinforcing steel bars**

Reinforcing steel bar was cut into 260 mm lengths, and cleaned with a wire brush to remove any loose corroded part and cleaned with a cloth towel. The cleaned reinforcing steel bars were weighed using a table top weight meter, the measurement representing the initial mass, m_i (g) of the reinforcing steel bar (m_i). A 100 mm long electric cable was soldered to one end of the pre-conditioned reinforcing steel bar before fixing into the wooden moulds. The attached electric cable was to enable electrical connection between the corroding reinforcing steel bars and the corrosion monitoring devices. The two ends of the reinforcing steel bars (30 mm to an end) were then coated with epoxy to prevent corrosion of the exposed ends during initial curing in water and when exposed to the environment. The schematic diagram of a typical pre-conditioned reinforcing steel bar is shown in Figure 3.7.

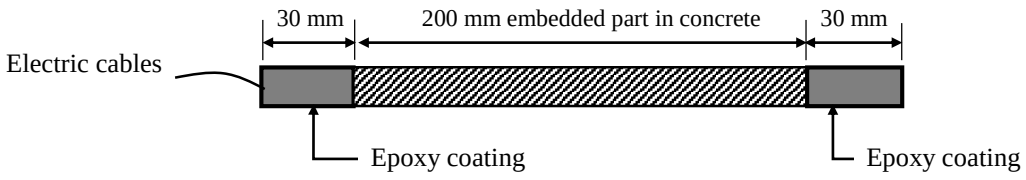

Figure 3:7 Schematic diagram of a pre-conditioned typical reinforcing steel bar

3.5.1 Concrete batching and mixing

The quantity of concrete for each test was batched based on the mass of the concrete constituents. However, it was difficult to have a particular type of concrete mix in a single batch because of a large number of samples required, therefore batching was done based on the volume of the mixer and the available number of moulds. For every mix, a 0.026 m^3 of concrete was considered to avoid incomplete mixing and spillage of concrete materials during mixing. Mixing was done in a horizontal drum mixer of 0.035 m^3 capacity at a laboratory ambient temperature of 23 ± 2^oC. The superplasticiser was added to the mixtures when necessary to control the workability. The workability of each concrete batch was measured using a slump test as described in SANS 5861-1:2006.

3.5.2 Casting and curing of the concrete specimens

Fresh concrete was cast horizontally into the respective moulds and compacted in two layers using a vibrating table and finished using a hand trowel. Immediately after the casting, specimens were covered with polyethene sheets for 24 ± 2 hours at a laboratory room temperature of 23 ± 2^oC. This was done to protect the fresh concrete from moisture loss while setting and hardening for handling. After curing for 24 ± 2 hours in the moulds, the concrete specimens were stripped and placed inside a water tank filled with water (at a temperature of 22 ± 2^oC) for a specified number of curing days depending on the type of test (Table 3.5).

3.6 Tests Procedures

3.6.1 Natural carbonation

The roof top of the Hillman building at the University of the Witwatersrand, Johannesburg was used for the outdoor sheltered and unsheltered exposure sites. A reinforced concrete tank positioned at the upper roof top of the Hillman building provided sheltered conditions for the concrete cube samples, while the exposed area of the lower rooftop provided the unsheltered conditions for the concrete cubes (see

Figures 3.1, 3.2 and 3.3). A laboratory room with a temperature of 22 ± 2ºC and relative humidity of 45 ± 5% was used to represent the indoor exposure.

Prior to exposure of the concrete samples, the environmental conditions (RH, temperature and air CO_2 concentration) of the exposure sites were measured daily at ±1400 hours for a year using a portable climate equipment (Combo IAQ meter). The micro-climate data was analysed for each exposure site in terms of minimum and maximum values for the winter and summer periods, thus showing the probable peak and low periods for concrete carbonation and reinforcing steel corrosion in the inland environment.

In the respective exposure sites, concrete samples were positioned at a spacing of about 30 to 50 mm with the cast faces touching the roof slab while other sides were exposed. The spacing of about 30 to 50 mm between each concrete cube was allowed to permit free air circulation around the exposed concrete faces. The concrete specimens positioned at their respective exposure sites are shown in Figures 3.1 to 3.3.

3.6.2 Accelerated carbonation

To shorten the corrosion initiation time of the reinforcements, it was decided to initiate corrosion by accelerating the carbonation of the cover concretes. This mechanism of initiating reinforcement corrosion was selected in preference to other methods such as impressed current/voltage and chlorides inclusion at the mixing stage of fresh concrete for the following reasons as stated by Ballim & Reid (2003):

- the hydration properties of the cement phase are not affected during the important early stages of cement hydration
- in practice chloride compounds are usually excluded from concrete mixes
- carbonation in the inland environment typically causes early corrosion initiation.

Therefore, a carbonation chamber with an internal relative humidity of 55 ± 5 % was used to accelerate the carbonation in the concretes (Jones et al. 2000). The chamber's humidity was achieved and maintained using a saturated salt solution of

potassium nitrate (KNO_3). The CO_2 concentration entering the chamber was regulated to 10% through control and monitoring system units attached to the chamber, as shown in Figure 3.8.

Figure 3:8 Accelerated carbonation chamber

A 10% CO_2 concentration was chosen to accelerate the carbonation process in a reasonable time limit (Morandeau *et al.*, 2015). The corrosion specimens and the unreinforced prisms used to monitor the progress of carbonation front were positioned in the chamber. To avoid CO_2 stagnation which could result into locally depressed partial pressures of CO_2 around the test specimens, a standard computer CPU fan (4-wire PWM controlled fans stated to operate at 2000 RPM) was provided at the base of the chamber to circulate the CO_2 (Jones *et al.*, 2000).

Carbonation test was carried out weekly by spraying a phenolphthalein solution on the freshly cut surface of the monitoring concrete prisms, and the extent of the carbonation front was observed. The extent of carbonation front was measured using a vernier caliper of 0.05 mm accuracy. The RC prism specimens were removed from the chamber when the observed carbonation front passed beyond the level of reinforcement and was made ready for exposure to the natural unsheltered environment.

3.6.3 Corrosion propagation

The pre-carbonated RC prisms were exposed to the outdoor unsheltered environment on the lower rooftop of Hillman building (University of the Witwatersrand) as shown in Figure 3.9. They were positioned such that the two adjacent cover depths were equally exposed to the environment. The concrete specimens were monitored daily (± 1400hrs) for the appearance of a first visible crack (visible to the naked eye) on the concrete cover. The observation was discontinued once a longitudinal crack (parallel to the line of reinforcement) appeared on the concrete cover surface. The appearance of a first visible crack on the surface of the concrete cover was considered in this study as the end of RC service life based on the fact that the appearance of visible crack impairs the aesthetic of the structure. It also allows other aggressive agents into the concrete resulting in a further deterioration (Alonso, Andradel and Diez, 1998). However, the width of the cracks was not measured due to variations in the crack width along the crack length.

A coulostatic method of linear polarization resistance was used to quantitatively assess the corrosion condition of the corroding reinforcing steels immediately after the first crack appeared on the cover concretes. A subsequent gravimetric mass loss measurement for the calculation of steel radius loss or corrosion amount required for cracking the cover concretes was later carried out on the RC specimens.

Figure 3:9 Pre-carbonated RC specimens exposed to natural unsheltered inland environment

3.7 Test Measurements

3.7.1 Concrete characterisation tests (Durability index)

The 28-day water sorptivity index (WSI) and oxygen permeability index (OPI) tests were used to characterise the quality of the concretes. The tests were carried out as specified in Concrete Durability Index Testing, Part 1 & 2 (2009) and SANS 3001-CO3- part 1-3 (2015). The same concrete disc samples were used for the two tests. This was possible because oxygen gas does not react with hardened concrete and water capillary in WSI test is at a low pressure. Hence, concrete microstructure was not affected due to the tests. Therefore, two durability indexes (OPI and WSI) were obtained from one sample.

Oxygen permeability index (OPI)

South African Oxygen Permeability index (OPI) test was used to measure the concrete permeability. The test is used to assess the overall micro- and macrostructure of the near surface of cast concrete, and is sensitive to the presence of macro-void and cracks within the concrete (Salvoldi, Beushausen and Alexander, 2015). The test is useful in assessing the state of compaction, the presence of bleed

void and the degree of connection between the pores and their sizes. Beushausen & Alexander (2008) found that the test is useful in studying the variation in concrete w/b ratio, binder type, and curing conditions. The OPI test results were found to be similar to other existing permeability test methods such as the Torrent permeability test and Cembureau methods (Beushausen and Alexander, 2008). Hence, OPI test procedure as specified in SANS 3001-CO3-2 (2015) was followed in this study.

The concrete cube specimens were cured in water for 28 days ± 2hours and two concrete cube samples from each concrete type were cored to obtain four concrete disc samples of size 70 ± 2 mm diameter and 30 ± 2 mm thickness. They were conditioned in an oven chamber at a temperature of 50 ± 2^{o}C for 7 days ± 4hrs. The oven chamber temperature and duration were selected to result in a minimum degree of microstructural alteration of the concrete disc samples, while still maintaining the internal moisture equilibrium (Alexander, Jaufeerally and Mackechnie, 2003). The samples were cooled in a desiccator for 3 hours before loading into the compressible collars subsequently fitted into the permeability loading rigs (Figure 3.10).

Oxygen gas was then allowed to flow through the concrete at an initial pressure of 100 ±5 kPa. As permeation occurred with time, a decrease in pressure with time was measured to the nearest 0.5 kPa and slopes of the log of pressure head versus time define the oxygen permeability coefficient (k) as expressed in Equation 3.1.

$$k = \frac{wVg}{RA}\left(\frac{d}{\theta t}\right) In\left(\frac{P_o}{P_t}\right) \qquad 3.1$$

where k is the coefficient of permeability (m/s), w (kg/mol) is the molecular mass of permeating gas, V is the volume of oxygen under pressure in permeameter (m^3), g (m/s^2) is acceleration due to gravity. R (N m K^{-1} mol^{-1}) is universal gas constant, which is 8313, d (m) is the average thickness of the specimen, θ(^{o}K) is the absolute temperature, P_o (kPa) is the oxygen pressure at the beginning of the test. P_t (kPa) is the oxygen pressure at the end of the test, and t (second) is the time for pressure to decrease from P_o to P_t. A (m^2) is the superficial cross-sectional area of a concrete sample. The coefficient of permeability (k_i) was calculated for each of the disc

specimens. The negative logarithm of an individual coefficient of permeability is the oxygen permeability index (Equation 3.2).

$$OPI_i = -\log_{10} k_i \qquad 3.2$$

Oxygen permeability index (OPI) of a concrete mixture is the average of four individual OPI values of that particular mix (Equation 3.3).

$$OPI = \left[\frac{1}{4}\left(OPI_1 + OPI_2 + OPI_3 + OPI_4\right)\right] \qquad 3.3$$

where OPI_i *(i = 1, 2, 3, 4)* is the calculated OPI of the specimens

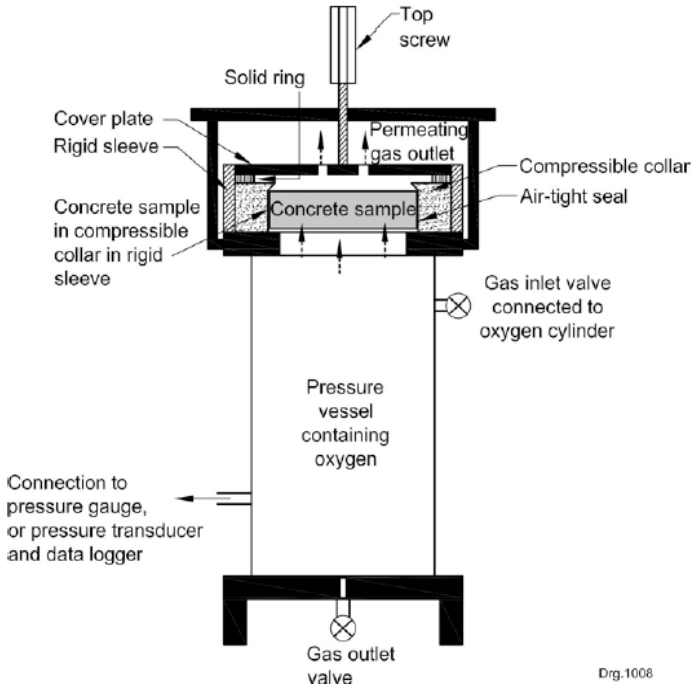

Figure 3:10 Oxygen permeability test set up rig (SANS 3001-CO3-2, 2015).

Water sorptivity index (WSI)

Water sorptivity test was done as specified by Concrete Durability Index Testing, Part 1 & 2 (2009). The sample number and preparation were similar to the oxygen permeability samples. The vertical curved side of the concrete disc samples were sealed with a packaging tape. The initial weight of the specimens, M_{so} (g) were taken to the nearest 0.01 g, after which they were partially immersed in a solution

of distilled water saturated with $Ca(OH)_2$ with one face exposed to the solution as shown in Figure 3.11.

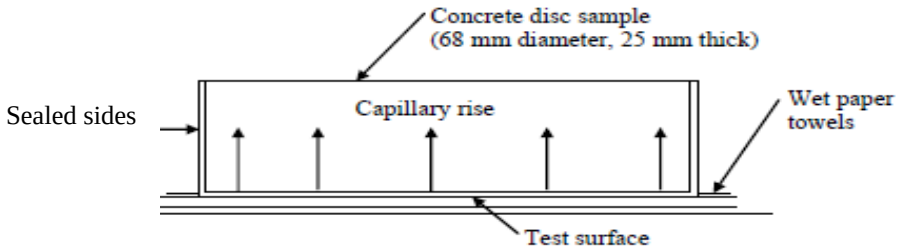

Figure 3:11 Schematic diagram of water sorptivity test adapted from Otieno (2008)

The weight of the partially immersed concrete discs, M_{st} (g) were measured to the nearest 0.01 g at 3, 5, 7, 9, 12, 16, 20 and 25 minutes. The samples were then placed inside a vacuum saturation tank which was vacuumed with the pressure of between -75 kPa and -80 kPa and maintained for three hours. After 3 hours ± 15 minutes, the tank was filled with calcium hydroxide solution to a level of 40 mm above the top of the top specimens. The chamber with concrete samples and calcium hydroxide solution was vacuumed at a pressure between -75 and -80 kPa for 1hour ± 15 minutes. The samples were allowed to soak for further 18 ± 1 hours before removing them, and surface dried with a paper towel and immediately weighed to an accuracy of 0.01g. The readings were recorded as the vacuum saturated mass (M_{sv}) to the nearest 0.01 g. Water sorptivity was calculated as:

$$S = \frac{Fd}{M_{sv} - M_{so}} \qquad 3.4$$

where, S (mm/hour$^{0.5}$) is the sorptivity, F is obtained as the slope of the best fit line from plotting M_{wt} against the $t^{0.5}$ in g/hour$^{0.5}$ and d is the average thickness of the specimens (mm). t is the time in hours after a sample was first exposed to water on its lower face and M_{wt} is obtained from Equation 3.5.

$$M_{wt} = M_{st} - M_{so} \qquad 3.5$$

The average of 4 water sorptivity measurements from the same concrete mix represents the WSI of that concrete mixture.

3.7.2 Carbonation depth

The carbonation depths of the concrete samples were measured at 6, 12, 18 and 24 months of the exposure to the natural inland environment. Three cube specimens per a concrete mixture were removed from each of the exposure sites at a testing period. The cube specimens were broken into two along the side faces using a masonry cutter improvised in the Amsler universal testing machine. The cut surface was cleaned of dust and loose particles immediately after the breaking. The extent of carbonation depth was determined by spraying the freshly cut surface with a solution of phenolphthalein (1% phenolphthalein in 70% ethyl alcohol). The sprayed concrete cut surface was left for 1hour ± 15 minutes. The carbonated zone showed no colouration while the purple-red zone with phenolphthalein solution showed an unaffected zone by carbonation.

Moreover, obvious distortions such as the presence of coarse aggregate particles or air voids near the surface were avoided and 12 measurements (3 measurements on each side) were taken. The depths of the carbonated zone was measured to an accuracy of 0.05 mm using a Vernier caliper. Due to lower depths of the carbonation zone observed in the 0.40 w/b ratio concretes, a magnifying glass with a magnification of X10 was used to observe their carbonation fronts. The procedure of carbonation measurement was repeated at 6, 12, 18 and 24 months of exposure to the natural inland environment for all the concrete cube specimens. An average of 36 readings on 3 identical specimens was reported as carbonation depth of that particular concrete mix at a testing period.

3.7.3 Reinforcement Corrosion current density

The measurement of the corrosion current density was carried out using a Coulostat V3 corrosion rate meter. The equipment is shown in Figures 3.12 and 3.13. It consists of three underneath silver/silver chloride reference and counter electrodes

as shown in Figure 3.13. Figure 3.14 shows the schematic measurement diagram of the Coulostat corrosion rate meter. The device operates using coulostatic a form of linear polarization resistance (LPR). This involves measurement of potential relaxation after the application of a few millisecond of known charge to the corroding reinforcing steel. The potential transient which is monitored over 30 seconds after the perturbation indicates the rate of corrosion in the steel. The theoretical principle of the coulostatic method is available in the literature (Suzuki, Kanno and Sato, 1980; Panasenko *et al.*, 1988). However, the working principle can be described briefly as follows:

when a small amount of charge pulse is applied to a corroding steel, its potential jumps from a lower corrosion potential to a higher potential. The resulting potential shift is expressed as:

$$\eta_o = \frac{\Delta q}{C_d} \qquad 3.7$$

where η_o is the initial potential shift, Δq is the applied charge (Coulomb) and C_d is the double layer capacitance of the steel specimen. The charge increment can be expressed by Equation 3.8

$$\Delta q = \frac{t_{pu} I_{app}}{A} \qquad 3.8$$

where t_{pu} (ms) is the pulse duration, I_{app} (mA) is the applied current, and A is the surface area of the reinforcing steel exposed to corrosion. The charge increment is then consumed by corrosion reaction which brings about a potential drift backward to the corrosion potential, E_{corr}. The potential decay proceeds exponentially with time and is expressed by the Equation 3.9 (Suzuki, Kanno and Sato, 1980; Panasenko *et al.*, 1988)

$$\eta_t = \eta_o \exp\left(\frac{-t}{C_d R_p}\right) \qquad 3.9$$

where η_t is the potential shift at time t, and R_p is the polarization resistance.

The Equation 3.9 can be used with the assumption that the charge increment is consumed only by corrosion reaction of the steel (Suzuki et al. 1980; Panasenko et al. 1988). The Equation 3.9 can be expressed in a logarithmic form as:

$$\log \eta_t = \log \eta_o - \frac{t}{2.3 C_d R_p} \qquad 3.10$$

An experimental plot of log η_t against t results is a straight line whose slope is $-1/2.3C_dR_p$ and R_p is then calculated from the slope of the line while C_d is obtained from the Equation 3.7. Corrosion current density i_{corr} is calculated by using the Stern-Geary concept (Equation 3.12).

$$i_{corr} = \frac{\beta}{R_p} \qquad 3.11$$

$$\beta = \frac{\beta_a \beta_c}{2.3(\beta_a + \beta_c)} \qquad 3.12$$

where β_a and β_b are the Tafel slopes obtained by Equation 3.13 (β_a is the anodic Tafel slope, and β_c is the cathodic Tafel slope)

$$\beta_{a,c} = \frac{\Delta \eta}{\log\{(t_3 - t_2)/(t_2 - t_1)\}} \qquad 3.13$$

Where t_1, t_2 and t_3 are the corresponding times during potential decay, measured in milliseconds. However, Coulostat V3 device uses the β value of 26 mV (Figure 3.16) as recommended by Andrade & Alonso (1996) for an active corroding steel reinforcement. The corresponding times, beta value and length factor are shown in Figure 3.16 as part of the input parameters for the corrosion current density calculation.

The corrosion current density measurements were taken with the instrument placed at the cover sides of the RC prism samples (Figure 3.12), such that the probes were aligned with the prism longitudinal axis (direction of the reinforcing steel). A wet sponge was used to maintain a connection between the electrodes and concrete specimen as shown in Figure 3.12. The Coulostat device impacts a charge impulse by forcing a small current (1~25 mA) through the counter electrode, concrete and corroding reinforcing steel (with a known surface area) for a duration (0~100 ms) and then sent back to the device via the common electrode connection.

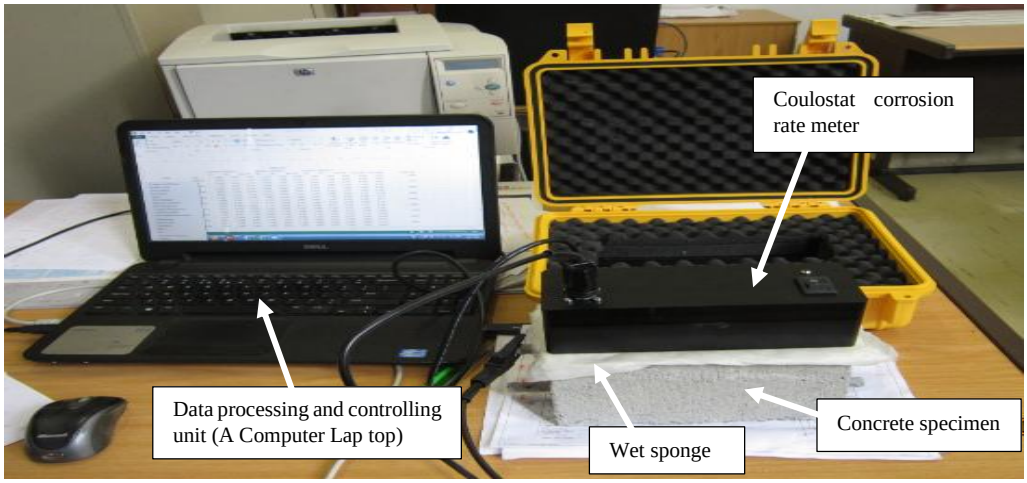

Figure 3:12 Photograph of Coulostat corrosion rate measurement set-up

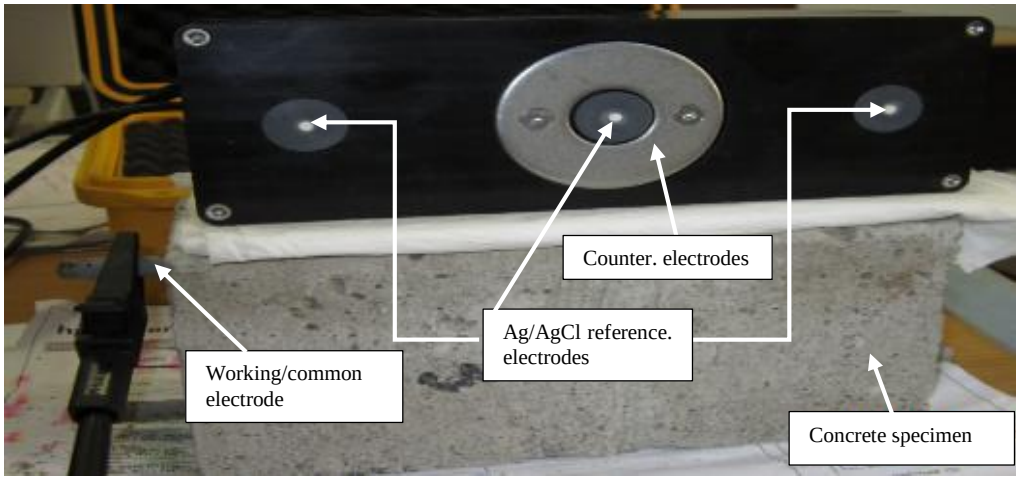

Figure 3:13 Photograph of Coulostat corrosion rate meter showing the underneath electrodes

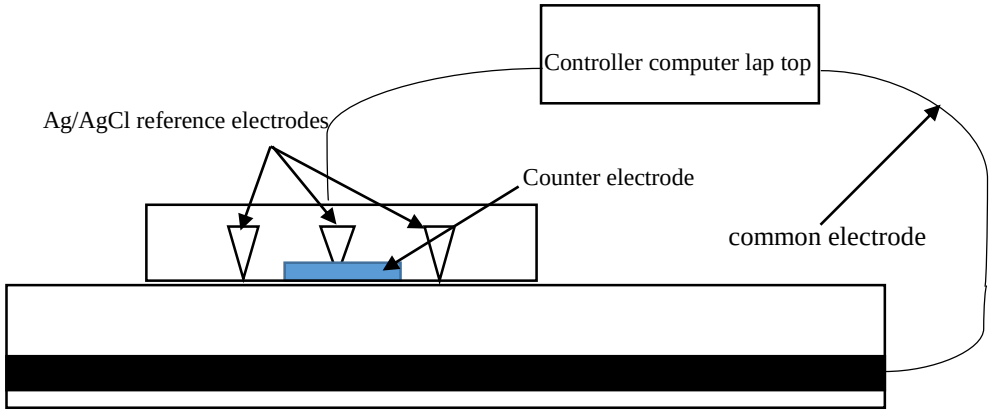

Figure 3:14 Schematic measurement diagram of Coulostat corrosion rate meter

For each of the electrodes, the average time before the pulse, during which the analysis estimated the pre-pulse potential of each electrode was set at 10 ms and post-pulse waiting time was set at 1 ms while potential decay time was set at 20 s (Figures 3.15 and 3.16). The length factor adjusts the effective area of reinforcing steel based on the measured potentials of the inner and outer electrodes. The device default value of 1 (length factor) was used which represents no adjustment to the effective surface area. The applied current was set at 12 mA for a duration of 12 ms, which falls between the recommended limit of 1-25 mA and 0-100 ms respectively as set by the manufacturer. The steel surface area used was varied depending on the diameter. However, the various steel surface areas used were 50.27 cm^2, 75.27 cm^2 and 125.68 cm^2 for 8 mm, 12 mm and 20 mm steel diameters respectively. Figure 3.17 shows a typical real-time potential graph after the potential decay of the second electrode.

The measurement was stopped after the potential had decayed close to the original potential value. The input data was immediately processed by the IDS analysis software installed on a laptop computer connected to the device (Figures 3.12 and 3.13). Figure 3.16 shows a typical corrosion current density measurement. The corrosion current density displayed on Coulostat device represents an average value of the three reference electrodes. Figure 3.17 shows the result of the non-linear curve-fitting process used to estimate the corrosion current density. Four corrosion current density readings on two identical samples (an equal w/b ratio, cover depth, reinforcing steel diameter and binder type) were taken, and their average was used to represent the corrosion current density of that particular concrete mix.

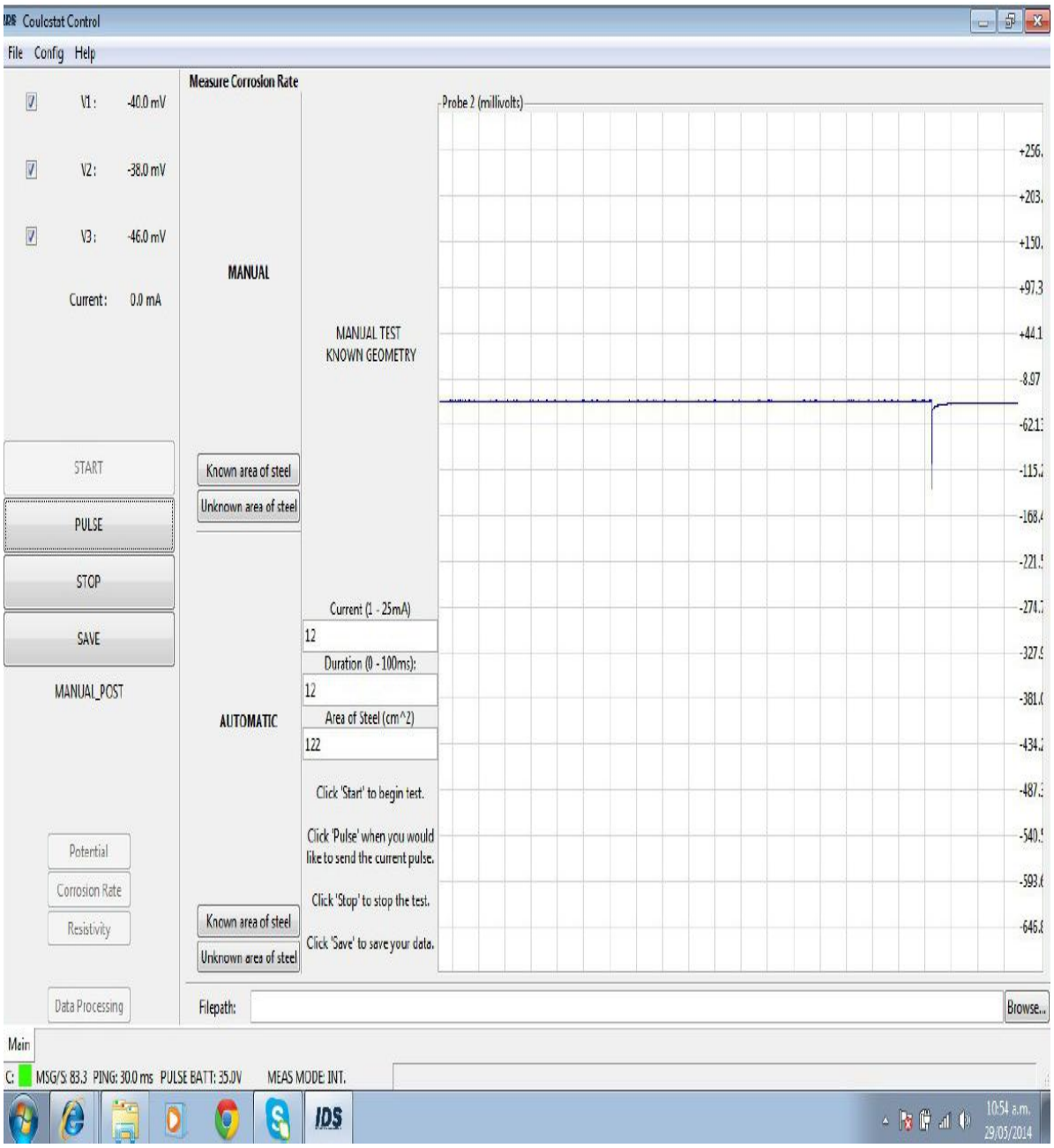

Figure 3:15 A typical Coulostat V3 input and data analysis page

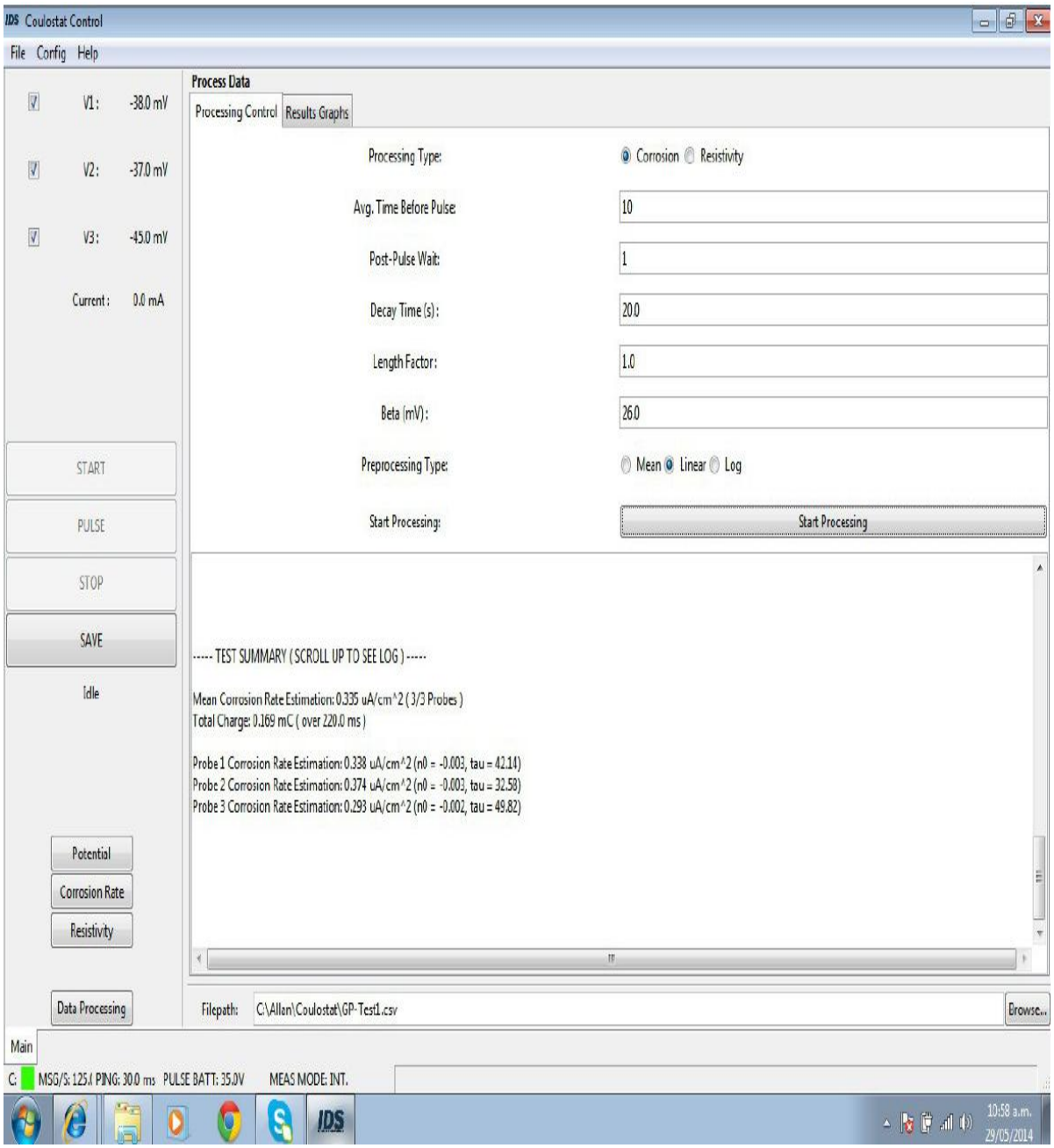

Figure 3:16 A typical result summary page for corrosion rate measurement

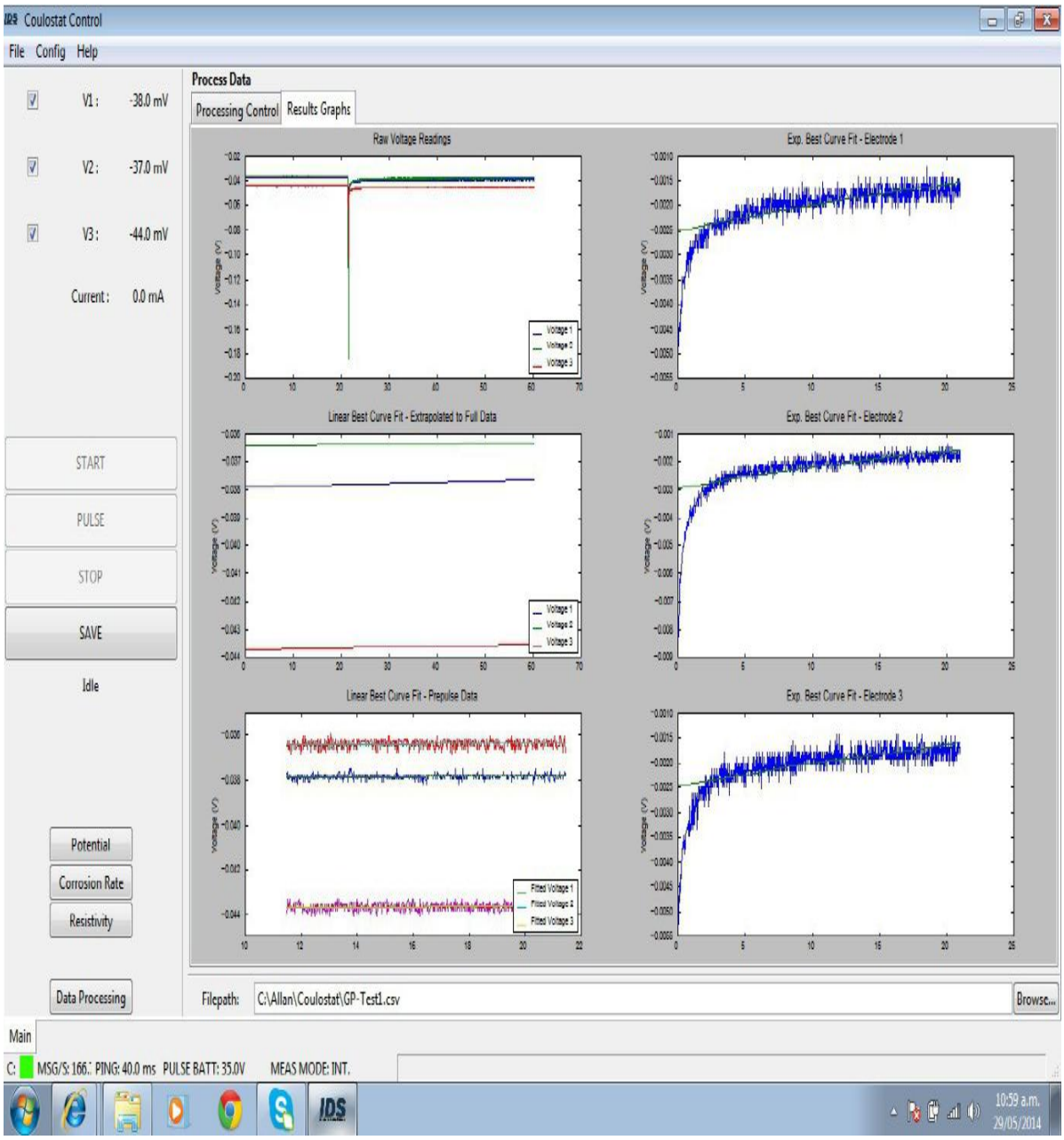

Figure 3:17 A typical result plots of corrosion current density

3.7.4 Gravimetric mass loss

Gravimetric mass loss method is a destructive technique of obtaining the mass of steel loss to corrosion (Busba, 2013; Rodriguez *et al.*, 1996; Andrade, Alonso and Molina, 1993). This approach was selected because it overcomes some practical difficulties usually experienced when interpreting results obtained by the electrochemical techniques. Therefore, gravimetric mass loss method as specified

by ASTM G1-3 (1999) was employed in this study to determine the amount of corrosion radius loss required to initiate a first visible cracking of the pre-carbonated concrete samples. Tuutti (1982) regarded the method as suitable for investigating the carbonation- induced corrosion propagation and for determining the amount of corrosion needed to initiate a surface crack in concrete. Busba (2013) used the technique to obtain a reliable estimate of the critical corrosion amount required to crack a cover concrete in the marine environment.

The test procedure followed is that contained in ASTM G1-3 (1999). The test was done immediately after measuring the corrosion current density at cracking of pre-carbonated cover concretes. The embedded corroding reinforcing steel bars were extracted and visually observed for the type of corrosion distribution (Figure 3.18).

Figure 3:18 Photograph of split reinforced concrete prisms showing the corroding reinforcements

The extracted corroding reinforcing steels were thoroughly wire-brushed using an electric machine fitted with a wire brush to remove the rust and adhered concrete before a chemical cleaning. The extracted wire brushed reinforcing steel were then cleaned in a chemical solution made with 500 ml of hydrochloric acid and 3.5 g of hexamethylene tetramine in 500 ml of reagent water. The solution was applied to the reinforcing steel's surface and then dried to remove the left over corroded portions from the corroding reinforcing steel bars. The process was repeated until the steels were visually observed to be free of rust. The mass, m_f (grams) of the

cleaned reinforcing steel bar was measured. The new mass (m_f) was deducted from the initial mass before corrosion, m_i (grams) (see Section 3.5 for m_i) to obtain the steel mass loss due to corrosion, m_l (grams) (Equation 3.14).

$$m_l = m_i - m_f \tag{3.14}$$

Four readings on 2 identical samples (an equal w/b ratio, cover depth, reinforcing steel diameter and binder type) were taken and their average was used to represent the corrosion steel mass loss of that particular concrete mix. The corrosion steel mass loss was converted to radial loss as follows:

Estimating reinforcement corrosion radius loss

Considering a given uniformly corroding reinforcing steel cross section shown in Figure 3.19, the volume change per unit length of the corroding reinforcing steel bar can be expressed as:

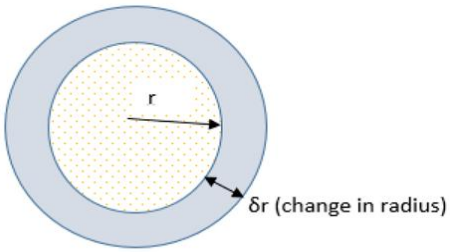

Figure 3:19 A schematic representation of a corroded reinforcing steel cross-section (homogeneous corrosion)

$$\delta v = \pi\left(r + \delta r\right)^2 - \pi r^2 \tag{3.15}$$

where δv (mm^3) is the change in volume per unit length due to the corrosion products expansion, δr (mm) is the change in radius or radius loss per unit length due to volumetric change in the steel cross-section, and r (mm) is the original radius of the reinforcing steel bar. Expanding the Equation 3.15 gives Equation 3.16 which can be further expressed as shown in Equation 3.17.

$$\delta v = \pi\left[r^2 + 2r\delta r + \delta r^2 \right] - \pi r^2 \tag{3.16}$$

$$\delta v = \pi\left(2r\delta r + \delta r^2\right) \quad 3.17$$

Normally, the radial loss δr in Equation 3.17 can be a very small decimal and the δr^2 is considerably smaller compared to r. Hence its effect can be ignored (Lu et al. 2010). The volume change per unit length can be re-written as:

$$\delta v = 2\pi r \delta r \quad 3.18$$

Applying Equation 3.18 to density, volume, and mass relationship expressed in Equation 3.19, the resulting Equation 3.20 can be used to calculate the amount of steel radius loss (critical corrosion penetration or amount of corrosion) required to cause a first visible surface crack on the concrete samples.

$$\rho = \frac{\delta m}{\delta v} \quad 3.19$$

$$\delta_r = \frac{m_l}{2\pi r \rho} \quad 3.20$$

where ρ (g/cm^3) is the density of the reinforcing steel bar, and m_l (g) is the measured steel mass loss of the reinforcing steel bar due to the corrosion. The corrosion rate by gravimetric mass loss method can be obtained by dividing the Equation 3.20 by the measured cracking time of the concrete cover, and the resulting equation can be expressed as:

$$I_{ML} = \frac{m_l}{2\pi r \rho t_c} \quad 3.21$$

where I_{ML} (μm/year) is the corrosion rate by gravimetric mass loss method and t_c (years) represent the time from the corrosion initiation to the time at which a first visible appears on the concrete.

3.7.5 Other tests

Compressive strength

The compressive strengths of concrete used to design mixes were obtained by performing a standard 100 mm cube crushing test. The specimens were tested in water saturated condition after initial curing in water for 28 days in accordance with

SANS 5863-2 (1994). Three cubes per a mixture were selected and crushed using a hydraulic Universal Testing Machine (UTM) at a loading rate of 0.3 MPa/sec. The results were expressed as the average of the three measurements for a mix.

Splitting tensile strength

Three unreinforced prisms for each mixture were tested for tensile strength after 28 days of initial curing in water. This was to study the influence of tensile strength on corrosion cracking performance of the concrete specimens. It was performed in accordance with SANS 6253:2006. The test specimens were loaded into the hydraulic compression machine in a splitting plane parallel to the prism axis. A wooden strip of size 6 mm x 13 mm x 200 mm was used to distribute the applied compressive stress across the contact surface. This was done by placing the wooden strip along the contact surface between the concrete and the steel loading bar. A compressive force was applied at the rate 8.02 kN/min as specified by SANS 6253:2006. Equation 3.22 was used to calculate the tensile strength in MPa.

$$f_{sp} = \frac{2P}{\pi A} \qquad 3.22$$

where f_{sp} (Mpa) is the split tensile strength, P (N) is the failure load, and A (mm^2) is the area of the splitting surface. Three prisms were tested for each concrete mixtures, and an average of the three measurements represent the split tensile for that particular mix.

3.8 Summary

This chapter described the laboratory and field studies undertaken to provide the data used to develop models for predicting carbonation rate and corrosion radius loss required to initiate the first visible crack in RC structures exposed to the South African inland environment. The experimental programme consisted of three main phases. Phase one was the concrete characterisation tests on the concrete samples, using the durability indicators (oxygen permeability and water sorptivity indices). Phase two was the carbonation tests carried out on the concrete samples initially

moist cured for 7 and 28 days in water before the exposure to the natural inland environment for 2 years. Phase three was the natural corrosion propagation tests carried out on the pre-carbonated concrete samples using Coulostat corrosion rate meter, and gravimetric mass loss method.

A total of 1155 cubes (100 mm x 100 mm x 100 mm) were cast using fifteen different concretes for the durability indicator, natural carbonation, and compressive strength tests. The concretes were made using five binder types (100 PC, 70/30 PC-FA, 50/50 PC-BS, 90/10 PC-SF and 60/30/10 PC-BS-SF) and three w/b ratios (0.95, 0.60 and 0.40).

For the corrosion propagation tests, a total number of 108 RC prism (100 mm x 100 mm x 200 mm) and 24 unreinforced concrete prisms (12 prisms for splitting tensile strength test and 12 prisms for accelerated carbonation monitoring) were cast using six different concretes. Concrete specimens were made using three binder types (100 PC, 70/30 PC-FA, and 50/50 PC-BS) and two w/b ratios (0.95 and 0.60). Other corrosion propagation experimental variables included the cover depth (12, 20 and 30 mm) and the reinforcing steel diameter (8, 12 and 20 mm). Concrete resistivity and half-cell potential (HCP) methods were used to qualitatively assessed corrosion condition of the concretes and the corroding reinforcing steel bars respectively. Linear polarization resistance (coloustatic) and gravimetric mass loss methods were used to quantitatively assessed the corrosion condition of the corroding reinforcing steels.

The analyses and discussion of the results are presented in Chapter 4 and documented for the development of the carbonation-induced corrosion initiation and propagation models in Chapter 5.

CHAPTER 4

4 EXPERIMENTAL RESULTS, ANALYSES AND DISCUSSION

4.1 Introduction

The experimental results and analyses of the laboratory and field-based investigation into carbonation-induced corrosion of different concrete mixtures are presented in this chapter. The chapter is divided into two parts. The first part presents the results, analyses and discussion of the data obtained from the early-age characterisation tests performed on different concretes and carbonation test of the concrete specimens exposed to the natural inland environment; while the second part presents the results, analyses, and discussion of the data obtained from the corrosion tests performed on the pre-carbonated RC prism specimens exposed to the outdoor unsheltered environment. The relationship among some selected variables that influence concrete carbonation and corrosion of reinforcement are established. The relationships are used in Chapter 5 to develop the models that can predict carbonation rate and steel radius loss required to initiate cracking in RC structures exposed to inland environment.

4.2 Exposure Conditions at the Concrete Sites

The daily measurements of relative humidity (RH), temperature (T) and atmospheric carbon dioxide concentration (CO_2) were carried out for a year at the concrete exposure sites. The results which are presented in Table 4.1 are divided into two periods of the year, namely winter and summer. The winter starts from April to September while the summer starts from October to March in South Africa. As shown in Table 4.1, the climatic measurements are classified into three exposure types which are indoor, outdoor sheltered and outdoor unsheltered. This exposure conditions were used to allow comparison of the results with those stated in BS EN 206-1 (2006) which has a similar classification.

As shown by the results presented in Table 4.1, the range of relative humidity measured at the indoor exposure site is relatively lower than the range of RH measured at the outdoor exposure sites for the two periods. For a given exposure

the range of relative humidity measured during the summer is higher than the range of humidity measured during the winter. The difference in RH between the two periods is more noticeable in the outdoor exposures than with the indoor exposure. The marked difference between the winter and summer relative humidity, especially for the outdoor exposures may be due to frequent rainfall during the summer period compared to the winter period. The summer time is noted for the highest amount of rainfall compared to the winter period which has scarce rainfall in South African inland environment. The results of the RH obtained at the concrete exposure locations are expected to have an impact on concrete deterioration in the inland environment.

Table 4:1 Exposure conditions at concrete specimen exposure sites (±1400 hours)

Periods	Indoor			Outdoor sheltered			Outdoor unsheltered		
	RH (%)	T (^oC)	CO_2 (ppm)	RH (%)	T(^oC)	CO_2 (ppm)	RH (%)	T (^oC)	CO_2 (ppm)
April-September	30 - 35	19 - 20	990 - 1200	35 - 60	10-19	300-550	30 - 55	10-19	300-550
October-March	35 - 40	20 - 23	650 - 850	70 - 80	16-20	250-400	60 - 80	16-22	250-350

Note: The exposure conditions are presented in range (Minimum – maximum). RH (relative humidity), T (temperature)

Carbonation reaction does not occur when concrete pores are either completely dry or completely saturated with water (Ballim and Lampacher, 1996). The optimum range of relative humidity for carbonation reaction to occur was noted by Ballim et al. (2009) to be between 40% and 60%, and optimum range of relative humidity of between 60 and 90% was noted for reinforcement corrosion. However, various authors differ slightly as to the optimum RH range for maximum carbonation and corrosion rates (Ballim and Lampacher, 1996). With the relative humidity ranges cited by Ballim, Alexander and Beushausen (2009), it seems that outdoor exposures will favour carbonation process more than corrosion process. However, the periodic rewetting of the outdoor concretes during the summer period can significantly reduce the rate of CO_2 diffusion through the saturated pores of cement paste matrix (Alexander, Mackechnie and Yam, 2007; Ballim and Lampacher, 1996). As shown

by this results, the range of relative humidity during the summer period tends to be in favour of corrosion activity for outdoor RC in the inland environment.

It is also evident from the results that the maximum and minimum temperatures measured during the summer period are higher compared to the maximum and minimum temperatures measured during the winter period. This suggests that a higher steel corrosion rate is expected during the summer periods compared to the winter period in the inland environment since an increase in temperature usually cause an increase in rate of chemical reaction (Tuutti, 1982). It is also observed from the results that the maximum and minimum CO_2 concentrations for the indoor exposure is about three times higher than the maximum and minimum CO_2 concentrations of the outdoor exposures. This can be attributed to the enclosed nature of the indoor site which restricts the free circulation of air. Therefore, it is expected that concretes exposed to this indoor environment will experience a relatively higher carbonation rate than those in the outdoor exposure sites. The CO_2 concentrations for the two outdoor exposures seem to be similar.

4.3 Quantification of Concrete Quality

Concrete quality is defined in this study as the characteristics of concrete that bear on its ability to satisfy the requirement of resisting the movement of moisture, oxygen, and CO_2 into or within the cover of hardened concrete. In this study, the concrete resistance to the movement of moisture, oxygen, and CO_2 within the concrete is measured using the concrete fluid transport parameters represented by the early-age oxygen permeability index (OPI) and water sorptivity index (WSI). The 28-day OPI and WSI terms used in this study are referred to as the OPI and WSI of the concretes cured for 28 days in water and tested between 30 to 40 days from casting.

This section presents the results of the 28-day OPI and WSI. Note that a higher OPI or a lower WSI value represents a less permeable concrete while a lower OPI or a higher WSI depicts a more permeable concrete. The capillary pores of a lesser permeable concrete are smaller and less connected to allow easy transport of the aggressive fluids than a more permeable concrete. In this study, a less permeable

concrete represent a good quality while a more permeable concrete depicts a poor quality concrete.

4.3.1 28-day oxygen permeability index

The results of the 28-day oxygen permeability test conducted on the different concrete disc specimens are shown in Table B1 of Appendix B. The 28-day oxygen permeability results are presented as both coefficient of oxygen permeability, k (m/s) and oxygen permeability index, OPI (-log k (m/s)). Each value shown in Table B1 of Appendix B represents an average of OPI measurements of four individual concrete disc specimens of the same concrete mix.

The mean values of 28-day OPI of the concretes are given with their standard error bars in Figure 4.1. A standard error bar shows the graphical representation of data variability. They are determined using this expression; $\mu \pm (\sigma / n^{0.5})$ where μ represents mean of a particular group of data, σ is the standard deviation of the same group of data and n is the number of measurements (Cumming, Fidler and Vaux, 2007).

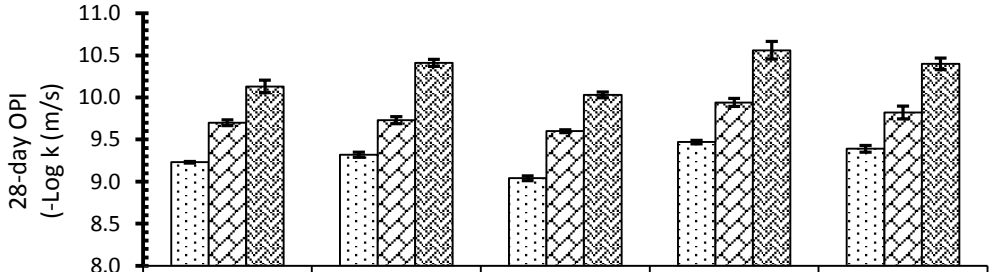

	PC	PC-FA	PC-BS	PC-SF	PC-BS-SF
0,95 w/b	9.23	9.32	9.04	9.47	9.39
0,60 w/b	9.70	9.73	9.60	9.94	9.82
0,40 w/b	10.13	10.41	10.03	10.56	10.40

Figure 4:1 28-day OPI results (error bars represents $\mu \pm (\sigma / n^{0.5})$)

The wider an error bar from the mean the higher the measurement variability. Standard error bar can also be used to show statistical significant difference between

two or more data groups (note that two or more error bars lapping each other indicate that there is no significant statistical difference between their means). In this study, the standard error bars are used to illustrate the variability and statistical significance of the data presented.

As shown in Figure 4.1 there are significant differences in the mean OPI values for the same concrete at different w/b ratios. Concrete becomes more permeable as w/b ratio increases. This effect is common to all the concrete types and can be attributed to the capillary porosity of their cement paste and interconnectivity of the pores which increase along with an increase in the w/b ratio (Salvoldi, 2010; Alhassan, 2014 and Ananmalay, 1996). Garboczi (1995) attributed the increased capillary porosity in high w/b ratio concrete to their low binder content which causes inefficient packing of the cement particles with the aggregates.

A discernible trend between the OPI and binder type is also noted but not as much as that between the OPI and w/b ratio. At the same w/b ratio, the SCM blended concretes are less permeable than the PC concretes. This can be due to the effect of pozzolanic reaction and complex products of hydration reaction of the SCM (forming new CSH phase) (Mehta, 1987). These products tend to block the capillary pores resulting in a denser microstructure with a finer pore structure (Mehta, 1987).

Even though, particle size of the SCM used in this study were not measured, it is well understood that SCM particles are smaller than PC particles, the feature of which is beneficial in controlling the width of cement packing with aggregates. The smaller SCM particles allow a better packing with the PC and aggregates which improve the concrete microstructure and consequently reduces its permeability. However, the BS blended concretes behaved differently and were more permeable compared to the other SCM concretes at all the w/b ratios considered. This can be attributed to the inability of the BS at an early age (28 days) to attain its full reactivity potential in refining its pore structure. The inability of the BS blend to reach its full reactivity potential at 28 days of moist curing may be due to the low PC content (50%) of the BS blended concrete mixture compared to the other SCM blended concretes. The trend noted for the permeability of the BS blended concretes was also reported by Tuutti (1982) and Ballim (1993). Tuutti (1982) ascribed it to

the presence of microcracks within the pores of BS concrete while Ballim (1993) attributed the low OPI values of the BS blended concretes to their low 28-day compressive strengths.

As shown by the standard error bars plotted on the mean values of the OPI (Figure 4.1), this study suggests that the order of permeability of the concretes from minimum to maximum is PC-SF→ PC-BSSF → PC-FA → PC → PC-BS for 0.95 and 0.40 w/b ratios. Moreover, it seems that there is no significance difference between the OPI of the PC and PC-FA concretes at 0.60 w/b ratio. This is also similar to PC-SF, and PC-BS-SF concretes at 0.60 w/b ratio. Therefore, for the 0.60 w/b ratio concretes the order of permeability from minimum to maximum is PC-SF/PC-BS-SF → PC-FA/PC → PC-BS. The improved performance of the SF blended concretes compared to the other concretes can be because of its early reactivity and high particle fineness as noted by various researchers (Terence, 2005; Arum and Moya, 2012; King, 2012; Buss, 2013). This is in line with the previous findings of Alhassan (2014); Ananmalay (1996) and Wong et al. (2009) where SF was regarded as an effective pozzolanic micro-filler in concrete.

The results of the OPI obtained in this study clearly reflect the influence of w/b ratio and binder type on the overall pore structure of the concretes. Therefore, OPI may be used as part of the input parameter in a model that can reasonably predict carbonation rate in different concretes.

4.3.2 28-day water sorptivity index

Water sorptivity test measures the rate of water absorption by capillary suction of an unsaturated concrete disc (Kropp and Alexander, 2007; Alexander, Ballim and Stanish, 2008). It is a sensitive parameter that provides useful information relating to the pore structure of concrete at the surface zone (Ballim, 1993). The results of the water sorptivity index (WSI) of the concretes are presented in Figure 4.2, where the WSI values are plotted against the w/b ratio and binder type. It is understood that OPI and WSI give an indication of the pore structure of concrete; therefore, much of the discussions on the OPI results will be similarly to that of WSI.

Using the standard error bars plotted on the mean values of the WSI to interpret the WSI results, the variation in the w/b ratio can be seen to have a marked effect on the WSI than the variation in the binder type. For an equal w/b ratio of 0.95, WSI of the PC concrete is higher than that of SCM blended concrete. As shown by the error bars, there is no clear difference among the WSI of the SCM blended concretes at the same 0.95 w/b ratio. As shown by the error bars (Figure 4.2) , there is no clear difference among the WSI of the SCM blended concretes at a constant w/b ratio of 0.95. Therefore, the 0.95 w/b concretes are classified into two groups (PC and SCM blended concretes) and the PC concrete has a greater WSI compared to the SCM blended concretes at a constant 0.95 w/b ratio. For 0.60 w/b ratio, replacing the PC with 30% FA and 50% BS respectively did not have any significant difference on WSI. However, at the same w/b ratio of 0.60, replacing PC with 10% SF at both binary and ternary compositions with the PC show some significant reductions in WSI. Therefore, the ranking order of WSI from maximum to minimum for the 0.60 w/b ratio is PC /PC-FA/ PC-BS → PC-SF/PC-BS-SF. For w/b ratio of 0.40, there is no significant difference among the concretes. Therefore, the WSI of the concretes were the same.

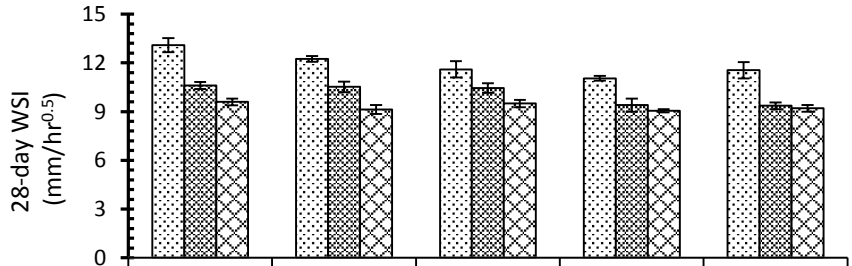

	PC	PC-FA	PC-BS	PC-SF	PC-BS-SF
0,95 w/b	13.10	12.25	11.60	11.05	11.55
0,60 w/b	10.60	10.52	10.45	9.40	9.36
0,40 w/b	9.60	9.13	9.50	9.05	9.20

Figure 4:2 28-day water sorptivity (WSI) results (error bars represents $\mu \pm (\sigma / n^{0.5})$)

The results of the WSI shown in Figure 4.2 suggests the following points:

(i) water sorptivity index is less sensitive to variation in the binder type at low and high w/b ratios (0.40 and 0.95)

(ii) For w/b ratio of 0.6, the WSI results showed no difference between the PC-FA and PC-BS concretes. This is also similar to the PC-SF, and PC-BS-SF concretes.

All these show the limitations WSI can present if used as an input parameters in the carbonation rate prediction models. Therefore, it seems that OPI is more appropriate to be used as an input parameter in carbonation rate models compared to WSI.

4.4 Compressive Strength and Split tensile strength

The 28-day compressive strength and split tensile strength results of the concretes are presented in Tables A1 and A2 of Appendix A. Each of the strength values represents an average of 3 individual concrete compressive strengths and tensile strengths respectively.

Figure 4.3 demonstrates the effect of w/b ratio variation and binder type on the compressive strength. The error bars show the compressive strength variability and the significant difference between the concrete mixtures. The results indicate that the variation in the w/b ratio is more significant to the compressive strength than a change in binder type. In all the concrete mixtures, the compressive strengths increase as the w/b ratio is reduced. This follows a normal trend in concrete, as reported by some previous studies (Ananmalay, 1996; Johnson, 2010; Otieno, 2008; Ikotun, 2010).

The effect of SCM on the concrete compressive strengths is shown in Figure 4.3. Apart from the BS blended concrete, the SCM blended concretes have their compressive strengths higher than the PC concrete for the same w/b ratios of 0.95 and 0.60. The lower compressive strength observed with the BS blended concretes at 0.95 and 0.60 w/b ratios can be due to the slower hydration and inactivity of the BS blend at higher w/b ratios. Essentially, the early strength development of a particular concrete mix is from hydration of the C3S component of the clinker.

Clark (2013) asserted that it is the dilution of the C3S by the SCM that reduce the setting time and early strength development of blended cement concretes. In this study, the dilution factor is greater in the BS blended concretes than other blended cement concretes used in this study. Hence, lower early compressive strength were observed in the slag concretes. However, for 0.40 w/b ratio, the SCM blended concretes have their compressive strengths higher than the PC concrete which can be due to a dense microstructure formed by the pozzolanic reaction of the SCM at low w/b ratio (Kayali & Zhu, 2005; Igarashi & Watanabe, 2006).

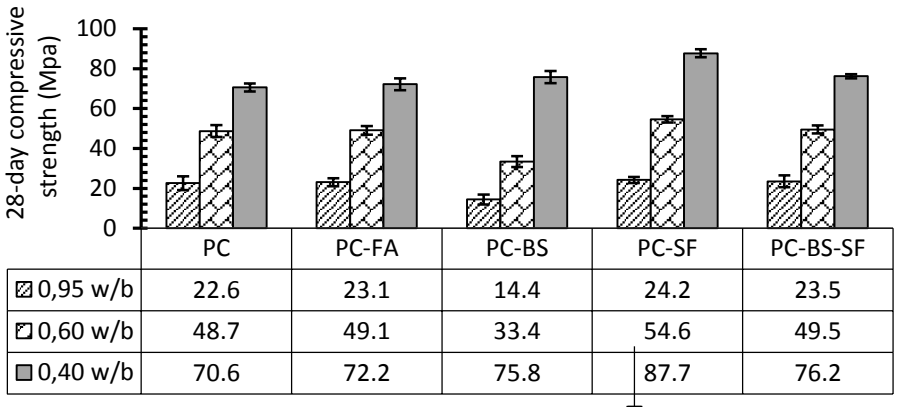

	PC	PC-FA	PC-BS	PC-SF	PC-BS-SF
0,95 w/b	22.6	23.1	14.4	24.2	23.5
0,60 w/b	48.7	49.1	33.4	54.6	49.5
0,40 w/b	70.6	72.2	75.8	87.7	76.2

Figure 4:3 28-day compressive strength results (error bars - $\mu \pm (\sigma / n^{0.5})$

Moreover, the concrete mixtures blended with SF have the highest compressive strengths compared to other concrete mixes for all the w/b ratios. This can be attributed to the increased fineness of SF, which contributes to an improvement in its reactivity and particle packing (micro-filler effect) of the cement with the aggregates. Thus the SF at both binary and ternary compositions with PC and BS can be used to densify the microstructure of a cement paste matrix.

The observed trends in the 28-day compressive strength results are similar to the trends in 28-day tensile strength results as shown in Table A4 of Appendix A. Even though, tensile strength is not normally specified during concrete design, the knowledge of tensile strength can be used to estimate the load under which cracking is initiated and propagated in concrete.

4.5 Carbonation Depth

The carbonation depths of the concretes were measured using the method described in Chapter 3 (Section 3.5.3). The results are presented in Tables C1, C2 and C3 of Appendix C. The typical plots of carbonation depths against the exposure times for the PC concretes exposed to an indoor environment are shown in Figure 4.4. The plots show that for a given concrete in an indoor environment, carbonation depth increases along with the exposure time and a higher carbonation depth is noticed with a higher w/b ratio. Similar trends were also observed for the concretes exposed to outdoor sheltered and unsheltered environments. Even though the trend of carbonation depth with exposure time is the same in all the concretes the depth of carbonation varied. This may be due to the influence of binder type, w/b ratio, duration of the initial moist curing conditions, and the climatic condition at the concrete exposure site.

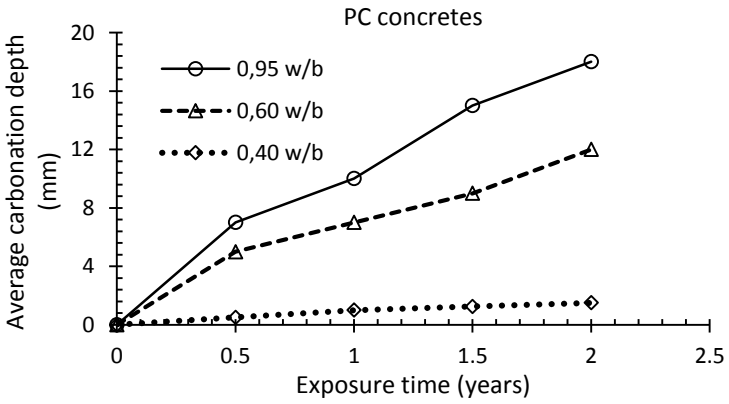

Figure 4:4 Carbonation depth versus exposure time – Indoor exposure

Apart from the SF blended concretes, the SCM blended concretes showed higher carbonation depths than the PC concrete for the same w/b ratio, curing age, and exposure condition. The effect of the initial moist curing duration is also observed on the concretes carbonation depth. A given concrete initially moist cured for 28 days before exposure to a particular environment showed a lower carbonation depth

compared to the same concrete subjected to seven days moist curing before exposure to the same environment.

For a given concrete mixture moist cured for a particular given time showed a higher carbonation depth at every ages of exposure to indoor environment compared to the same concrete exposed to outdoor environment for the same ages. It is also noticed that for a similar w/b ratio, curing age and binder type, a concrete exposed to the outdoor sheltered environment has a higher carbonation depth compared to the same concrete exposed to the outdoor unsheltered environment. In this study, carbonation rate is used to express the carbonation resistance of the concrete. The next section (4.6) discusses the results of the carbonation rate of the concretes.

4.6 Carbonation Rate

Carbonation rate is defined as the progress of the carbonation front in concrete with time. It is used to assess the carbonation resistance of different concretes, and is influenced by w/b ratio, binder type, duration of initial curing condition, and climatic conditions at the exposure site and duration of the exposure. Moreover, carbonation rate allows variability to be quantified in individual concretes and can also be used to model time to corrosion initiation of steel in concrete.

Based on the 2 years measurements of average carbonation depth of the concretes exposed to the natural inland environment, carbonation depths were plotted against the square root of the exposure time. A linear regression line was fitted to each of the carbonation data as shown in Appendix C, Figures C1 to C6. The slope of the regression line represents the carbonation rate (K_c) of a particular concrete mixture and as illustrated in Equation 4.1 (Note that the carbonation depth was assumed to be zero at the beginning of the exposure).

$$d = K_c t^{0.5} \qquad 4.1$$

where, Kc (mm/year$^{0.5}$) is the carbonation rate, d (mm) is the average carbonation depth and t (years) is the duration of the exposure. The coefficients of correlation (R^2) are well above 90% in most of the concretes. Some concretes with low R^2 (<

90%) may be due to displacement and handling of the specimens during the exposure to the natural environment. Carbonation rate (K_c) of the concretes are presented in Figures 4.5 and 4.6, and the following points are evident:

i. For a given binder type, w/b ratio and moist curing duration, carbonation rate is greater in indoor exposure than outdoor exposure conditions. For the same concrete, carbonation rate is greater in outdoor sheltered conditions compared to outdoor unsheltered conditions.

ii. For a given binder type, curing duration and exposure environment, the carbonation rate increases with increasing w/b ratio.

iii. For a given w/b ratio, exposure condition and duration of initial moist curing condition, the order of carbonation rate (minimum to maximum) in terms of the binder type is PC-SF → PC-BS-SF → PC→PC-FA → PC-BS

iv. A given concrete initially moist cured for 28 days before exposure to a particular environment shows a lower carbonation rate compared to the same concrete which was initially moist cured for seven days before exposure to the same environment.

The influence of the exposure conditions, w/b ratio, binder type and initial moist curing age on the carbonation coefficient are discussed in sections 4.6.1, 4.6.2 and 4.6.3.

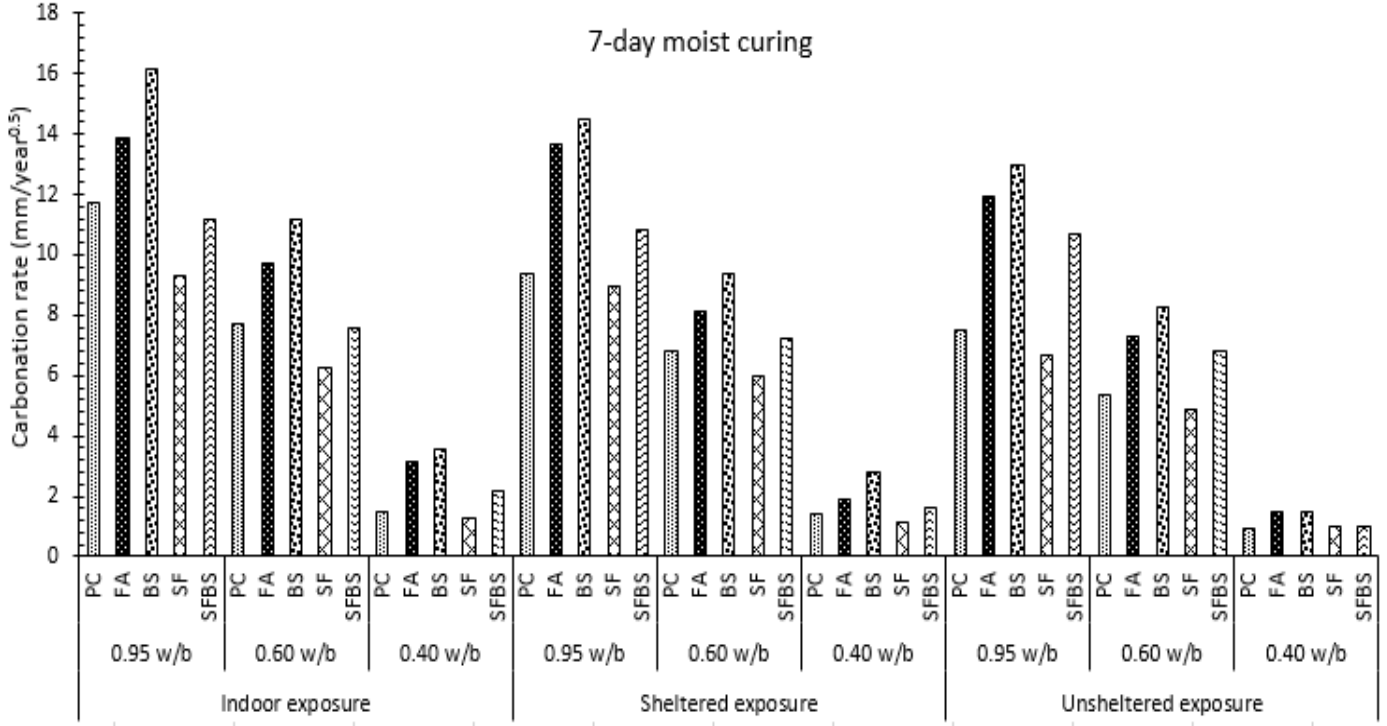

Figure 4:5 Carbonation rate versus water/binder ratio, binder type and exposure conditions for the concretes initially moist cured for

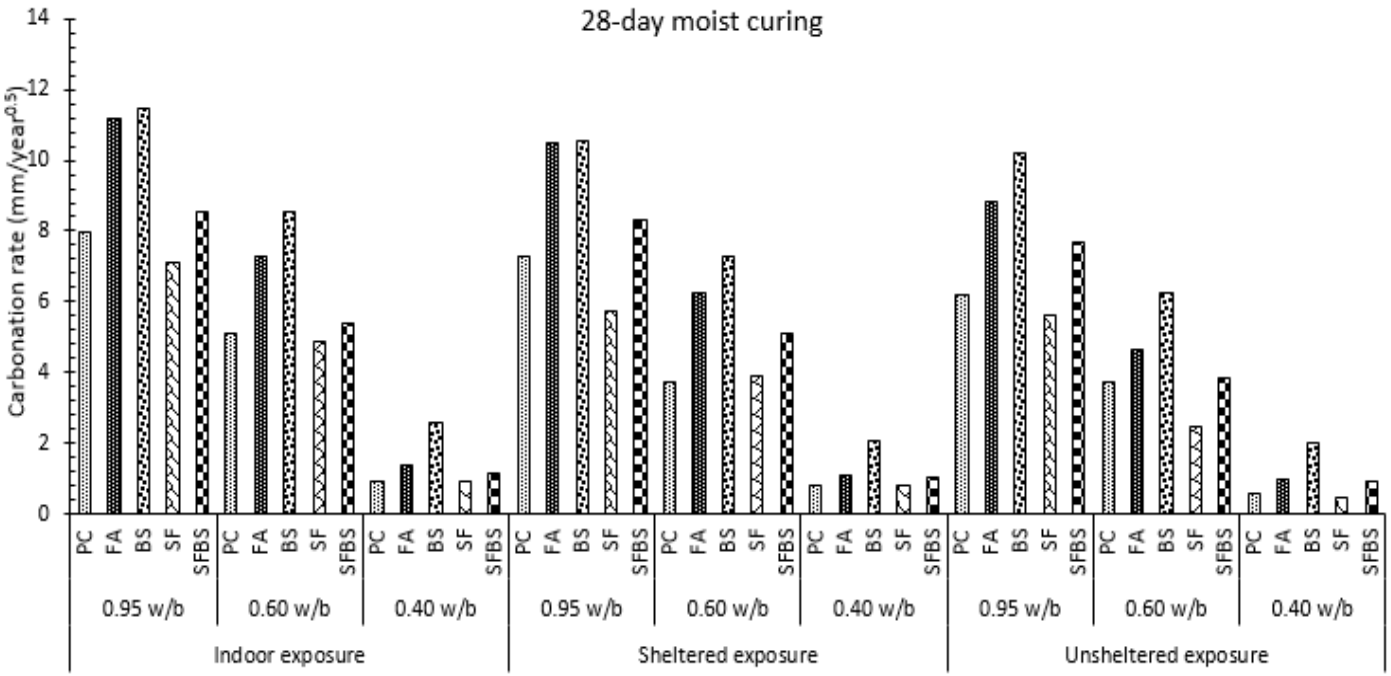

Figure 4:6 Carbonation rate versus water/binder ratio, binder type and exposure conditions for the concretes initially moist cured for 28 days

4.6.1 The effect of natural exposure conditions on carbonation rate

The effect of the indoor, outdoor sheltered, and outdoor unsheltered exposure conditions on the concrete carbonation rates are shown in Figures 4.5 and 4.6. It can be observed from Figures 4.7 and 4.8 that for a given concrete initially cured for a specified period; the indoor exposed concretes have the highest carbonation rates compared to the concretes exposed to the outdoor environmental conditions. This can be due to the higher concentration of CO_2 found in the indoor environment compared to the outdoor CO_2 concentration. Moreover, it seems that the relative humidity of the indoor environment does not support optimum carbonation reaction as shown in Table 4.1. This shows that the carbonation reaction of the indoor exposed concrete is controlled by the CO_2 diffusion rather than the exposure relative humidity and it is made possible by the available water within the concrete pore network.

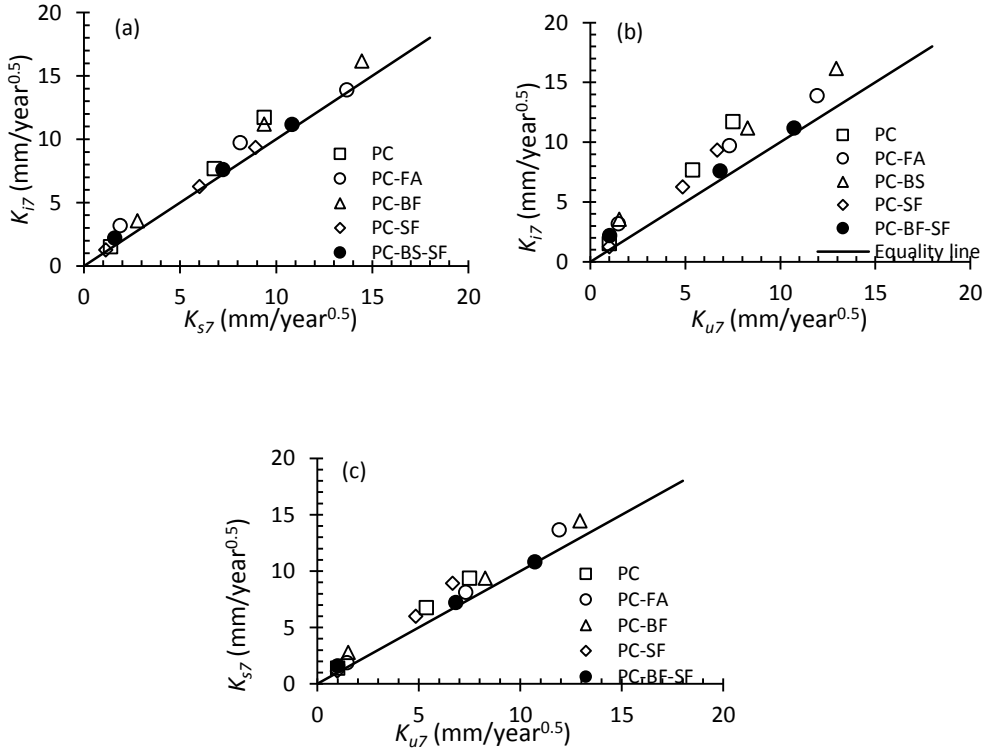

Figure 4:7 (a) Indoor carbonation rate (K_{i7}) versus outdoor sheltered carbonation rate (K_{s7}) (b) Indoor carbonation rate (K_{i7}) vs outdoor unsheltered carbonation rate (K_{u7}) (c) Outdoor sheltered (K_{s7}) vs outdoor unsheltered (K_{u7})

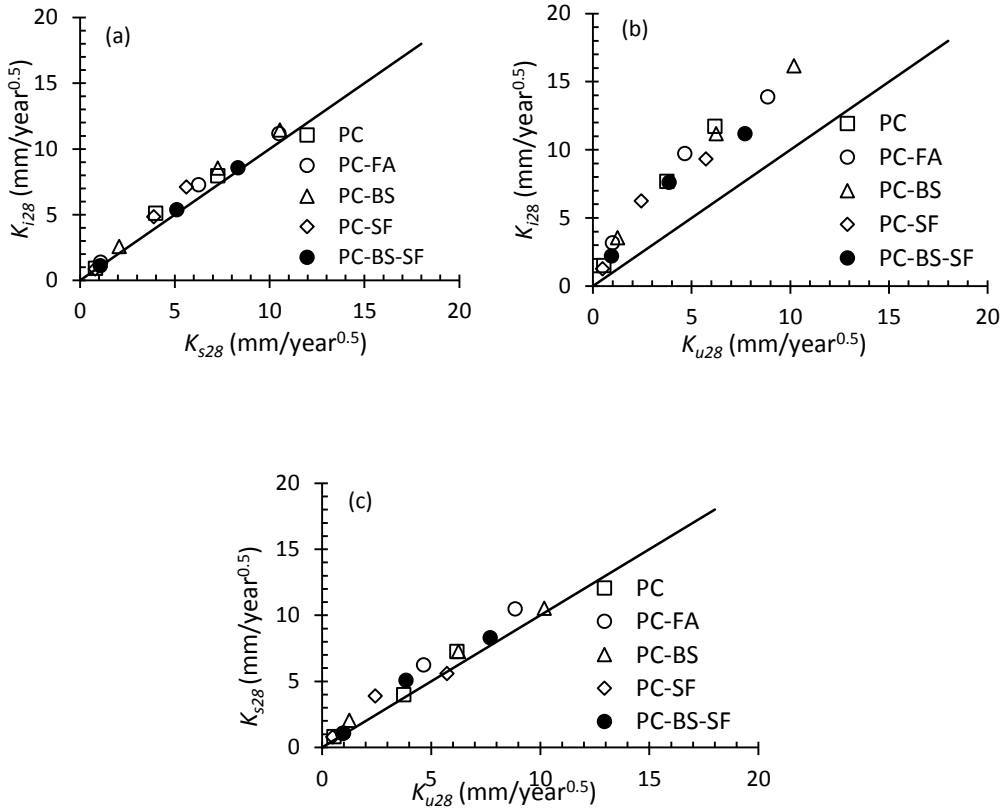

Figure 4:8 (a) Indoor carbonation rate (K_{i28}) versus outdoor sheltered carbonation rate (K_{s28}) (b) Indoor carbonation rate (K_{i28}) vs outdoor unsheltered carbonation rate (K_{u28}) (c) Outdoor sheltered (K_{s28}) vs outdoor unsheltered (K_{u28})

In comparing the two outdoor exposure conditions of sheltered and unsheltered as shown in Figures 4.7 and 4.8, it is evident that carbonation rate is higher in the sheltered concretes than the unsheltered concretes. This is because capillary pores of the outdoor exposed concretes are usually filled with moisture during the wet season thereby hindering CO_2 diffusion into the concrete pores. The carbonation reaction can only proceed once samples have dried sufficiently to the depth at which the process stopped (Ananmalay, 1996; Hills *et al.*, 2015). This shows that for a concrete exposed externally to the inland environment, carbonation reaction is controlled by the length of wetting and drying periods.

The carbonation rate results obtained in this study verify the results of Nischer, (1984), where three years carbonation tests on concretes exposed to an outside unsheltered condition of rain shower showed a reduced carbonation rate in comparison to an indoor exposed concrete. Wierig (1984) also reported that

concrete walls protected from rain showed greater carbonation rate compared to the same structure exposed to rain.

4.6.2 The effect of w/b ratio and binder type on carbonation rate

To show the effect of w/b ratio and binder type on carbonation rate of the concretes, the carbonation rate was plotted against w/b ratio and binder type (Figures 4.5 and 4.6). As shown by the plots, for a given concrete exposed to a certain inland environment, the carbonation rate increases with an increase in w/b ratio. This may is due to the increased concrete capillary pore sizes and their interconnectivity at a high w/b ratio since w/b ratio primarily determines the gel/space ratio, capillary porosity and concrete permeability (Garboczi, 1995). The increased carbonation rate of the high w/b ratio concrete may also be attributed to the fact that the amount of Portlandite decreases with an increase in w/b ratio as there is less cementitious material present in higher w/b ratios (Salvoldi, Beushausen and Alexander, 2015). This trend is similar to the observation made by Houst & Wittmann (1994) in an experiment that involved varying w/b ratio from 0.40 to 0.80 and measuring the corresponding effective diffusivity of CO_2 in the concrete. The corresponding effective diffusivity increased by 20 to 25% when the w/c ratio varied from 0.40 to 0.80. The trend was also evident from the permeation test results of the concretes as shown in Figure 4.1, even though oxygen gas was used as the permeating fluid.

Similar results about the effect of w/b ratio on carbonation rate of different concretes have also been reported in the literature (Tuutti, 1982; Alhassan, 2014; Salvoldi, Beushausen and Alexander, 2015). The decrease in carbonation rates of the concretes at a lower w/b ratio was attributed to the fact that the cumulative pore volume and the amount of pores are reduced compared to concrete with high w/b ratio concretes. Therefore, it can be concluded that concrete with low w/b ratio show superior resistance to carbonation.

The influence of binder type on the carbonation rate of the concretes for each of the exposure site is also shown in Figures 4.5 and 4.6. It is evident that for a constant w/b ratio, the SCM blended concretes showed higher carbonation rates compared to the PC concretes exposed to the same environment. However, SF concretes at a

binary composition with BS and PC showed a superior carbonation resistance compared to the PC, FA and BS blended concretes. This observation is consistent with the trend reported by other previous researchers (Ananmalay, 1996; Khunthongkeaw, Tangtermsirikul and Leelawat, 2006; Neville, 2011; Alhassan, 2014; Salvoldi, Beushausen and Alexander, 2015).

Despite the fact that the pore structure of SCM blended concretes are very dense as a result of their finer particle size and their filler effect with PC and aggregates, their carbonation rates are higher compared to the PC concretes. This suggests that pore structure may not be the only parameter that control the carbonation rate in concrete. In a similar work, Alhassan (2014) asserted that there is a greater influence of carbonating material present in hydrated cement paste of concrete on carbonation rate. For a given w/b ratio, the amount of $Ca(OH)_2$ in the SCM blended concrete is lower compared to that of PC concrete. This is usually because of the reduction in the PC content of the SCM blends. The available $Ca(OH)_2$ in the SCM concrete is partly consumed during the pozzolanic reaction of the SCM (Dalage and Aitcin, 1983; Terence, 2005). The pozzolanic reaction of the SCM blend reduces the amount of calcium hydroxide available for carbonation reaction and can be responsible for the faster rate of carbonation in the SCM blended concretes.

It is well noted by many studies that, the reactivity of SF at early age is higher due to its particle fineness, this depicts a greater consumption of Ca $(OH)_2$ with an expectation that carbonation rate would be greater in SF blended concrete than the PC concrete. The improved performance of SF blended concrete can be attributed to its lower permeability as as a result of its particle fineness and high PC content compared to FA and BS (Terence, 2005; Arum and Moya, 2012; King, 2012; Buss, 2013). This shows that permeability controls carbonation rate more than the reactivity of SF in SF blended concrete.

4.6.3 Effect of initial moist curing duration on carbonation rate

The effect of the initial moist curing duration on concrete carbonation rates is illustrated in Figure 4.9. It is evident that for a given concrete in exposure, extending the initial moist curing duration from 7 days to 28 days reduces the carbonation

rate. The percentage reduction in carbonation rate of the concretes when the initial moist curing duration was varied from 7 days to 28 days are presented in Table 4.2. The decrease in the carbonation rate due to the extension in the early-age curing conditions may be because of the fact that extending the moist curing duration increases the degree of hydration (Garboczi, 1995). During hydration, the capillary porosity decreases due to consumption of water producing hydration products that fill the capillary pore spaces. As the hydration continues, the size of the capillary pores and the connectivity between the pores decreases, particularly at the cover zone.

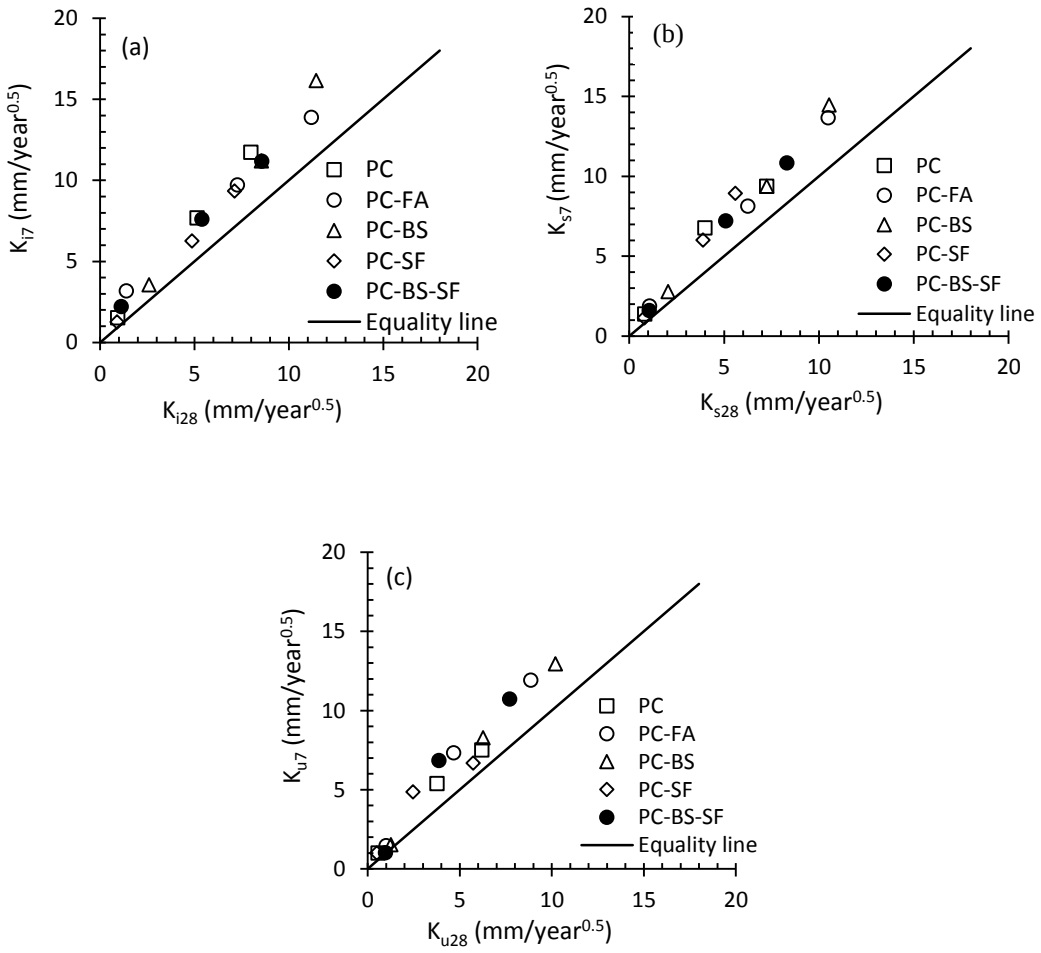

Figure 4:9 (a) Indoor carbonation rate (K_{i7}) vs indoor carbonation rate (K_{i28}) (b) sheltered carbonation rate (K_{s7}) vs sheltered carbonation rate (K_{s28}) (c) Outdoor unsheltered (K_{u7}) vs outdoor unsheltered (K_{u28})

Several findings about the beneficial effect of increasing the initial moist curing duration of concrete on hardened properties of concrete have been reported in the literature (Ballim 2003; Alonso and Andrade (2007); Owens (2009); Molina, (1992); Scrivener & Nernati (1996); Nagataki & Ohga (1986) and Tsukayama (1980)). They attested to the fact that increasing the duration of the initial moist curing of concrete improves the concrete microstructure which in turn influences its hardened properties, hence, the concrete service life is affected.

Table 4:2 Percentage reduction in carbonation rate K_c (mm/year$^{0.5}$) due to extension of the initial curing period from 7 days to 28 days

Binder type	PC			PC-FA			PC-BS			PC-SF			PC-BS-SF		
w/b ratio	0.95	0.60	0.40	0.95	0.60	0.40	0.95	0.60	0.40	0.95	0.60	0.40	0.95	0.60	0.40
% Reduction in K_i	32	33	38	19	25	56	29	24	27	24	22	29	23	29	49
% Reduction in K_s	23	41	41	23	23	43	27	23	26	37	35	30	23	29	34
% Reduction in K_u	18	30	45	26	36	33	21	24	18	14	50	52	28	44	7

Moreover, extending the initial moist curing of concrete is not the only method of reducing carbonation rate in concrete in an exposure condition. Other methods such as reducing the w/b ratio seems to offer greater reductions in carbonation rate of the concretes compared to extending the initial moist curing duration as shown in Tables 4.2 to 4.4. For example, a PC-FA concrete of 0.95 w/b ratio exposed to the indoor environment was initially moist cured in water for seven days. The same PC-FA concrete was initially moist cured for 28 days in water, the percentage reduction in carbonation rate as shown in Table 4.2 is 19%. Reducing the w/b ratio from 0.95 to 0.60 for the same concrete in a similar environment gives a carbonation rate reduction of 30% (Table 4.3). A further reduction of the w/b ratio from 0.60 to 0.40 gives a carbonation rate reduction of 67% which is the highest compared to extending the early-age moist curing duration from 7 to 28 days. The trend is similar in all the concretes in the other exposures.

This analysis shows that reducing the w/b ratio seems to be more effective and sustainable (in terms of water conservation) in reducing the carbonation rate in concrete than extending the duration of the initial moist curing.

Table 4:3 Percentage reduction in carbonation rate, K_c (mm/year$^{0.5}$) due to decrease in w/b ratio from 0.95 to 0.60

	PC	PC-FA	PC-BS	PC-SF	PC-BS-SF
% Reduction in K_i	34	30	31	32	23
% Reduction in K_s	28	41	35	33	33
% Reduction in K_u	28	39	36	27	28

Table 4:4 Percentage reduction in carbonation rate, K_c (mm/year$^{0.5}$) due to decrease in w/b ratio from 0.60 to 0.40

	PC	PC-FA	PC-BS	PC-SF	PC-BS-SF
% Reduction in K_i	80	67	68	80	74
% Reduction in K_s	78	77	70	81	78
% Reduction in K_u	81	80	82	80	85

4.7 Relationship between Carbonation Rate and Permeability

Carbonation reaction and permeability of concrete occur within the concrete pore network system therefore, a relationship between the carbonation rate and oxygen permeability index is expected. An approach was made in this study to correlate the carbonation rate of the concrete initially cured for 28 days in water to their corresponding 28-day oxygen permeability index using regression analysis of least squares method. The regression analysis of least squares method was based on the experimental data of the concretes 28-day OPI and their corresponding 2-year carbonation data.

In the statistical analyses, each concrete mixture data of PC, PC-FA, PC-BS, PC-SF and PC-BS-SF for a particular carbonation exposure condition was individually used to find a linear regression line that fit the data quite well as shown in Figure 4.10 to 4.12. Some considerations were given to other forms of regression plots

such as power, logarithms, and exponential functions and linear function appears to fit the data with their coefficient of correlations (R^2) very close to unity with 95% confidence level. However, it is observed that different concretes do not correlate well with each other. This may be due to the effect of binder chemistry on their carbonation rates (Salvoldi, Beushausen and Alexander, 2015). This may bring a difficulty in developing a generalised model that shows the effect of different binders on carbonation rate..

The trend in the relationship between the carbonation rate and the early-age OPI of the concretes suggests a negative linear correlation. This can be interpreted to mean that an improvement in the quality of concrete reduces the concrete carbonation rate for all the exposures.

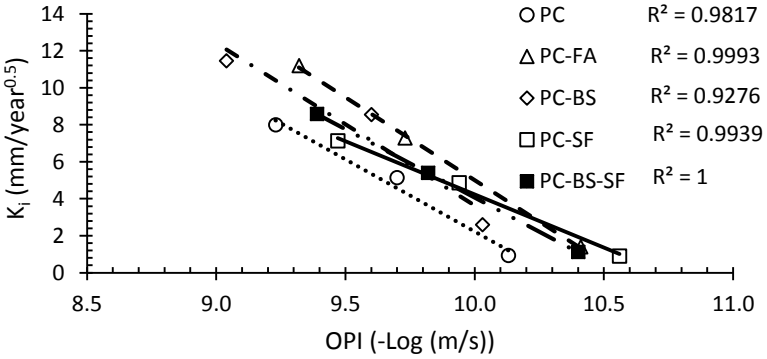

Figure 4:10 Relationship between K_i (indoor exposure carbonation rate) and OPI

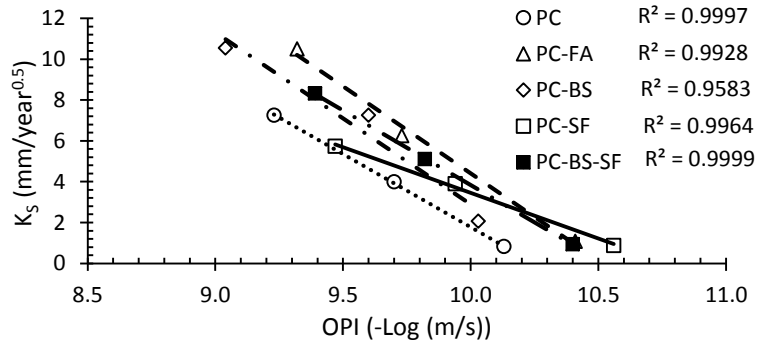

Figure 4:11 Relationship between K_s (sheltered exposure carbonation rate) and OPI

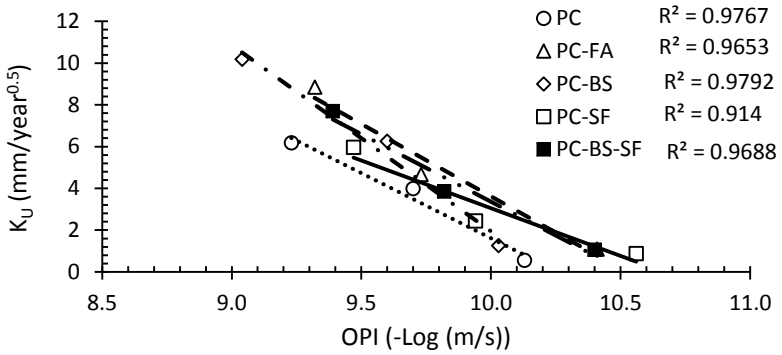

Figure 4:12 Relationship between K_u (unsheltered exposure carbonation rate) and OPI

4.8 Corrosion Propagation Test Results, Analyses and Discussion

This part presents the test results, analyses and discussion of corrosion propagation in the pre-carbonated concrete samples exposed to the natural inland unsheltered environment. Concretes were made using three binder types (100 PC, 70/30 PC-FA, and 50/50 PC-BS) and two w/b ratios (0.95 and 0.60). Other corrosion propagation experimental variables included cover depth (12, 20 and 30 mm) and reinforcing steel diameter (8, 12 and 20 mm).

The corrosion of the reinforcing steel bars was initiated by carbonation and propagated by exposing the RC samples to the unsheltered natural inland environment. The corrosion extent of the reinforcements was assessed immediately a visible crack appeared on the concrete cover using electrochemical (linear polarisation resistance). Gravimetric mass loss method was used to measure the amount of steel radius loss required to initiate the first visible crack in the concretes. The reinforcement corrosion test results are presented, analysed, and discussed in term of corrosion current density, reinforcement radius loss, corrosion rate and time to initiate a first visible crack on the cover concretes (cracking time). The associated factors that influenced the corrosion propagation in the exposed concrete samples are discussed.

4.8.1 Reinforcement corrosion current density

The corrosion current density was measured electrochemically using a Coulostat V3 instrument as described in Chapter 3. The measurements were taken immediately after the appearance of the first visible crack on the concrete; the results are presented in Figures 4.13 to 4.16. (Note: corrosion current density referred to in this section is an average of 4 readings on 2 RC specimens having the same w/b ratio, cover depth, and reinforcement diameter). Even though visible cracks were evident on the cover concretes, the steel corrosion current density results were influenced by the cover depth, w/b ratio, and binder type. The results trends are discussed as follows:

i. For a given concrete at a constant cover depth, increasing or decreasing the reinforcing steel diameter seems not to have any significant trend with the corrosion

current density as evident from Figures 4.13, 4.14 and 4.15. Therefore, ignoring the effect of the reinforcing steel diameter on the corrosion current density, a clearer trend is obtained as shown in Figure 4.16.

ii. The steel corrosion current density increases with a reduction in cover depth. This is because the reinforcement placed at a lower cover depth has more access to oxygen and moisture than reinforcement positioned at a higher cover depth for a given concrete.

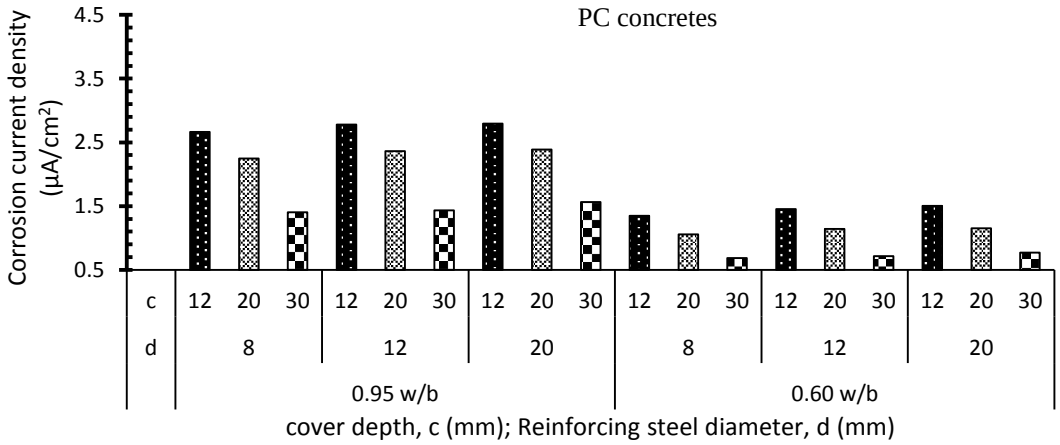

Figure 4:13 Corrosion current density results (PC concretes)

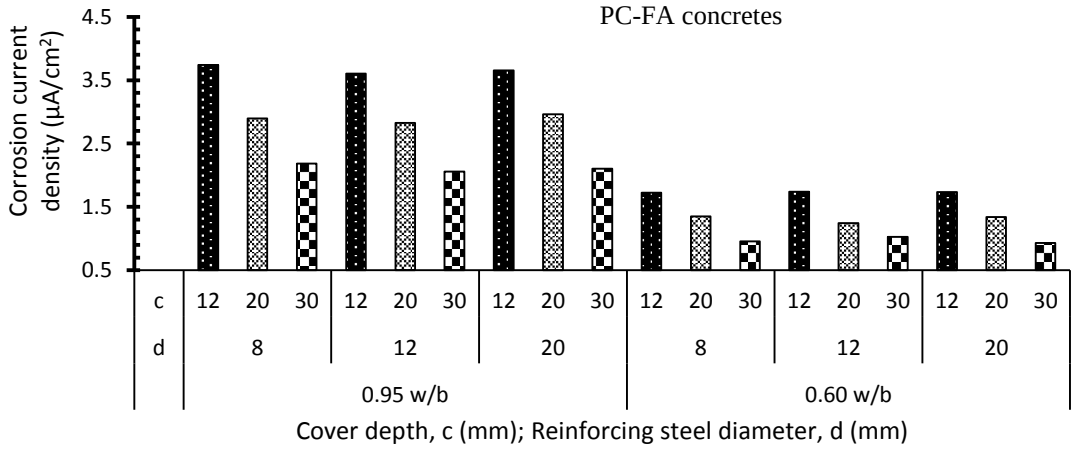

Figure 4:14 Corrosion current density results (PC-FA concretes)

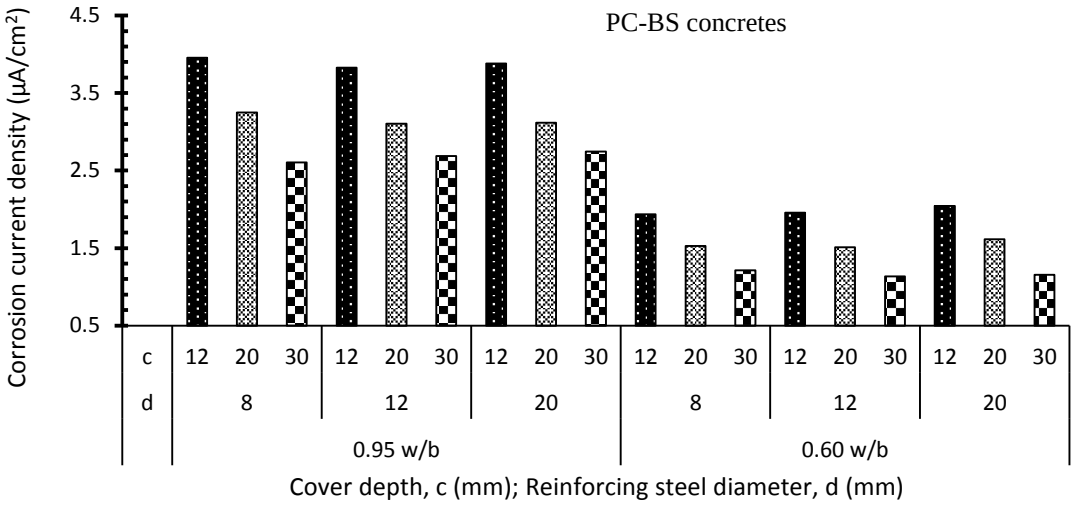

Figure 4:15 Corrosion current density results (PC-BS concretes)

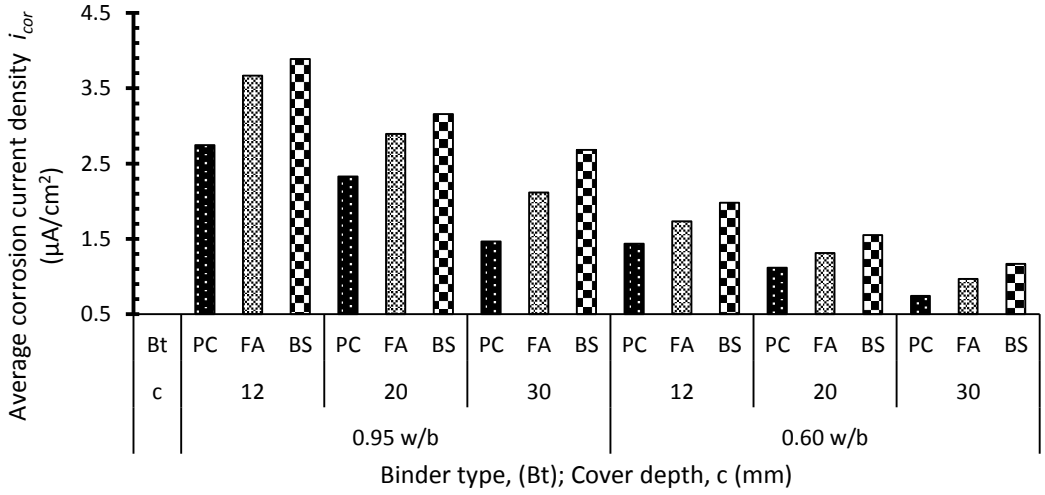

Figure 4:16 Average corrosion current density results

iii. As presented in Figure 4.16, the SCM blended concretes have higher steel corrosion current density compared to the PC concretes and BS blended concretes that have the highest steel corrosion current density at all the w/b ratios and cover depths. The trend is similar to the trend observed in the carbonation rate results of the concretes. Similar findings of the effect of SCM on carbonation-induced corrosion have been reported in the literature (Arachchige, 2008; Gonzalez, Feliu

and Rodrigues, 1996). The increase in the corrosion current density of the SCM concretes was attributed to their reduced calcium hydroxide content due to SCM pozzolanic and carbonation reactions. The carbonation and pozzolanic reactions of the SCM blended concretes tend to marginally reduce the ionic concentration of the pore solution, particularly the calcium ions. This increases the ionic mobility of the concrete pore solution resulting in greater corrosion activity of the carbonated SCM concretes (Dhir, Jones and Mccarthy, 1992; Gallucci and Scrivener, 2007; Arachchige, 2008; Thiéry, Faure and Bouteloup, 2011).

Moreover, Tuutti (1982), Hakkinen (1993) and Parrott (1994) attributed the increased corrosion current of SCM blended concretes compared to PC concrete to the presence of micro-cracks and coarse capillary porosity usually found with SCM blended concretes when carbonated with a relative high (> 10%) percentage of CO_2. The increased porosity of the concrete can permit the transport of moisture and oxygen into the concrete and can be responsible for the increase in corrosion current of the SCM blended concretes.

Further, Tuutti (1982) attributed the high rate of corrosion found in BS blended concrete to its chemical composition which gives the concrete a higher hygroscopicity (affinity for water). Additionally, it should be noted that all the corrosion RC specimens were initially moist cured for seven days in water. Such duration of moist curing condition may not be sufficient for the hydration of the BS and FA blends at 0.60 and 0.95 w/b ratios to develop a refined pore microstructure that could compare with PC in resisting carbonation-induced corrosion (Tuutti 1982).

Figure 4.16 also shows that for a given concrete, corrosion current reduces with a reduction in the w/b ratio. This may be because the dense structure of the cement paste which is a feature of a good quality concrete can disrupt the diffusion of oxygen and movement of moisture in the concrete, resulting in low corrosion current. This is similar to the results obtained by Kulakowski, Pereira and Dal (2009) and Tuutti (1982), where corrosion current intensity was increased due to an increase in w/b ratio. This was also evident from the carbonation test results of the concretes.

4.8.2 Steel corrosion radius loss required for cover cracking

The steel mass loss due to corrosion was measured as described in section 3.7.4. The results are presented in Appendix D with the equivalent concrete specimen cover depth and reinforcing steel diameter. The reinforcing steel mass losses were converted to the amount of corrosion products or steel radius loss (δ_r) required to initiate a first visible crack on the cover concrete using Equation 3.20 for a uniform corrosion (characteristic of carbonation-induced corrosion as evident from visual observation of the corroding specimens). The results of the steel radius loss are presented in Figure 4.17, and the variations in the amount of corrosion products required for cracking can be observed with the concretes.

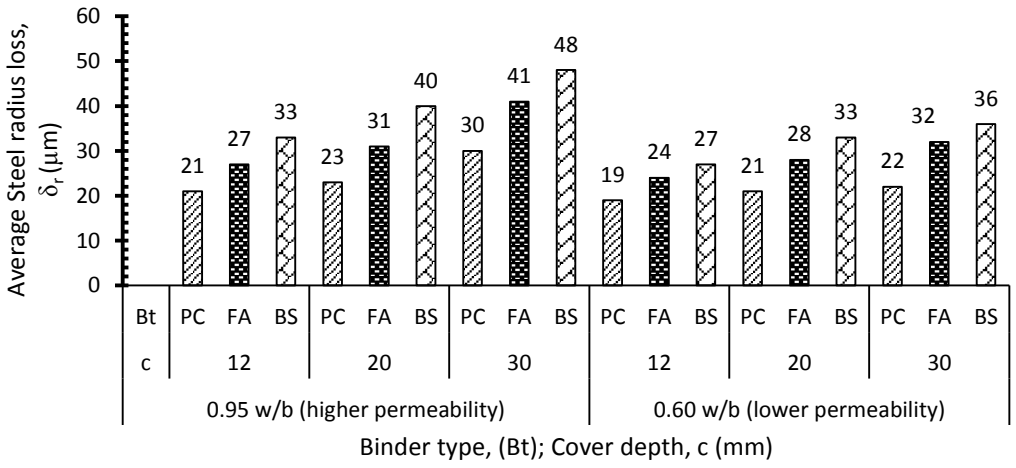

Figure 4:17 Average steel radius loss required to initiate cover concrete cracking

As shown by the results in Figure 4.17, the amount of corrosion needed to initiate a first visible crack in the concretes of 0.95 w/b ratio ranged between 21 µm to 51 µm considering the cover depths and the binder types. The amount of corrosion required to initiate cracking of the cover concretes range between 18 µm to 40 µm for concrete specimens of 0.60 w/b ratio for the cover depths and the binder types.

It should be noted that the values obtained in this study are steel radius losses and can be multiplied by a factor of 2 to convert them to diameter losses for easy

comparison with some literature values that express theirs in term of diameter or section losses. Tuutti (1982) and Parrot (1994) suggested that around 100 µm section loss is required to crack cover concrete while others (Andrade, Alonso and Molina, 1993; Almusallam, Al-Gahtani and Aziz, 1996; Rodriguez *et al.*, 1996) reported that about 6 to 130 µm of corrosion is required to crack concrete. The range of steel section loss required for cracking the cover concretes obtained in this study is in agreement with some literature results. This shows that the data from this study can be relied on and can be used in developing a model that can predict time to induce corrosion crack in concrete. Figure 4.17 also shows variations in the amount of corrosion products required to initiate a first visible crack on the concrete which seem to be influenced by the variations in depth and quality of the cover concrete (binder type and w/b ratio).

- **Effect of concrete quality on steel radius loss required for cover cracking**

In this study concrete quality was quantified using a durability index parameter (28-day OPI). The OPI was as well used to describe the amount of pores and their connectivity within the test concretes. It is primarily affected by the binder type and w/b ratio of the concrete mix. A concrete with high w/b ratio is more permeable and can be characterised to have large pores that are well connected compared to a concrete with low w/b ratio. The large connected pores in a permeable concrete can permit the diffusion of oxygen and movement of moisture within the concrete for a further corrosion deterioration. The large connected pores can also serve as repositories for the corrosion products before initiating a cover crack (Tuutti 1982).

As shown in Figure 4.17 for a given concrete specimen, the amount of corrosion steel radius loss required to induce the first cracking at the cover concrete is higher in a more permeable concrete than a less permeable concrete. This can be attributed to the fact that a larger amount of corrosion is required to fill the larger pore spaces in a more permeable concrete than a smaller pore spaces available in a less permeable concrete before initiating a cover crack . For example, at a constant cover depth of 20 mm, there are 9%, 10% and 18% reductions in the amount of corrosion required for cracking, when w/b ratio changes from 0.95 to 0.60 in the PC, PC-FA and PC-BS blended concrete specimens respectively. This shows that improving

the quality of concrete by reducing its permeability (i.e reducing the w/b ratio) irrespective of the binder type has a beneficial effect in reducing the amount of radial loss to corrosion in reinforcing steel bar. A similar trend was observed by Alonso, Andradel and Diez (1998) and Tuutti (1982) where a lower w/b ratio concrete required a lesser amount of corrosion to initiate cover cracking. This was because of the less void space being available to accommodate the corrosion products in concrete with low w/b ratio.

The use of the SCM in partial replacement of PC in the concretes resulted in a higher corrosion steel radius loss required for cracking compared to a PC concrete specimen at the same cover depth and w/b ratio. At a constant cover depth and w/b ratio, this study suggests the increasing order of corrosion steel radius loss as: PC-→PC-FA→PC-BS. The reason for the larger steel radius loss found with the BS concretes compared to the FA and PC concretes may be due to large coarse capillary pores usually found with carbonated BS blended concretes (Tuutti, 1982; Parrott, 1994; Thiéry, Faure and Bouteloup, 2011; Hornbostel, Larsen and Geiker, 2013; Morandeau *et al.*, 2014, 2015).

The effect of accelerated carbonation on SCM concrete microstructure was investigated by Thiéry, Faure and Bouteloup (2011). It was found that the proportion of coarse capillary pores increased in the SCM concretes with high w/b ratio, while there was a systematic reduction in total porosity of the PC concretes at the same w/b ratio. The increased capillary porosity found in the pozzolanic materials was due to the decalcification of pozzolanic C-S-H by carbonation which resulted in poorly-hydrated silica gel of a lower molar volume. This led to a significant reduction in the volume of calcium carbonate in the solid phase (Gallucci and Scrivener, 2007; Thiéry, Faure and Bouteloup, 2011).

- **Effect of cover depth on steel radius loss required to initiate cover cracking**

The effect of cover depth on the amount of corrosion needed for cracking the concrete specimens are shown in Figure 4.18. For a given w/b ratio and binder type, increasing the cover thickness increases the amount of radius loss required for the cover cracking. This can be attributed to the fact that the amount of pores and their volumes are increased in a larger cover depth compared to a smaller cover thickness

for the same concrete mixture. A larger cover depth serves as a better storage void for the corrosion products without developing a cracking stress on the surrounding concrete. Corrosion crack is only initiated on the cover concrete after the pores are filled with the corrosion products (Tuutti, 1982).

Even though a larger cover would offer more protection to the reinforcement from the aggressive agents than a smaller cover, excessive trading-off the quality of concrete for an increased cover depth should be avoided in RC design and construction. This is because there is no early indication that the reinforcing steel is at risk of corrosion-induced structural failures in a thick lower quality cover. The steel reinforcement may be severely weakened before corrosion is detected. The corrosion weakened reinforcing steel can jeopardize the structural integrity of such RC structure. Therefore, to ensure a durable structure as part of the requirement for an extended service life of RC structure, both concrete quality, and cover depth should be proportioned adequately in an aggressive (carbonation) environment.

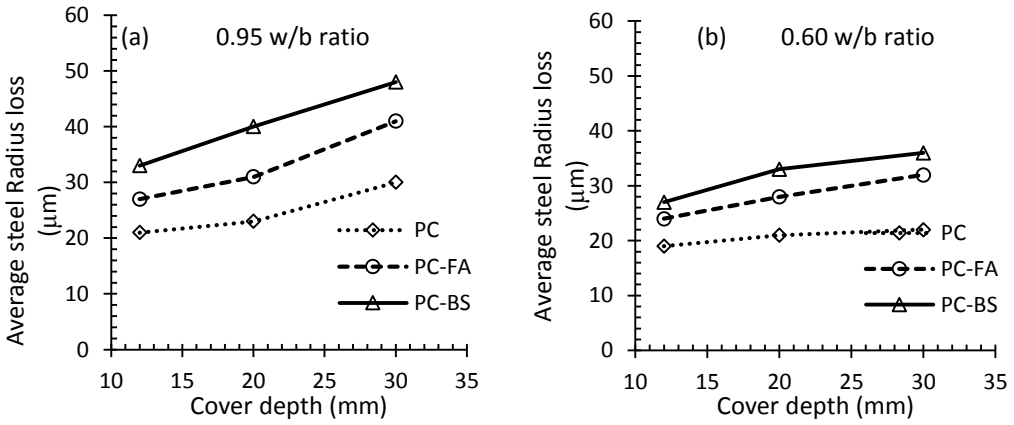

Figure 4:18 Average steel radius loss versus cover depths (a) 0.95 w/b ratio (b) 0.60 w/b ratio

4.8.3 Reinforcement corrosion rate

The corrosion rates were obtained using the gravimetric mass loss and linear polarisation resistance methods highlighted in sections 3.7.3 and 3.7.4. The corrosion current density, i_{cor} ($\mu A/cm^2$) obtained by the linear polarisation

resistance method was converted to corrosion rate, I_{RP} (μm/year) by multiplying the corrosion current density by a factor of 11.6 (see Appendix G). The gravimetric steel mass loss, m_l (g) was also converted to corrosion rate, I_{ML} (μm/year) using Equation 3.21. The results of the two measurements are presented in Tables D1-2, D2-2 and D3-2 of Appendix D while Figure 4.19 shows the measured corrosion rate by the gravimetric mass loss method.

As presented in Tables D1-2, D2-2 and D3-2 of Appendix D, the trends in the results of the corrosion current density and corrosion rate are similar. Therefore, the explanation of various influencing factors on the corrosion current density results still hold for the corrosion rate results. The corrosion rate influencing factors are not discussed in detail in this section.

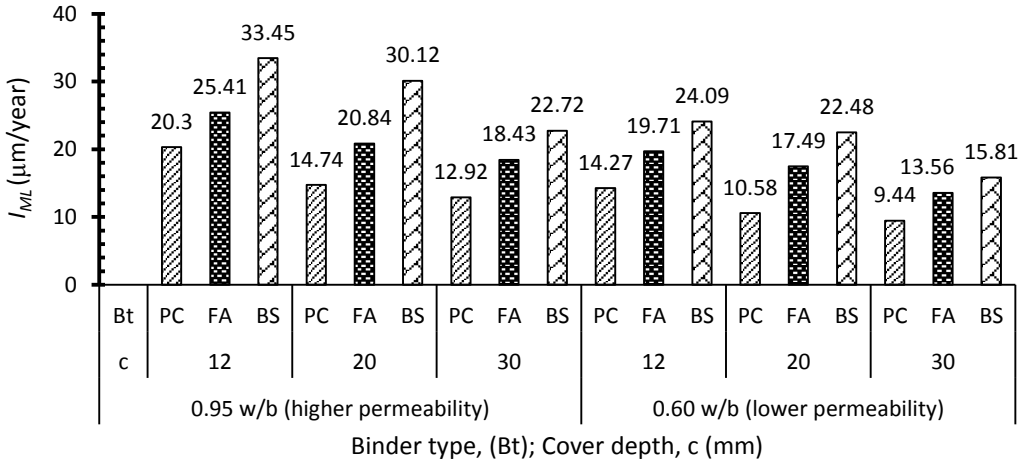

Figure 4:19 Measured Average corrosion rate results

It is evident from Figure 4.19 that corrosion rate is higher in a smaller cover depth compared to a bigger cover depth for a given concrete and w/b ratio. This may be due to the accessibility of the reinforcing steel to the environment in a thinner cover depth compared to a thicker cover depth. The influence of binder type on the corrosion rate is also shown in Figure 4.19 where it is evident that corrosion rates in the SCM blended concretes are higher than the PC concretes at all the cover depths and w/b ratios. The highest corrosion rate is found with the PC-BS concretes for the two w/b ratios and cover depths considered. The increased corrosion rate

found with the SCM concretes may be because of their increased porosity caused by the carbonation of their C-S-H (Arachchige, 2008).

The influence of concrete quality on the corrosion rate is also noted in the corrosion rate results presented in Figure 4.19. A lesser permeable concrete has a lower corrosion rate while a more permeable concrete has a higher corrosion rate at a constant cover depth and binder type as shown in Figure 4.19.

Figure 4.20 shows that for a given w/b ratio and binder type, average corrosion rate increased with a decrease in cover depth. This trend is observed in all the binder types and w/b ratios and may be due to the accessibility of oxygen and moisture to the reinforcement in shallow cover depth.

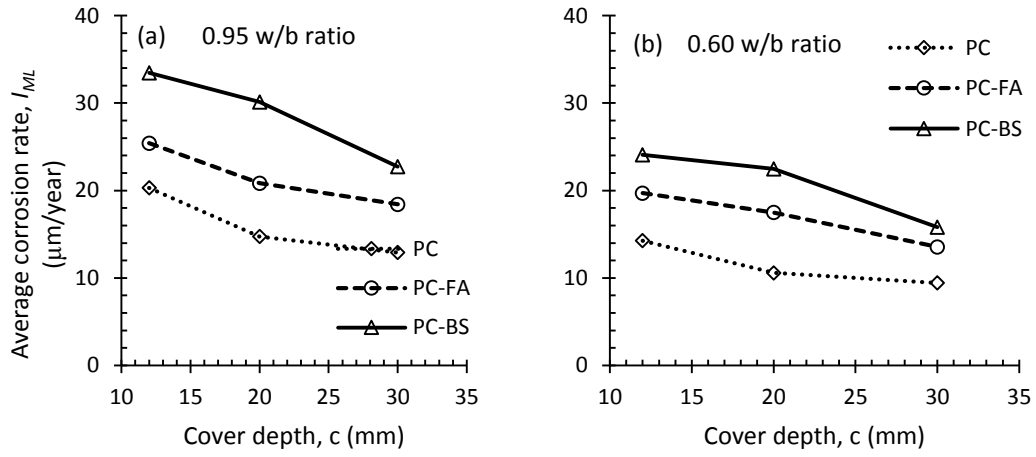

Figure 4:20 Average corrosion rate versus cover depth (a) 0.95 w/b ratio (b) 0.60 w/b ratio

Figure 4.21 shows the comparison between the two corrosion rate results (I_{Ml} and I_{Rp}). The comparison of the two measurements is important in reinforcement corrosion context whether the two corrosion rates (I_{Ml} and I_{Rp}) can be used interchangeably. Various methods for assessing interchangeability of two data are available in literature, the most popular in concrete context is by checking the agreement between the two corrosion rate data by using a line of equality in a comparison plot of the two data set. Even though other advanced statistical methods can be employed to check the level or the limit of agreement between two data, this was not considered in this study, as it is not part of the study objectives.

The comparison plot of the two corrosion rates shows a level of agreement between the two corrosion rates results. However, the majority of the corrosion rates obtained by using linear polarisation resistance method seem to be higher than the corrosion rates obtained by the gravimetric mass loss method as shown by the plots in Figure 4.21. This may be partly due to complexity in the corrosion system where less stable iron oxides independently (without any significant interaction with the parent steel) tend to oxidise further. The combination of the corrosion current generated during the initial iron oxidation and the oxidation of the less stable oxides can be responsible for the higher corrosion current density measured by the polarisation resistance method. Similar observation was made by Liu (1996) where concrete exposed to an outdoor unsheltered environment was tested for corrosion rate using linear polarisation resistance and gravimetric mass loss methods.

Besides, Ballim & Reid (2003) asserted that the hypothesis that iron oxidation is the only chemical reaction taking place at the anode site of a corrosion cell might be wrong. They concluded that other competing chemical reactions (oxidation of other chemical elements of steel such as Manganese (Mg) and Vanadium (V) etc might also be taken place at the corrosion sites which in combination with the iron oxidation might increase the linear polarisation corrosion current density.

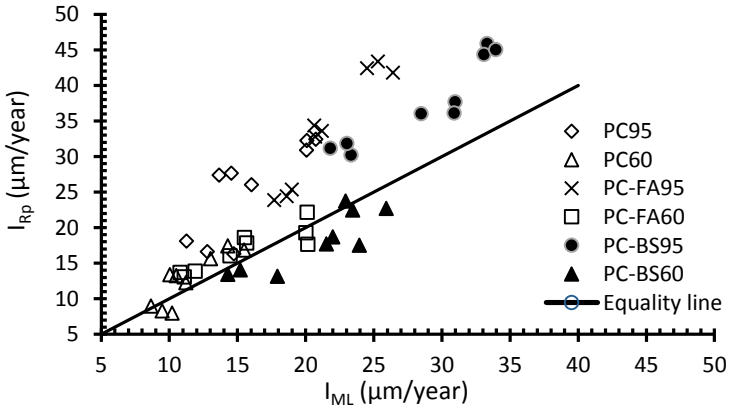

Figure 4:21 Comparison between the I_{RP} and I_{ML}

4.8.4 Corrosion morphology and concrete cover cracking time

The time to corrosion-induced cracking of cover concrete is a significant parameter in service life estimation of RC structure. In this study, cracking time is the time between the corrosion initiation (this is an assumption, corrosion is initiated when there is sufficient oxygen and moisture around the reinforcement) and corrosion propagation to the appearance of a first visible crack on the cover concrete. Corrosion-induced cover concrete cracking is caused by the expansive pressure of the corrosion products which fill the concrete capillary pores and induces a tensile stress in the concrete around the reinforcing steel. The cumulative increase in pressure causes crack to develop when the tensile resistance of the concrete is exceeded (Alonso, Andradel and Diez, 1998).

Figure 4.22 shows a photograph of some of the corrosion cracked carbonated concrete specimens and continuous cracking along the line of the reinforcement can be observed on the specimens. The visual observation of the extracted steels showed a uniform corrosion along the embedded length of the reinforcing steel (Figure 3.18). This can be attributed to the fact that the corrosion was induced by carbonation.

Figure 4:22 Pre-carbonated concretes with visible cracks along the line of reinforcement after exposure to unsheltered inland environment

The results of the cracking time of the pre-carbonated concrete specimens made with three binder types and two w/b ratios are presented in Figure 4.23. The cracking time in these plots represents an average cracking time of two identical (in terms of binder type, w/b ratio and cover depth) concrete specimens. It is evident from Figure 4.23 that binder type, w/b ratio and cover depth influence the cracking time of the concretes. For an equal w/b ratio and cover depth the SCM blended concretes have shorter cracking times compared to the PC concretes. This may be due to the effect of carbonation and pozzolanic reactions of the SCM blended concretes which increased their corresponding corrosion rates. The PC-BS concretes showed shortest cracking times. Part of the reason for this performance of the PC-BS concretes may be because of their lower 28-day tensile strengths compared to PC and FA concretes for equal w/b ratio and cover depth.

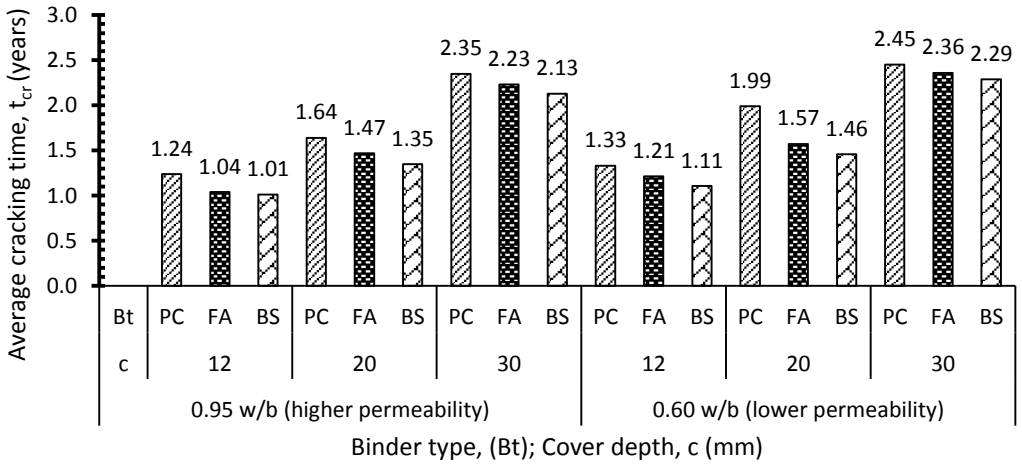

Figure 4:23 Observed average cracking time of the RC prisms

Also, for a given binder type and cover depth, it was expected that concrete with smaller pores (lower w/b ratio or lower permeability) would require a shorter time to be filled with the corrosion products before a first surface crack is initiated. However, the delay in crack initiation found with concrete with smaller pores can be attributed to their lower corrosion rate and higher tensile strength resistance. This shows that improving the concrete quality in terms of reducing the concrete

permeability is an option that can be used to extend the corrosion cover cracking time of RC structure exposed to the unsheltered inland environment.

For a given cover depth and binder type, the controlling factor for the corrosion cracking process (radius loss required for cracking and cracking time) is the permeability of the concrete which is controlled by the mix w/b ratio. Even though controlling the w/b ratio of a mix is a good practice to achieve a durable concrete that can withstand corrosion cracking, a good compaction and extended curing duration must also be considered for RC structures that will have extended service life.

The effect of cover depth on the cracking time is shown in Figure 4.24. For a given concrete, increasing the cover depth extends the time to cracking of the cover concrete. This may be because increase in cover depth increases the amount and volume of concrete pores that are available and required to be filled before initiating cracking of the cover concrete. The trend observed in Figure 4.24 corresponds to the results obtained by Lu, Jin and Liu (2011) in a corrosion experimental investigation where an increase in cracking time of a thicker cover depth was attributed to the extended time it took the corrosion materials to fill the larger cover depth compared to a smaller cover depth.

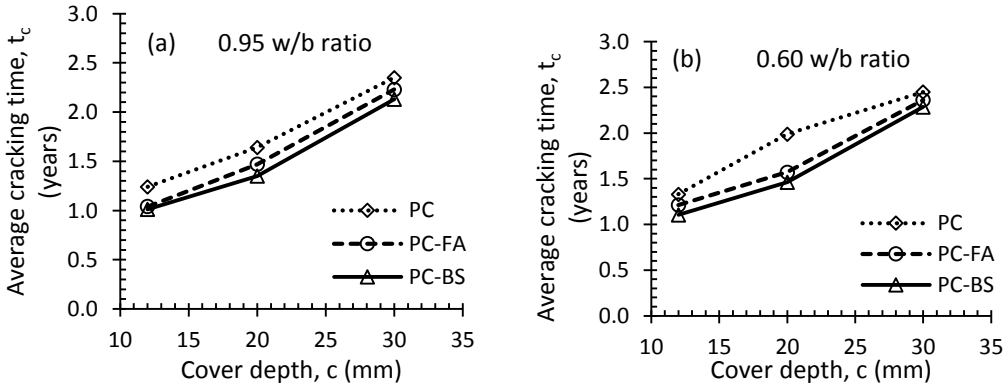

Figure 4:24 Average cover cracking time versus cover depth (a) 0.95 w/b (b) 0.60 w/b

Increasing the cover depth can be a good practice and can be beneficial to improving the durability of RC structure (Lu, Jin and Liu, 2011). However, caution must be

taken not to excessively trade off a thicker cover depth for a lower quality concrete. This is to prevent corrosion-induced structural failure in a thicker cover, as there may not be any early indication that the reinforcing steel is at risk of corrosion-induced structural failure in a thicker cover. The steel reinforcement may have been severely weakened before corrosion is detected in a thicker cover, this can jeopardize the structural integrity of such RC structure. Therefore, to ensure the structural durability of reinforced concrete structure, both concrete quality and cover depth should be proportioned adequately in carbonation environment.

4.9 Conclusion

This Chapter has presented the analyses and discussion of the results obtained from the experimental work reported in Chapter 3. In this section, a summary of the outcomes is presented, and some trends and conclusions are generalised to draw useful insights. The areas that need further research are also highlighted.

The results of the early-age concrete characteristics (oxygen permeability and water sorptivity indexes, compressive and tensile strength) obtained in this study clearly reflect the influence of w/b ratio and binder type on concrete quality. It was also observed from the results that w/b ratio, binder type, extent of the initial moist curing conditions and exposure climate affected the carbonation resistance of the concretes. Similar trends to the carbonation results were noticed with the corrosion tests results. The influence of the investigated variables on the concrete early-age characteristics, carbonation rate and steel radius loss required to cause cover cracking and time to corrosion-induced cracking are summarised as follows:

1. Binder type

(a) At the same w/b ratio, SCM blended concretes were less permeable than PC concretes. This was due to the effect of pozzolanic reaction and complex products of hydration reaction of the SCM which tend to block the capillary pores resulting in a denser microstructure with a finer pore structure. Another reason was better packing of the SCM with the aggregates and cement particles which improved the SCM concrete microstructure. However, PC-BS concretes were more permeable compared to the other SCM concretes in all the w/b ratios considered. This was

attributed to the inability of the PC-BS concrete at early age (28 days) to attain its full reactivity potential and refine its pore structure possibly due to its PC content.

(b) There was no clear difference between water sorptivity results of the PC and the SCM concretes at the same w/b ratios of 0.95 and 0.60. At a lower w/b ratio of 0.40 all the concretes had a similar WSI.

(c) Apart from the PC-BS concretes, all the SCM concretes had higher compressive strengths compared to PC concretes for the same w/b ratio. Similar trends to that of compressive strength results were also observed with the split tensile strength results

(d) Apart from the concretes containing SF, all the SCM concretes showed higher carbonation rate compared to the PC concrete at the same w/b ratio, exposure and extent of the initial moist curing conditions. This effect was attributed to the dominating influence of carbonation and pozzolanic reactions of the SCM. The superior performance of PC-SF concretes in resisting carbonation reaction was attributed to the increased reactivity of SF due to its particles fineness and high PC content compared to the other SCM concrete.

(e) A higher corrosion rate and a larger amount of corrosion radius loss required to initiate a first visible cover crack were found with the SCM concretes compared to the PC concrete at the same w/b ratio and cover depth. This consequently led to their early cracking times and was attributed to the pozzolanic and carbonation reaction of the SCM concretes.

2. Water/binder ratio

(a) For a given binder type, increasing the w/b ratio resulted in a more porous concrete. This was attributed to the capillary porosity of the cement paste and interconnectivity of the pores which increased with increase in the w/b. This trend was observed in all the concretes.

(b) For a given w/b ratio and duration of initial moist curing condition, compressive and tensile strengths increased with a decrease in the w/b ratio. The trend was noticed in all the concretes.

(c) For a given concrete exposed to a certain inland environment, carbonation rate increased with increase in w/b ratio. This was attributed to an increase in the concrete capillary pore sizes and their interconnectivity at a higher w/b ratio.

3. Exposure conditions

(a) The range of relative humidity measured at the indoor exposure site was relatively lower than the range of RH measured at the outdoor exposure sites for the winter and summer periods.

(b) For a given exposure the range of relative humidity measured during summer period was higher than the range of humidity measured during winter period. The difference in RH between the two periods was more noticed with the outdoor exposures than with the indoor exposure. The significant difference between the RH of the two outdoor exposures was attributed to the frequent rainfall during the summer period compared to the winter period in South Africa.

(c) The climatic results of the inland environment showed that the maximum and minimum temperatures measured during the summer period are higher compared to the maximum and minimum temperatures measured during the winter period.

(d) It was evident from the results that the highest and lowest CO_2 concentrations for the indoor exposure were about three times greater than the maximum and minimum CO_2 levels of the outdoor exposures. This was due to the enclosed nature of the indoor site which restricts the free circulation of air. The CO_2 concentrations for the two outdoor exposures were similar.

(d) For a given concrete, carbonation rate was seeing greater in indoor exposure than the outdoor exposures. This is due to the climatic conditions of the inland environment.

4. Duration of initial moist curing conditions

(a) For a given concrete in exposure, extending the initial moist curing period from 7 days to 28 days reduced the carbonation rate. This was attributed to the fact that extending the wet curing duration increased the degree of hydration which decreased the size and connectivity between the capillary pores.

(b) Reducing the w/b ratio is more efficient and sustainable in lowering the carbonation rate in concrete than extending the duration of the initial moist curing.

5. Cover depth

(a) For a given w/b ratio and binder type, corrosion initiation increased with increase in cover depth. The trend was common to all the concretes and was due to the greater proportion of carbonating material in a thicker cover than a thinner cover depth.

(b) For a given w/b ratio, the amount of steel radius loss required to initiate a cover crack increased with increase in cover depth. This was because the amount of pores and their volumes were higher in a deeper cover depth compared to a shallow cover thickness for the same concrete mixture. The higher amount and volume of capillary pores in a larger cover depth required a larger amount of radius loss to fill the pores before initiating the first visible crack.

(d) At a constant w/b ratio and binder type cracking time of the cover concrete increased with the increasing cover depth

6. Reinforcing steel diameter

For a given concrete at a constant cover depth, increasing or decreasing the reinforcing steel diameter seemed not to have any significant trend with the corrosion current density and the amount of steel radius loss required to initiate cracking results. The insignificant trend with the variation in reinforcing steel diameter was also evident in the concretes' cracking time results.

4.10 Specific Conclusion

Concerning the experimental results presented, analysed and discussed in this chapter, the following general observations can be made:

(a) The results of the oxygen permeability index obtained in this study clearly reflected the influence of w/b ratio and binder type on the overall pore structure of the concretes than water sorptivity index. The results appear to indicate that OPI is a more sensitive measure of changes in the developmental phase of cement

microstructure than water sorptivity. This presents OPI as an appropriate parameter that can be used in a model that can reasonably predict carbonation rate in concrete. This parameter along with cover depth can be used to predict the amount of radius loss required for corrosion cover cracking.

(b) The w/b ratio and duration of initial moist curing conditions significantly influenced the carbonation rate in concrete. However, from the results and analysis presented, using a reduced w/b ratio offered a greater reduction in carbonation rate than extending the initial moist curing conditions of the concretes. For example, PC-FA concrete having 0.95 w/b ratio exposed to the indoor environment was initially wet cured in water for seven days when the same PC-FA concrete was initially moist cured for 28 days in water, the percentage reduction in carbonation rate was 19%. Increasing the w/b ratio from 0.95 to 0.60 for the same concrete in a similar environment gave a carbonation rate reduction of 30%. A further reduction of w/b ratio from 0.60 to 0.40 w/b ratio gave carbonation rate reduction of 67% which is higher compared to extending the early-age moist curing duration. This analysis showed that reducing the w/b ratio is more effective and sustainable in reducing carbonation rate in concrete than extending the length of the initial moist curing from 7 to 28 days.

(c) The corrosion test results indicated greater corrosion in the concretes blended with the SCM than in the PC concretes, and the BS concrete has more corrosion at the same cover depth and w/b ratio. The reason for higher corrosion activity in the SCM blended concretes was due to the accelerated carbonation of their pozzolanic C-S-H. This increased the capillary porosity of the SCM blended concretes which consequently increased their amount of corrosion radius loss required to initiate cracking on their cover. This shortened their corrosion propagation periods. This action can be seen to be disadvantageous to the use of SCM in concrete exposed to the inland environment.

(d) It should be noted that all the RC specimens were initially moist cured for seven days in water. Such extent of wet curing may not be sufficient for the hydration of BS and FA blends at 0.60 and 0.95 w/b ratios to develop a refined pore microstructure that could compare well with PC concrete in resisting carbonation-

induced corrosion. Although, the initial moist curing duration was not among the experimental variables considered for the corrosion propagation in this study. An investigation into the influence of initial moist curing duration on corrosion cracking performance of SCM concrete is therefore recommended for further study. This will help in arriving at a meaningful conclusion about the effective use of SCM in resisting carbonation-induced corrosion.

This chapter has shown that a proper durability design that takes into account concrete quality and adequate cover depth are essential for a more controlled durability and service life of reinforced concrete structures in the inland environment. The combination of good concrete quality and adequate cover depth, when provided for a RC structure, can withstand the aggressiveness of the inland environment. These measures will reduce concrete carbonation rate, amount of steel radius loss required for cracking and consequently increase the time to corrosion-induced cover concrete cracking.

The next chapter deals with the development of the empirical carbonation-induced corrosion initiation and propagation models based on the results and analyses presented in this chapter.

CHAPTER 5

5 DEVELOPMENT OF SERVICE LIFE MODELS

5.1 Introduction

This chapter deals with the service life modeling of reinforced concrete structures exposed to the natural inland environment. This is presented as a two-stage model namely the corrosion initiation and the corrosion propagation periods. The experimental results presented, analysed and discussed in Chapter 4 are used as the basis for developing the carbonation-induced corrosion initiation and propagation models. In the propagation stage, a model to estimate the amount of corrosion that will be required to initiate a first visible crack on cover concrete is developed. The two models are developed using linear regression analysis of least squares method. The regression analyses, results, and interpretations of the regression models are presented and discussed in this chapter. The chapter also includes the model's graphical illustrations and the comparisons with the existing corrosion initiation and corrosion propagation models. The applications of the models are also illustrated.

5.2 Statistical Modelling

Regression analysis is one of the most commonly used statistical techniques for studying the behaviour of a dependent variable as a function of independent variables (Silva, Neves and de Brito, 2014). In a linear regression analysis, the relationship between dependent and independent variable can be expressed using a mathematical representation of the form:

$$y = \beta_o + \beta_1 x_1 + \varepsilon \qquad 5.1$$

For a multiple linear regression analysis, the relationship between a dependent variable and independent variables can be expressed using a mathematical representation of the form:

$$y = \beta_o + \beta_1 x_1 + \beta_2 x_2 + \beta_j \, x_j \, ...\varepsilon \qquad 5.2$$

where y represents a dependent (predicted) variable, βo, $\beta_1 \ldots$, βj represent regression coefficients and $x_i \ldots, x_j$ represent independent (predictor) variables, and

ε is the random error of the model. The model expressed in Equation 5.1 is only used when a significant independent variable is involved in the regression analysis. When several other significant variables are included in the regression analysis, the Equation 5.2 can be employed. For carbonation rate and corrosion radius loss modelling, a multiple regression analysis is used because the combined effects of more than one significant variables on carbonation rate as well as the amount of radius loss are examined.

It should be noted that multiple linear regression analysis can only be used when the input variables are not correlated with each other to avoid multicollinearity effects that can jeopardise the reliability and validity of the regression (Montgomery and Runger, 2011; Silva, Neves and de Brito, 2014). Also, regression models are valid for values of the regressor variables within the range of the original data (Montgomery & Runger, 2011).

5.3 Carbonation-Induced Corrosion Initiation Model

The dependence of carbonation depth on time can be expressed using the square root of time rule as expressed in Equation 4.1 (Schiessl, 1988).

$$d_c = K_c t^{0.5} \qquad 4.1$$

where t (years) is the exposure time, d_c (mm) is the carbonation depth, and K_c (mm/years$^{0.5}$) is the carbonation rate.

Various studies have examined the adequacy of the square root of time law in expressing carbonation depth with time in concrete exposed to natural environmental conditions. Alexander, Mackechnie and Yam (2007) established the adequacy of square root of exposure time for concrete carbonation in Johannesburg locality. This was based on the relative uniform exposure conditions of Johannesburg location throughout the year. Thus, 0.5 value was decided upon in this study for the exponent factor of the exposure time.

The initiation time of corrosion is defined as the time required for the carbonation front to reach the level of the reinforcing steel and initiate corrosion. At this point,

carbonation depth becomes the cover depth and using the square root of time rule expressed in Equation 5.2, the initiation time is given as:

$$t_i = \left[\frac{c}{K_c}\right]^2 \qquad 5.3$$

where t_i (years) is the time to corrosion initiation, c (mm) is the cover depth, and K_c (mm/years$^{0.5}$) is the carbonation rate which depends on the concrete pore network system, chemical composition of the pore solution and the exposure conditions. Concrete pore network system and chemical composition of pore solution depend on the binder type, w/b ratio and the duration of initial moist curing condition.

Carbonation rate is fundamentally a durability indication that is expected to consider all the variables relating to environmental aggressiveness and characteristics of concrete (Silva, Neves and de Brito, 2014). Hence, carbonation rate may be difficult to estimate and to model carbonation-induced steel corrosion initiation time can be a complex task. The application of multiple linear regression analysis has been used by many researchers to overcome some of the modelling challenges especially when it involves more than one influencing variable that can be numeric or non-numeric.

In this study, natural carbonation rate is modelled using a multiple linear regression analysis of least squares method. Some of the significant factors influencing carbonation rate are well captured in this model and can be used in estimating carbonation rate in RC structure. The estimated carbonation rate is applied to the square root of time law to predict the time to corrosion initiation in RC structures when the concrete cover thickness is known.

5.3.1 Carbonation rate prediction model

The results of carbonation depth measured within the two years of the concretes (PC, PC-FA, PC-BS, PC-SF and PC-BS-SF) exposure to the inland environment were used to establish a general empirical relationship between the depth of carbonation and the exposure time. The concretes were manufactured using three w/b ratios (0.95, 0.60, 0.40) and initially cured for 7 and 28 days in water before

the exposure to three different exposure conditions within the inland environment (Indoor, outdoor sheltered and outdoor unsheltered). The climatic conditions of the exposure environment were already highlighted in Section 4.1 of Chapter 4 and therefore will not be discussed further in this section.

Concrete early deterioration starts from its exposed surface, hence a knowledge of its surface properties is important to predict its performance against carbonation (Ballim and Alexander, 2005). The fact that the reinforcing steel is close to the near surface makes the cover concrete an important factor in concrete early deterioration. This means that prescription of rate-controlling factors of concrete early deterioration, that is the operating environmental conditions and quality of concrete in terms of transport properties become important parameters in the carbonation rate prediction model. Further, w/b ratio determines the fluid transport properties of concrete. Thus including both w/b ratio and fluid transport properties in a multiple linear regression model would violate the standard linear regression assumption especially variable collinearity (Montgomery & Runger, 2011).

Having ascertained the significance effects of binder, permeability, duration of initial moist curing and exposure conditions on carbonation rate, a carbonation rate model is developed as shown in Equations 5.4. The model is in form of multiple linear regression (least squares) having the OPI (representing concrete permeability), exposure conditions (indoor, outdoor sheltered and outdoor unsheltered) and moist curing duration (7 and 28 days) as the predictor or independent variables and the carbonation rate as the response or dependent variable. The variables are further classified as continuous (variable that can be expressed in numbers) and categorical (variables that can be expressed other than numbers) variables as shown in Table 5.1. The categorical variables include the exposure conditions and duration of the initial moist curing while continuous variables are the carbonation rate and the OPI.

To allow the modelling operation to be carried out with the categorical variables, they were coded as dummy variables as shown in Tables 5.2 and 5.3. There are three possible values for the exposure variables and two possible values for the curing variables. In general, if the original data has x categorical values, the model

will require x-1 dummy variables. Therefore, the exposure variable is coded as two dummy variables in three categories namely: indoor, outdoor sheltered and outdoor unsheltered. The early-age curing variable is coded as one dummy variable under two categories of 7-day and 28-day. Each dummy variable was programmed to take the value of 0 or 1.

Table 5:1 Characterisation of the input and output variables

Variable	Variable type	Range of value
28-day OPI (-Log k (m/s))	Continuous	9.04 - 10.56
Exposure type	Categorical	1 - 0
initial moist Curing	Categorical	1 - 0
Carbonation rate, K_c (mm/year^{05})	Continuous	0.48 - 16.16

Table 5:2 Dummy variable coding for the exposure conditions

Type of exposure condition	Dummy variables	
	x_1	x_2
Indoor	1	0
Outdoor sheltered	0	1
Outdoor unsheltered	0	0

Table 5:3 Dummy variable coding for the curing

Duration of the initial curing condition	Dummy variables
	x_1
7-day	1
28-day	0

The carbonation rate modelling was based on 18 observations for a binder type which was performed using a multiple linear regression analysis of least squares method. The outputs of the analysis are presented in Tables E1 to E5 of Appendix E, which include the regression statistics, analysis of variance (ANOVA), regression coefficients and the parameters that can be used to test the adequacy of the regression model. Based on the multiple linear regression analysis the true

relationship between the carbonation rate and the associated influences is given as

$$K_{c,j} = \beta_3 - \beta_4(OPI) + \beta_5 I_{Indoor} + \beta_6 I_{Sheltered} + \beta_7 I_{Unsheltered} + \beta_8 I_{C7} + \beta_9 I_{C28} \quad 5.4$$

where $K_{c,j}$ (mm/year$^{0.5}$) represents carbonation rate of a particular concrete expressed in terms of its binder type, j (PC, PC-FA, PC-BS, PC-SF and PC-BS-SF) as shown in Table 5.4. For example $K_{c,PC}$ means the estimated carbonation rate of the PC concrete. The OPI represents 28-day oxygen permeability index and subscripts C7 and C28 represent 7 and 28 days moist curing conditions. Table 5.4 shows the coefficients associated with the predictor variables. The possible value of I shown in Equation 5.4 is 1 or 0. The value of I is 0 if its subscript does not apply to the concrete in question and 1 if it does apply to the concrete in question.

Table 5:4 Regression coefficients and adjusted R^2 for Equation 5.4

Carbonation rates, $K_{c,j}$ (mm/year$^{0.5}$)	Regression constants	Regression coefficients						R^2
	β_3	β_4	β_5	β_6	β_7	β_8	β_9	
$K_{c,pc}$	81.50	8.08	1.77	0.88	0	1.75	0	0.9381
$K_{c,PC\text{-}FA}$	93.97	9.08	1.91	1.05	0	2.11	0	0.9787
$K_{c,PC\text{-}BS}$	103.90	10.00	2.18	1.01	0	2.23	0	0.9439
$K_{c,PC\text{-}SF}$	60.70	5.80	1.43	0.87	0	1.51	0	0.9547
$K_{c,PC\text{-}BS\text{-}SF}$	84.60	8.14	0.83	0.51	0	1.91	0	0.9787

Table 5.4 also shows the adequacy of the regression model, the adjusted R^2 (usually used for testing the adequacy of multiple regression models (Montgomery & Runger, 2011) is greater than 0.93 at 95% confidence level in all the concretes. The analysis of the regression results shows that more than 93% of the variability in the carbonation rate can be explained by the three input variables (concrete permeability, exposure conditions, and duration of initial moist curing conditions). The remaining less than 7% can be due to other causes that were not investigated in this study. It is therefore concluded that the model has a high correlation between the output and input variables for all the concretes. The proposed model demonstrates that the input variables are capable of describing the carbonation rate.

Moreover, as shown in Tables E1 to E5 of Appendix E, the statistical significance P-values for the OPI, indoor exposure, unsheltered exposure and curing variables are lower than 5% (allowed P-value obtained from statistic t-test). The statistical significance P-values for the outdoor sheltered exposure variable in all the models are greater than 5% at a 95% confidence level. Even though the significance P-value for the outdoor exposure is greater than 0.05 at a 95% confidence level, this does not mean that outdoor sheltered exposure variable can be ignored in the model.

Figure 5.1 shows the plot of the predicted and measured carbonation rate of the concretes. The comparison between the predicted and measured carbonation rates is determined using a line whose slope is equal to 1 (equality line) as shown in Figure 5.1.

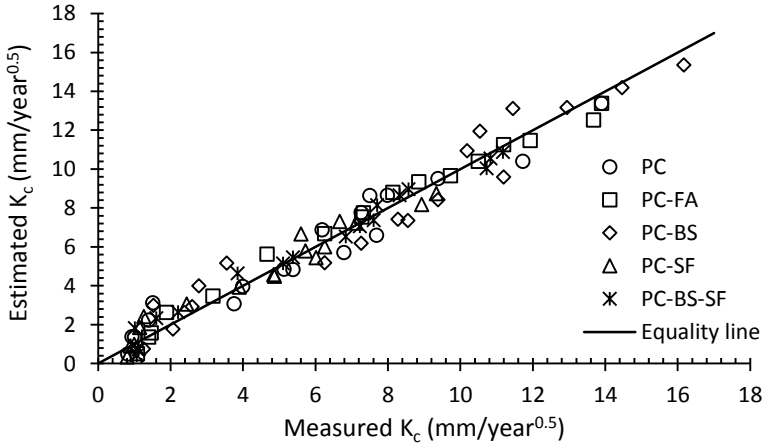

Figure 5:1 Measured values versus estimated values of K_c (mm/year$^{0.5}$)

It can be observed that both data points lie closer to the line of equality which means that the models predict carbonation rate quite well with a reasonable level of accuracy. The model is adequate to predict carbonation rate in concrete with more than 95% of the standard residuals (the difference between measured and predicted carbonation rates) are within the recommended intervals of -2 and +2 (Montgomery & Runger, 2011) in all the variables as shown in Appendix H.

5.3.2 Carbonation depth prediction model

The carbonation depth prediction equation is obtained by using square root of time law (Equation 4.1). The resulting carbonation depth equation is expressed as:

$$d_{c,j} = K_{c,j}\sqrt{t} \qquad 5.5$$

where $d_{c,j}$ (mm) represents the depth of carbonation of a particular concrete expressed regarding its binder type, j (PC, PC-FA, PC-BS, PC-SF, and PC-BS-SF). $K_{c,j}$ (mm/year$^{0.5}$) represents the carbonation rate of that particular concrete, and t (year) is the exposure time.

The model presented in Equation 5.5 enables the prediction of time-dependent carbonation depth of concrete regarding the three selected natural inland exposure conditions, duration of early-age moist curing and 28-day OPI. The proposed depth of carbonation model can be used to estimate the depth of carbonation in both new and existing RC structures. Such information can be used for strategic planning and maintenance of RC structures exposed to the natural inland environment.

5.3.3 Time to corrosion initiation prediction model

The time to corrosion initiation model for the concretes can be expressed as shown in Equation 5.6 which is obtained by using the square root of time rule. The proposed time to corrosion initiation model can be used to predict the time to initiate corrosion in RC structure exposed to the inland environment when the cover depth and carbonation rate of that particular concrete are known.

$$t_{i,j} = \left[\frac{c}{K_{c,j}}\right]^2 \qquad 5.6$$

where $t_{i,j}$ (year) represents the time to corrosion initiation of a particular concrete expressed regarding its binder type, j (PC, PC-FA, PC-BS, PC-SF, and PC-BS-SF). $K_{c,j}$ (mm/year$^{0.5}$) represents the carbonation rate of that particular concrete, and c (mm) is the cover thickness..

The time to corrosion initiation model developed in this study is based on the initial assumption that corrosion is initiated immediately the carbonation front reaches the

steel surface. Although, in reality, corrosion can only be initiated in the presence of sufficient oxygen and moisture. Equation 5.6 shows that initiation time of reinforcement corrosion in concrete is dependent on concrete cover depth and carbonation rate; while the carbonation rate is a function of many other parameters investigated in this study such as concrete permeability, exposure conditions, and duration of initial moist curing. The binder type also has a considerable influence on the carbonation rate as shown by the variations in the model coefficients.

The graphical representation of the proposed time to corrosion initiation model result is illustrated in Figures 5.2 to 5.5. The values for the model parameters were arbitrarily selected to show the potential of using the empirical time to corrosion initiation model to objectively compare potential durability performance of concrete with different permeability, exposure conditions, early-age moist curing duration, binder type and cover depth. The values adopted for the model parameters are within the range of experimental data to avoid unrealistic predictions.

The analysis was done by varying a particular input parameter while other input parameters were kept constant. The graphical results are presented in Figures 5.2 to 5.5. The model trends and the influence of various parameters on the predicted time to corrosion initiation are shown and discussed in the preceding sub-sections.

(i) Effect of cover depth on predicted time to corrosion initiation

Cover depth is an essential parameter in service life estimation of reinforced concrete structures. It serves as a physical barrier to delay the ingress of harmful species from reaching the reinforcing steel in the concrete. It can be seen from the results presented in Figure 5.2 that predicted time to corrosion initiation increases when concrete cover depth is increased from 0 mm through to 100 mm for a given exposure. This is because the proportion of carbonating material in a bigger cover is greater compared to a smaller cover depth. It is understood that the greater the amount of carbonating material in concrete the longer time it takes carbonation reaction to being completed.

It is also observed in Figure 5.2 that the variation in the predicted time to corrosion initiation is quite distinct at some greater cover depths compared to the lower cover depths. This may be attributed to the early drying of the concrete surface

immediately after wetting of the outdoor concretes which allows early resumption of carbonation in a lower cover depth. This shows that at some lower cover depths variation in the inland exposure conditions may not have any significant effect on natural carbonation process in concrete.

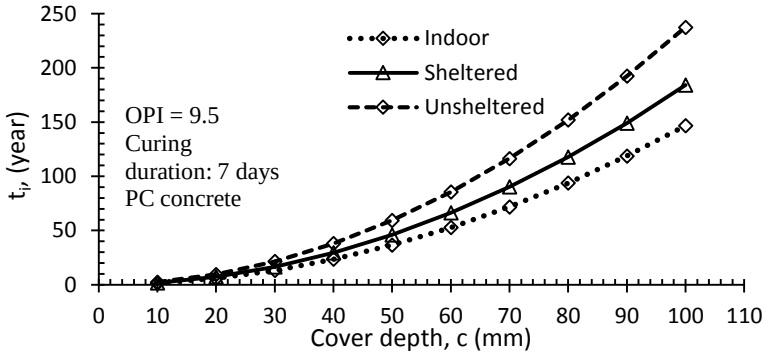

Figure 5:2 Predicted time to corrosion initiation (t_i) vs concrete cover depth

(ii) Effect of exposure conditions on the predicted time to corrosion initiation

Figures 5.2 and 5.3, also show the influence of the exposure conditions on the predicted time to corrosion initiation at some cover depths and concrete qualities. It can be observed that the predicted initiation times are longer for the concretes exposed to outdoor environments compared to indoor exposed concretes. For the outdoor exposed concrete, the predicted time to corrosion initiation is greater for the outdoor unsheltered concrete compared to the sheltered concrete. This can be attributed to the frequent wetting of the outdoor unsheltered concrete by the rain which hinders the flow of CO_2 when concrete pores are saturated with water. In the case of the indoor concrete, its shorter predicted time to corrosion initiation can be due to the relatively higher concentration of CO_2 in the indoor environment compared to outdoor exposures as found by this study.

(iii) Effect of concrete quality on the predicted time to corrosion initiation

Figure 5.3 shows the relationship between the predicted time to corrosion initiation and the concrete quality. It is found that at a constant cover depth and exposure conditions the predicted time to corrosion initiation increases with the increasing concrete quality. This trend is the same in all the exposure conditions as shown by

Figure 5.3. A more permeable (low quality) concrete is usually characterised by many and large interconnected capillary pores, which can easily allow the penetration of CO_2 and moisture into concrete leading to a higher carbonation rate. The easy passage of CO_2 and moisture into a more permeable concrete reduces the time to corrosion initiation of such a concrete compared to a less permeable concrete which is usually characterised by smaller pore spaces. Additionally, the amount of carbonating material is smaller and can be easily consumed by the carbonation reaction in a lower quality concrete compared to a higher quality concrete. Furthermore, the effect of the exposure conditions on high quality concrete is more distinct compared to the lower quality concrete.

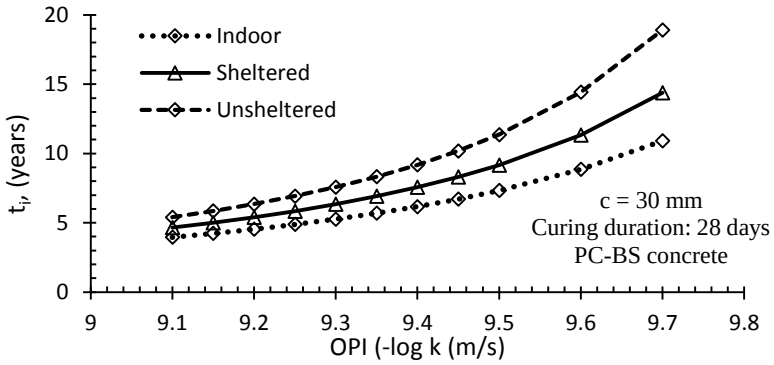

Figure 5:3 Predicted time to corrosion initiation vs concrete quality (OPI)

The variations in the predicted time to corrosion initiation with binder types is shown in Figure 5.4 assuming that the concretes have the same OPI, cover depth and exposed to the same environmental conditions. The order of ranking (longest to shortest) of the predicted time to corrosion initiation is given as PC-SF → PC → PC-BS-SF → PC-FA → PC-BS. This order of ranking shows the dominating influences of permeability and pozzolanic activities of the binders on their predicted time to corrosion initiation.

The proposed model also reflects the importance of early-age moist curing duration, on the concretes. A concrete initially moist cured for 28 days can be seen with an extended predicted time to corrosion initiation compared with a similar concrete moist cured for seven days as shown in Figure 5.5. This is due to the higher degree

of hydration experienced by the concrete left in water for a longer duration compared to the same concrete left in water for a shorter period.

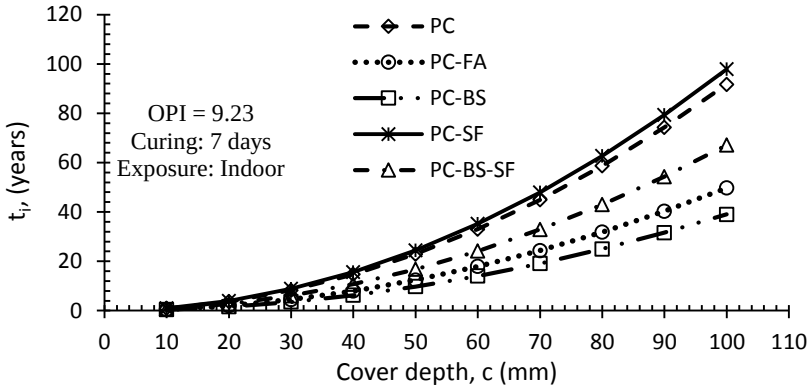

Figure 5:4 Effect of binder type on the predicted time to corrosion initiation

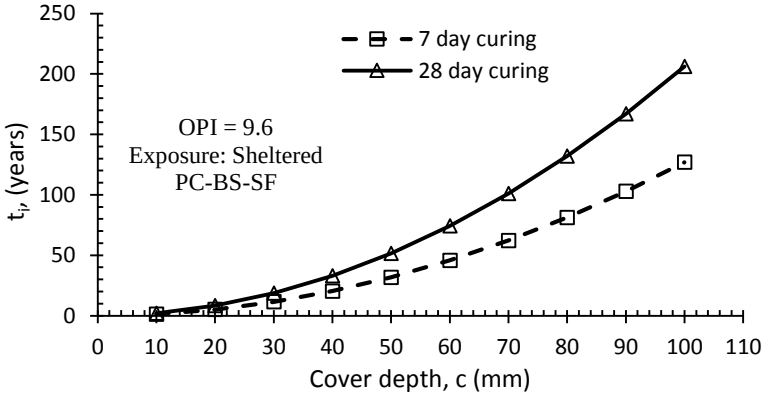

Figure 5:5 Effect of initial curing duration on the predicted time to corrosion initiation

5.4 Comparison with some Existing Models

In this section, the proposed time to corrosion initiation model is compared with those developed by RILEM 14 (1996) and Alhassan (2014). The two existing models were selected because they were developed using data obtained from natural carbonation test which is similar to this study and the RILEM's model is widely used. In addition, early-age concrete characteristics were used as part of the input variables in both models.

The selected corrosion initiation models and their input parameters are summarised in Table 5.5. The cover depths were chosen arbitrarily. However, they are within (SANS 10100:2-2000, 1992) specification for RC structural durability. The 28-day compressive strength corresponding to OPI value of 9.73 was used to represent the concrete 28-day compressive strength. The moist curing age of 28 days was adopted where necessarily to be applied in the models.

Table 5:5. Selected corrosion initiation models and their input parameters

Ref.	Models	Model parameters and coefficients
RILEM 14 (1996)	$t_i = \left[\frac{c}{C_{env} C_{air} a (f_{cu})^{-b}}\right]^2$	Cover depth c,$10 \leq c \leq 70$ mm Compressive strength, f_{cu} (48.7 MPa) Exposure coefficient, (C_{env}): Outdoor sheltered (1.00), outdoor unsheltered (0.50) Air content coefficient, C_{air} (1.00) Binder type: (PC) constants, a (1800) and b (-1.70)
Alhassan , (2014)	$t_i = \left[\frac{c}{72.32 - 6.82(\text{OPI}) + \beta'}\right]^2$	Binder type (PC) Cover depth, c(mm): $10 \leq c \leq 70$ mm Concrete quality, OPI (9.73) Exposure types β': Indoor (0) Outdoor sheltered (1.07) and Outdoor unsheltered (-2.07)
Present study	$t_i = \left[\frac{c}{81.50 - 8.08(OPI) + 1.77 I_{Indoor} + 0.88 I_{Sheltere} + 0 I_{Unsheltered} + 1.75 I_{C7} + 0 I_{C28}}\right]^2$	Cover depth, c: $10 \leq c \leq 70$ mm. Binder type (PC) Concrete quality, OPI (9.73) 28-day moist curing duration Exposure types: Indoor, Outdoor sheltered and Outdoor unsheltered

The predicted time to carbonation-induced corrosion initiation from the three models using the input parameters in Table 5.5 is presented in Figures 5.6 and 5.7 where the three models can be seen to have similar trends. The three models propose that for a given concrete in an exposure environment, increasing the cover depth extends the predicted time to corrosion initiation. For a given cover depth, the

predicted time to corrosion initiation by the three models is higher for the outdoor unsheltered concrete compared to the outdoor exposed concretes.

Using the t_i predicted by this model as a reference, Figures 5.6 and 5.7 show that RILEM's model overestimates the initiation time compared to the Alhassan and the current model for the two outdoor exposure environments. The reason may be because RILEM's model was built using compressive strength as one of the predictor parameters which measures the concrete bulk property of rather than the near surface property that affects the durability of concrete.

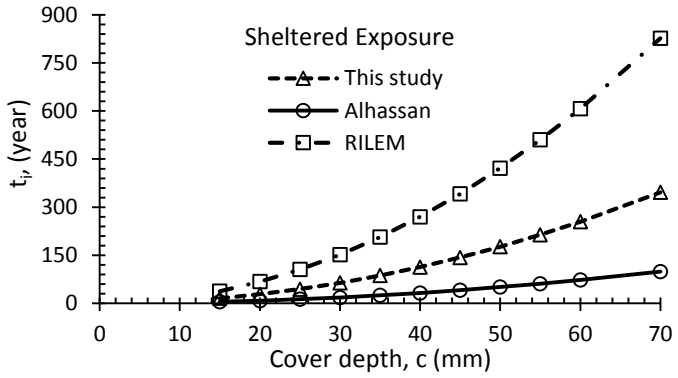

Figure 5:6 Comparison of the RILEM's, Alhassan's and the proposed time to carbonation induced corrosion initiation (t_i) model

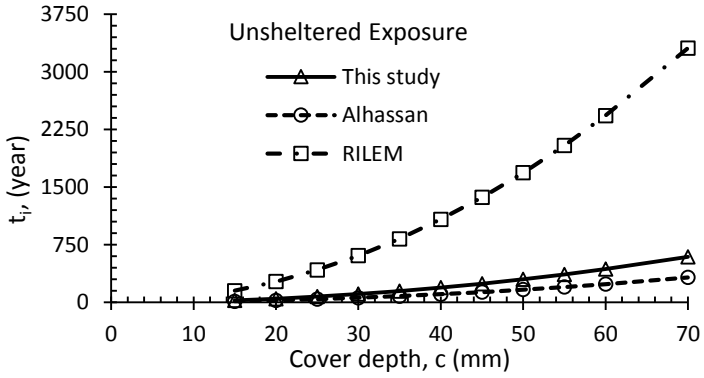

Figure 5:7 Comparison of the RILEM's, Alhassan's and the proposed time to carbonation induced corrosion initiation (t_i) models

The overestimation of the t_i by the RILEM's model might be because RILEM used Swedish outdoor environment to obtain the carbonation data utilized in the modeling. It is understood that Swedish climate is more humid than the South African inland climate. Previous research show that Swedish climate has a mean annual relative humidity of 80% (Relative humidity in Stockholm (Tuutti, 1982)) while the South African inland climate has an average annual relative humidity of 59% (Relative humidity in Johannesburg (Alexander, Mackechnie and Yam, 2007). It is understood that CO_2 diffusion in concrete can be very low in the humid environment (Tuutti, 1982). This may contribute to the extended initiation time predicted by RILEM's model compared to this study and Alhassan's model.

For the sheltered exposed concretes, the predicted corrosion initiation time by the proposed model is higher than the Alhassan's model. This may be because underneath the bridge of a busy motorway in Johannesburg was used by Alhassan for the sheltered exposure site while rooftop of the Hillman building at the University of the Witwatersrand, Johannesburg was employed by the current study. Previous studies have shown that CO_2 concentration is higher in motorway areas due to the greater emission of CO_2 by the vehicle traffic (Tuutti, 1982; Ballim and Lampacher, 1996; Alhassan, 2014). This increases the rate of carbonation which consequently reduces the time to corrosion initiation.

The Alhassan's model predicted a slightly lower corrosion initiation time compared to the present model for the unsheltered concretes at all the cover depths as shown in Figure 5.7. The reason might be because of the difference in elevation of about 15 m between the two roof slabs that were used to position the outdoor unsheltered concretes in the two studies. Alhassan used the top roof slab of the Hillman building while the current study used the lower roof slab to represent the unsheltered exposure. Even though, it was expected that the predicted initiation time would be greater at the higher elevation compared to the lower elevation due to the high concentration of CO_2 usually found in lower elevation (Stewart, Wang and Nguyen, 2011; Peng and Stewart, 2014); the shading from the adjacent walls can reduce the rate of early drying of the concrete surface each time it rained. This can delay the resumption of carbonation, especially at higher cover depths as shown in Figure 5.7

and might be responsible for the delay in the time to corrosion initiation of the unsheltered concrete as predicted by this study.

For the indoor exposure conditions, Figure 5.8 shows that the predicted time to corrosion initiation seems to be slightly higher in the Alhassan's model compared to the present model, especially at the higher cover depths. This may be due to the exposure conditions of the indoor sites used by the two models. The proposed model used a laboratory room in the Hillman building to represent the indoor site while Alhassan indoor exposure site was a vehicle parking basement floor at Senate building of the University of the Witwatersrand. Carbonation rate is usually higher in vehicle parking areas due to the higher CO_2 concentration and its constant discharge from the vehicular movement compared to a laboratory room used by this study. Therefore, it is expected that the predicted time to corrosion initiation would be delayed in the present model compared to the Alhassan's model. The RILEM's model does not include the indoor exposure in its experimental design. Therefore it is not included in this indoor exposure comparison analysis.

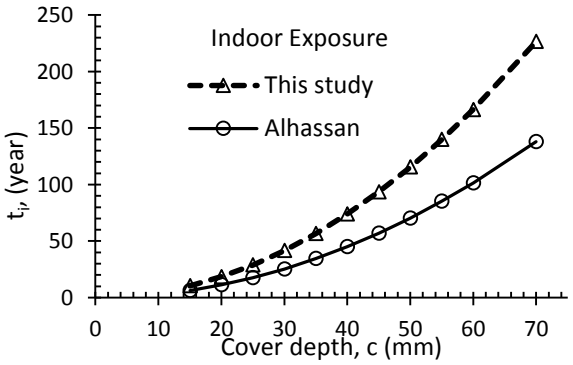

Figure 5:8 Comparison between the Alhassan's and proposed carbonation induced corrosion initiation time (t_i) model

5.4.1 Summary

The time to corrosion initiation prediction model develop in this study was compared with other similar models regarding predicting the time to corrosion initiation. The results showed that corrosion initiation models cannot be generalised

due to the variations observed with the models' predictions. This can be attributed to :

(i) heterogeneity of the concrete material
(ii) variations in the concrete early-age characteristics used in the modelling procedures and
(iii) differences in the experimental exposure environment used in obtaining the modeling data.

Therefore, at this point, it's hard to identify the most plausible model, a reasonable model would have to depend on the choice of model input parameters that impacts carbonation mechanism, and the predictions must be realistic.

Moreover, the proposed initiation model considered the influence of permeability (pore network system) binder type (binder chemistry), cover depth, initial moist curing age and exposure conditions on carbonation rate. The considerations given to these variables in this present model, and its realistic predictions make it more confident and reliable in predicting the corrosion initiation time.

5.5 Modelling the Propagation Phase of Carbonation-Induced Corrosion

The carbonation-induced corrosion propagation phase is the time between the corrosion initiation (assumed to be the time at which carbonation front reaches the reinforcement steel) to the time at which a specified level of corrosion-induced damage state is attained on reinforced concrete structure (Busba and Sagues, 2013). In this study, the level of corrosion-induced damage that is adopted as the limit state is the first appearance of a visible crack along the line of reinforcement.

A first visible crack is formed on corroding RC when the corrosion products completely filled the concrete pores and air void spaces surrounding the reinforcement and exerted an expansive pressure that is greater than the tensile capacity of the concrete surrounding the reinforcing steel. This means that a knowledge of the amount of steel radius loss required to fill the concrete pores and air void spaces and a reliable estimate of projected corrosion rate are necessary for predicting time to cover cracking of a corroding RC structure (Jamali *et al.*, 2013).

The amount of steel radius loss, pore spaces and depth of cover concrete become real important parameters that can be useful in predicting the time to corrosion propagation in concrete. A reliable prediction of corrosion propagation period is required for a realistic estimate of the total and remaining service life of a corroding RC structure.

As shown in Chapter 4, the steel radial loss required for cracking is strongly influenced by the concrete quality, cover depth and binder type. The variables are used as the input parameters in a multiple regression analysis to predict the amount of radius loss required to initiate a first visible crack in the concrete. Knowing the estimated amount of radius loss or corrosion amount needed for a cover concrete damage and the rate at which the corrosion is being produced, Faraday's law can be used to estimate the time needed for the damage to occur.

5.5.1 Predicting corrosion steel radius loss required for cracking

Based on the carbonation-induced corrosion experimental data presented, analysed and discussed in Chapter 4, a multiple linear regression (MLR) analysis of least squares method is used to establish an empirical relationship among the corrosion experimental variables investigated. The radius loss or the amount of corrosion required to initiate a first visible cracking represents the response variable while the predictor variables are cover depth (c), 28-day OPI, and binder type. The selection of these predictor variables was based on their empirical relationships with the steel radius loss established in Chapter 4. The model variables are classified as continuous (numerical) and categorical (non-numerical) variables as shown in Table 5.6 with their range of values obtained from the corrosion tests.

To allow the modelling operation to be carried out with the categorical variable, it was coded as a dummy variable as shown in Table 5.7. The binder type variable is coded as 2 dummy variables under 3 categories of PC, PC-FA, and PC-BS. Each dummy variable was programmed to take the value of 0 or 1.

The corrosion radius loss modelling was based on 54 observations which were performed using a regression analysis (least squares method). The outputs of the analysis are presented in Table F of Appendix F, which include the regression

statistics, analysis of variance (ANOVA) and the coefficients associated with the predictor variables included in the model. The values of these coefficients are given by Equation 5.7.

$$\delta_r = 142.158 + 0.557(c) - 12.580(\text{OPI}) - 11.829I_{PC} - 3.422I_{FA} - 0I_{BS} \qquad 5.7$$

where the only two possible values of I are 1 and 0. The value of I is 0 if its subscript does not apply to the concrete in question and it is 1 if it does apply to the concrete in question. δr (μm) represents the radius loss, OPI represents 28-day oxygen permeability index, and c (mm) is the cover depth.

Table 5:6 Characterisation of the input and output variables

Variables	Variable types	Range of values
28-day OPI (-Log k (m/s))	Continuous	9.04 - 9.73
Binder type	Categorical	1 - 0
Radius loss, δ_r (μm)	Continuous	18.23 - 51.13

Table 5:7 Dummy variable coding for Binder type

Binder types	Dummy variables	
	x_1	x_2
PC	1	0
PC-FA	0	1
PC-BS	0	0

The regression statistics, analysis of variance (ANOVA), and the regression coefficients are presented in Table F of Appendix F which can be used for testing the validity and adequacy of the model. The adjusted R^2 (usually used for testing the adequacy of multiple regression models (Montgomery & Runger, 2011) of the model is 0.8967 at 95% level of confidence. This shows that the model could account for well above 88% of the variations in the output variable.

For statistical reliability and validity of a regression model, it is general understood that the total significance F-value and statistical P-value (statistical t-test) for the

model predictor variables must be less than 0.05. As shown by the model analysis of variance (ANOVA), the total significance F-value and the significance P-values of the variables are less than 0.05 at 95% confidence level. This means that the proposed model is reliable and valid for the predictor variables considered. The proposed model shows the significant impact of the concrete pore network system (measured by the 28-day OPI), cover depth and the binder type on the amount of radius loss required to initiate the first visible cover crack.

Figure 5.9 shows the comparison of the proposed model prediction and measured amount of radius loss needed to initiate the first cracking. As shown in Figure 5.9, the data points are closer to the line of equality which shows that there is a reasonable level of agreement between the predicted and the corresponding measured amount of radius loss required for cracking the concretes. The proposed model could quite well predict the corrosion amount or radius loss needed to initiate a visible fist crack in the concrete.

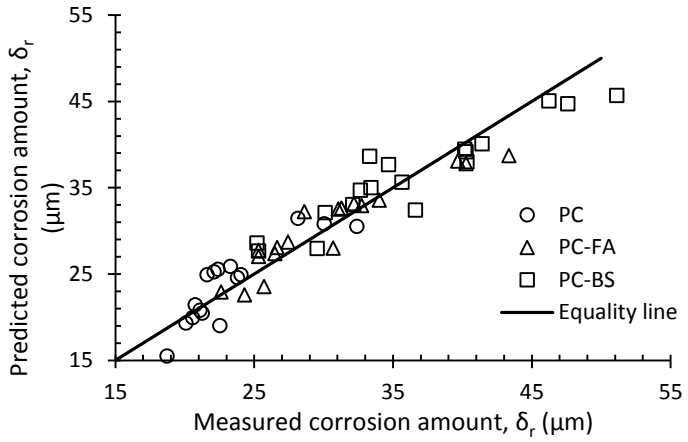

Figure 5:9 Comparison between the predicted and measured corrosion amount required for cover cracking

5.6 Graphical Representation of the Proposed Steel Radius loss Model

The graphical representations of the proposed corrosion radius loss model showing the influence of cover depth, permeability (concrete quality) and binder type on model predictions are presented in Figures 5.10 and 5.11. The input parameters used

for the graphical illustration of the radius loss model are shown in Table 5.8. The input parameters are arbitrarily selected but are within the experimental range of values. This is to demonstrate the potential of using the proposed empirical radius loss model to objectively compare potential durability performance of concrete exposed to a unsheltered environment with different cover depth, permeability and binder type.

Table 5:8 Input parameters for graphical representation of Equation 5.7

Cover depth, *c* (mm)	OPI (-$\log_{10}$ k (m/s))	Binder type
$10 \leq c \leq 100$	9.73	PC, PC-FA, PC-BS
30	$9.04 \leq OPI \leq 9.73$	PC, PC-FA, PC-BS

where k (m/s) is permeability coefficient

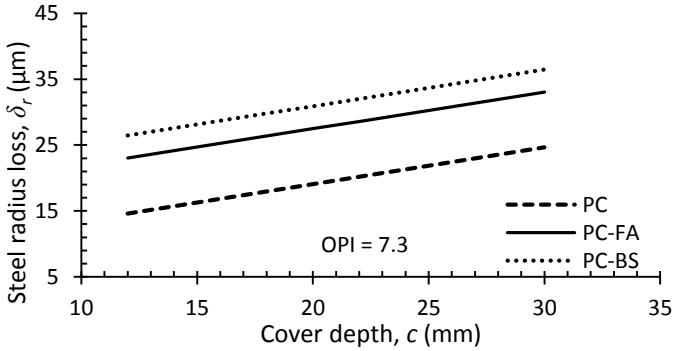

Figure 5:10 Plot of the predicted steel radius loss versus Cover depths

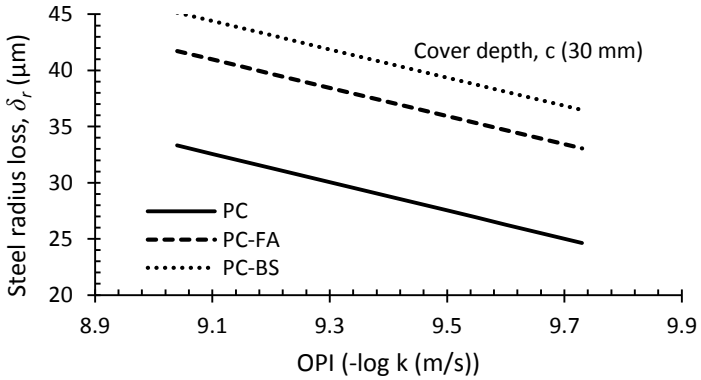

Figure 5:11 Plot of the predicted steel radius loss versus OPI

The followings are evident from the graphical representation of the proposed steel radius loss model shown in Figures 5.10 and 5.11.

- The predicted steel radius loss needed for crcking is sensitive to the variations in the concrete permeability, cover depth and binder type.
- The predicted steel radius loss required for cracking is greater in the SCM blended cement concretes than the equivalent PC concretes.
- Increasing the cover depth at a constant concrete quality increases the predicted steel radius loss needed for cracking the cover concrete. This can be attributed to the fact that the amount of pores and their volumes are increased in a larger cover depth compared to a smaller cover depth for the same concrete mixture. This shows that increasing the cover depth is a direct measure to improve the structural durability of RC structure (Lu, Jin and Liu, 2011)(Lu, Jin and Liu, 2011). However, care must be taken to avoid excessive cover depth in RC structures.
- Keeping other parameters in the model constant and increasing the concrete quality in terms of reducing the permeability can be seen to reduce the steel radius loss required for cracking. This may be because lesser permeable concrete is characterised by a smaller void spaces which require a lower amount of corrosion before initiating a first crack. The PC concrete shows the lowest predicted steel radius loss while the PC-BS concrete has the biggest predicted steel radius loss.

5.7 Evaluation of the Proposed Cover Cracking model

In this study, an attempt was made to evaluate the performance of the proposed cracking model using the slab experimental data of Liu (1996) and comparing the output with some selected existing cracking models (Morinaga, 1989; Rodrigu*ez et al*., 1996; Alonso, Andradel and Diez, 1998; Torres-Acosta and Sagues, 2004). The slab experimental data of Liu (1996) was considered because it is based on outdoor corrosion testing of RC slabs exposed to real environmental conditions over an extended period. The choice of previous models was selected because they are empirical models and their input parameters are available in this study; they have a

precise order of presentation which make them easy to implement. However, it is expected that there will be some variations in their output results due to:

i. differences in the experimental exposure environment,
ii. changes in experimental procedures used to propagate the corrosion,
iii. variations in concrete material characteristics
iv. theoretical assumptions used in developing the models.

The current and the selected previous models and the summary of their experimental procedures, exposure environments, test concrete characteristics used to obtain the modelling data are shown in Table 5.9. It should be noted that the selected previous corrosion cracking models were developed using data from accelerated corrosion tests (by method of admixing chloride and impressed current) this is because there is little information about carbonation-induced corrosion cracking model in the literature. The information availabe in the literature were not expanded to include predictive corrosion cracking model.

As demonstrated by the models in Table 5.9, it will be difficult to establish a general trend in the relationship between concrete quality and the models' predictions because only the current and Rodriguez *et al.* (1996) models include a concrete material property as part of their input variables. Other models are only based on geometric parameters (cover depth and reinforcement diameter) which may pose a limitation to their application.

The corrosion experimental data of Liu (1996) used for evaluating this proposed model is shown in Table 5.10 where the primary experimental variable is cover depth, and steel diameter variable is only varied for specimen SL4. The concrete mixtures are similar in all the slab samples. Performance evaluation results of the models are shown in Figure 5.12, where comparison between the predicted amount of steel radius loss calculated by the models and the measured amount of steel radius loss is shown. It is clear that the predicted amount of radius loss results with the models vary significantly apart from the steel radius loss predictions of Morinaga's model that is closer to the measured values of slabs 1 and 4.

The results show a general trend of increased amount of radius loss at cracking with increasing cover depth as shown in Figure 5.12. The predicted steel radius loss from

the present proposed model is in good agreement with the experimentally observed steel radius loss and predictions of other previous models (Figure 5.12). This shows the adequacy of the proposed model in predicting the amount of carbonation-induced corrosion steel radius loss required for cover concrete cracking.

Table 5:9 Selected previous and proposed empirical steel radius loss models

Reference	Model	Specimens	Corrosion test procedure
Rodriguez et al., (1996)	$\delta_r = 83.8 + 7.4\frac{c}{d} - 22.6 f_t$	Singly reinforced concrete blocks 15 x 15 x 38 cm, f_t = 2.4-3.85 MPa, w/c (0.52, 0.6,0.65) d (3, 8, 10, 12, 16 mm, c (10, 15, 20, 30, 50, 70 mm	3% calcium chloride (by weight of cement) and 10 and 100 μA/cm^2 external current
Alonso, Andradel and Diez, (1998)	$\delta_r = 7.53 + 9.32\frac{c}{d}$	Singly reinforced concrete blocks 15 x 15 x 38 cm, f_t = 2.4-3.85 MPa, w/c (0.52, 0.6,0.65) d (3, 8, 10, 12, 16 mm, c (10, 15, 20, 30, 50, 70 mm	3% calcium chloride (by weight of cement) and 10 and 100 μA/cm^2 external current
Morinaga (1989)	$\delta_r = 0.602d\left[1 + \frac{2c}{d}\right]^{0.85}$	Hollow and singly reinforced cylinders 100 and 150 mm diameters 100 mm high, d = 9, 19 and 25 mm	Series 1: hydraulic pressure; Series 2: 0.5%, 1% and 5% calcium chloride (by weight of cement) and 1.5, 3, 6 nd 12 V external voltage
Torres-Acosta and Sagues (2004)	$\delta_r = 11\left(\frac{c}{d}\right)\left(1 + \frac{c}{L}\right)^2$	Singly reinforced cylinders, c = 27.5-65.7 mm, d = 21 mm; Series B: 140 x 140x 406 mm singly reinforced beams, d = 6 and 13 mm; c = 13-39 mm, fc = 40.53 MPa, L = 8-390 mm	2% calcium chloride and 100μmcm^{-2} external current
This study	$\delta_r = 142.16 + 0.56c - 12.58(OPI) - 11.83I_{PC} - 3.42I_{FA} - 0I_{BS}$	100x100x200 mm; 0.95, 0.6 w/b; c = 12, 20, 30 mm	Pre-carbonated and natural unsheltered exposure

δr = radius loss at cracking; c = cover depth; d = reinforcing steel diameter; f_t = 28-day tensile strength; L = corroding length of steel

Table 5:10 Experimental data for the slab specimens (Liu 1996)

Specimen Reference	d (mm)	c (mm)	f_c (MPa)	f_t (MPa)
SL1	16	48	32	3.35
SL2	16	70	32	3.35
SL3	16	27	32	3.35
SL4	12.7	52	32	3.35

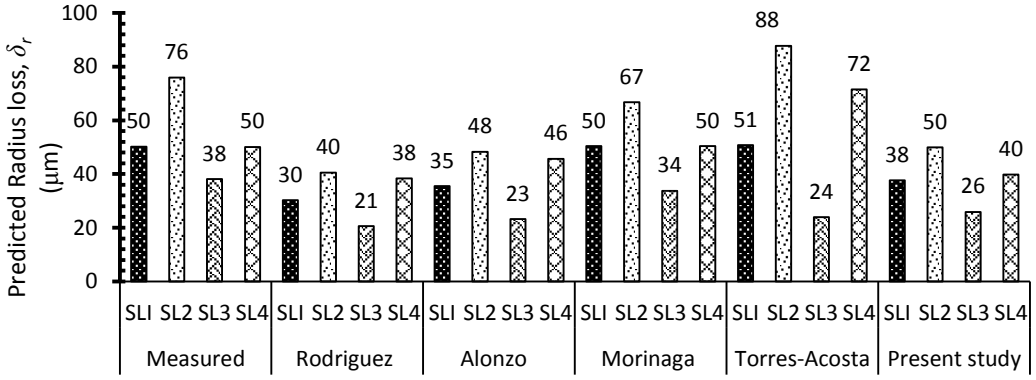

Figure 5:12 Comparison between the predicted radius loss and measured steel radius loss of slab specimens of Liu (1996)

Moreover, the proposed durability based steel radius loss model compared well in trend with the observed experimental results and the predictions of previous models. Therefore, the steel radius loss prediction by this present model can be relied upon. The predictions are reasonable and can be applied to estimate the amount of steel radius loss required for cracking RC structures of different durability properties and cover depths. The information of which can be used along with the estimate of projected corrosion rate from a reliable model to predict the service life of new RC structures and remaining service life of corroding RC structures exposed to the unsheltered inland environment.

5.8 Summary

Multiple linear regression by the least squares method have been used to develop a proposed carbonation rate model that can be used to predict time to corrosion

initiation in different concretes exposed to the inland environments (indoor, outdoor sheltered and unsheltered from rain). The damaging effect of carbonation on concretes exposed to the unsheltered inland environment was also modelled using multiple linear regression. The data utilized for the models was obtained from the experimental procedures highlighted in Chapter 3. The various significant parameters identified in Chapter 4 and their relationships were used to develop the robust models that can be used to estimate carbonation rate and steel radius loss in damaged RC structures. The models' predictions are quite well and are in good agreement with the experimentally observed values. Even though the proposed carbonation rate and steel radius loss models are empirical, they provide reasonable predictions when compared to other previous empirical models.

Lastly, it is evident that the proposed models can give a reasonable service life estimation of RC structures. The outcome of these models can help the design engineer in the choice of quality and cover depth of concrete to achieve a desirable durability of RC structures prone to carbonation in an inland environment. Also, the owners of RC structures can have information on the service life of their concrete even before construction. The application of the proposed models is not restricted to planning and design stage of new concrete; it can also be applied to an existing corroding RC structure for estimation of remaining service life. The service life information will help engineer in scheduling maintenance plan for their RC structure, and concrete owners can have information on how long their concrete can last before repairs.

CHAPTER 6

6 CONCLUSION AND RECOMMENDATIONS

6.1 Introduction

This research was aimed at developing performance-based predictive carbonation-induced corrosion initiation and propagation models for RC structures exposed to the inland environment. The intention of the study was (i) to understand the transport mechanisms of fluid substances (CO_2, oxygen, and moisture) in concretes exposed to the natural inland environment (ii) to understand the carbonation-induced corrosion initiation, and propagation processes in RC structures exposed to the natural inland environment (iii) to quantify from durability point of view the initiation and propagation phases of carbonation-induced corrosion as part of the service life of corrosion affected RC structures.

To achieve the aims and objectives of the study, the experimental method to obtain the data for the modeling was designed in three phases as follows:

Phase 1- concrete early-age characteristics

Phase 2- corrosion initiation in different concretes

Phase 3- corrosion propagation in various pre-carbonated concretes.

The early-age characterisation experiments were carried out in the laboratory to investigate and quantify the combined influence of binder type and w/b ratio on the early-age concrete characteristics (28-day OPI, WSI, compressive strength and tensile strength). Carbonation tests were carried out in the field to investigate and quantify the combined influence of concrete quality (binder type, w/b ratio, and initial moist curing duration) and inland exposure conditions on carbonation rate. The corrosion tests were carried out to investigate and quantify the combined influence of binder type, w/b ratio, cover depth and reinforcing steel diameter on corrosion characteristics of the RC exposed to the natural inland environment. The experiments were performed in the laboratory and the field. The experimental details were presented in Chapter 3 while the results were presented, analysed and discussed in Chapter 4. The experimental results presented, analysed and discussed in Chapter 4 were used to develop a carbonation-induced corrosion initiation and

propagation models. This chapter deals with the general conclusions, practical implications, and recommendations for further study.

6.2 Effect of concrete quality on the concrete early-age characteristics and carbonation-induced steel corrosion

Concrete quality was varied in this study using five binder types (PC, PC-FA, PC-BS, PC-SF and PC-BS-SF) and three w/b ratios (0.40, 0.60 and 0.95) and quantified using oxygen permeability index and water sorptivity index obtained from the 28-day OPI and WSI tests. Concrete quality was observed to influence the concrete early-age characteristics which consequently impacted the carbonation-induced corrosion resistance of the concretes. The following general conclusions are therefore made regarding the effect of concrete quality on the concrete early-age characteristics and carbonation-induced corrosion resistance:

1. Binder type

(a) At the same w/b ratio, SCM blended cement concretes were less permeable than PC concretes. The order of ranking (maximum to minimum) of the binders regarding their OPI result at 0.95 and 0.40 w/b ratios is PC-SF→ PC-BS-SF → PC-FA → PC → PC-BS. At 0.60 w/b ratio, the order of OPI ranking from maximum to minimum is PC-SF/PC-BS-SF → PC-FA/PC → PC-BS.

(b) For the WSI results, at 0.95 w/b ratio, the order of ranking from maximum to minimum is PC→ PC-SF/PC-BS-SF/PC-FA/PC-BS. At 0.60 w/b ratio, the order of ranking is PC /PC-FA/ PC-BS → PC-SF/PC-BS-SF. At w/b ratio of 0.40, WSI values of the concretes are the same which presents OPI as an appropriate parameter that can be used in a model that can reasonably predict carbonation rate in concrete.

(c) Apart from the BS blended concretes, all the concretes blended with the SCM have their compressive strength higher than the PC concretes at the same w/b ratio. Similar trends to the compressive strength results were also observed with the split tensile strength results

(d) Apart from the concretes containing SF, all the SCM blended cement concretes showed higher carbonation rates compared to the PC concretes of the same w/b ratio, exposure condtions, and extent of the initial moist curing conditions. This effect was due to the dominating influence of carbonation and pozzolanic reactions of the SCM. The superior performance of SF blended concretes in resisting carbonation reaction was attributed to the increased reactivity of SF due to its high degree of fineness and high PC contents compared to the other SCM.

(g) Higher corrosion current density and larger amount of steel radius loss required to initiate a first visible cover cracking were found with the SCM concretes compared to the PC concrete at the same w/b ratio and cover depth. This consequently led to their early cracking times. The reason for the higher corrosion activities in the SCM blended concretes was because of accelerated carbonation of their pozzolanic C-S-H which increased their porosity relatively compared to the PC concretes.

2. Water/binder ratio

(a) For a given binder type, increasing the w/b ratio resulted in a more porous concrete. This was due to the capillary porosity of the cement paste and interconnectivity of the pores which increased with an increase in w/b ratio. This trend was observed in all the concretes.

(b) For a given w/b ratio and duration of initial moist curing, compressive and tensile strengths increased with a decrease in w/b ratio. All the concretes showed a similar pattern.

(c) For a given concrete exposed to a certain inland environment, carbonation rate increased with an increase in w/b ratio. This was attributed to increasing concrete capillary pore size and their interconnectivity at a higher w/b ratio.

(d) For a given cover depth, the corrosion current density, amount of steel radius loss required to initiate the first cover cracking and cracking time of cover concrete increased with an increase in w/b ratio. This was attributed to the higher permeability associated with increasing w/b ratio. This trend was

evident in all the concretes. However, the concrete cracking time reduced with an increase in w/b ratio

4. Duration of the initial moist curing conditions

   For a given concrete exposed to an environment, extending the initial moist curing period from 7 days to 28 days reduced the carbonation rate for a given concrete. This was attributed to the fact that extending the moist curing duration increased the concrete degree of hydration which consequently reduced the size of the capillary pores and the connectivity between the pores.

This study showed that a change in concrete quality due to a change in w/b ratio has a relatively more marked effect on concrete characteristics and carbonation-induced corrosion resistance than a change in concrete quality due to a change in binder type or extending the initial moist curing conditions. Extending the duration of the initial moist curing had a more marked effect on time to carbonation-induced corrosion initiation than changing the binder type.

In general, it can be concluded that concrete quality is an important parameter in the control of carbonation-induced corrosion. The quality of a concrete can be improved by using a lower w/b ratio and extending the period of initial moist curing condition of the concrete. Apart from the methods highlighted in this study to improve concrete quality on site, adherence to good site practices will also improve the quality of concrete on site to a large extent. This will ensure an excellent durability that will guarantee the expected RC service life.

6.3 Effect of concrete cover depth on carbonation-induced corrosion

Three cover depths of 12, 20 and 30 mm and three reinforcing steel diameters of 8, 12 and 20 mm were used in the carbonation-induced corrosion experiment. The following general conclusions were made about the influence of cover depth and reinforcing steel diameter on corrosion current density and corrosion steel radius loss required to initiate a crack on the cover concretes and their cracking time of the cover concrete:

(a) For a given w/b ratio, and binder type, corrosion initiation time increased with increase in cover depth..

(b) For a given concrete quality, the amount of radius loss required to initiate a cover cracking increased with increasing cover depth.

(c) Corrosion-induced cover cracking time increased with increasing cover depth for a given concrete quality

(d) For a given concrete quality and cover depth, variation in the reinforcing steel diameter seemed not to have any significant trend with the corrosion measurements

The impact of increasing cover depth was observed to improve the carbonation-induced corrosion resistance of the concretes at both initiation and propagation stages of the corrosion. Therefore, it can be concluded that cover depth is an important parameter in the control of carbonation-induced corrosion in concrete exposed to the natural inland environment. However, it should be noted that the vulnerability of reinforcement to corrosion in terms of cover depth (i.e., protecting the reinforcement) and quality of concrete (i.e., permeability and pore solution alkalinity) interact with the environment in a way that determines whether or not the environment is aggressive for the concrete reinforcement. The values of cover depth specified in the national codes are usually for the protection of reinforcement against corrosion in RC structures. However, care must be taken not to trade-off cover depth (reducing cover) with reduced w/b ratio or extended initial curing duration.

The near surface of the concrete is usually susceptible to higher permeability caused by the higher cement paste content and locally increased w/b ratio at the surfaces cast against the impermeable formwork. Similarly, floated concrete surfaces may be more porous than the bulk of the concrete due to bleeding and settlement of the coarse aggregates. In these cases, any locally reduced concrete cover depth will considerably reduce the durability of the RC structure in any exposure. Therefore, cover depth and quality of the cover concrete must be balanced to have a durable concrete that can withstand the aggressiveness of the natural inland environment.

It is recognised that cover depth concrete is susceptible to cracking under the influence of external loads. Thermal cracking, plastic shrinkage, and carbonation shrinkage cracking have been reported in the literature to be common in concrete cover. However, cracking is inevitable in RC structures and may not indicate an undue lack of durability provided the crack widths are within the acceptable limits specified in the building national codes.

Additionally, specifying smaller cover depth with corresponding smaller allowable crack widths and using an excessive amount of reinforcement in a section with a high bending moment and a shear force may have adverse effects on durability. These measures are clearly unsustainable in terms of obtaining a long service life.

Therefore, a good quality and adequate cover depth will ensure a high concrete resistance to early deterioration. A good quality concrete can be achieved by using cost effective methods such as appropriate choice of binder, concrete mixture, duration of initial curing conditions and good site practices (i.e. adequate compaction)

6.4 Empirical Carbonation-induced Corrosion Initiation Model

The results of carbonation depth of the PC, PC-FA, PC-BS, PC-SF and PC-BS-SF concretes measured within two years of their exposure to the inland environment (indoor, sheltered and unsheltered from rain) were used to establish their carbonation rates. The concretes were manufactured using 3 w/b ratios (0.95, 0.60 and 0.40) and initially cured for 7 and 28 days in water before the exposure to three different exposure conditions in the inland environment (Indoor, outdoor sheltered and outdoor unsheltered).

A linear relationship between carbonation rate and OPI as well as exposure conditions and initial curing duration was established using a multiple linear regression of least squares method. The relationship is shown in Equation 5.4.

$$K_{c,j} = \beta_3 - \beta_4(OPI) + \beta_5 I_{Indoor} + \beta_6 I_{Sheltered} + \beta_7 I_{Unsheltered} + \beta_8 I_{C7} + \beta_9 I_{C28} \qquad 5.4$$

The predicted carbonation rate by this model compared reasonably with the measured carbonation rates. The carbonation rate equation was further developed

into carbonation depth and carbonation-induced corrosion initiation time using a square root of time law, as shown in Equations 5.5 and 5.6.

$$d_{c,j} = K_{c,j}\sqrt{t} \qquad 5.5$$

$$t_{i,j} = \left[\frac{c}{K_{c,j}}\right]^2 \qquad 5.6$$

The graphical illustration of the corrosion initiation prediction model show the influence of binder type, cover depth, concrete quality, exposure conditions and curing on the predicted carbonation-induced corrosion initiation time.

The proposed carbonation-induced corrosion initiation model predictions were compared with some existing models' predictions. The variations found with their predictions were attributed to the difference in input parameters, local environmental conditions at the concrete exposure sites, mixture compositions used in obtaining the primary data used in the modelling. Even though some variations were observed with the predictions, the proposed carbonation-induced corrosion initiation model have similar trends with the selected previous models and compared well with them. It can be useful to the engineers in the following areas:

(i) selection of a suitable concrete cover depth and quality as well as the exposure conditions for a longer service life

(ii) determining the duration of corrosion initiation periods in different concrete mixtures.

(iii) importantly, the model can form an integral part of service life model of RC structures which can be used to plan and schedule maintenance strategy.

With the proposed carbonation-induced corrosion initiation model, a client will have timely information about how long their structure can last before planning for maintenance.

6.5 Empirical Carbonation-induced Corrosion cracking Model

The concrete data used to model the corrosion propagation phase were manufactured using three binder types (PC, PC-FA, and PC-BS), two w/b ratios (0.95 and 0.60), three reinforcing steel diameters (8, 12 and 20 mm) and three cover depths (12, 20 and 30 mm). The concretes were initially cured for 7 days in water before carbonation under accelerated laboratory conditions. The pre-carbonated concretes were exposed to the natural unsheltered inland environment till a first visible crack was seen on the concrete surface. The gravimetry mass loss method was used to measure the amount of the steel radius loss required to initiate the first visible crack on the concrete surface. The radius loss parameter was used with the OPI, cover depth and binder type in a multiple linear regression of least squares method to model the carbonation-induced radius loss in the concretes. The linear equation representing the model is given in Equation 5.7.

$$\delta_r = 142.158 + 0.557(c) - 12.580(\text{OPI}) - 11.829I_{PC} - 3.422I_{FA} - 0I_{BS} \qquad 5.7$$

The graphical illustration and practical implementation of the prediction model showed the influence of cover depth and concrete quality on the predicted carbonation-induced corrosion radius loss. The model was compared with some selected existing empirical steel radius loss models using a natural corrosion experimental data from a literature (Liu 1996). It was found that the predictions of this proposed model follow similar trends with the selected previous models.

Even though some variations were noted with the models' predictions the proposed steel radius loss model was comparable with other previous models. The variations in their predictions were attributed to the model input parameters, experimental exposure climate and methods in obtaining the primary data used for the modelling (accelerated and natural corrosion). The variations in the predictions of the models show that a paticular model cannot be generalised in application.

The proposed model can be developed further to estimate the cover concrete cracking time using the Faraday's assumption as illustrated by Rodriguez & Andrade (1990) for a known corrosion current density (Equation 2.48).

$$t_{cr} = 86.96\frac{\delta_r}{i_{cor}} \qquad 2.48$$

where t_{cr} (years) is the cracking time and i_{cor} ($\mu A/cm^2$) is a known corrosion current density which is classified by Andrade et al. (1993) in terms of corrosion damage risk. The corrosion risks are classified as: Negligible risk which corresponds to i_{cor} < 0.1 $\mu A/cm^2$; low risk which corresponds to i_{cor} between 0.1 and 0.5 $\mu A/cm^2$, moderate risk corresponds to i_{cor} between 0.5 and 1 $\mu A/cm^2$ and high risk corresponds to i_{cor} > 1 $\mu A/cm^2$.

However, the classifications made by Andrade et al. (1993) may not be realistic since corrosion current density is understood to be largely influenced by the depth and quality of cover concrete. Therefore, a corrosion current density model that is sensitive to both depth and quality of concrete is important for a better estimation of corrosion current density. Such corrosion current density model can be included in a corrosion damage model which when combined with initiation model can be used to estimate service life of corroding RC structures exposed to the unsheltered inland environment. This presents an opportunity for further research.

6.6 Practical Implications and Limitations of the Models

The practical demonstration of the models' applications showed that improving the quality and depth of cover concrete improved the structural durability of RC structures when exposed to the inland environment. However, these proposed models are limited to (i) the inland environment and (ii) the range of parameters for which the models are valid. Other limitations are mainly associated with the experimental set-up and scope used in this study as presented in Chapter 1. Therefore, it is important to take caution when extrapolating these models to include values outside those studied. Additionally, having ascertained that the quality and depth of cover concrete are important for the structural durability of RC structure exposed to the inland environment, it is important to distinguish their degree of sensitivity to service life. This can be an area for further research.

The models are capable of providing a realistic (the model output values are closer to the actual or real measurements) estimate of carbonation-induced corrosion initiation and propagation times for concrete. They provide framework in which suitable combinations of concrete quality, cover depth, and exposure conditions can

be selected and optimised during the design stage or repair stage of damaged RC structures. The result of this study can be used as a guide for the design of durable RC structures that can withstand the exposure conditions of inland environment. It can also be used for optimisation of inspections and priorities of data collection for research studies.

6.7 Contributions to Knowledge

Based on the experimental results and their trends, corrosion initiation and propagation models were proposed. The proposed corrosion initiation model incorporates the combined influence of concrete quality (concrete penetrability, binder type, and duration of initial moist curing duration) and exposure conditions on carbonation rate; while the corrosion propagation model incorporates the combined influence of concrete quality (permeability and binder type) and cover depth on the steel radius loss required to initiate concrete cover cracking. With a known cover depth, binder type, initial moist curing duration, and exposure condition, the proposed carbonation rate model can be used to quantify the corrosion initiation period of RC structures. This is with the assumption that corrosion is initiated immediately carbonation front reaches the reinforcememt.

Moreover, using a relevant carbonation-induced corrosion rate model, with a known concrete permeability, binder type, and cover depth, the proposed steel radius loss model can be used to estimate the corrosion propagation period of RC structures exposed to the unsheltered inland environment. According to the conceptual service life model proposed by Tuutti (1982) mentioned in Chapter 1, the addition of the two periods (initiation and propagation) is refered to as the service life of RC structure.

The outcome of these models can help the design engineer in the choice of quality and cover depth of concrete to achieve a given service life. The models' application is not restricted to planning or designing stage of new concrete; it can also be applied to an existing corroding RC structure for estimation of remaining service life. Concrete construction stakeholders can have information on the life span of

their RC structures before maintenance. The information will help engineers in scheduling maintenance plans for RC structures.

6.8 Recommendations for Further Research

Based on the findings of this study, the following recommendations for future study are given:

Corrosion initiation

- It is recommended that carbonation experimental studies with a large variation in w/b ratio be conducted. This will produce a significant variation in the results and can improve the precision of the models
- The present corrosion initiation prediction model was based on two years carbonation data from natural exposure conditions. There is a need to extend the exposure time to cover more than two years. Such information can be used to calibrate the present carbonation-induced corrosion initiation model for site applications.
- The proposed carbonation-induced corrosion initiation prediction model can be validated and calibrated in the form of a research study. This will involve using a long-term data from a large scale specimen.
- In this study, concretes were assumed to be in the un-cracked state. However, this may not be a reasonable assumption for a typical concrete where plastic shrinkage and micro cracks are inevitable. Several types of research conducted on cracked concrete had been in marine exposure environment which cannot be generalised. It is therefore important to investigate carbonation of cracked concrete in both accelerated and natural carbonation environment. This will be useful in estimating the corrosion initiation time in cracked concrete exposed to the inland environment.
- Although, it is understood that high-pressure carbonation test is faster compared to natural carbonation test. However, high-pressure carbonation can destroy the cover concrete micro-structure especially the weak cover concretes. It is important to establish a relationship between high-pressure carbonation test and natural carbonation test.

Corrosion propagation

- The proposed propagation model considered the effect of the cover thickness and concrete quality to be the dominating factors in corrosion propagation in concrete. However, analytical prediction of Bhargava et al., (2006) suggests that spacing of reinforcing steel in the concrete might as well contribute to cracking of the cover concrete. However, this can be investigated using a beam with multiple reinforcing steels to develop an empirical cracking model that will include a spacing factor. The result can be compared with the analytical prediction of Bhargava *et al.* (2006)
- The current study assumed the absence of micro-crack on the surface of the concrete, however, this might not be the case with some concrete types. The effect of pre-existing crack on carbonation-induced corrosion can be investigated to determine the service life of such concretes.
- Although, it is generally understood that corrosion may not be serious in Johannesburg area. In order words, the environmental factors may not have any direct influence on corrosion of reinforced concrete structures. However, the effect of moisture and temperature from external sources such as lake, dam, and pond on the nearby RC structures can be investigated in carbonation environment along with structural design and concrete penetrability parameters.
- It is generally understood that extending the duration of initial moist curing improves the concrete micro-structure; importantly the SCM blended concretes. The effect of initial moist curing duration on steel corrosion in different carbonated SCM concretes when exposed to the inland environment is therefore recommended for investigation and the result compared with PC concrete.
- The proposed cover cracking model can be validated and adjusted in the form of a research study. This will involve using a long-term data from large scale specimen.

7 REFERENCES

Adewole, K. K., Ajagbe, W. O. and Arasi, I. A. (2015) 'Determination of appropriate mix ratios for concrete grades using Nigerian', *Leonardo Electronic Journal of Practices and Technologies*, (26), pp. 79–88.

Ahmad, S. (2003) 'Reinforcement corrosion in concrete structures, its monitoring and service life prediction—a review', *Cement and Concrete Composites*, 25(4–5), pp. 459–471. doi: 10.1016/S0958-9465(02)00086-0.

Ahmad, S. (2009) 'Techniques for inducing accelerated corrosion of steel in concrete', *The Arabian Journal for Science and Engineering*, 34(2), pp. 95–104.

Al-Harthy, A. S., Mullard, J. and Stewart, M. G. (2011) 'Concrete cover cracking caused by steel reinforcement corrosion', *Magazine of Concrete Research*, 63(9). doi: 10.1680/macr.2011.63.9.655.

Alexander, M. G., Ballim, Y. and Mackechnie, J. M. (2007) *Durability Index Testing Procedure Manual*. Cape Town, South Africa: Department of Civil Engineering, University of Cape Town.

Alexander, M. G., Ballim, Y. and Stanish, K. (2008) 'A framework for use of durability indexes in performance-based design and specifications for reinforced concrete structures', *Materials and Structures*, 41(5), pp. 921–936. doi: 10.1617/s11527-007-9295-0.

Alexander, M. G., Jaufeerally, H. and Mackechnie, J. R. (2003) *Structural and durability properties of concrete made with Corex slag - Research monograph, Department of Civil Engineering, University of Cape Town*. Cape Town, South Africa.

Alexander, M. G., Mackechnie, J. R. and Yam, W. (2007) 'Carbonation of concrete bridge structures in three South African localities', *Cement and Concrete Composites*, 29(10), pp. 750–759. doi: 10.1016/j.cemconcomp.2007.06.005.

Alexander, M. G. and Mindess, S. (2005) *Aggregates in Concrete (Modern Concrete Technology)*. 1st edn. NY, USA: Taylor & Francis Group, London.

Alexander, M. G., Santhanam, M. and Ballim, Y. (2010) 'Durability design and specification for concrete structures-the way forward', *International Journal of Advances in Engineering Sciences and Applied Mathematics*, 2(3), pp. 96–105.

Alhassan, A. Y. (2014) *Effects of materials and micro-climate variations on predictions of carbonation rate in reinforced concrete in inland environment*. PhD Thesis, University of the Witwatersrand, Johannesburg, South Africa.

Almusallam, A. A., Al-Gahtani, A. S. and Aziz, A. R. (1996) 'Effect of

reinforcement corrosion on bond strength', *Construction and Building Materials*, 10(2), pp. 123–129. doi: 10.1016/0950-0618(95)00077-1.

Alonso, C., Andradel, C. and Diez, J. M. (1998) 'Factors controlling cracking of concrete affected by reinforcement corrosion', *Materials and Construction*, 31, pp. 435–441.

Alonso, C., Andradel, C. and Gonzalez, J. . (1988) 'Relationship between resistivity and corrosion rate of reinforcement in carbonated mortar made with several cement types', *Cement and Concrete Composites*, 8, pp. 687–698.

Ananmalay, N. (1996) *Characterising the strength and durability performance of South African Silica fume concretes*. MSc thesis. University of the Witwatersrand, Johannesburg, South Africa.

Andersson, K., Allard, B., Bengtsson, M. and Magnusson, B. (1989) 'Chemical composition of cement pore solutions', *Cement and Concrete Research*, 19(3), pp. 327–332. doi: 10.1016/0008-8846(89)90022-7.

Andrade, C. and Alonso, C. (1996) 'Corrosion rate monitoring and on-site', *Construction and Building Materials*, 10(5), pp. 315–328.

Andrade, C., Alonso, C. and Molina, F. J. (1993) 'Cover cracking as a function of bar corrosion□: Part 1-Experimental test', *Materials and Structures*, 26(8), pp. 453–464.

Andrade, C., Rio, O., Castillo, A., Castellote, M. and D'Andrea, R. (2006) 'An NDT Performance related proposal based on electrical resistivity to the specification of concrete durability', in *RILEM International Workshop 'Performance based evaluation and indicators for concrete dura-buility'*. Madrid, Spain: RILEM Publications SARL.

Apostolopoulos, C. a. and Papadakis, V. G. (2008) 'Consequences of steel corrosion on the ductility properties of reinforcement bar', *Construction and Building Materials*, 22(12), pp. 2316–2324. doi: 10.1016/j.conbuildmat.2007.10.006.

Arachchige, A. D. M. (2008) 'Influence of cement content on corrosion resistance', *Proceedings of the ICE - Construction Materials*, 161(1), pp. 31–39. doi: 10.1680/coma.2008.161.1.31.

Arum, C. and Moya, D. (2012) 'Effect of packing densities of aggregates on the workability and compressive strength', in *4th West Africa Built Environment Research*, pp. 301–314.

ASTM C876 (1991) *Standard test method for half-cell potentials of uncoated reinforcing steel in concrete*. ASTM C876-91.

ASTM G1-3 (1999) *ASTM G1 Standard Practice for Preparing, Cleaning, and Evaluation Corrosion Test Specimens*.

ASTM G1-3 (2011) *Standard Practice for Preparing, Cleaning, and Evaluating Corrosion Test Specimens*. West Conshohocken, PA.

Balafas, I. and Burgoyne, C. J. (2010) 'Environmental effects on cover cracking due to corrosion', *Cement and Concrete Research*. Elsevier Ltd, 40(9), pp. 1429–1440. doi: 10.1016/j.cemconres.2010.05.003.

Ballim, Y. (1993) 'Curing and the durability of OPC, fly ash and blast-furnace slag concretes', *Materials and Structures*, 26, pp. 238–244.

Ballim, Y. and Alexander, M. G. (2005) 'Towards a performance based specification for concrete durability', in *African Concrete Code symposium*. Libya, pp. 206–218.

Ballim, Y., Alexander, M. G. and Beushausen, H. (2009) 'Durability of concrete', in Owens, G. (ed.) *Fulton's Concrete Technology*. 9th edn. Midrand: Cement and Concrete Institute, South Africa, pp. 155–188.

Ballim, Y. and Lampacher, B. J. (1996) 'Long-term carbonation of concrete structures in the Johannesburg environment', *SAICE*, pp. 5–9.

Ballim, Y. and Reid, J. C. (2003) 'Reinforcement corrosion and the deflection of RC beams - An experimental critique of current test methods', *Cement and Concrete Composites*, 25(6), pp. 625–632. doi: 10.1016/S0958-9465(02)00076-8.

Basheer, M., Russell, D. P. and Rankin, G. I. B. (1999) 'Design of concrete to resist carbonation', in Lacasse, M.A. and Vanier, D.J.(Institute of Research in Construction, Ottawa, C. (ed.) *8th International Conference on Durability of Building Materials and Components (8dbmc)*. Vancouver, Canada: National Research Council, Canada, pp. 423–435.

Bazant, Z. (1979) 'Physical model for steel corrosion in concrete sea structures - theory', *Journal of the Structural Division ASCE*, pp. 1137–1153.

Beushausen, H. and Alexander, M. (2009) 'Performance-based service life design of reinforced concrete structures using durability indicators', in *ConcreteLife 09*.

Beushausen, H. and Alexander, M. G. (2008) 'The South African durability index tests in an international comparison', *Journal of the South African Institution of Civil Engineering*, 50(1), pp. 25–31.

Beushausen, H., Alexander, M. G., Andrade, C., Basheer, M., Baroghel-Bouny, V., Corbett, D., d'Andrea, R., Goncalves, A., Guilbaud, J., Jacobs, F., Monteiro, A. V., Nanukuttan, S. V., Otieno, M., Polder, R. and Torrent, R. (2016) 'Application

Examples of Performances-Based Specification and Quality Control', in Beushausen, H. and Fernandez Luco, L. (eds) *Performance-Based Specifications and Control of Concrete Durability - State-of-the Art Report RILEM TC 230-PSC*. London, UK: RILEM Publications Springer, pp. 197–266.

Bhargava, K., Ghosh, a. K., Mori, Y. and Ramanujam, S. (2006) 'Analytical model for time to cover cracking in RC structures due to rebar corrosion', *Nuclear Engineering and Design*, 236(11), pp. 1123–1139. doi: 10.1016/j.nucengdes.2005.10.011.

Bier, T. A., Kropp, J. and Hilsdorf, H. . (1987) 'Carbonation and realkalinisation of concrete and hydrated cement paste', in *Durability of Construction Materials*. London, UK: RILEM, Chapman & Hall, pp. 927–934.

Bjegovic, D., Serdar, M., Oslakovic, I. ., Jacobs, F., Beushausen, H., Andrade, C., Monteiro, A. V., Paulini, P. and Nanukuttan, S. (2016) 'Test Methods for Concrete Durability Indicators', in Beushausen, H. and Luco, L. F. (eds) *Performance-Based Specifications and Control of Concrete Durability State-of-the-Art Report RILEM TC230-PSC*. London, UK: RILEM Publications Springer, pp. 51–105.

Borges, P. H. R., Costa, J. O., Milestone, N. B., Lynsdale, C. J. and Streatfield, R. E. (2010) 'Carbonation of CH and C–S–H in composite cement pastes containing high amounts of BFS', *Cement and Concrete Research*, 40(2), pp. 284–292. doi: 10.1016/j.cemconres.2009.10.020.

BS EN 206-1:2000 (2000) *Concrete - Part 1: Specification, perfformance, production and conformity, European Standard, REu de Stasst, B-1050*. Brussels, Belgium: British Standard Institution (BSI).

BS EN 934-2 (2009) *Admixtures for concrete, mortar and grout. Concrete admixtures. Definitions, requirement, conformity, making and labelling*. British Standard Institution (BSI).

Busba, E. R. (2013) *Effect of Localized Corrosion of Steel on Chloride-Induced Concrete Cover Cracking in Reinforced Concrete Structures*. University of South Florida.

Busba, E. and Sagues, A. A. (2013) 'Critical localised corrosion penetration of steel reinforcement for concrete cover cracking', in *NACE CORROSION 2013 CONFERENCE & EXPO*. Houston, Texas: NACE International, pp. 1–14.

Buss, K. (2013) *Ternary combination concretes using GGBS , fly ash & limestone*. PhD Thesis, University of Dundee, Dundee, UK.

Calavera, J. (2001) 'Evaluacion resistente de enstructuras', in *de hormigon armado*. Madrid, Spain.

Ceukelaire, L. De, Nieuwenburg, D. Van, De Ceukelaire, L., Van Nieuwenburg, D., Ceukelaire, L. De, Nieuwenburg, D. Van, De Ceukelaire, L., Van Nieuwenburg, D., Ceukelaire, L. De and Nieuwenburg, D. Van (1984) 'Accelerated carbonation of a blast-furnace cement concrete', *Cement and Concrete Research*, 23(2), pp. 239–249. doi: 10.1016/0008-8846(93)90109-M.

Chang, C.-F. F. and Chen, J.-W. W. (2006) 'The experimental investigation of concrete carbonation depth', *Cement and Concrete Research*, 36(9), pp. 1760–1767. doi: 10.1016/j.cemconres.2004.07.025.

Chernin, L. and Val, D. V. (2011) 'Prediction of corrosion-induced cover cracking in reinforced concrete structures', *Construction and Building Materials*, 25(4), pp. 1854–1869. doi: 10.1016/j.conbuildmat.2010.11.074.

Chi, J. M., Huang, R. and Yang, C. C. (2002) 'Effects of carbonation on mechanical properties and durability of concrete using accelerated testing method', *Journal of Marine Science and Technology*, 10(1), pp. 14–20.

Clark, M. (2013) *Clinker C3S paramount*, *https://www.cemnet.com/*. Available at: https://www.cemnet.com/Articles/story/151799/clinker-c3s-paramount.html (Accessed: 23 June 2017).

Cumming, G., Fidler, F. and Vaux, D. L. (2007) 'Error bars in experimental biology', *The Journal of Cell Biology*, 177(1), pp. 7–11. doi: 10.1083/jcb.200611141.

Czarnecki, L. and Woyciechowski, P. (2015) 'Modelling of concrete carbonation; Is it a process unlimited in time and restricted in space?', *Bulletin of the Polish Academy of Sciences: Technical Sciences*, 63(1), pp. 43–54. doi: 10.1515/bpasts-2015-0006.

Dalage, P. and Aitcin, P. . (1983) 'Influence of condensed silica fume on the pore-size distribution of concretes', *Industrial and engineering Chemistry product Research and Development*, 22(2), pp. 286–290.

Dhir, R. K., Hewlettt, P. C. and Chanz, Y. N. (1989) 'Near-surface characteristics of concrete□: prediction of carbonation resistance', *Magazine of Concrete Research*, 41(148), pp. 137–143.

Dhir, R. K., Jones, M. R. and Mccarthy, M. J. (1992) 'Pulverized4 uel ash concrete: carbonation-induced reinforcement corrosion rates', *Proceedings of the Institution of Civil Engineers, Structures & Buildings*, 94(3), pp. 335–342.

Diamond, S. (1981) 'Effects of Two Danish Fly ashes on Alkali Content of Pore Solutions of Cement-Fly ash Pastes', *Cement and Concrete Research*, 11(c), pp. 383–394.

Federation International du Béton (fib Bulletin) (2000) *Bond of reinforcement in concrete: State-of-art Report, Bulletin no. 10*. Second edi. Swizerland: International Federation for Structural Concrete (fib). Available at: http://books.google.co.za/books?id=jLrMEPdSz2QC.

Fitzpatrick, M. (2014) 'The new 400ppm World: CO2 Measurement at Mauna Loa Continue to climb', *Union of Concerned Scientist*.

de Fontenay, C. . (1985) 'A study of the effect of concrete admixtures, concrete composition and exposure conditions on carbonation', in *First International Conference on Deterioration and Repair of reinforced concrete structures*. Bahrain.

Galan, I., Andrade, C., Pedro, M. and Miguela, S. (2010) 'Sequestration of CO2 by Concrete Carbonation', *Environmental Science Technology*, 44(8), pp. 3181–3186.

Gallucci, E. and Scrivener, K. (2007) 'Crystallisation of calcium hydroxide in early age model and ordinary cementitious systems', *Cement and Concrete Research*, 37(4), pp. 492–501. doi: 10.1016/j.cemconres.2007.01.001.

Garboczi, E. J. (1995) 'Microstructure and transport properties of concrete', in Kropp, J. and Hilsdorf, H. . (eds) *Performance Criteria for Concrete Durability*. London: E & FN SPON, pp. 198–212.

Garboczi, E. J. and Bentz, D. P. (1996) 'The Dilute Limit', in *American Society of Civil Engineers, Proceedings of the Fourth Materials Conference*. Washington, DC,: American Society of Civil Engineers.

Gonzalez, J. ., Feliu, S. and Rodrigues, P. (1996) 'Some questions on the corrosion of steel in concrete. Part II: Corrosion mechanism and monitoring, service life prediction and protection methods', *Materials and Structures*, 29(2), pp. 97–104.

Gowers, K. R., Millard, S. G., Gill, J. S. and Gill, R. P. (1994) 'Programmable Linear Polarisation Meter for Determination of Corrosion Rate of Reinforcement in Concrete Structures', *British Corrosion Journal*, 29(1).

Guangling, S. and Ahmad, S. (1998) *Corrosion of steel in concrete, causes, detection and prediction: state-of the-art review: Report 4*. Vermont South, Australia.

Gulikers, J. (1999) 'Numerical Simulation of Corrosion Rate Determination by Linear Polarisation', in Andrade, C., Alonso, C., Fullea, J., Polimon, J., and Rodriguez, J. (eds) *Measurement and Interpretation of the On-site Corrosion Rate*. Madrid, Spain: RILEM Publications SARL, pp. 145–156.

Hakkinen, T. (1993) 'The influence of slag content on the microstructure, permeability and mechanical properties of concrete, part 2, Technical and theoretical examinations', *Cement and Concrete Composites*, 23(Type 2), pp. 518–

530.

Haque, M. N. and Al-Khaiat, H. (1997) ‘Carbonation of concrete structures in hot dry coastal regions’, *Cement and Concrete Composites*, 19(2), pp. 123–129. doi: 10.1016/S0958-9465(96)00047-9.

Haque, M. N., Al-Khaiat, H. and John, B. (2007) ‘Climatic zones-A prelude to designing durable concrete structures in the Arabian Gulf’, *Building and Environment*, 42(6), pp. 2410–2416. doi: 10.1016/j.buildenv.2006.04.006.

Heiyantuduwa, R. and Alexander, M. G. (2009) ‘Studies on prediction models for concrete durability’, in Alexander, M. G. (ed.) *Concrete Repair, Rehabilitation and Retrofitting II*. Taylor & Francis Group, London, pp. 303–310.

Hills, T. P., Gordon, F., Florin, N. H. and Fennell, P. S. (2015) ‘Statistical analysis of the carbonation rate of concrete’, *Cement and Concrete Research*, 72, pp. 98–107. doi: 10.1016/j.cemconres.2015.02.007.

Hornbostel, K., Larsen, C. K. and Geiker, M. R. (2013) ‘Relationship between concrete resistivity and corrosion rate – A literature review’, *Cement and Concrete Composites*. Elsevier Ltd, 39, pp. 60–72. doi: 10.1016/j.cemconcomp.2013.03.019.

Houst, Y. F. and Wittmann, F. H. (1994) ‘Influence of porosity and water content on the diffusivity of CO2 and O2 through hydrated cement paste’, *Cement and Concrete Research*, 24(6), pp. 1165–1176. doi: 10.1016/0008-8846(94)90040-X.

Igarashi, S. and Watanabe, A. (2006) ‘Effects of pozzolanic reaction on the evolution of coarse capillary pore structure and phase constitution in cement pastes with mineral admixtures’, in Kovler, K. (ed.) *ConcreteLife’06 - International RILEM-JCI Seminar on Concrete Durability and Service Life Planning: Curing, Crack Control, Performance in Harsh Environments*. RILEM Publications SARL, pp. 83–93.

Ikotun, J. O. (2010) *Benefits of utilising oil drill cuttings as filler replacement in cement and ternary cement concretes*. MSC Thesis, University of Dundee, Dundee, UK.

Ikotun, J. O. and Ekolu, S. O. (2012) ‘Essential parameters for strength-based service life modeling of reinforced concrete structures - a review’, in Alexander, M. G., Beushausen, H. D., Dehn, F., and Moyo, P. (eds) *Proceedings of 3rd Intl. Conf. on Concrete Repair, Rehabilitation and Retrofitting (ICCRRR)*. Cape Town, South Africa: CRC Press: Taylor & Francis Group, pp. 433–438.

Jaffer, S. J. and Hansson, C. M. (2009) ‘Chloride-induced corrosion products of steel in cracked-concrete subjected to different loading conditions’, *Cement and Concrete Research*. Elsevier Ltd, 39(2), pp. 116–125. doi:

10.1016/j.cemconres.2008.11.001.

Jamali, A., Angst, U., Adey, B. and Elsener, B. (2013) 'Modeling of corrosion-induced concrete cover cracking: A critical analysis', *Construction and Building Materials*, 42, pp. 225–237. doi: 10.1016/j.conbuildmat.2013.01.019.

Johnson, J. B. (2010) *Bond Strength of Corrosion Resistant Steel Reinforcement in Concrete*. MSC Thesis, University of Virginia, Virginia, US.

Jones, M. ., Dhir, R. ., Newlands, M. . and Abbas, A. M. . (2000) 'A study of the CEN test method for measurement of the carbonation depth of hardened concrete', *Materials and Structures*, 33(March), pp. 135–142.

Kayali, O. and Zhu, B. (2005) 'Corrosion performance of medium-strength and silica fume high-strength reinforced concrete in a chloride solution', *Cement and Concrete Composites*, 27(1), pp. 117–124. doi: 10.1016/j.cemconcomp.2004.02.040.

Khunthongkeaw, J., Tangtermsirikul, S. and Leelawat, T. (2006) 'A study on carbonation depth prediction for fly ash concrete', *Construction and Building Materials*, 20(9), pp. 744–753. doi: 10.1016/j.conbuildmat.2005.01.052.

King, D. (2012) 'The Effect of Silica Fume on the Properties of Concrete as Defined in Concrete Society Report 74, Cementitious Materials', in *37th Conference on Our World In Concrete & Structures: 29 - 31 August 2012*. Singapore.

Kokubu, M. and Nagatakis, S. (1989) 'Carbonation of concrete with fly ash and corrosion of reinforcement in 20 years tests', *ACI Materials Journal SP-114-14*, pp. 315–329.

Kropp, J. and Alexander, M. (2007) *Transport mechanisms and reference tests, Non-Destructive Evaluation of the Penetrability and Thickness of the Concrete Cover - State-of-the-Art Report of RILEM Technical Committee 189-NEC*. Edited by R. Torrent and L. Fernandez Luco. RILEM Publications SARL.

Kulakowski, M. P., Pereira, F. M., Dal, D. C. C. and Molin, D. C. C. D. (2009) 'Carbonation-induced reinforcement corrosion in silica fume concrete', *Construction and Building Materials*. Elsevier Ltd, 23(3), pp. 1189–1195. doi: 10.1016/j.conbuildmat.2008.08.005.

Liang, M. and Lin, S. (2003) 'Mathematical modeling and applications for concrete carbonation', *Journal of Marine Science and Technology*, 11(1), p. 2003.

Litvan, G. . and Meyer, A. (1986) 'Carbonation of granulated blast furnace slag cement concrete during twenty years of field exposure', in *2nd International Conference on fly ash, silica fume, slag and natural pozzolans in concrete ACI SP-91*. Madrid, Spain, pp. 1445–1462.

Liu, Y. (1996) *Modeling the time-to-corosion cracking of the cover concrete in chloride contaminated concrete structures*. PhD thesis, Virginia Polytechnic Institute and State University, Blacksburg, Virginia, US.

Liu, Y. P. and Weyers, R. E. (1998) 'Modeling the time to corrosion cracking in chloride contaminated reinforced concrete structures', *ACI Materials Journal*, 95(6), pp. 675–681.

Loo, Y. H., Chin, M. S., Tam, C. T. and Ong, K. C. G. (1994) 'A carbonation prediction model for accelerated carbonation testing of concrete', *Magazine of Concrete Research*, (168), pp. 191–200.

Lu, C. H., Liu, R. G. and Jin, W. L. (2010) 'A model for predicting time to corrosion-induced cover cracking in reinforced concrete structures', in Ohga, H. (ed.) *Fracture Mechanics of Concrete and Concrete Structures - Assessment, Durability, Monitoring and Retrofitting of Concrete Structures*. Seoul: 2010 Korea Concrete Institute, pp. 967–975.

Lu, C., Jin, W. and Liu, R. (2011) 'Reinforcement corrosion-induced cover cracking and its time prediction for reinforced concrete structures', *Corrosion Science*. Elsevier Ltd, 53(4), pp. 1337–1347. doi: 10.1016/j.corsci.2010.12.026.

El Maaddawy, T. A. and Soudki, K. A. (2003) 'Effectiveness of Impressed Current Technique to Simulate Corrosion of Steel Reinforcement in Concrete', *Journal of Materials in Civil Engineering*, 15(1), pp. 41–47. doi: 10.1061/(ASCE)0899-1561(2003)15:1(41).

El Maaddawy, T. and Soudki, K. (2007) 'A model for prediction of time from corrosion initiation to corrosion cracking', *Cement and Concrete Composites*, 29(3), pp. 168–175. doi: 10.1016/j.cemconcomp.2006.11.004.

Matsuzawa, K., Kitsutaka, Y. and Tsukagoshi, M. (2010) 'Effect of humidity on rate of carbonation of concrete exposed to high-temperature environment', in *International symposium on the ageing management & maintenance of nuclear power plants*, pp. 109–114.

Mehta, P. . (1993) *Concrete Structure Properties and Materials*. Englewood Cliffs: Prentice-Hall, Inc., Englewood Cliffs, N.J. 07632.

Mehta, P. K. (1987) 'Pozzolanic and Cementitious By-Products as Mineral Admixtures for Concrete - A critical Review', *Proceedings of the First ACI/CANMET. International Conference on the Use of Fly Ash, Silica Fume, Slag, and Other Mineral By-Products in Concrete, Montebello, Canada,Vol. 1, ACI SP-79*, 1, pp. 1–46.

Mikhailov, A. ., Strekalov, P. . and Panchenko, Y. . (2008) 'Atmosheric corrosion

of metals in regios of cold and extremely cold climate (a review)', *Protection of Metals*, 44(7), pp. 1–16.

Mindess, S., Young, J. ., Sidney, M. and Young, F. (1981) *Concrete*. Englewood cliffs NJ: Prentice-Hall, Inc.

Molina, L. (1992) 'On predicting the influence of curing conditions on the degree of hydration', *Stockholm□: Cement och Betong Institututet*. CBI-rapporter, 1992:5.

Montgomery, D. C. and Runger, G. C. (2011) *Applied statistics and probability for Engineers*. 5 edn. Danvers: John Wiley and Sons, Inc.

Morandeau, A., Thiéry, M., Dangla, P., Thi?ry, M. and Dangla, P. (2014) 'Investigation of the carbonation mechanism of CH and C-S-H in terms of kinetics, microstructure changes and moisture properties', *Cement and Concrete Research*. Elsevier Ltd, 56, pp. 153–170. doi: 10.1016/j.cemconres.2013.11.015.

Morandeau, A., Thiéry, M., Dangla, P., Thi?ry, M., Dangla, P., Thiéry, M. and Dangla, P. (2015) 'Impact of accelerated carbonation on OPC cement paste blended with fly ash', *Cement and Concrete Research*. Elsevier Ltd, 67, pp. 226–236. doi: 10.1016/j.cemconres.2014.10.003.

Morinaga, S. (1989) *Prediction of service lives of reinforced concrete buildings based on rate of corrosion of reinforcing steel*. Skimiza Corporation, Japan.

Mullard, J. A. and Stewart, M. G. (2009) *Corrosion-induced Cver Cracking of RC Structures: New Experimental Data and Predictive Models*. New South Wales, Australia.

Nagataki, S., Ohga, H. and Kim, E. K. (1986) 'Effect of Curing Conditions on the Carbonation of Concrete with Fly Ash and the Corrosion of Reinforcement in Long-Term Tests', *ACI Special Publication*, 91, pp. 521–540. doi: 10.14359/10086.

Naik, T. . (1997) 'Concrete Durability as Influenced by Density and / or Porosity', in *Cement and Concrete Institute of Mexico Symposium "World of Concrete*. Guadalajara, Mexico, p. 13.

Nasser, A., Clément, A., Laurens, S. and Castel, A. (2010) 'Influence of steel-concrete interface condition on galvanic corrosion currents in carbonated concrete', *Corrosion Science*. Elsevier Ltd, 52(9), pp. 2878–2890. doi: 10.1016/j.corsci.2010.04.037.

Neville, A. . (2011) *Properties of concrete*. 4th edn. Essex, England: Pearson Prentice Hall.

Newhouse, C. and Weyers, R. (1996) 'Modelling the measured time to corrosion cracking-techniques to assess the corrosion activity of steel reinforced concrete

structures', *ASTM STP 1276*, pp. 3–22.

Nischer, P. (1984) 'Influence of concrete quality and environment on carbonation', in *RILEM Seminar*. Hannover, pp. 231–238.

Otieno, M. (2008) *Corrosion propagation in cracked and uncracked concrete*. MSc thesis, Unviversity of Cape Town, Cape Town, South Africa.

Otieno, M., Alexander, M. G. and Beushausen, H. (2010) *Transport mechanisms in concrete - Corrosion of steel in concrete (initiation, propagation and factors affecting - Assessment of Corrosion*. Cape Town.

Otieno, M. B. (2014) *The Development of Empirical Chloride-induced Corrosion Rate Prediction Models for Cracked and Uncracked Steel Reinforced Concrete Structures in the Marine Tidal Zone*. PhD Thesis, University of Cape Town.

Otieno, M. B., Beushausen, H. D. and Alexander, M. G. (2011) 'Modelling corrosion propagation in reinforced concrete structures – A critical review', *Cement and Concrete Composites*. Elsevier Ltd, 33(2), pp. 240–245. doi: 10.1016/j.cemconcomp.2010.11.002.

Owens, G. (ed.) (2009) *Fulton's concrete technology*. Ninth. Midrand: Cement & Concrete Institute, South Africa.

Panasenko, S. A., Makarchenko, N. ., Oleshchenko, N. ., Bitchenko, O. ., Grishchuk, V. . and Danilov, F. . (1988) 'A pulsed coulostatic method of evaluating the protective properties and corrosion resistance of coatings', *Fiziko-Khimicheskaya Mekhanika Materialov*, 3, pp. 25–27.

Pantazopoulou, S. . and Papoulia, K. D. (2001) 'Modeling Cover-cracking due to Reinforcement Corrosion in RC Structures', *Journal of Engineering Mechanics*, 127(April), pp. 342–351.

Papadakis, V. G., Fardis, M. N. N. and Vayenas, C. G. G. (1992) 'Effect of composition , environmental factors and cement-lime mortar coating on concrete carbonation', *Materials and Structures*, 25(5), pp. 293–304. doi: 10.1007/BF02472670.

Papadakis, V. G. and Vayenas, C. G. (1991) 'Experimental investigation and mathematical modeling of the concrete carbonation problem', *Chemical Engineering Science*, 46(5/6), pp. 1333–1337.

Papavinasam, S. (2008) 'Evolution of External Pipeline Coatings for Corrosion Protection – A Review', *CORROSION REVIEWS*, 26(5–6).

Park, R. and Pauay, T. (1975) *Reinforced concrete structures*. NY, USA: John Wiley & Sons, Inc.

Parrott, L. J. (1987) *A Review of Carbonation in Reinforced Concrete*. Cement & Concrete Association of Great Britain.

Parrott, L. J. (1994) 'A study of carbonation-induced corrosion', *Magazine of Concrete Research*, 46(166), pp. 23–28. doi: 10.1680/macr.1994.46.166.23.

Patel, R. G., Parrott, L. J., Martin, J. A. and Killoh, D. C. (1985) 'Gradients of microstructure and diffusion properties in cement paste caused by drying', *Cement and Concrete Research*, 15(2), pp. 343–356. doi: 10.1016/0008-8846(85)90046-8.

Peng, L. and Stewart, M. G. (2014) 'Climate change and corrosion damage risks for reinforced concrete infrastructure in China', *Structure and Infrastructure Engineering*. Taylor & Francis, 2479(April), pp. 1–18. doi: 10.1080/15732479.2013.858270.

Perrie, B. (2009) 'Strength of hardened concrete', in Owens, G. (ed.) *Fulton's Concrete Technology*. Ninth. Midrand: Cement & Concrete Institute, South Africa, pp. 97–110.

Pihlajavaara, S. E. (1984) 'SESSION I Some results of the effect of carbonation on the porosity and pore size distribution of cement paste', pp. 521–527.

Polder, R. B. (2001) 'Test methods for on site measurement of resistivity of concrete a RILEM TC-154 technical recommendation', pp. 125–131.

Pommersheim, J. and Clifton, J. (2010) 'Prediction of concrete service-life', *Materials and Construction*, 85(1).

Powers, T. C. (1948) 'A Discussion of cement Hydration in relation to the curing of concrete', in *Proceedings of the Twenty-Seventh Annual Meeting of the Highway Research Board*. Washington, D.C.: Highway Research Board, pp. 178–188.

Proverbio, E. (1999) 'Sensitivity and Reliability of embedded Polarisation Resistance Probes in Concrete Structures: Full scale and Laboratory Experiences', in Andrade, C., Alonso, C., Fullea, J., Polimon, J., and Rodrigues, J. (eds) *Measurement and Interpretation of the On-site Corrosion Rate*. Madrid, Spain: RILEM Publications SARL, pp. 167–175.

Quillin, K. (2001) *Modelling degradation processes affecting concrete*. London, UK: BRE center for concrete construction.

Raphael, M. and Shalon, R. (1964) 'Corrosion of reinforcing steel in hot countries', in *RILEM Bulletin*. RILEM, pp. 29–45.

Rashid, M. H., Khatun, S., Kamal Uddin, S. M. and Nayee, M. A. (2010) 'Effect of Strength and Covering on Concrete Corrosion', *European Journal of Scientific Research.*, 4, pp. 492–499.

Reardon, E. ., James, B. . and Abouchar, J. (1989) ‘High pressure carbonation of cementitious grout’, *Cement and Concrete Research*, 19(c), pp. 385–399.

RILEM 14 (1996) *Durability Design of Concrete Structures*. Edited by E. V. A. Sarja. London: E & FN SPON.

Rodriguez, J. and Andrade, C. (1990) ‘Load-bearing capacity loss in corroding structures’, in *ACI Convention*. Toronto.

Rodriguez, J., Ortega, L., Casal, J. and Diez, J. (1996) ‘Corrosion of reinforcement and service life of concrete structures’, in Sjostrom, C. (ed.) *Durability of Building Materials and Components 7*. London, UK: E & FN SPON, pp. 117–126.

Rostam, S. (2000) ‘Service Life Design of Concrete Structures - an Experience-Based Discipline Becoming Scientific’, *Structural Engineering and Materials - Centenary Celebration*.

Saetta, A. V. and Vitaliani, R. V. (2004) ‘Experimental investigation and numerical modeling of carbonation process in reinforced concrete structures Part I: Theoretical formulation’, *Cement and Concrete Research*, 34, pp. 571–579. doi: 10.1016/j.cemconres.2003.09.009.

Sagues, A. A., Moreno, E. I., Morris, W. and Andrade, C. (1997) *Carbonation in concrete and effect on steel corrosion*. Tampa.

Salvoldi, B. G. (2010) *Modeling the carbonation of concrete using early age oxygen permeability index tests*. University of Cape Town.

Salvoldi, B. G., Beushausen, H. and Alexander, M. G. (2015) ‘Oxygen permeability of concrete and its relation to carbonation’, *Construction and Building Materials*. Elsevier Ltd, 85, pp. 30–37. doi: 10.1016/j.conbuildmat.2015.02.019.

Sanjuan, M. A., Andrade, Ã. C. and Cheyrezy, M. (2003) ‘Concrete carbonation tests in natural and accelerated conditions’, *Advances in Cement Research*, (4), pp. 171–180.

SANS 10100:1-2000 (2000) *The structural use of concrete Part 1: Design*. Pretorial: South African Beureau of Standards.

SANS 10100:2-2000 (1992) *South African Standard:The structural use of concrete Part 2: Materials and execution of work*. Pretoria.

SANS 1083 (2006) *South African Standard: Aggregates from natural sources-Aggregates for concrete*.

SANS 3001-CO3-2 (2015) *South African Natioanl Standard Civil engineering test methods Part CO3-2□: Concrete durability index testing — Oxygen permeability test*. Pretoria.

SANS 50197-2□: 2000 (2000) *South African National Standard Cement Part 2□: Conformity evaluation*.

SANS 5861-1□: 2006 (2006) *South African National Standard Concrete tests Part 1□: Mixing fresh concrete in the laboratory*.

SANS 5863-2 (1994) *Concrete testing-Compressive strength of hardened concrete*.

SANS 6253□: 2006 (2006) *South African National Standard Concrete tests — Tensile splitting strength of concrete*.

SANS 920: 2011 (2011) *South African National Standard: Steel bars for concrete reinforcement*.

Schiessl, P. (1988) *Corrosion of Steel in Concrete, Report of Technical Committee 60-CSC*. Chapman and Hall, London, New York, 1988.

Schubert, P. (1987) 'Carbonation behaviour of mortals and concretes made with fly ash', in *Kathrine and Bryant Mather International conference on Concrete Durability*. USA: ACI SP-100, pp. 1945–1962.

Scrivener, K. L. and Nernati, K. M. (1996) 'The percolation of Pore space in cement paste/aggregate zone of concrete', *Cement and Concrete Research*, 26(1), pp. 35–40.

Shanmugavadivu, P. ., Kumar, P., Sarathivelan and Karthikeyan (2014) 'Corrosion behavior of concrete with partial replacement of cement with Rice Husk', *Advances in Materials and Corrosion*, 3, pp. 1–4.

Shetty, A. (2011) 'Effect of Loss of Bond Strength Due to Corrosion in Reinforced Concrete Members', *International Journal of Earth Sciences & Engineering*, 4(6), pp. 879–884.

Shetty, A., Venkataramana, K., Gogoi, I. and Praveen, B. B. (2012) 'Performance Enhancement of TMT Rebar in Accelerated Corrosion', *Journal of Engineering Research*, 2(1), pp. 14–17. doi: 10.5923/j.jce.20120201.03.

Silva, A., Neves, R. and de Brito, J. (2014) 'Statistical modelling of carbonation in reinforced concrete', *Cement and Concrete Composites*, 50, pp. 73–81. doi: 10.1016/j.cemconcomp.2013.12.001.

Sisomphon, K. and Franke, L. (2007) 'Carbonation rates of concretes containing high volume of pozzolanic materials', *Cement and Concrete Research*, 37(12), pp. 1647–1653. doi: 10.1016/j.cemconres.2007.08.014.

Sohail, M. G. (2013) *Corrosion of Steel in Concrete: Development of an Accelerated Test by Carbonation and Galvanic Coupling*. PhD Thesis, Universite de Toulouse.

Song, H. and Saraswathy, V. (2007) ‘Corrosion Monitoring of Reinforced Concrete Structures - A Review’, *International Journal of Electrochemical Science*, 2, pp. 1–28.

Song, H. W. and Kwon, S. J. (2007) ‘Permeability characteristics of carbonated concrete considering capillary pore structure’, *Cement and Concrete Research*, 37, pp. 909–915. doi: 10.1016/j.cemconres.2007.03.011.

Soroka, I. (2003) *Concrete in hot climate: modern concrete technology*. CRC Press.

South Africa Department of National Treasury (2010) *Reducing Greenhouse Gas Emissions: The Carbon Tax Option, Reducing Greenhouse Gas Emissions and Facilitating The Transition To A Green Economy Pretoria: Department of National Treasury, South Africaa*. Available at: http://www.treasury.gov.za/public comments/Discussion Paper Carbon Taxes 81210.pd.

Stewart, M. G., Wang, X. and Nguyen, M. N. (2011) ‘Climate change impact and risks of concrete infrastructure deterioration’, *Engineering Structures*. Elsevier Ltd, 33(4), pp. 1326–1337. doi: 10.1016/j.engstruct.2011.01.010.

Suzuki, M., Kanno, K.-I. and Sato, Y. (1980) ‘An application of the coulostatic method to corrosion rate measurements’, *Wertstoffe und korrosion*, 31, pp. 364–370.

Terence, C. H. (2005) *Silica Fume User’s Manual*. FHWA-IF-05-016. Lovettsville, VA.

Thiery, M., Dangla, P., Villain, G., Platret, G. and Central, L. (2005) ‘A prediction model for concrete carbonation based on coupled CO 2 -H 2 O-ions transfers and chemical reactions’, in *10 DBMC International Conference On Durability of Building Materials and Components*. LYON, FRANCE.

Thiéry, M., Faure, P. and Bouteloup, J. (2011) ‘Effect of Carbonation on the Microstructure and Moisture Properties of Cement - Based Materials’, in *International conference on Durability of Building Material and Components*. Porto-Portugal, pp. 1–8.

Torrent, R., D’Andrea, R., Goncalves, A., Jacobs, F., Imamoto, K., Kanellopoulos, A., Khrapko, M., Monteiro, A. V. and Nanukuttan, S. (2016) ‘Prescriptive Durability Specifications’, in Beushausen, H. and Luco, L. F. (eds) *Performance-Based Specifications and Control of Concrete Durability State-of-the-Art Report RILEM TC230-PSC*. London, UK: RILEM Publications Springer, pp. 19–49.

Torres-Acosta, A. A. and Sagues, A. . (2004) ‘Concrete Cracking by Localized Steel Corrosion - Geometric Effect’, *ACI Materials Journal*, 101(6), pp. 501–507.

Turk, K., Karatas, M. and Gonen, T. (2012) ‘Effect of Fly Ash and Silica Fume on

compressive strength, sorptivity and carbonation of SCC', *KSCE Journal of Civil Engineering*, 17(1), pp. 202–209. doi: 10.1007/s12205-013-1680-3.

Tuutti, K. (1982) *Corrosion of Steel in Concrete*. Stockholm: Swedish Cement and Concrete Research Institute S-100 44 Stocholm.

Uhlig, H. and Revie, R. (1985) *Corrosion and corrosion control*. Third. J Wiley & Sons.

Vennesland, Ø., Raupach, M. and Andrade, C. (2007) 'Recommendation of Rilem TC 154-EMC: "Electrochemical techniques for measuring corrosion in concrete"—measurements with embedded probes', *Materials and Structures*, 40(8), pp. 745–758. doi: 10.1617/s11527-006-9219-4.

Vesikari, E. (1988) *Service life of concrete structures with regard to corrosion of reinforcement*. Espoo, Finland.

Villain, G., Thiery, M. and Platret, G. (2007) 'Measurement methods of carbonation profiles in concrete: Thermogravimetry, chemical analysis and gammadensimetry', *Cement and Concrete Research*, 37(8), pp. 1182–1192. doi: 10.1016/j.cemconres.2007.04.015.

Visser, J. H. M. (2012) 'Accelerated carbonation testing of mortar with supplementary cementing materials - Limitation of the acceleration due to drying', *HERON*, 57(3).

Wierig, H. (1984) 'Longtime studies on the carbonation of concrete under normal outdoor exposuretle', in *Proceedings of the RILEM seminar on the durability of concrete structures*. Hannover, Germany: RILEM.

Wong, H. S., Buenfeld, N. R. and Head, M. K. (2006) 'Estimating transport properties of mortars using image analysis on backscattered electron images', *Cement and Concrete Research*, 36(8), pp. 1556–1566. doi: 10.1016/j.cemconres.2006.05.002.

Zhou, K. (2005) *Models for Predicting Corrosion-induced Cracking, Spalling/Delamination of Rehabilitated RC Bridge Decks*. University of Ottawa.

Zhou, Y., Gencturk, B., Willam, K. and Attar, A. (2014) 'Carbonation-Induced and Chloride-Induced Corrosion in Reinforced Concrete Structures', *Journal of Materials in Civil Engineering.*, 10.1061/(A. doi: 10.1061/(ASCE)MT.1943-5533.0001209.

APPENDICES

Appendix A: Experimental data and preliminary results

Table A1: Coarse aggregate sieve analysis result

Sieve size	Mass retained (g)	Mass Passing (g)	Cumulative % mass passing	Cumulative % mass retained
26.5 mm	0.0	6000.9	100.0	0.0
19 mm	1206.4	4794.5	79.9	20.1
13.2 mm	3795.3	999.2	16.6	83.4
9.5 mm	850.0	149.2	2.5	97.5
Pan	149.2			
Sample size	6000.9 g			

Coarse aggregate fineness modulus = 201/100 = 2.01
Nominal and maximum aggregate size = 19 mm

Table A2: Sand aggregate sieve analysis results

Sieve size	Mass retained (g)	Mass Passing (g)	Cumulative % mass passing	Cumulative % mass retained
4750 µm	56.8	1762.7	96.9	3.1
2360 µm	285.4	1477.3	81.2	18.8
1180 µm	326.8	1150.5	63.2	36.8
600 µm	450.1	700.4	38.5	61.5
300 µm	384.5	315.9	17.4	82.6
150 µm	229.2	86.7	4.8	95.2
75 µm	71.3	15.4	0.8	99.2
Pan	15.4			
Sample size	1819.5 g			

Sand aggregate fineness modulus = 298/100 = 2.98
Nominal sand aggregate size = 2.36 mm

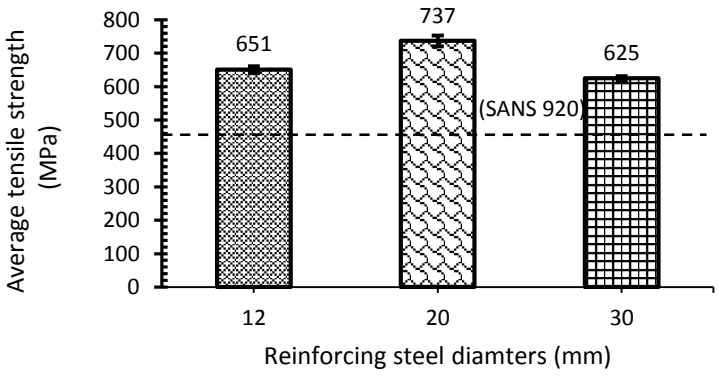

Figure A1: Average tensile strength of the reinforcing steel bars

Table A3: Compressive strength of the concretes

Concrete label	w/b	Compressive Strength					
		7 days moist cured			28 days moist cured		
		Mean (MPa)	Standard Deviation (MPa)	Coefficient of Variation (%)	Mean (MPa)	Standard Deviation (MPa)	Coefficient of Variation (%)
PC	0.95	18.5	1.4	7.4	22.6	3.5	15.4
	0.60	36.8	1.9	5.2	48.7	3.6	7.3
	0.40	59.6	2.4	4.1	70.6	1.4	2.0
PC-FA	0.95	15.9	2.2	15.1	23.1	1.1	4.5
	0.60	30.7	6.6	21.5	51.9	2.2	4.3
	0.40	45.5	7.2	15.5	72.2	4.7	6.5
PC-BS	0.95	9.7	3.1	32.3	14.4	2.5	17.1
	0.60	18.7	1.9	10.4	33.4	2.7	8.1
	0.40	51.6	3.0	5.9	75.8	7.8	7.2
PC-SF	0.95	18.2	4.4	24.2	24.2	0.5	1.9
	0.60	33.6	4.2	12.9	54.6	1.6	2.9
	0.40	67.0	0.3	0.5	87.7	4.9	5.6
PC-SF-BS	0.95	19.3	4.1	21.0	24.5	7.0	22.3
	0.60	25.1	6.9	27.4	49.1	2.0	4.6
	0.40	52.3	5.3	10.1	76.2	1.0	1.3

Table A4: Split tensile strength of the concretes

Concrete label	w/b ratio	Split tensile strength		
		Mean (MPa)	Standard Deviation (MPa)	Coefficient of Variation (%)
PC	0.95	2.1	0.3	13.2
	0.60	4.9	0.2	4.9
	0.40	7.5	0.4	5.4
PC-FA	0.95	2.0	0.3	13.3
	0.60	4.5	0.5	10.0
	0.40	8.1	1.4	17.5
PC-BS	0.95	0.6	0.3	45.4
	0.60	3.5	0.5	13.4
	0.40	8.3	1.0	12.4
PC-SF	0.95	2.9	0.3	11.7
	0.60	4.9	0.3	6.7
	0.40	9.0	1.0	10.6
PC-SF-BS	0.95	2.4	0.3	12.3
	0.60	4.1	0.4	8.9
	0.40	8.1	0.2	2.0

Appendix B: Experimental results: Durability index (OPI and WSI)

Table B1: 28-day coefficient of permeability (*k*) and oxygen permeability index (OPI) results

Concrete label	w/b	Coefficient of permeability (*k*)		Oxygen permeability index, OPI -Log k (m/s)
		Average *k* x 10^{-10} (m/s)	COV (%)	
PC	0.95	5.87	57.6	9.23
	0.60	1.99	90.9	9.70
	0.40	0.76	66.5	10.12
FA	0.95	4.86	24.7	9.31
	0.60	1.86	31.9	9.73
	0.40	0.39	92.3	10.41
BS	0.95	9.15	25.9	9.04
	0.60	2.50	27.1	9.60
	0.40	0.95	56.5	10.02
SF	0.95	3.40	25.9	9.47
	0.60	1.18	57.9	9.93
	0.40	0.31	87.9	10.52
PC-SF-BS	0.95	4.05	22.5	9.39
	0.60	1.55	39.8	9.81
	0.40	0.41	85.3	10.39

Table B2: Water sorptivity index (WSI) results

Concrete label	w/b	Water sorptivity index (WSI)			
		7 days cured		28 days cured	
		Average WSI ($mm/hr^{0.5}$)	COV (%)	Average WSI ($mm/hr^{0.5}$)	COV (%)
PC	0.95	16.7	15.9	13.1	6.9
	0.60	11.0	5.1	10.6	12.6
	0.40	9.7	9.1	7.9	11.4
PC-FA	0.95	26.9	78.7	10.0	38.9
	0.60	13.0	16.3	9.1	6.1
	0.40	9.1	5.9	6.6	12.3
PC-BS	0.95	19.1	10.4	11.6	10.2
	0.60	12.4	23.8	8.5	8.9
	0.40	9.8	9.9	6.8	3.4
PC-SF	0.95	14.5	16.1	10.3	24.0
	0.60	9.5	11.7	7.6	6.4
	0.40	9.2	4.8	6.0	21.8
PC-SF-BS	0.95	15.6	3.4	10.1	9.9
	0.60	10.5	11.3	9.0	19.6
	0.40	8.9	11.1	7.1	10.2

Appendix C: Experimental results - Carbonation test results

Table C1: Average carbonation depth of the concretes (indoor environment)

Concrete label	w/c	7-day curing				28- day curing			
		Exposure duration (years)				Exposure duration (years)			
		0.5	1.0	1.5	2.0	0.5	1.0	1.5	2.0
		Average depth of carbonation (mm)				Average depth of carbonation (mm)			
PC	0.95	7.0	10.0	15.0	18.0	4.0	8.0	10.0	12.0
	0.60	5.0	7.0	9.0	12.0	3.0	5.0	6.0	8.0
	0.40	0.5	1.0	1.3	1.5	0.1	0.2	0.3	0.3
PC-FA	0.95	9.0	13.0	17.0	20.0	7.0	10.0	14.0	17.0
	0.60	6.0	10.0	12.0	14.0	4.0	7.0	9.0	11.0
	0.40	1.0	2.0	2.5	3.0	0.1	0.2	0.3	0.3
PC-BS	0.95	10.0	17.0	20.0	23.0	8.0	14.0	17.0	21.0
	0.60	7.0	10.0	14.0	17.0	6.0	8.0	10.0	13.0
	0.40	1.5	2.5	3.0	4.0	0.1	0.2	0.3	0.3
PC-SF	0.95	7.0	10.0	11.0	13.0	3.0	4.5	5.0	6.0
	0.60	4.0	5.0	8.0	9.0	1.5	2.5	3.0	3.5
	0.40	0.5	1.0	1.3	1.5	0.1	0.2	0.3	0.3
PC-SF-BS	0.95	8.0	12.0	14.0	15.0	5.0	9.0	11.0	12.0
	0.60	5.0	8.0	9.0	11.0	2.0	4.0	5.0	6.0
	0.40	0.5	1.0	1.3	1.5	0.1	0.2	0.3	0.3

Table C2: Average carbonation depth of the concretes (sheltered environment)

Concrete label	w/c	7-day curing				28-day curing			
		Exposure duration in years				Exposure duration in years			
		0.5	1.0	1.5	2.0	0.5	1.0	1.5	2.0
		Average depth of carbonation (mm)				Average depth of carbonation (mm)			
PC	0.95	5.0	9.0	12.0	14.0	4.0	7.0	9.0	11.0
	0.60	4.0	6.0	9.0	10.0	2.0	4.0	5.0	6.0
	0.40	0.5	1.0	1.3	1.5	0.1	0.2	0.3	0.3
PC-FA	0.95	10.0	15.0	18.0	20.0	6.0	10.0	14.0	15.0
	0.60	6.0	8.0	10.0	12.0	4.0	6.0	8.0	9.0
	0.40	0.5	1.0	1.3	1.5	0.1	0.2	0.3	0.3
PC-BS	0.95	9.0	15.0	18.0	22.0	6.0	10.0	13.0	16.0
	0.60	5.0	9.0	12.0	140	4.0	7.0	9.0	11.0
	0.40	1.0	1.5	2.0	2.0	0.1	0.2	0.3	0.3
PC-SF	0.95	7.0	8.0	11.0	13.0	5.0	7.0	9.0	10.0
	0.60	4.0	6.0	8.0	9.0	3.0	5.0	6.0	8.0
	0.40	0.5	1.0	1.3	1.5	0.1	0.2	0.3	0.3
PC-SF-BS	0.95	7.0	11.0	14.0	15.0	5.0	9.0	10.0	12.0
	0.60	5.0	8.0	9.0	11.0	1.5	5.0	7.0	8.0
	0.40	0.5	1.0	1.3	1.5	0.1	0.2	0.3	0.3

Table C3: Average carbonation depth of the concretes (unsheltered environment)

Concrete label	w/c	7-day curing				28-day curing			
		Exposure duration in years				Exposure duration in years			
		0.5	1.0	1.5	2.0	0.5	1.0	1.5	2.0
		Average depth of carbonation (mm)				Average depth of carbonation (mm)			
PC	0.95	4.0	7.0	10.0	11.0	3.0	6.0	8.0	9.0
	0.60	3.0	5.0	7.0	8.0	2.0	4.0	5.0	6.0
	0.40	0.5	1.0	1.3	1.5	0.1	0.2	0.3	0.3
PC-FA	0.95	7.0	11.0	15.0	18.0	5.0	9.0	11.0	15.0
	0.60	5.0	8.0	9.0	10.0	3.0	4.0	6.0	7.0
	0.40	1.0	1.0	1.3	1.5	0.1	0.2	0.3	0.3
PC-BS	0.95	8.0	12.0	15.0	16.0	7.0	9.0	13.0	15.0
	0.60	6.0	8.0	10.0	12.0	4.0	6.0	8.0	9.0
	0.40	0.5	1.0	1.3	1.5	0.1	0.2	0.3	0.3
PC-SF	0.95	5.0	6.0	8.0	10.0	4	6.0	8.0	8.0
	0.60	3.0	5.0	6.0	7.0	2.5	4.0	6.0	6.5
	0.40	0.5	0.75	1.0	1.02	0.1	0.2	0.3	0.3
PC-SF-BS	0.95	8.0	11.0	13.0	15.0	4.0	8.0	10.0	11.0
	0.60	5.0	7.0	9.0	9.0	3.0	5.0	7.0	7.0
	0.40	0.5	1.0	1.25	1.5	0.1	0.2	0.3	0.3

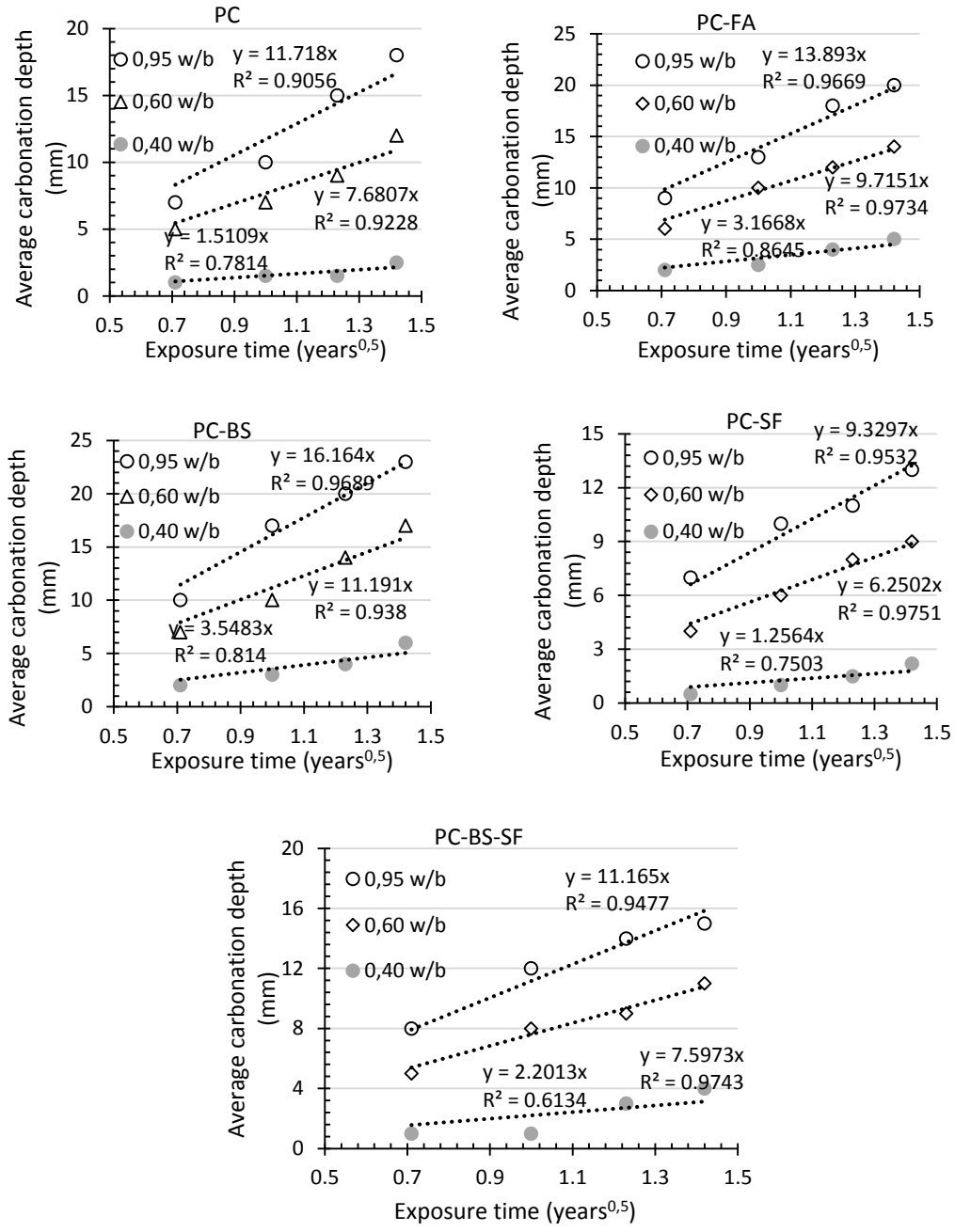

Figure C1 Average carbonation depth versus square root of the exposure time (7-day cured concretes exposed to indoor environment)

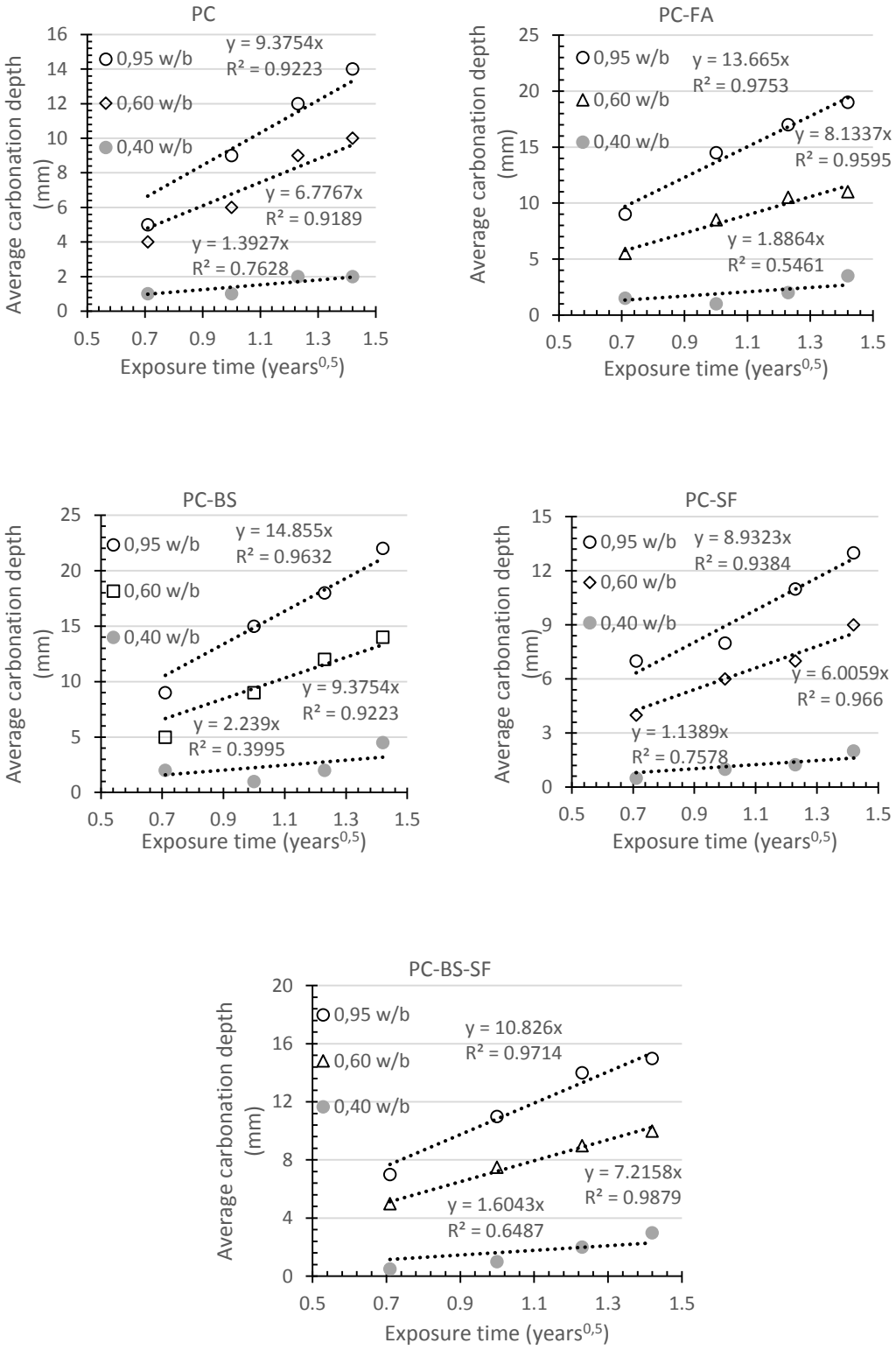

Figure C2: Average carbonation depth versus square root of the exposure time (7-day cured concretes exposed to outdoor sheltered environment)

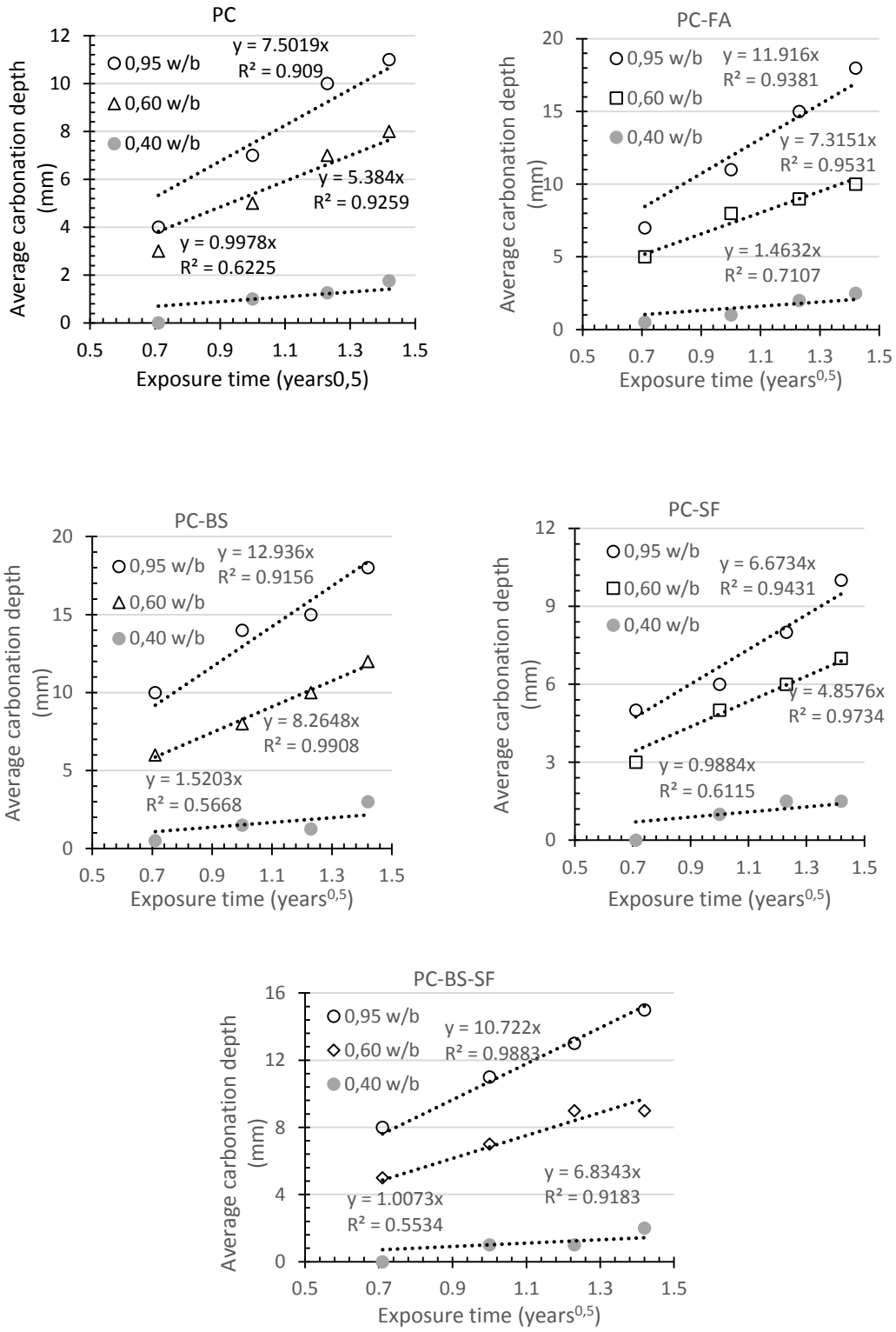

Figure C3: Average carbonation depth versus square root of the exposure time (7-day cured concretes exposed to outdoor unsheltered environment

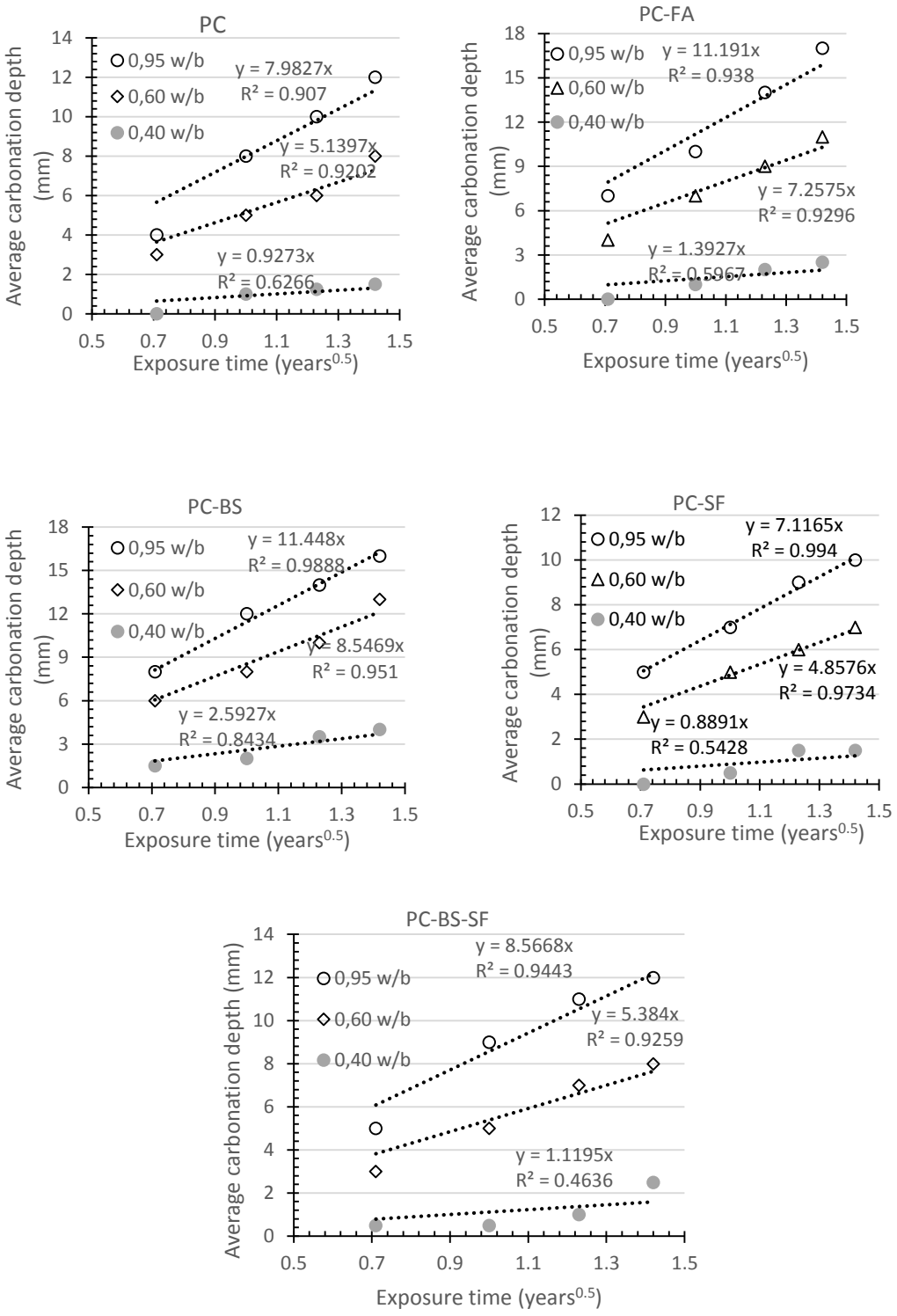

Figure C4: Average carbonation depth versus square root of the exposure time (28-day cured concretes exposed to indoor environment)

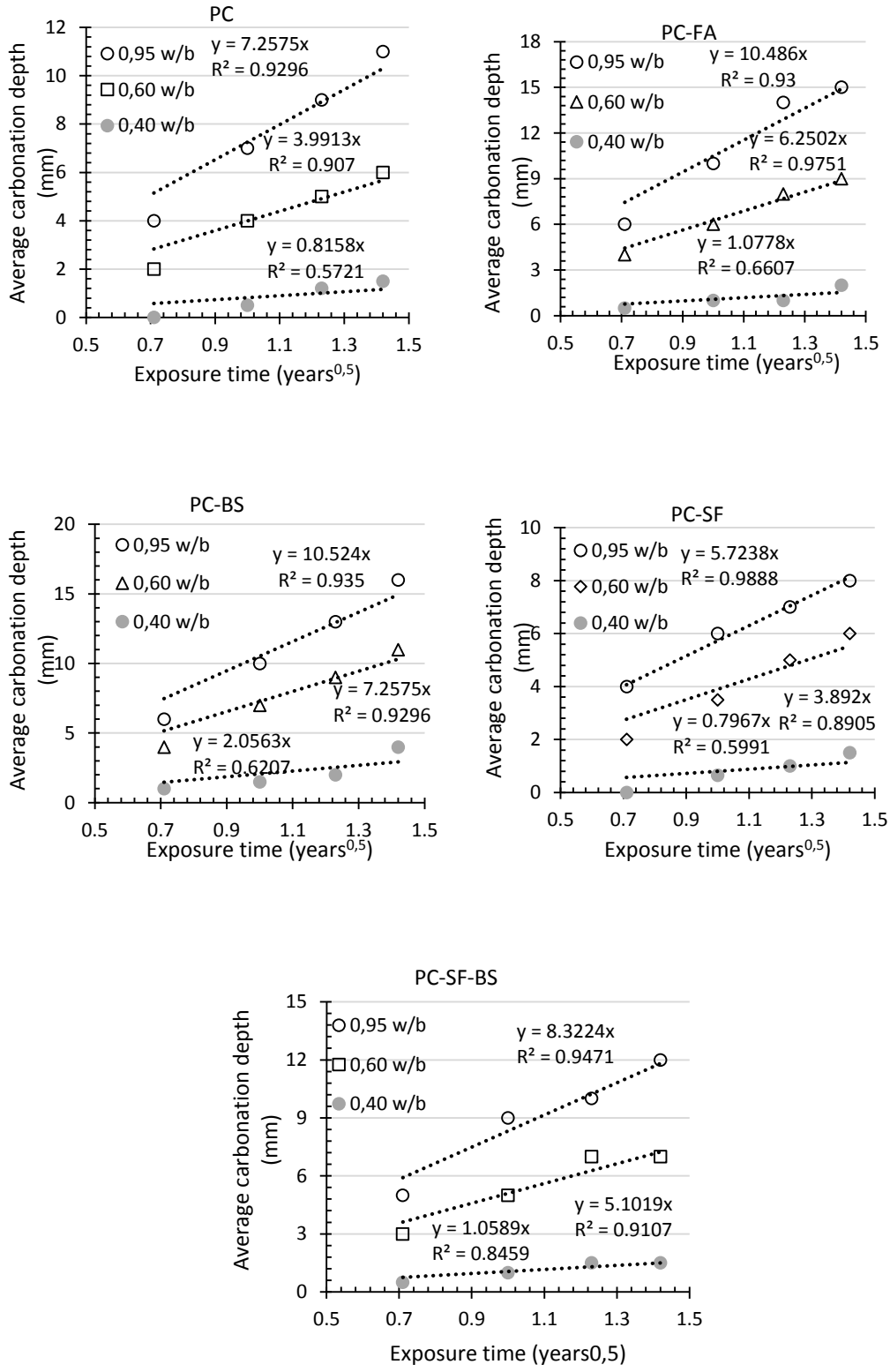

Figure C5: Average carbonation depth versus square root of the exposure time (28-day cured concretes exposed to outdoor sheltered environment)

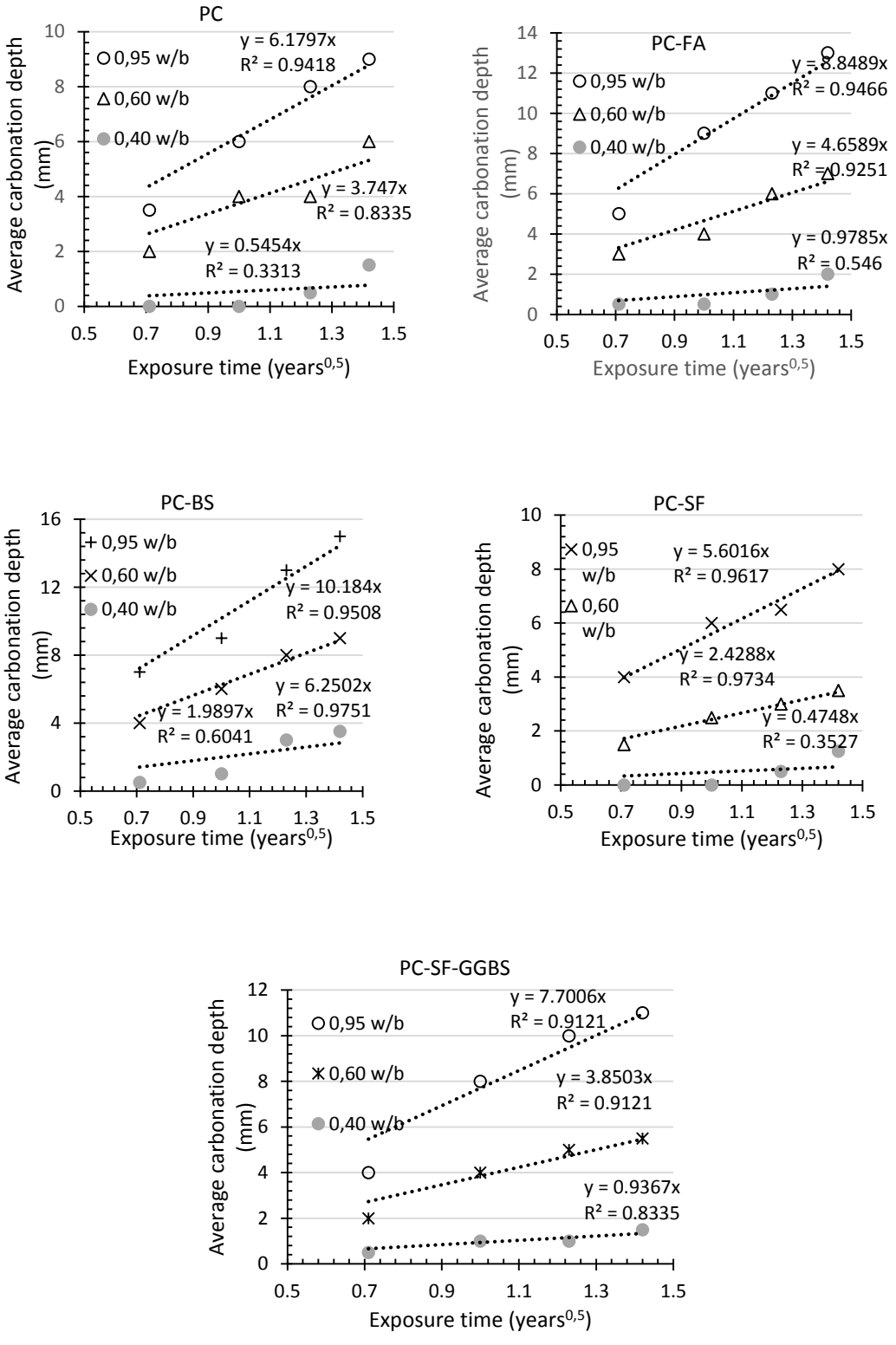

Figure C6: Average carbonation depth versus square root of the exposure time (28-day cured concretes exposed to outdoor unsheltered environment)

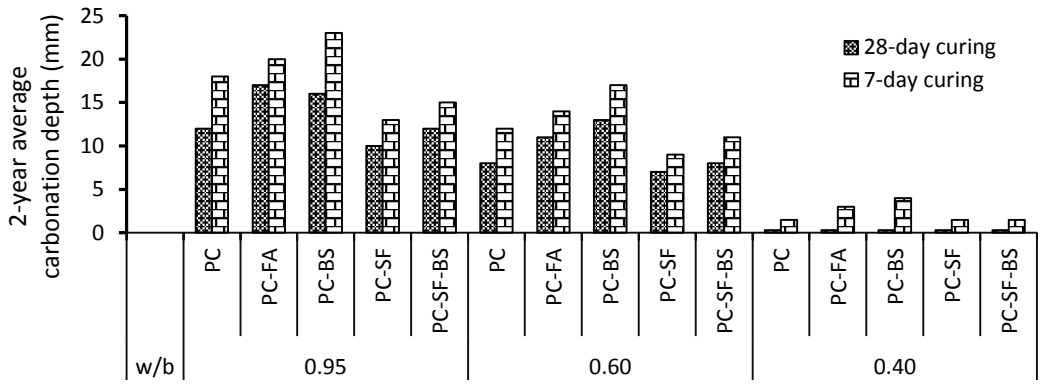

Figure C7: Effect of binder type, curing age and w/b ratio on 2-year indoor concrete carbonation depth

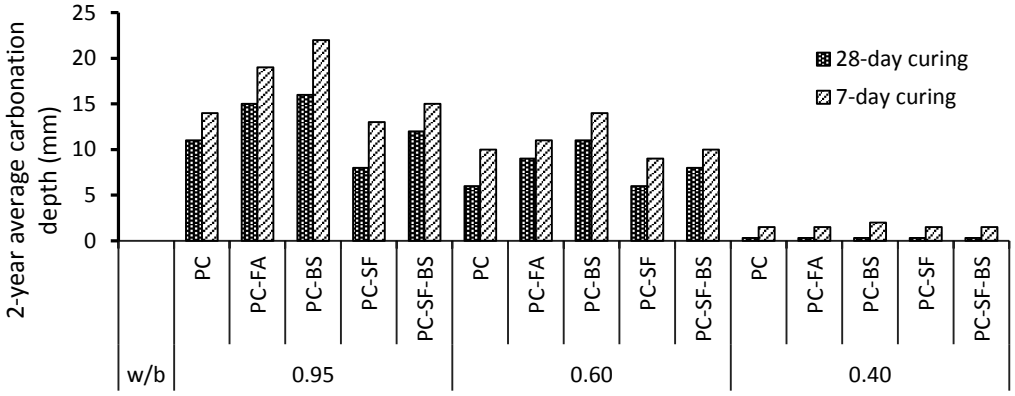

Figure C8: Effect of binder type, curing age and w/b ratio on 2-year outdoor sheltered concrete carbonation depth

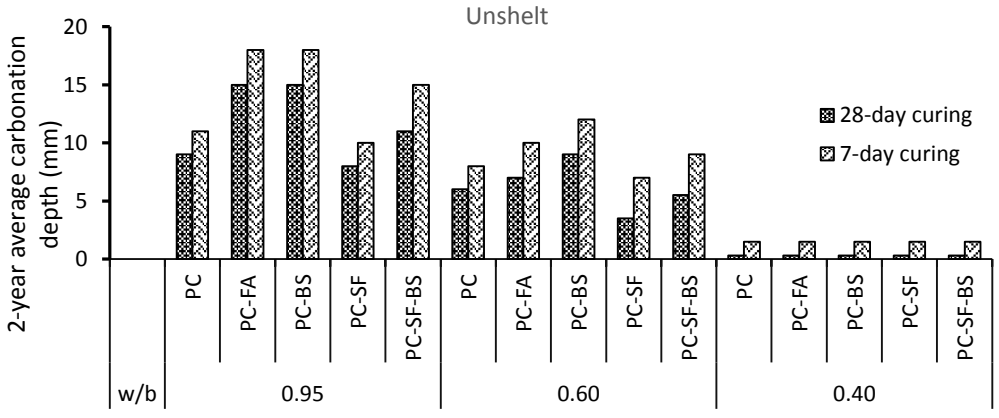

Figure C9: Effect of binder type, curing age and w/b ratio on 2-year outdoor unsheltered concrete carbonation depth

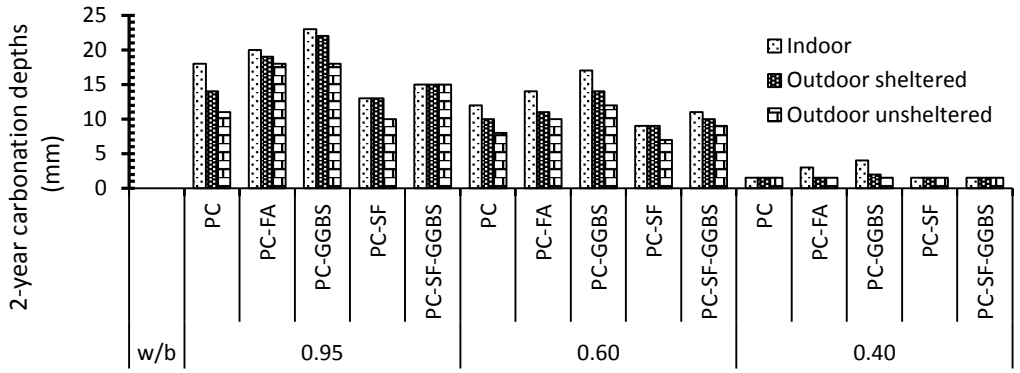

Figure C10: Effect of binder type and exposure type on 2-year carbonation depths of the concretes cured at 7days

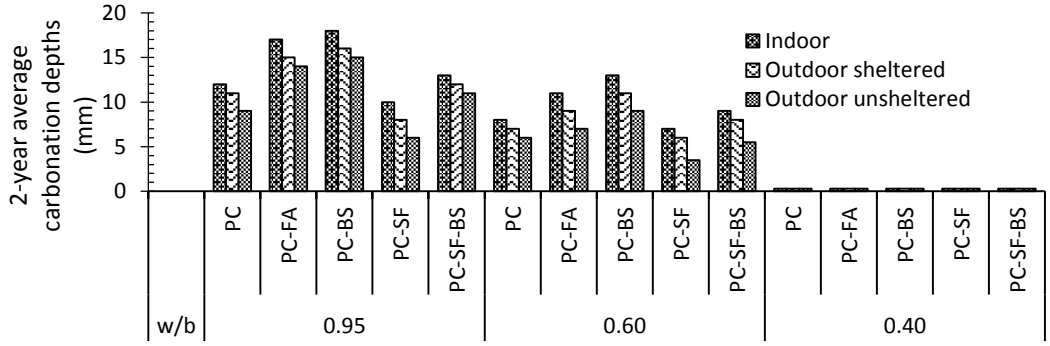

Figure C11: Effect of binder type and exposure type on 2-year carbonation depths of the concretes cured at 28 days

Table C4: Carbonation rate of the concretes

Binder type	w/c	7-day curing			28-day curing		
		Average carbonation rate, K_7 (mm/years$^{0.5}$)			Average carbonation rate, K_{28} (mm/years$^{0.5}$)		
		Indoor	Sheltered	Unsheltered	Indoor	Sheltered	Unsheltered
PC	0.95	11.72	9.38	7.50	7.98	7.26	6.18
	0.60	7.68	6.78	5.38	5.13	3.99	3.75
	0.40	1.51	1.39	1.00	0.93	0.82	0.55
PC-FA	0.95	13.89	13.67	11.92	11.19	10.49	8.85
	0.60	9.72	8.13	7.32	7.28	6.25	4.66
	0.40	3.17	1.89	1.46	1.39	1.08	0.98
PC-BS	0.95	16.16	14.46	12.94	11.45	10.54	10.18
	0.60	11.19	9.38	8.27	8.55	7.26	6.25
	0.40	3.55	2.78	1.52	2.59	2.06	1.25
PC-SF	0.95	9.33	8.93	6.67	7.12	5.60	5.72
	0.60	6.25	6.01	4.85	4.86	3.89	2.44
	0.40	1.26	1.14	0.99	0.89	0.80	0.48
PC-BS-SF	0.95	11.17	10.83	10.72	8.57	8.32	7.70
	0.60	7.60	7.22	6.83	5.384	5.10	3.85
	0.40	2.20	1.60	1.01	1.12	1.06	0.94

Appendix D: Experimental results - Concretes corrosion propagation data

Table D1-1: Corrosion propagation data - PC concretes

Binder Type	w/b	d (mm)	c (mm)	Average initial mass (g)	Average final mass (g)	Mass loss (g)
PC	0.95	8	12	102.53	101.69	0.84
		8	20	102.98	102.03	0.95
		8	30	102.88	101.60	1.28
		12	12	231.52	230.27	1.25
		12	20	232.16	230.85	1.31
		12	30	228.77	226.99	1.78
		20	12	625.65	623.60	2.05
		20	20	630.55	628.25	2.30
		20	30	634.40	631.62	2.78
	0.60	8	12	101.98	101.26	0.72
		8	20	100.88	99.99	0.89
		8	30	100.78	99.84	0.94
		12	12	228.38	227.26	1.12
		12	20	228.60	227.41	1.19
		12	30	228.28	227.00	1.28
		20	12	617.86	616.01	1.85
		20	20	627.07	625.04	2.03
		20	30	622.20	619.99	2.21

Table D1-2: Corrosion propagation results - PC concretes

Binder Type	w/b	d (mm)	c (mm)	c/d	Corrosion current density ($\mu A/cm^2$)	Mass loss (g/cm^2)	Surface Area (cm^2)	Amount of corrosion, δr (μm)	Cracking time (years)	Corrosion rate by mass loss (μm/year)	Corrosion rate, Rp (μm/year)	28-day tensile strength (MPa)	28-day OPI (-log k (m/s)
PC	0.95	8	12	1.50	2.66	0.017	50.27	21.26	1.06	20.06	30.90	2.05	9.23
		8	20	2.50	2.25	0.019	50.27	24.05	1.50	16.03	26.04	2.05	9.23
		8	30	3.75	1.41	0.025	50.27	32.40	2.20	14.73	16.31	2.05	9.23
		12	12	1.00	2.78	0.017	75.41	21.09	1.05	20.09	32.24	2.05	9.23
		12	20	1.67	2.36	0.017	75.41	22.11	1.62	13.65	27.39	2.05	9.23
		12	30	2.50	1.43	0.024	75.41	30.04	2.35	12.78	16.61	2.05	9.23
		20	12	0.60	2.80	0.016	125.68	20.76	1.00	20.76	32.43	2.05	9.23
		20	20	1.00	2.39	0.018	125.68	23.29	1.60	14.56	27.68	2.05	9.23
		20	30	1.50	1.56	0.022	125.68	28.15	2.50	11.26	18.13	2.05	9.23
	0.60	8	12	1.50	1.35	0.014	50.27	18.23	1.40	13.02	15.65	4.87	9.70
		8	20	2.50	1.06	0.018	50.27	22.53	2.01	11.21	12.25	4.87	9.70
		8	30	3.75	0.69	0.019	50.27	23.80	2.33	10.21	7.97	4.87	9.70
		12	12	1.00	1.45	0.015	75.41	18.90	1.22	15.49	16.85	4.87	9.70
		12	20	1.67	1.14	0.016	75.41	20.08	1.91	10.51	13.25	4.87	9.70
		12	30	2.50	0.72	0.017	75.41	21.60	2.28	9.47	8.29	4.87	9.70
		20	12	0.60	1.50	0.015	125.68	18.73	1.31	14.30	17.45	4.87	9.70
		20	20	1.00	1.15	0.016	125.68	20.56	2.05	10.03	13.36	4.87	9.70
		20	30	1.50	0.77	0.018	125.68	22.38	2.59	8.64	8.96	4.87	9.70

Table D2-1: Corrosion propagation data – PC-FA concretes

Binder Type	w/b	d (mm)	c (mm)	Average initial mass (g)	Average final mass (g)	Mass loss (g)
FA	0.95	8	12	101.90	100.90	1.00
		8	20	101.78	100.65	1.13
		8	30	102.28	100.69	1.59
		12	12	224.73	223.15	1.58
		12	20	223.78	221.94	1.84
		12	30	224.60	222.25	2.35
		20	12	636.22	633.51	2.71
		20	20	638.16	634.98	3.18
		20	30	636.40	632.12	4.28
	0.60	8	12	100.85	99.89	0.96
		8	20	100.92	99.92	1.00
		8	30	100.78	99.54	1.24
		12	12	228.38	227.04	1.34
		12	20	228.52	226.95	1.57
		12	30	228.10	226.16	1.94
		20	12	618.65	616.11	2.54
		20	20	627.07	624.04	3.03
		20	30	623.45	620.09	3.36

Table D2-2: Corrosion propagation results – PC-FA concretes

Binder Type	w/b	d (mm)	c (mm)	c/d	Corrosion current density ($\mu A/cm^2$)	Surface Area (cm^2)	Mass loss (g/cm^2)	Amount of corrosion (μm)	Cracking time (years)	Corrosion rate by mass loss (μm/year)	Corrosion rate, Rp (μm/year)	28-day tensile strength (MPa)	28-day OPI (-log k (m/s)
PC-FA	0.95	8	12	1.50	3.74	50.27	0.020	25.32	1.00	25.32	43.38	1.95	9.31
		8	20	2.50	2.90	50.27	0.022	28.61	1.35	21.19	33.59	1.95	9.31
		8	30	3.75	2.19	50.27	0.032	40.25	2.12	18.99	25.36	1.95	9.31
		12	12	1.00	3.60	75.41	0.021	26.66	1.01	26.40	41.81	1.95	9.31
		12	20	1.67	2.83	75.41	0.024	31.05	1.50	20.70	32.77	1.95	9.31
		12	30	2.50	2.06	75.41	0.031	39.66	2.24	17.70	23.88	1.95	9.31
		20	12	0.60	3.66	125.68	0.022	27.44	1.12	24.50	42.41	1.95	9.31
		20	20	1.00	2.96	125.68	0.025	32.20	1.56	20.64	34.37	1.95	9.31
		20	30	1.50	2.11	125.68	0.034	43.34	2.33	18.60	24.42	1.95	9.31
	0.60	8	12	1.50	1.73	50.27	0.019	24.30	1.26	19.29	20.01	4.50	9.73
		8	20	2.50	1.35	50.27	0.020	25.32	1.42	17.83	15.68	4.50	9.73
		8	30	3.75	0.96	50.27	0.025	31.39	2.40	13.08	11.09	4.50	9.73
		12	12	1.00	1.74	75.41	0.018	22.61	1.28	17.67	20.17	4.50	9.73
		12	20	1.67	1.25	75.41	0.021	26.49	1.65	16.06	14.45	4.50	9.73
		12	30	2.50	1.03	75.41	0.026	32.74	2.36	13.87	11.90	4.50	9.73
		20	12	0.60	1.73	125.68	0.020	25.72	1.16	22.17	20.12	4.50	9.73
		20	20	1.00	1.34	125.68	0.024	30.68	1.65	18.59	15.52	4.50	9.73
		20	30	1.50	0.93	125.68	0.027	34.02	2.48	13.72	10.78	4.50	9.73

Table D3-1: Corrosion propagation data – PC-BS concretes

Concrete Type	w/b	d (mm)	c (mm)	Average initial mass (g)	Average final mass (g)	Mass loss (g)
PC-BS	0.95	8	12	102.95	101.66	1.29
		8	20	100.00	98.41	1.59
		8	30	100.82	98.94	1.88
		12	12	227.99	226.01	1.98
		12	20	225.37	222.99	2.38
		12	30	227.75	225.01	2.74
		20	12	627.10	623.58	3.52
		20	20	621.07	616.98	4.09
		20	30	623.15	618.10	5.05
	0.60	8	12	102.05	101.05	1.00
		8	20	101.80	100.61	1.19
		8	30	102.70	101.33	1.37
		12	12	226.12	224.37	1.75
		12	20	227.80	225.63	2.17
		12	30	227.10	224.71	2.39
		20	12	632.95	630.46	2.49
		20	20	636.05	632.88	3.17
		20	30	631.08	627.79	3.29

Table D3-2: Corrosion propagation resultss – PC-BS concretes

Concrete Type	w/b	d (mm)	c (mm)	c/d	Corrosion current density ($\mu A/cm^2$)	Surface Area (cm^2)	Mass loss (g/cm^2)	Amount of corrosion (μm)	Cracking time (years)	Corrosion rate by mass loss (μm/year)	Corrosion rate, Rp (μm/year)	28-day tensile strength (MPa)	28-day OPI (-log k (m/s)
PC-BS	0.95	8	12	1.50	3.96	50.27	0.026	32.66	0.98	33.32	45.89	0.55	9.04
		8	20	2.50	3.25	50.27	0.032	40.25	1.30	30.96	37.69	0.55	9.04
		8	30	3.75	2.61	50.27	0.037	47.59	2.04	23.33	30.24	0.55	9.04
		12	12	1.00	3.83	75.41	0.026	33.41	1.01	33.08	44.38	0.55	9.04
		12	20	1.67	3.11	75.41	0.032	40.16	1.41	28.49	36.02	0.55	9.04
		12	30	2.50	2.69	75.41	0.036	46.24	2.12	21.81	31.16	0.55	9.04
		20	12	0.60	3.88	125.68	0.028	35.64	1.05	33.94	45.03	0.55	9.04
		20	20	1.00	3.12	125.68	0.033	41.41	1.34	30.91	36.14	0.55	9.04
		20	30	1.50	2.75	125.68	0.040	51.13	2.22	23.03	31.85	0.55	9.04
	0.60	8	12	1.50	1.94	50.27	0.020	25.32	1.08	23.44	22.46	3.56	9.60
		8	20	2.50	1.53	50.27	0.024	30.12	1.40	21.52	17.71	3.56	9.60
		8	30	3.75	1.21	50.27	0.027	34.68	2.28	15.21	14.06	3.56	9.60
		12	12	1.00	1.96	75.41	0.023	29.53	1.14	25.91	22.69	3.56	9.60
		12	20	1.67	1.51	75.41	0.029	36.62	1.53	23.93	17.53	3.56	9.60
		12	30	2.50	1.13	75.41	0.032	40.33	2.25	17.93	13.15	3.56	9.60
		20	12	0.60	2.05	125.68	0.020	25.21	1.10	22.92	23.72	3.56	9.60
		20	20	1.00	1.61	125.68	0.025	32.10	1.46	21.99	18.70	3.56	9.60
		20	30	1.50	1.16	125.68	0.026	33.31	2.33	14.30	13.42	3.56	9.60

Appendix E: Regression analysis output – Carbonation rates

Table E1: Regression analysis result: PC concretes

Regression Statistics	
Multiple R	0.9686
R Square	0.9381
Adjusted R Square	0.9191
Standard Error	0.9612
Observations	18

ANOVA

	df	*SS*	*MS*	*F*	*Significance F*
Regression	4	182.0446	45.5111	49.2557	0.0000
Residual	13	12.0117	0.9240		
Total	17	194.0563			

	Coefficients	*Standard Error*	*t Stat*	*P-value*	*Lower 95%*	*Upper 95%*
Intercept	81.4945	5.9883	13.6089	0.0000	68.5574	94.4315
OPI	-8.0843	0.6164	-13.1146	0.0000	-9.4160	-6.7525
Indoor	1.7650	0.5550	3.1803	0.0072	0.5661	2.9639
Sheltered	0.8767	0.5550	1.5797	0.1382	-0.3223	2.0756
7_Curing	1.7500	0.4531	3.8620	0.0020	0.7711	2.7289

Table E2: Regression analysis result: PC-FA concretes

Regression Statistics	
Multiple R	0.9893
R Square	0.9788
Adjusted R Square	0.9722
Standard Error	0.7430
Observations	18

ANOVA

	df	*SS*	*MS*	*F*	*Significance F*
Regression	4	330.8819	82.7205	149.8384	0.0000
Residual	13	7.1768	0.5521		
Total	17	338.0587			

	Coefficients	*Standard Error*	*t Stat*	*P-value*	*Lower 95%*	*Upper 95%*
Intercept	93.973	3.842	24.461	0.000	85.674	102.273
OPI	-9.080	0.390	-23.306	0.000	-9.921	-8.238
Indoor	1.908	0.429	4.449	0.001	0.982	2.835
Sheltered	1.053	0.429	2.455	0.029	0.127	1.980
7_Curing	2.111	0.350	6.027	0.000	1.354	2.868

Table E3: Regression analysis result: PC-BS concretes

Regression Statistics	
Multiple R	0.9716
R Square	0.9439
Adjusted R Square	0.9267
Standard Error	1.2639
Observations	18

ANOVA

	df	*SS*	*MS*	*F*	*Significance F*
Regression	4	349.5540	87.3885	54.7053	0.0000
Residual	13	20.7667	1.5974		
Total	17	370.3208			

	Coefficients	*Standard Error*	*t Stat*	*P-value*	*Lower 95%*	*Upper 95%*
Intercept	103.902	7.049	14.740	0.000	88.674	119.131
OPI	-10.284	0.735	-13.993	0.000	-11.872	-8.697
Indoor	2.180	0.730	2.987	0.010	0.604	3.756
Sheltered	1.012	0.730	1.386	0.189	-0.565	2.588
7_Curing	2.236	0.596	3.752	0.002	0.948	3.523

Table E4: Regression analysis result: PC-SF concretes

Regression Statistics	
Multiple R	0.9771
R Square	0.9547
Adjusted R Square	0.9407
Standard Error	0.7077
Observations	18

ANOVA

	df	*SS*	*MS*	*F*	*Significance F*
Regression	4	137.124	34.281	68.439	0.000
Residual	13	6.512	0.501		
Total	17	143.636			

	Coefficients	*Standard Error*	*t Stat*	*P-value*	*Lower 95%*	*Upper 95%*
Intercept	60.695	3.748	16.193	0.000	52.598	68.793
OPI	-5.799	0.374	-15.517	0.000	-6.606	-4.991
Indoor	1.427	0.409	3.491	0.004	0.544	2.309
Sheltered	0.870	0.409	2.129	0.053	-0.013	1.753
7_Curing	1.514	0.334	4.539	0.001	0.794	2.235

Table E5: Regression analysis result: PC-BS-SF concretes

Regression Statistics	
Multiple R	0.989274936
R Square	0.978664899
Adjusted R Square	0.972100252
Standard Error	0.611351722
Observations	18

ANOVA

	df	*SS*	*MS*	*F*	*Significance F*
Regression	4	222.877	55.719	149.081	0.000
Residual	13	4.859	0.374		
Total	17	227.736			

	Coefficients	*Standard Error*	*t Stat*	*P-value*	*Lower 95%*	*Upper 95%*
Intercept	84.600	3.449	24.531	0.000	77.149	92.050
OPI	-8.144	0.348	-23.388	0.000	-8.896	-7.391
Indoor	0.832	0.353	2.356	0.035	0.069	1.594
Sheltered	0.513	0.353	1.454	0.170	-0.249	1.276
7_Curing	1.904	0.288	6.608	0.000	1.282	2.527

Appendix F: Regression analysis output – corrosion propagation

Table F1: Regression analysis result

SUMMARYOUTPUT

Regression Statistics	
Multiple R	0.951058
R Square	0.904511
Adjusted R Square	0.896716
Standard Error	2.582403
Observations	54

ANOVA

	df	*SS*	*MS*	*F*	*Significance F*
Regression	4	3095.3247	773.8312	116.0374	0.0000
Residual	49	326.7716	6.6688		
Total	53	3422.0963			

Regression coefficients

	Coefficients	*Standard Error*	*t Stat*	*P-value*	*Lower 95%*	*Upper 95%*
Intercept	142.1580	13.5852	10.4642	0.0000	114.8575	169.4584
OPI	-12.5800	1.4523	-8.6620	0.0000	-15.4986	-9.6615
cover	0.5572	0.0477	11.6763	0.0000	0.4613	0.6531
PC	-11.8287	0.8862	-13.3478	0.0000	-13.6095	-10.0478
PC-FA	-3.4216	0.9108	-3.7566	0.0005	-5.2520	-1.5913

Table F2: Comparison between the proposed and some previous steel radius loss models

Specimen designation	Measured δ_r (μm)	Rodriguez δ_r (μm)	Alonzo δ_r (μm)	Morinaga δ_r (μm)	Torres-Acosta δ_r (μm)	Present study δ_r (μm)
SL1	50	30	35	50	51	38
SL2	76	40	48	67	88	50
SL3	38	21	23	34	24	26
SL4	50	38	46	50	72	40

Appendix G: Derivation of a multiplying factor (11.6) for converting corrosion current density (μA/cm^2) to corrosion rate (μm/year)

From mass loss, the corrosion current density can be converted to corrosion rate using the Faraday's law:

$$m_l = \frac{i_{cor} A t}{nF}$$

where m_l (g) is the mass of iron consumed, i_{cor} (Ampere/m^2) is the corrosion current density, A (g/mol) is the atomic weight of the ions being dissolved, F (C/mol) is the Faraday's constant taken as 96500 C/mol and t (seconds) is the time. The n (moles of electrons per mole of iron corroded) is valency of the corrosion reaction which depends on chemical composition of the reaction products usually taken as 2. Corrosion rate can be expressed as:

Corrosion rate, $I_{cor}(m_i / At) = \frac{i_{cor}}{nF}$

It should be noted that coulomb is a product of corrosion current and time (C = Ampere x second), therefore the rate of corrosion can be expressed as moles of iron per square metre per second which can be converted to grams per square meter per day (g/m^2.day) by multiplying the atomic weight of the metal and 86400 second/day.

For example, an iron corrodes at a corrosion current density of 1A/m^2, the corrosion rate can be calculated as:

$$I_{cor} = \frac{A}{m^2}\frac{(55.85g/mol(Fe))(86400s/d)}{\frac{2molee^-}{mol(Fe)}(96500A.s/molee^-)} = \frac{4825440}{193000} = 25g/m^2.day$$

To convert the corrosion rate to steel radial loss assuming that the steel density is 7.86 x 10^6 g/m^3, therefore

$$I_{cor} = \frac{25g/m^2day(365day/year)}{7.86x10^6 g/m^3} = 0.00116m/year$$

Therefore, a current density of 1 A/m^2 (1 μA/cm^2) is equivalent to a metal loss of 0.00116 m/year (11.6 μm/year).

Appendix H: Regression analysis outputs in a CD

File 1: Carbonation rate data and regression analysis outputs

File 2: Corrosion steel radius loss data and regression analysis outputs

The File 1 and 2 contain the carbonation rate and corrosion steel radius loss regression analysis input and outputs. The regression analysis output contains the regression statistics, analysis of variance (ANOVA) and regression coeficients.

Regression statistic table: The regression statistics contain the multiple R, R squared, adjusted R squared, standard error of the regression and observations. They measure the Goodness of fit of the regression model which show how well the calculated linear regression equation fits a particular data.

ANOVA table: The ANOVA table contains the sum of squares (SS), regression mean square (MS) = regression SS/regression degree of freedom (df), residual MS = mean square error (residual SS/ residual degree of freedom), F (overall F test for the null hypothesis) and significance F (the significance associated P-value).

Regression coefficients: The regression coefficients give specific information about the output variables which are categorised into 6 columns as shown in the files.

Column 1 contains the coefficients of the intercept (y-axis) and output variables which show the least square estimate of the output variables and the intercept. The coefficients in the column1 gives the linear regression equation.

Column 2 contains the standard error (the least squares estimate of the standard error) of the output variables and the intercept

Column 3 represents the T Statistics of the output variables and the intercept for the null hypothesis vs the alternate hypothesis

Column 4 shows the P values of the output variables and the intercept which are used in testing the hypothesis

Column 5 shows lower 95% of the output variables and the intercept which represents the lower boundary for the confidence interval.

Column 6 is the upper 95% of each of the output variables and the intercept which represents the upper boundary for the confidence interval.